



UNIVERSIDAD DE GRANADA

Departamento de Ecología

Organic matter distribution and dynamics in marine ecosystems.

Field, experimental and remote sensing approaches

TESIS DOCTORAL

Eva Ortega Retuerta



Granada, Septiembre 2008

Editor: Editorial de la Universidad de Granada
Autor: Eva Ortega Retuerta
D.L.: GR. 2100-2008
ISBN: 978-84-691-6364-1



UNIVERSIDAD DE GRANADA

Departamento de Ecología

Organic matter distribution and dynamics in marine ecosystems.
Field, experimental and remote sensing approaches

Memoria presentada por la Licenciada Eva Ortega Retuerta para aspirar al Grado de Doctora por la Universidad de Granada

Fdo: Eva Ortega Retuerta

Directores

Dra. Isabel Reche Cañabate
Departamento Ecología
Universidad de Granada

Dr. Carlos M. Duarte Quesada
Institut Mediterrani d'Estudis Avancats
Consejo Superior de Investigaciones Científicas (CSIC)

Granada, Septiembre 2008

Dra. Isabel Reche Cañabate

Profesora titular del departamento de Ecología de la Universidad de Granada

Dr. Carlos M. Duarte Quesada

Profesor de Investigación del Institut Mediterrani d'Estudis Avançats
(IMEDEA, CSIC)

Certifican

Que los trabajos de investigación desarrollados en la memoria de la tesis doctoral "Organic matter distribution and dynamics in marine ecosystems: field, experimental and remote sensing approaches" son aptos para ser presentados por la Licenciada Eva Ortega-Retuerta antes el tribunal designado para optar al grado de Doctora por la Universidad de Granada.

Para que así conste, en cumplimiento de las disposiciones vigentes, se extiende el presente certificado a 1 de septiembre de 2008.

Fdo: Dra. Isabel Reche Cañabate

Fdo. Dr. Carlos M. Duarte Quesada

Durante el desarrollo de esta tesis doctoral (2004-2008), Eva Ortega Retuerta disfrutó de una beca de Formación del Profesorado Universitario otorgada por el ministerio de Educación y Ciencia.

Este trabajo ha sido financiado por los proyectos ICEPOS (REN2002-04165-CO3) y DISPAR (CGL2005-00076), otorgados por los ministerios de Ciencia y Tecnología y Educación y Ciencia, y el proyecto europeo THRESHOLDS (CTM2005-24238-E).

A mis padres.

*What we know is a drop,
what we don't know is an ocean.*

(Sir Isaac Newton)

AKNOWLEDGEMENTS

... y tras mucho caminar, por fin llegué al principio. Ahora puedo pararme a respirar, tomar aliento, y mirar hacia atrás tras cruzar la meta del cuatrocientos vallas más largo de mi vida. Una meta que nunca habría alcanzado sin el apoyo de todos los que me habéis estado ayudando a pasar obstáculos durante estos años.

En primer lugar, mi más sincero agradecimiento a mis directores de tesis. A Isabel Reche, por permitirme conocer este mundillo y transmitirme como nadie su pasión por la ciencia, aun avisándome el primer día de que cuán larga iba a ser esta carrera. A Carlos Duarte, por darme la oportunidad de “zambullirme” en la oceanografía y aprender de su amplísima experiencia.

A todo el departamento de ecología e instituto del agua de la universidad de Granada por acogerme y acompañarme durante este tiempo. En especial quiero agradecer a Elvi el haberme allanado el camino con su ayuda y apoyo, a Carolina su asesoramiento continuo en materia de papeleos, y a Oti el haber estado ahí para lo que hiciera falta. También a Antonio, Andrés, Jorge, Nacho, Natalie y todo el batallón de alumnos, ayudantes y amigos que han colaborado de alguna forma, desde pesando un reactivo hasta contándome un chiste, para que todo mi trabajo llegara a buen puerto.

I Acknowledgements

A todos los participantes en las campañas oceanográficas ICEPOS y Thresholds; en especial, a Susana Agustí, y Tom Frazer, de cuya colaboración han salido varios de los capítulos de esta tesis, por compartir su ciencia conmigo. También gracias a Regino Martínez, María Calleja, y Rocío Santiago, por facilitarme datos de carbono y nutrientes, y a los técnicos de la Unidad de Tecnología Marina de Barcelona por su profesionalidad y humanidad.

A Pep Gasol, por darme un curso acelerado de citometría de flujo en el Institut de Ciències del Mar de Barcelona del que he sacado buen rendimiento, y por estar siempre disponible para resolverme dudas.

Thanks to the members of Biogeosciences division in the Alfred Wegener Institute (Germany) for their hospitality during my stay in 2005. I would like to specially acknowledge Uta Passow for introducing me to “the TEP world” and for kindly supervising my work during these last years. Also thanks to Sebastian, Elena, Sévrine and Sven for making Bremerhaven a warmer place.

Thanks to my colleagues of the Institute for Computational Earth System Science (University of California, USA), and especially to Dave Siegel, for a productive and nice stay with them. I would like also to acknowledge Norm Nelson, Chantal Schwan and Stéphane Maritorena for their help with computing and more.

Thanks to Karen Patterson and David Thomas for sharing with me their CDOM data. Also thanks to the SeaWiFS Bio-Optical archive and storage system (SeaBASS), particularly to Greg Mitchell, PI of AMLR cruises, for CDOM data, to the National Snow and Ice Data Center and the NASA Ocean Biology Processing Group for providing satellite data, and the NOAA/ National Weather Service for providing AAO Index data.

A Fran Pérez, gracias por conseguir que esta tesis luzca mejor.

Y, por último, a todos los que me habéis hecho reír y disfrutar durante todos estos años. Porque sólo con buen ánimo se hace un buen trabajo, gracias a todos los que habéis ayudado en esta tesis sin hablarme de ciencia.

A todos mis compañeros de la antigua biblioteca, actual sala X, y futuro incierto, así como a mis vecinas de casita, pobladores de pasillos, laboratorios y rincones perdidos del departamento e instituto, compañeros de cafés y partidos

de voley-cemento, porque con vosotros hasta quejarse es divertido. Perdonad si no os nombro a todos, pero todos estáis aquí.

A mis amigos de biología, porque con ellos comencé mi andadura. Gracias en especial a María la Rubia, por hacerse de la “familia”.

A Pepe por estos catorce años de vallas, salud y rock.

A mis niñas de Jerez: Ana, Elena, Inma y Sonia, por crecer conmigo.

A mis “esposos”, Jesús y Jorge, porque son imprescindibles.

A mi familia, los Ortega y los Retu, por ser tan chulos. Gracias especialmente al abuelo Mariano, que siempre siguió mis viajes dedo en atlas, y a mi hermano Alva, por estar dispuesto a chincharme toda la vida.

A Kim, por quererme tanto.

Y finalmente, a mis padres, José Luis y Eva. Por ser los mejores sufridores, críticos, ídolos, fans, maestros, alumnos, amigos... os dedico este libro.

INDEX

Abstract (in Spanish)	23
Introduction.....	35
Significance of Organic Matter in the Ocean.....	35
Classifying Ocean Organic Matter	36
Bacterial and sunlight transformation of DOM.....	38
Chromophoric Dissolved Organic Matter (CDOM).....	38
Marine Gel phase. Transparent Exopolymer Particles (TEP)	40
General objectives.....	42
References.....	43
Material and Methods	49
Study site characterization.....	49
Southern Ocean.....	49
Mediterranean Sea	50
North Sea	51
Sampling protocols.....	52

Chemical and Biological Analyses	60
Chromophoric dissolved organic matter (CDOM)	60
Transparent Exopolymer Particles (TEP).....	61
Dissolved Monosaccharides (DMCHO) and polysaccharides (DPCHO).....	62
Dissolved Organic Carbon concentration.....	63
Chlorophyll <i>a</i>	63
Bacterial Abundance	63
Bacterial Production.....	65
References.....	67

Chapter 1 : **Chromophoric dissolved organic matter in marine ecosystems: distribution and controlling factors. 73**

Ortega-Retuerta, E., Pulido-Villena, E., Agustí, S., Duarte, C.M., and Reche, I.	
Introduction	75
Material and Methods.....	77
Results.....	78
Discussion	87
References.....	91

Chapter 2 : **Role of photoreactions on chromophoric dissolved organic matter dynamics in marine ecosystems and further influence on bacterioplankton..... 97**

Ortega-Retuerta, E., Pulido-Villena, E., Duarte, C.M., and Reche, I.	
Introduction	99
Material and Methods.....	100
Results.....	108
Discussion	119
References.....	123

Chapter 3: **Chromophoric dissolved organic matter generation by bacterioplankton and Antarctic krill in the Southern Ocean and Mediterranean Sea. 127**

Ortega-Retuerta, Frazer, T.K., Duarte, C.M., and Reche, I.

Introduction	129
Material and Methods	131
Results.....	136
Discussion	146
References.....	150

Chapter 4: **Dynamics of Chromophoric dissolved and detrital organic matter (CDM) using remote sensing in the Southern Ocean: data validation, temporal dynamics, and global warming implication. 155**

Ortega-Retuerta, E., Siegel, D.V., Duarte, C.M., and Reche, I.

Introduction	157
Material and Methods	163
Results.....	169
Discussion	178
References.....	184

Chapter 5: **Uncoupled distribution of transparent exopolymer particles and dissolved carbohydrates in the Southern Ocean.....191**

Ortega-Retuerta, E., Pulido-Villena, E., Agustí, S., Duarte, C.M., and Reche, I.

Introduction	193
Material and Methods	194
Results.....	195
Discussion	202
References.....	207

Chapter 6: Role of bacterioplankton on transparent exopolymer particles formation in the Mediterranean Sea.....213

Ortega-Retuerta, E., Duarte, C.M., and Reche, I.

Introduction	215
Material and Methods	218
Results.....	221
Discussion	233
References.....	238

Chapter 7: Impact of UVB on transparent exopolymer particles. 245

Ortega-Retuerta, E., Passow, U., Duarte, C.M., and Reche, I.

Introduction	247
Material and Methods	249
Results.....	254
Discussion	264
References.....	267

General Summary..... 271

Conclusions (in English) 283

Conclusions (in Spanish)..... 285

List of abbreviations 289

Appendix: Publications..... 291

RESUMEN

DISTRIBUCIÓN Y DINÁMICA DE LA MATERIA ORGÁNICA DISUELTA EN ECOSISTEMAS MARINOS: APROXIMACIONES DE CAMPO, EXPERIMENTALES, Y DE SATÉLITE

Eva Ortega-Retuerta

El océano es uno de los principales reservorios de carbono reactivo de la superficie terrestre. El contenido de carbono inorgánico disuelto, con 38000 Pg C, es un orden de magnitud superior al resto de depósitos de carbono reactivo (Hedges, 2002), mientras que se estima que 685 Gt de carbono se encuentran en forma de carbono orgánico disuelto, cantidad comparable a la masa de carbono inorgánico que reside en la atmósfera. El flujo de carbono entre la atmósfera y el océano se aproxima a los 70 Pg C por año, del mismo orden de magnitud que el intercambio de carbono entre la atmósfera y la biota de sistemas terrestres. En consecuencia, una perturbación mínima en los procesos de producción o retirada de carbono orgánico en el océano podría tener un gran impacto sobre el intercambio de carbono con la atmósfera. Además, los factores que controlan la distribución y dinámica de la materia orgánica disuelta (MOD) tienen gran importancia en relación al flujo descendente y almacenamiento de carbono orgánico en el océano profundo (Carlson, 2002).

En esta tesis doctoral me he centrado en el estudio de dos fracciones del conjunto de carbono orgánico. Por un lado, la materia orgánica disuelta cromofórica (CDOM), y por otro, las partículas exopoliméricas transparentes (TEP).

La CDOM es una mezcla de compuestos que representan el subconjunto de la MOD ópticamente activo, tanto en el espectro visible como ultravioleta (Nelson and Siegel, 2002; Coble, 2007). Esta fracción de la MOD juega un papel fundamental en los ciclos del carbono y otros elementos como mediadora de reacciones fotoquímicas (Kieber et al., 1989; Mopper et al., 1991; Kieber et al., 1999) y como reguladora de la transmisión de la luz a través de la columna de agua, protegiendo a los organismos contra el daño causado por la luz ultravioleta (Arrigo and Brown, 1996; Anderson et al., 2001; Williamson et al., 2001) o controlando la disponibilidad de luz fotosintéticamente activa (Kalle, 1966; Bricaud et al., 1981). En los últimos años, el interés creciente en el estudio de la CDOM se debe, además, a que es un componente principal en medidas ópticas del color del océano realizadas por teledetección, con la consiguiente interferencia sobre la precisión de los datos de producción primaria obtenidos por satélite (Siegel et al., 2002; Siegel et al., 2005).

Las TEP son un tipo de partículas de naturaleza adhesiva, y susceptibles de ser teñidas con azul de alcián (Aldredge et al., 1993). Estas partículas se forman predominantemente por la polimerización abiótica de precursores disueltos, principalmente mono- y polisacáridos, que son excretados por microorganismos (Passow and Aldredge, 1994; Passow, 2000). Las TEP forman parte de forma significativa en el flujo descendente en sistemas marinos, ya que debido a su alta adherencia actúan como la matriz intersticial de agregados macroscópicos, formados por compuestos orgánicos e inorgánicos, que son conocidos como “nieve marina”. La formación y sedimentación de nieve marina es una ruta principal de retirada de carbono de la superficie del océano hacia aguas profundas (Aldredge et al., 1993; Passow et al., 2001; Passow, 2002).

En esta tesis he abordado el estudio de estos dos conjuntos de materia orgánica mediante distintas aproximaciones: observaciones directas de campo, experimentos para evaluar los procesos de aporte y pérdida, y dinámicas a largo plazo mediante el uso de la teledetección. He centrado mi investigación en dos ecosistemas marinos de características contrastadas: la península antártica en el océano Sur, y el mar Mediterráneo, además de dos estaciones situadas en el mar del Norte.

El ecosistema marino del océano Sur se caracteriza por una variabilidad estacional extrema, temperaturas bajas, y la influencia del avance y retirada anual de la capa de hielo (Smetacek and Nicol, 2005; Ducklow et al., 2007). Aunque representa un 10% del total de la superficie oceánica, este océano tiene un impacto global en la circulación de las masas de agua, y también en el ciclo del carbono a través de la formación y transporte meridional de aguas enriquecidas en nutrientes (agua Antártica inferior, Webb and Suginoara, 1997) y un sumidero de CO₂ antropogénico (Sarmiento et al., 1998; Takahashi et al., 2002). El océano Sur es una de las zonas llamadas “high nutrient-low chlorophyll” (con nutrientes elevados y clorofila baja). Esta denominación se refiere a zonas donde, a pesar de encontrar altas concentraciones de macronutrientes, la concentración de clorofila es relativamente baja (Minas et al., 1986). En esta zona esta restricción probablemente es debida a la limitación por luz (Smith et al 1992), o por micronutrientes, especialmente hierro (Debaar et al., 1995; Pakulski et al., 1996).

El mar Mediterráneo es un mar semiabierto, rodeado por Europa, Asia y África, que representa el 0.7% de la superficie total del océano y 0.3% de su volumen. A pesar de su reducido tamaño, muestra circulación termohalina y procesos de formación de aguas densas, como un “océano en miniatura”. Asimismo, es un área única en que la evaporación excede a la precipitación más los aportes terrestres (Chen et al., 2003), y ha sido uno de los primeros donde el calentamiento global se ha evidenciado y cuantificado (Bethoux et al., 1998). La principal entrada de agua al sistema viene de aguas superficiales, pobres en nutrientes, que entran desde el océano Atlántico a través del estrecho de Gibraltar. Este proceso conduce al sistema a un estado general de oligotrofia. Así, el mar Mediterráneo es una zona considerada “low nutrient-low chlorophyll” (nutrientes bajos, clorofila baja).

Por último, también he estudiado sucintamente algunos puntos del mar del Norte, concretamente en la bahía de Alemania. En esta zona, la poca profundidad y la influencia de grandes ríos aseguran una alta productividad.

Capítulo 1: **Materia orgánica disuelta cromofórica en ecosistemas marinos: distribución y factores de regulación.**

En este capítulo se describe la variabilidad geográfica y vertical (primeros 200 m) de la CDOM, caracterizada mediante coeficientes de absorción, absorción molar y valores de la pendiente espectral, en los diferentes sistemas de estudio. Cabe resaltar de los resultados los altos valores de CDOM observados en el océano Sur (valor medio de $a_{325} = 0.39 \text{ m}^{-1}$), especialmente en aquellas regiones donde se observó un deshielo reciente, como el oeste del mar de Weddell. En comparación, el Mediterráneo mostró valores más bajos de CDOM, con un valor medio de $a_{325} = 0.11 \text{ m}^{-1}$, aunque los valores más altos de CDOM se encontraron en las estaciones del mar del Norte (valor medio de $a_{325} = 1.72 \text{ m}^{-1}$). En las estaciones del mar de Bellingshausen (Océano Sur) y Mediterráneo, se observó un empobrecimiento en CDOM en las aguas de la capa de mezcla superior, probablemente debido a pérdidas por fotodegradación, mientras que se observaron valores mayores de CDOM bajo esta capa. La ausencia de relación de la CDOM con la concentración de carbono orgánico disuelto, así como con otras variables físicas y biológicas, subrayan la naturaleza compleja de esta fracción de la materia orgánica.

Capítulo 2: **El papel de las fotoreacciones sobre la dinámica de la materia orgánica disuelta cromofórica en sistemas marinos y su influencia sobre el bacterioplancton.**

La fotoreactividad de la materia orgánica disuelta puede conducir a una pérdida de la absorbancia por fotodegradación o, por el contrario, a un aumento en la absorbancia mediado por fotohumificación. En este capítulo, se determinó experimentalmente la fotoreactividad de la CDOM en diferentes lugares de estudio. La fotodegradación fue el proceso predominante en la mayoría de lugares de estudio del océano Sur y mar del Norte, mientras que la fotohumificación predominó en aquellos lugares que presentaron valores iniciales de CDOM bajos (mares de Bellingshausen y Mediterráneo). Estos resultados señalan el carácter reactivo de la CDOM sometida a la radiación solar natural, susceptible de ser modificada significativamente en un plazo de pocos días.

En la segunda sección, estudiamos experimentalmente el efecto de la presencia de fotoproductos de la CDOM sobre el crecimiento del bacterioplancton. Un efecto de fotodegradación previa de la CDOM supuso una inhibición a corto

plazo de la abundancia y producción bacterianas, debido posiblemente a la presencia de radicales tóxicos (especies de oxígeno reactivas).

Capítulo 3: **Generación de materia orgánica disuelta cromofórica por el bacterioplancton y el krill antártico en el océano Sur y el mar Mediterráneo.**

En este capítulo usamos una aproximación experimental para estudiar la generación de CDOM por bacterias en el océano Sur y el mar Mediterráneo y por la especie de krill antártico *Euphasia superba* en el océano Sur. El bacterioplancton generó CDOM de forma significativa, con tiempos de duplicación de meses, contribuyendo de forma importante a la dinámica local de CDOM. Además, la magnitud y la calidad de la CDOM generada por bacterias dependieron de la presencia de fotoproductos en el agua. Por otro lado, el krill antártico, una especie clave en la red trófica del océano Sur, demostró jugar un papel fundamental en la generación de CDOM, tanto directamente, con tiempos de duplicación de menos de un día dentro de “swarms” (acumulaciones de krill), como indirectamente promoviendo el crecimiento bacteriano y su consiguiente generación de CDOM.

Capítulo 4: **Dinámica de la materia orgánica disuelta y detrítica cromofórica obtenida por teledetección en la península Antártica: Validación de datos, dinámica temporal e implicaciones del cambio global.**

En este capítulo estudiamos las dinámicas de CDM a largo plazo en la península Antártica utilizando datos de satélite. En primer lugar, comprobamos la validez del algoritmo semianalítico GSM (Garver-Siegel-Maritorea) en la obtención de datos de CDM en superficie en el océano Sur comparando datos coincidentes de campo y de satélite obtenidos usando este algoritmo. Posteriormente, estudiamos dinámicas estacionales e interanuales en la península Antártica de CDM y sus posibles factores reguladores (clorofila, temperatura, extensión de hielo, radiación fotosintéticamente activa) empleando datos de satélite. A diferencia de lo obtenido en campo, pudimos observar dinámicas acopladas tanto espacial como temporalmente de CDM y clorofila. Este resultado implicaría que la CDM está, en última instancia, mediada por la clorofila, probablemente a través del procesado bacteriano de la materia orgánica de origen algal, o que ambas variables se en-

cuentran regulados por los mismos factores, esto es, el avance y retirada anual de hielo o los cambios interanuales del índice de oscilación antártica.

Capítulo 5: **Distribuciones desacopladas de las partículas exopoliméricas transparentes (TEP) y carbohidratos disueltos en el océano Sur.**

En este capítulo, describimos la variabilidad geográfica y vertical de TEP y carbohidratos disueltos en el área de la península Antártica, y evaluamos la contribución de estos compuestos dentro de los conjuntos de materia orgánica disuelta y particulada. Asimismo, exploramos la importancia del fito- y bacterioplancton como reguladores. La concentración media de las TEP fue de $15.4 \mu\text{g XG eq l}^{-1}$ ($11.6 \mu\text{g C l}^{-1}$). Los monosacáridos y polisacáridos disueltos mostraron valores medios de 4.3 y $8.6 \mu\text{mol C l}^{-1}$ respectivamente. TEP y carbohidratos disueltos no se relacionaron de forma significativa en campo, pero se observó una correlación negativa entre mono- y polisacáridos. Por otro lado, la clorofila fue la mejor variable descriptora de las variaciones de las TEP sobre la capa de mezcla, mientras que la producción bacteriana explicó los cambios de TEP bajo esta capa, lo que subrayó la relación directa entre TEP y actividad bacteriana en aguas alejadas de la influencia algal.

Capítulo 6: **El papel del bacterioplancton en la dinámica de las partículas exopoliméricas transparentes en el mar Mediterráneo.**

Las TEP se han ligado tradicionalmente a la evolución de afloramientos de fitoplancton. Sin embargo, el papel de las bacterias parece ser más complejo, ya que éstas son a la vez productoras y consumidoras tanto de las TEP como de sus precursores. En este capítulo se estudió la variabilidad geográfica de TEP y carbohidratos disueltos en el mar Mediterráneo, poniendo énfasis en el papel regulador de las bacterias. Se realizaron experimentos para determinar el efecto neto del bacterioplancton sobre la dinámica de TEP. Las TEP mostraron valores medios de $21.4 \mu\text{g XG eq l}^{-1}$, mientras que los monosacáridos y polisacáridos disueltos mostraron valores medios de 2.7 y $2.4 \mu\text{mol C l}^{-1}$ respectivamente. TEP y carbohidratos disueltos no se relacionaron significativamente en campo, mientras que la producción bacteriana fue el principal factor regulador de los TEP en esta área. Los resultados experimentales confirmaron que las bacterias pueden generar TEP de forma directa y que se pueden duplicar los valores de TEP in situ en 4 días debido a la actividad bacteriana.

Capítulo 7: **Impacto de la radiación UVB sobre las partículas exopoliméricas transparentes**

Actualmente, la información disponible sobre los posibles efectos de la radiación ultravioleta sobre la formación y degradación de partículas es muy limitada. En este capítulo, empleamos diferentes aproximaciones experimentales para evaluar el papel de la radiación solar, tanto ultravioleta B (UVB) como visible, sobre la fotogeneración y fotólisis de las TEP. Aunque no se evidenció una fotogeneración significativa de TEP, se demostró que los TEP pueden ser dispersados en su totalidad en menos de 3 días debido a la acción de la radiación UVB. Este proceso puede tener consecuencias significativas en la dinámica de TEP en la superficie del océano.

REFERENCES

- ALLDREDGE, A.L., U. PASSOW and B.E. LOGAN (1993) The abundance and significance of a class of large, transparent organic particles in the ocean. *Deep-Sea Research Part I-Oceanographic Research Papers*. 40: 1131-1140.
- ANDERSON, S., R. ZEPP, J. MACHULA, D. SANTAVY, L. HANSEN and E. MUELLER (2001) Indicators of UV exposure in corals and their relevance to global climate change and coral bleaching. *Human and Ecological Risk Assessment*. 7: 1271-1282.
- ARRIGO, K.R. and C.W. BROWN (1996) Impact of chromophoric dissolved organic matter on UV inhibition of primary productivity in the sea. *Marine Ecology-Progress Series*. 140: 207-216.
- BETHOUX, J.P., B. GENTILI and D. TAILLIEZ (1998) Warming and freshwater budget change in the Mediterranean since the 1940s, their possible relation to the greenhouse effect. *Geophysical Research Letters*. 25: 1023-1026.
- BRICAUD, A., A. MOREL and L. PRIEUR (1981) Absorption by dissolved organic matter of the sea (yellow substance) in the UV and visible domains. *Limnology and Oceanography*. 26: 43-53.
- CARLSON, C.A. (2002) Production and removal processes. In: D. A. Hansell and C. A. Carlson (eds.) *Biogeochemistry of marine dissolved organic matter*. Academic Press, San Diego, California.
- CHEN, C.A., K. LIU and R. MACDONALD (2003) Continental margin exchanges. In: M. J. R. Fasham (ed.) *Ocean Biogeochemistry*. Springer, Berlin Heidelberg New York. pp. 53-97.
- COBLE, P.G. (2007) Marine optical biogeochemistry: The chemistry of ocean color. *Chemical Reviews*. 107: 402-418.
- DEBAAR, H.J.W., J.T.M. DEJONG, D.C.E. BAKKER, B.M. LOSCHER, C. VETH, U. BATHMANN and V. SMETACEK (1995) Importance of Iron for Plankton Blooms and Carbon-Dioxide Drawdown in the Southern-Ocean. *Nature*. 373: 412-415.
- DUCKLOW, H.W., K. BAKER, D.G. MARTINSON, L.B. QUETIN, R.M. ROSS, R.C. SMITH, S.E. STAMMERJOHN, M. VERNET and W. FRASER (2007) Marine pelagic ecosystems: The West Antarctic Peninsula. *Philosophical Transactions of the Royal Society B-Biological Sciences*. 362: 67-94.
- HEDGES, J.I. (2002) Why dissolved organic matter? In: D. A. Hansell and C. A. Carlson (eds.) *Biogeochemistry of marine dissolved organic matter*. Academic Press, San Diego, California.

- KALLE, K. (1966) The problem of gelbstoff in the Sea. *Oceanography and Marine Biology: Annual Reviews* 4: 91-104.
- KIEBER, D.J., J. MCDANIEL and K. MOPPER (1989) Photochemical source of biological substrates in seawater: implications for carbon cycling. *Nature*. 341: 637-639.
- KIEBER, R.J., A. LI and P.J. SEATON (1999) Production of nitrite from the photodegradation of dissolved organic matter in natural waters. *Environmental Science & Technology*. 33: 993-998.
- MINAS, H.J., M. MINAS and T.T. PACKARD (1986) Productivity in upwelling areas deduced from hydrographic and chemical fields. *Limnology and Oceanography*. 31: 1182-1206.
- MOPPER, K., X.L. ZHOU, R.J. KIEBER, D.J. KIEBER, R.J. SIKORSKI and R.D. JONES (1991) Photochemical degradation of dissolved organic carbon and its impact on the oceanic carbon cycle. *Nature*. 353: 60-62.
- NELSON, N.B. and D.A. SIEGEL (2002) Chomophoric DOM in the open ocean. In: D. A. Hansell and C. A. Carlson (eds.) *Biogeochemistry of marine dissolved organic matter*. Academic Press, San Diego.
- PAKULSKI, J.D., R.B. COFFIN, C.A. KELLEY, S.L. HOLDER, R. DOWNER, P. AAS, M.M. LYONS and W.H. JEFFREY (1996) Iron stimulation of Antarctic bacteria. *Nature*. 383: 133-134.
- PASSOW, U. (2000) Formation of transparent exopolymer particles, TEP, from dissolved precursor material. *Marine Ecology-Progress Series*. 192: 1-11.
- PASSOW, U. (2002) Production of transparent exopolymer particles (TEP) by phyto- and bacterioplankton. *Marine Ecology-Progress Series*. 236: 1-12.
- PASSOW, U. and A.L. ALLDREDGE (1994) Distribution, size and bacterial colonization of transparent exopolymer particles (TEP) in the ocean. *Marine Ecology-Progress Series*. 113: 185-198.
- PASSOW, U., R.F. SHIPE, A. MURRAY, D.K. PAK, M.A. BRZEZINSKI and A.L. ALLDREDGE (2001) The origin of transparent exopolymer particles (TEP) and their role in the sedimentation of particulate matter. *Continental Shelf Research*. 21: 327-346.
- SARMIENTO, J.L., T.M.C. HUGHES, R.J. STOUFFER and S. MANABE (1998) Simulated response of the ocean carbon cycle to anthropogenic climate warming. *Nature*. 393: 245-249.
- SIEGEL, D.A., S. MARITORENA and N.B. NELSON (2005) Independence and interdependencies among global ocean color properties: Reassessing the bio-

optical assumption. *Journal of Geophysical Research-Oceans*. 110.

SIEGEL, D.A., S. MARITORENA, N.B. NELSON, D.A. HANSELL and M. LORENZIKAYSER (2002) Global distribution and dynamics of colored dissolved and detrital organic materials. *Journal of Geophysical Research-Oceans*. 107.

SMETACEK, V. and S. NICOL (2005) Polar ocean ecosystems in a changing world. *Nature*. 437: 362-368.

TAKAHASHI, T., S.C. SUTHERLAND, C. SWENEY, A. POISSON, N. METZL, B. TILBROOK, N. BATES, R. WANNINKHOF, R.A. FEELY, C. SABINE, J. OLAFSSON and Y. NOJIRI (2002) Global sea-air CO₂ flux based on climatological surface ocean pCO₂, and seasonal biological and temperature effects. *Deep-Sea Research Part II-Topical Studies in Oceanography*. 49: 1601-1622.

WEBB, D.J. and N. SUGINOHARA (1997) Vertical Mixing in the ocean. *Nature*. 409.

WILLIAMSON, C.E., P.J. NEALE, G. GRAD, H.J. DE LANGE and B.R. HARGREAVES (2001) Beneficial and detrimental effects of UV on aquatic organisms: Implications of spectral variation. *Ecological Applications*. 11: 1843-1857.

INTRODUCTION

SIGNIFICANCE OF ORGANIC MATTER IN THE OCEAN

The ocean is one of the major reservoirs of reactive carbon on the Earth. The organic carbon content of living marine organisms is about 2 Gt C, trivial compared with both seawater dissolved organic matter (DOM) and non-living particulate organic matter (POM) (Hedges and Oades, 1997). These non-living materials mostly constitute the waste products of the dynamic cycling between carbon fixation and consumption in the ocean. The dissolved organic matter (DOM) pool in the ocean is estimated to contain 685 Gt C, and represents the second largest reactive carbon pool after oceanic dissolved inorganic carbon, a value comparable to the mass of inorganic carbon in the atmosphere (Fig. i.1). Hence, small perturbations in the production or sink terms in the oceanic DOM pool would strongly impact the balance between oceanic and atmospheric CO₂. A net oxidation of only 1% of this DOM pool would generate a CO₂ flux larger than that produced annually by fossil fuel combustion (Hedges, 2002). DOM also has ecological significance as substrate for bacterioplankton. Global net primary production in the ocean is estimated to be around 50 Pg C y⁻¹ (Hedges, 1992; Field et al., 1998), 80% of which takes place in the open ocean, and around 20-40% of carbon fixed by phytoplankton is processed by bacterioplankton through the microbial loop (Azam et al., 1983). Bacterioplankton can regulate DOM composition through the selective consumption of labile compounds and subsequent release of humic-like (chromophoric) substances (Tranvik, 1993; Kawasaki and Benner, 2006) that

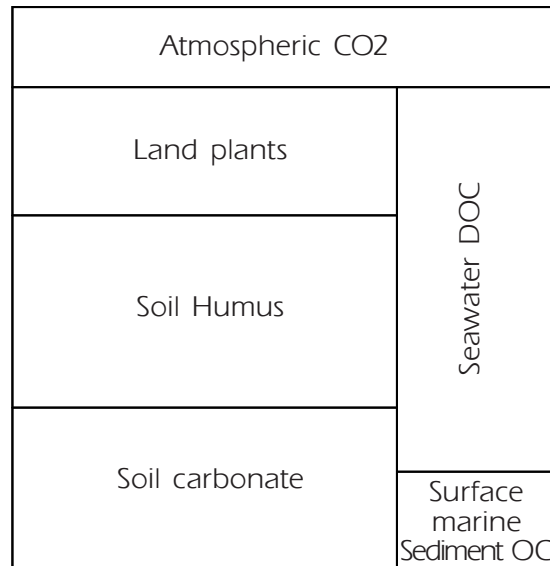


Figure i.1. Active atmospheric, land and ocean carbon reservoirs. Areas are proportional to carbon mass. Adapted from Hedges (1992).

appear to be refractory. The production of this material can comprise a significant proportion of total DOM pool extending the residence time of organic carbon in the water column with obvious consequences for carbon cycling (Brophy and Carlson, 1989; Ogawa et al., 2001). A net DOM accumulation has been observed in the ocean surface, ultimately due to the uncoupling of biological production and microbial consumption processes. About 1.2 Pg y⁻¹, corresponding to a 15-25% of new production, accumulates in surface waters and is available for export to the deep ocean before microbial utilization (Hansell and Carlson, 1998).

CLASSIFYING OCEAN ORGANIC MATTER

Traditionally, marine organic matter has been operationally divided into dissolved and particulate phases according to filtration procedures. Organic matter retained on filters that vary from 0.1 to 1 μm and made of different materials (polycarbonate, glassfiber, cellulose ester, etc) is considered “particulate”, whereas organic matter passing the filters is considered “dissolved”. This classification has ecological implications, as particulate organic carbon can sediment from surface to deep waters, while dissolved materials stay in the water column. The vast majority of the organic matter in the ocean (>97%) exists in the dissolved fraction (Sharp, 1973). The major fraction of DOM in the ocean water column, according

to ultrafiltration techniques, has low molecular weight (less than 1 kDa), accounting for about 65-80% of bulk DOM, while the high molecular weight DOM is a minor fraction (20-35% for >1 kDa and 2-7% of >10 kDa) and more abundant in the surface ocean.

However, organic matter in the ocean occurs as a size continuum of truly dissolved, colloidal and particulate phases (Sharp, 1973; Amon and Benner, 1994). It has been evidenced that dissolved colloids can spontaneously assemble forming polymer particles, reaching a reversible equilibrium with DOM pool (Chin et al., 1998). About a 10% of surface seawater DOM can be spontaneously assembled forming micro- and macrogels (Chin et al., 1998).

The classification of organic matter in size classes connects with other sorting criteria such as its age, reactivity, chemical composition, or optical properties. For instance, DOM of high molecular weight has been observed to have a contemporary origin (i.e. younger than a few decades) in contrast to an older and diagenetically altered DOM of low molecular weight (Santschi et al., 1995). DOM is also classified into at least three fractions according to its reactivity. Refractory DOM is the largest fraction (>90%, Ogawa and Tanoue, 2003) and it is dominated by compounds of low molecular weight with turnover on scales of centuries to millennia. Biologically labile DOM is composed by dissolved free molecules such as neutral monosaccharides or aminoacids. Their rapid turnover rates (from minutes to days) maintain these compounds at nanomolar concentrations in the open ocean (Keil and Kirchman, 1999; Skoog et al., 1999). Lastly, the semilabile fraction of DOM is reactive over months to years and it accumulates in surface waters (Carlson and Ducklow, 1995; Cherrier et al., 1996).

Several attempts have been done to characterize chemically DOM (e.g. C to N ratios). However, most DOM in the ocean remains uncharacterized (Williams and Druffel, 1987; Hedges et al., 2000). Indeed, the contribution of the major chemical constituents, i.e., amino acids, carbohydrates and lipids, may not exceed 30% of bulk DOM (Ogawa and Tanoue, 2003).

DOM has also been classified based on its optical properties (absorbance and fluorescence). The portion of the DOM that absorbs solar radiation is known as "gelbstoff", "gilvin", "yellow matter" or, more widely accepted, "chromophoric dissolved organic matter" (Nelson and Siegel, 2002).

Organic matter classes are interconnected within the size-reactivity continuum by formation, degradation and transformation processes driven by different physical and biological factors. In the present thesis, we will focus on the role of bacterioplankton and solar radiation.

BACTERIAL AND SUNLIGHT TRANSFORMATION OF DOM

Bacterioplankton are a central component of the ocean carbon cycle. These organisms are the main consumers of organic carbon in the ocean, and bacterial production represents a major pathway whereby DOM is converted into POM. But bacteria are not only consumers but also sources of organic matter through different mechanisms such as the direct release of different compounds, or due to viral lysis or grazing. Microbial processes are known to play a major role in generating refractory DOM from labile material or chromophoric dissolved organic matter from non-chromophoric compounds (Brophy and Carlson, 1989; Ogawa et al., 2001).

Solar radiation has a strong impact on carbon cycling. Apart from its obvious influence in primary productivity, many DOM transformations are initiated by the reaction with sunlight. For instance, photoreactions can alter DOM optical properties, molecular weight, or chemical composition. They can also fuel or short-circuit the microbial loop through the phototransformation of biorefractory compounds into labile or vice versa. In addition, DOM photoreactions can represent a direct sink of organic carbon through photomineralization into inorganic forms such as carbon monoxide or dioxide, a source of inorganic forms such as dimethyl sulfide or reactive oxygen species.

In this thesis I selected two major pools of non-living organic matter in the ocean: chromophoric dissolved organic matter and the fraction of the marine gel phase composed by transparent exopolymer particles.

CHROMOPHORIC DISSOLVED ORGANIC MATTER (CDOM)

Chromophoric DOM (CDOM) represents a variable fraction (from 20 to 70%) of total DOM formed by light-absorbing compounds (Coble, 2007).

The increasing interest in the study of CDOM in marine and freshwater systems is related to its role regulating the attenuation and quality of light available

for photosynthesis and other photoprocesses (Blough and deVecchio, 2002; Nelson and Siegel, 2002; Coble, 2007).

Light absorption of CDOM approximates to a negative exponential function throughout the UV and visible light spectra, hence showing maxima of absorbance at in the UV and blue portions (Bricaud et al., 1981). The slope parameter provides a measure of how rapidly the absorbance decreases when increasing wavelength (Bricaud et al., 1981).

CDOM controls the penetration of UVB, determining the water potential protection for organisms (Arrigo and Brown., 1996; Anderson et al., 2001; Williamson et al., 2001). CDOM is responsible of more than 50% of non-water attenuation at 443 nm (Nelson and Siegel, 2002; Siegel et al., 2002). Thus, it also controls the availability of photosynthetically active radiation (Kalle, 1966; Bricaud et al., 1981). This fact has an applied interest in the development of algorithms for chlorophyll *a* and primary productivity estimations from satellite measurements (Siegel et al., 2005). Finally, CDOM is essentially photoreactive. Sunlight reacts with chromophoric groups resulting in a variety of reactions that have a significant impact in the cycling of carbon and other elements (Kieber et al., 1989; Kieber et al., 1999; Mopper and Kieber, 2000; Toole et al., 2003; Coble, 2007).

Like the whole DOM pool in the ocean, CDOM is largely uncharacterized. CDOM has been traditionally linked to terrestrial humic and fulvic acids transported via rivers and runoff to the ocean, and would account for an unknown fraction of the background level of CDOM in the open sea (Nelson et al., 1998; Nelson and Siegel, 2002). However, terrestrial DOM is known to represent less than 5% of the total DOM in the open ocean (Opsahl and Benner, 1998). Hence, marine humic and fulvic acids mostly result from the reaction of fatty acids, sugars, amino acids and other small molecules released by phytoplankton (Harvey et al., 1983) that polymerize to form CDOM in the presence of UV radiation (Harvey et al., 1983) or mediated by microbial transformations (Nelson et al., 1998; Rochelle-Newall and Fisher, 2002). Among the non-humic components of marine CDOM are amino acid and peptides, nucleic acid and bases, urea, and other low molecular weight (LMW) compounds (Nelson and Siegel, 2002). To date, CDOM is frequently measured based in its optical properties (absorbance and fluorescence). The fact that marine DOM can emit a blue fluorescence when irradiated with UV light was recognized first by Kalle in 1949 and attributed to

CDOM. Since then, fluorescence techniques, both with single excitation or generating excitation-emission matrixes, are being used to provide useful information of CDOM chemical properties.

Due to the simplicity of the determination of CDOM absorbance spectra, some attempts have been done to use this measurement as an indicator of DOC concentration. However, co-variation between these two parameters appear to hold only in areas where mixing between rivers and seawater control distribution of both CDOM and DOC. In the open ocean, an uncoupling or even a near-inverse relationship between DOC and CDOM is observed both in temporal dynamics (Nelson et al., 1998) and in depth profiles (Hansell, 2002), reflecting that these two parameters are governed by different sources and sinks or are formed and recycled at different timescales.

Despite CDOM distribution and dynamics have been studied for decades, we are still far from achieving a complete knowledge about its chemical composition, production and removal processes.

MARINE GEL PHASE. TRANSPARENT EXOPOLYMER PARTICLES (TEP)

The marine gel phase covers the whole size continuum of organic matter, from colloidal (1 kDa) microgels to macroscopic particles (mm) (Fig. i.2).

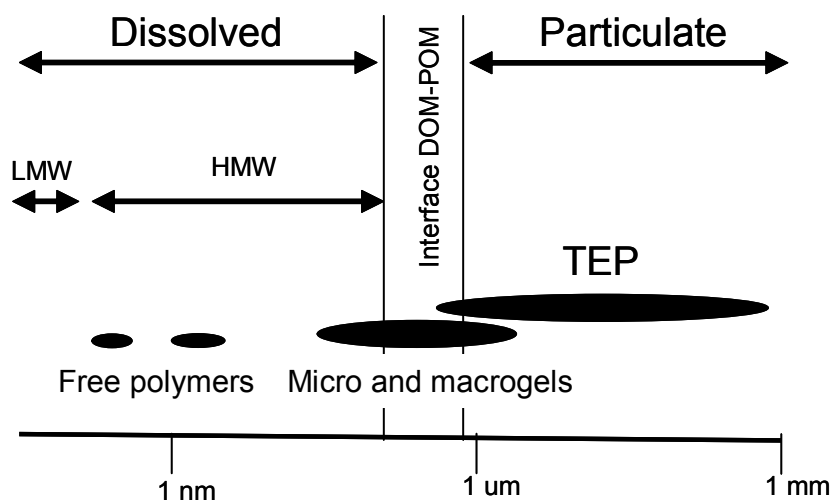


Figure i.2. Scheme of the different classes of organic matter along the size continuum. Adapted from Verdugo et al. (2004).

Within the size continuum from dissolved to particulate, TEP are large, sticky particles, formed by the spontaneous polymerization of dissolved precursors, mostly “acidic” polysaccharides (DPCHO) released by microorganisms (Alldredge et al., 1993; Passow and Alldredge, 1994; Passow, 2000). TEP are detected by staining with Alcian Blue, a cationic copper phthalocyanine dye that complexes carboxyl ($-\text{COO}^-$) and half-ester sulfate (OSO_3^-) reactive groups of acidic polysaccharides. The chemical composition of TEP is not exactly known. They are also a chemically diverse group of particles that may vary depending on their origin.

Due to their stickiness, TEP can act as the interstitial matrix to form larger aggregates of organic and inorganic compounds, known as marine snow, that sediment through the water column. Because TEP are formed directly from DOM, they represent a potentially highly significant pathway by which DOM can be transformed into POM and sequestered via sedimentation. Moreover, since TEP are essentially carbohydrate particles, their biogeochemistry should differ from organisms by an enrichment of carbon relative to the expected C:N:P ratio of 106:16:1 given by Redfield et al. (1963). Therefore, sedimentation of TEP may even lead to a selective export of carbon from surface to deep waters. However, owing to the low density of TEP, they can also ascend through the water column and accumulate in the surface (Azetsu-Scott and Passow, 2004; Mari, 2008) with significant implications for gas-exchange between the ocean and the atmosphere (Wurl and Holmes, 2008).

There is still insufficient information about TEP distribution in the ocean, and advances into an extended database on TEP in the global ocean, along with the understanding of their generation and losses processes, can give us insights on the ocean carbon cycle.

GENERAL OBJECTIVES

The main goals of this thesis were:

1. To describe the geographical and vertical distribution of chromophoric dissolved organic matter in three contrasting marine ecosystems, and to experimentally determine the CDOM photoreactivity (photobleaching and photohumification) and CDOM generated by organisms, evaluating their contribution to CDOM dynamics in the study systems.
2. To validate the algorithm Garver-Siegel-Maritorena (GSM01) for satellite estimations of CDM in the Antarctic Peninsula, and to study long-term dynamics of CDM in this area exploring the potential seasonal and non-seasonal drivers using remote sensing data.
3. To study the geographical and vertical distribution of transparent exopolymer particles (TEP) and dissolved carbohydrates (DMCHO, DPCHO) assessing their significance within the dissolved and particulate organic carbon pools, and to experimentally determine the role of bacterial TEP formation and UVB radiation affecting TEP dynamics.

In Fig. i.3 we show a conceptual scheme of the different approaches used to perform this study.

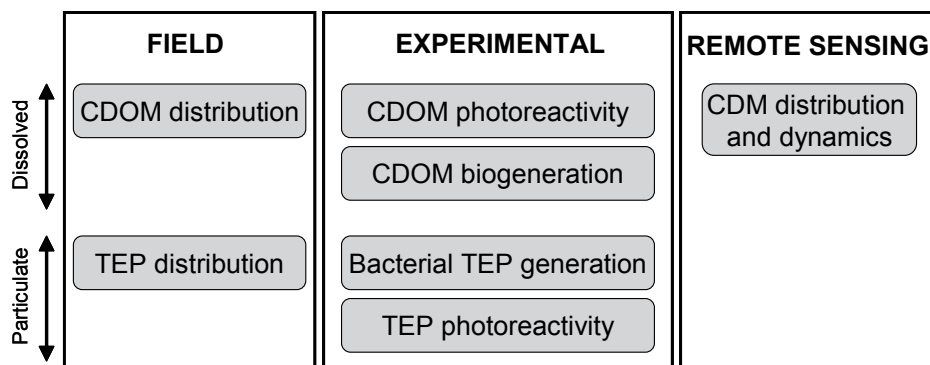


Figure i.3. Major objectives of the present thesis work.

REFERENCES

- ALLDREDGE, A.L., U. PASSOW and B.E. LOGAN (1993) The abundance and significance of a class of large, transparent organic particles in the ocean. *Deep-Sea Research Part I-Oceanographic Research Papers*. 40: 1131-1140.
- AMON, R.M.W. and R. BENNER (1994) Rapid cycling of high-molecular-weight dissolved organic matter in the ocean. *Nature*. 369 549-552.
- ANDERSON, S., R. ZEPP, J. MACHULA, D. SANTAVY, L. HANSEN and E. MUELLER (2001) Indicators of UV exposure in corals and their relevance to global climate change and coral bleaching. *Human and Ecological Risk Assessment*. 7: 1271-1282.
- ARRIGO, K.R. and C.W. BROWN. (1996) Impact of chromophoric dissolved organic matter on UV inhibition of primary productivity in the sea. *Marine Ecology-Progress Series*. 140: 207-216.
- AZAM, F., T. FENCHEL, J.G. FIELD, J.S. GRAY, L.A. MEYERREIL and F. THINGSTAD (1983) The ecological role of water-column microbes in the sea. *Marine Ecology-Progress Series*. 10: 257-263.
- AZETSU-SCOTT, K. and U. PASSOW (2004) Ascending marine particles: Significance of transparent exopolymer particles (TEP) in the upper ocean. *Limnology and Oceanography*. 49: 741-748.
- BLOUGH, N.V. and R. DELVECCHIO (2002) Chromophoric DOM in the coastal environment. *In*: D. A. Hansell and C. A. Carlson (eds.) *Biogeochemistry of Marine Dissolved Organic Matter*. Academic Press, San Diego. pp. 547- 578.
- BRICAUD, A., A. MOREL and L. PRIEUR (1981) Absorption by dissolved organic matter of the sea (yellow substance) in the UV and visible domains. *Limnology and Oceanography*. 26: 43-53.
- BROPHY, J.E. and D.J. CARLSON (1989) Production of biologically refractory dissolved organic carbon by natural seawater microbial populations. *Deep-Sea Research A: Oceanographic research papers*. 36: 497-507.
- CARLSON, C.A. and H.W. DUCKLOW (1995) Dissolved organic carbon in the upper ocean of the central equatorial Pacific Ocean, 1992 - daily and finescale vertical variations. *Deep-Sea Research Part II-Topical Studies in Oceanography*. 42: 639-656.
- CHERRIER, J., J.E. BAUER and E.R.M. DRUFFEL (1996) Utilization and turnover of labile dissolved organic matter by bacterial heterotrophs in eastern north

- Pacific surface waters. *Marine Ecology-Progress Series*. 139: 267-279.
- CHIN, W.C., M.V. ORELLANA and P. VERDUGO (1998) Spontaneous assembly of marine dissolved organic matter into polymer gels. *Nature*. 391: 568-572.
- COBLE, P.G. (2007) Marine optical biogeochemistry: The chemistry of ocean color. *Chemical Reviews*. 107: 402-418.
- FIELD, C.B., M.J. BEHRENFELD, J.T. RANDERSON and P. FALKOWSKI (1998) Primary production of the biosphere: integrating terrestrial and oceanic components. *Science*. 281: 237-240.
- HANSELL, D.A. (2002) DOC in the Global Ocean Carbon Cycle *In*: D. A. Hansell and C. A. Carlson (eds.) *Biogeochemistry of marine dissolved organic matter*. Academic Press, San Diego.
- HANSELL, D.A. and C.A. CARLSON (1998) Net community production of dissolved organic carbon. *Global Biogeochemical Cycles*. 12: 443-453.
- HARVEY, G.R., D.A. BORAN, L.A. CHESAL and J.M. TOKAR (1983) The structure of marine fulvic and humic acids. *Marine Chemistry*. 12: 119-132.
- HEDGES, J.I. (1992) Global biogeochemical cycles: progress and problems. *Marine Chemistry*. 39: 67-93.
- HEDGES, J.I. (2002) Why dissolved organic matter? *In*: D. A. Hansell and C. A. Carlson (eds.) *Biogeochemistry of marine dissolved organic matter*. Academic Press, San Diego, California.
- HEDGES, J.I., G. EGLINTON, P.G. HATCHER, D.L. KIRCHMAN, C. ARNOSTI, S. DERENNE, R.P. EVERSLED, I. KOGEL-KNABNER, J.W. DE LEEUW, R. LITCKE, W. MICHAELIS and J. RULLKOTTER (2000) The molecularly-uncharacterized component of nonliving organic matter in natural environments. *Organic Geochemistry*. 31: 945-958.
- HEDGES, J.I. and J.M. OADES (1997) Comparative organic geochemistries of soils and marine sediments. *Organic Geochemistry*. 27: 319-361.
- KALLE, K. (1966) The problem of gelbstoff in the Sea. *Oceanography and Marine Biology: Annual Reviews*. 4: 91-104.
- KAWASAKI, N. and R. BENNER (2006) Bacterial release of dissolved organic matter during cell growth and decline: Molecular origin and composition. *Limnology and Oceanography*. 51: 2170-2180.
- KEIL, R.G. and D.L. KIRCHMAN (1999) Utilization of dissolved protein and amino acids in the northern Sargasso Sea. *Aquatic Microbial Ecology*. 18: 293-300.

- KIEBER, D.J., J. MCDANIEL and K. MOPPER (1989) Photochemical source of biological substrates in seawater: implications for carbon cycling. *Nature*. 341: 637-639.
- KIEBER, R.J., A. LI and P.J. SEATON (1999) Production of nitrite from the photodegradation of dissolved organic matter in natural waters. *Environmental Science & Technology*. 33: 993-998.
- MARI, X. (2008) Does ocean acidification induce an upward flux of marine aggregates? *Biogeosciences* 5: 1023-1031.
- MOPPER, K. and D.J. KIEBER (2000) Marine photochemistry and its impact on carbon cycling *In*: S. d. Mora, S. Demers and M. Vernet (eds.) *The Effects of UV Radiation in the Marine Environment*, vol. 10. Cambridge University Press, Cambridge. pp. 101-129.
- NELSON, N.B. and D.A. SIEGEL (2002) Chromophoric DOM in the open ocean. *In*: D. A. Hansell and C. A. Carlson (eds.) *Biogeochemistry of marine dissolved organic matter*. Academic Press, San Diego.
- NELSON, N.B., D.A. SIEGEL and A.F. MICHAELS (1998) Seasonal dynamics of colored dissolved material in the Sargasso Sea. *Deep-Sea Research Part I-Oceanographic Research Papers*. 45: 931-957.
- OGAWA, H., Y. AMAGAI, I. KOIKE, K. KAISER and R. BENNER (2001) Production of refractory dissolved organic matter by bacteria. *Science*. 292: 917-920.
- OGAWA, H. and E. TANOUE (2003) Dissolved organic matter in oceanic waters. *Journal of Oceanography*. 59: 129-147.
- OPSAHL, S. and R. BENNER (1998) Photochemical reactivity of dissolved lignin in river and ocean waters. *Limnology and Oceanography*. 43: 1297-1304.
- PASSOW, U. (2000) Formation of transparent exopolymer particles, TEP, from dissolved precursor material. *Marine Ecology-Progress Series*. 192: 1-11.
- PASSOW, U. and A.L. ALLDREDGE (1994) Distribution, size and bacterial-colonization of transparent exopolymer particles (TEP) in the ocean. *Marine Ecology-Progress Series*. 113: 185-198.
- ROCHELLE-NEWALL, E.J. and T.R. FISHER (2002) Production of chromophoric dissolved organic matter fluorescence in marine and estuarine environments: an investigation into the role of phytoplankton. *Marine Chemistry*. 77: 7-21.
- SANTSCHI, P.H., L.D. GUO, M. BASKARAN, S. TRUMBORE, J. SOUTHON, T.S. BIANCHI, B. HONEYMAN and L. CIFUENTES (1995) Isotopic evidence for the contemporary origin of high molecular weight organic matter in oceanic envi-

- ronments. *Geochimica et Cosmochimica Acta*. 59: 625-631.
- SHARP, J.H. (1973) Size classes of organic carbon in seawater. *Limnology and Oceanography*. 18: 441-447.
- SIEGEL, D.A., S. MARITORENA and N.B. NELSON (2005) Independence and interdependencies among global ocean color properties: Reassessing the bio-optical assumption. *Journal of Geophysical Research-Oceans*. 110.
- SIEGEL, D.A., S. MARITORENA, N.B. NELSON, D.A. HANSELL and M. LORENZIKAYSER (2002) Global distribution and dynamics of colored dissolved and detrital organic materials. *Journal of Geophysical Research-Oceans*. 107.
- SKOOG, A., B. BIDDANDA and R. BENNER (1999) Bacterial utilization of dissolved glucose in the upper water column of the Gulf of Mexico. *Limnology and Oceanography*. 44: 1625-1633.
- TOOLE, D.A., D.J. KIEBER, R.P. KIENE, D.A. SIEGEL and N.B. NELSON (2003) Photolysis and the dimethylsulfide (DMS) summer paradox in the Sargasso Sea. *Limnology and Oceanography*. 48: 1088-1100.
- TRANVIK, L.J. (1993) Microbial transformations of labile organic matter into humic-like matter in seawater. *FEMS Microbiology Ecology*. 12: 177-183.
- VERDUGO, P., A.L. ALLDREDGE, F. AZAM, D.L. KIRCHMAN, U. PASSOW and P.H. SANTSCHI (2004) The oceanic gel phase: a bridge in the DOM-POM continuum. *Marine Chemistry*. 92: 67-85.
- WILLIAMS, P.M. and E.R.M. DRUFFEL (1987) Radiocarbon in dissolved organic matter in the central North Pacific Ocean. *Nature*. 330: 246-248.
- WILLIAMSON, C.E., P.J. NEALE, G. GRAD, H.J. DE LANGE and B.R. HARGREAVES (2001) Beneficial and detrimental effects of UV on aquatic organisms: Implications of spectral variation. *Ecological Applications*. 11: 1843-1857.
- WURL, O. and M. HOLMES (2008) The gelatinous nature of the sea-surface microlayer. *Marine Chemistry*. 110: 89-97.

MATERIAL AND METHODS

1. STUDY SITE CHARACTERIZATION

· Southern Ocean

The Southern Ocean ecosystem is characterized by an extreme seasonal variability in incident solar radiation, low temperatures, and the influence of the annual advance and retreat of sea ice (Smetacek and Nicol, 2005; Ducklow et al., 2007). Despite it represents only about a 10% of the total ocean surface, its global impact on water mass circulation and carbon cycling is very significant. On one hand, the Southern Ocean redistributes nutrients around the global ocean through nutrient-rich deep water formation and subsequent meridional transfer as Antarctic Bottom water, returning these nutrients to intermediate and surface waters of lower latitudes (Webb and Suginozara, 1997). On the other hand, its cold waters represent a significant sink of anthropogenic CO₂ (Sarmiento et al., 1998; Takahashi et al., 2002), although this process has been recently controversial (Caldeira and Duffy, 2000; Gurney et al., 2002).

Specifically, the Antarctic Peninsula is one of the most vulnerable areas to global warming, where air surface temperature trends reveal a warming rate (around 5°C during the last 50 years) that exceeds any other observed globally (Vaughan et al., 2003). In addition, a significant decrease in the ice extent has also been evidenced (Oppenheimer, 1998; Smith and Stammerjohn, 2001).

The Antarctic Peninsula is located in the Pacific sector of the Southern Ocean, between 58° and 70° S and between 80 and 50° W, with relatively warm and low saline waters from the Eastern Bellingshausen Sea to cold and saline waters from Western Weddell Sea that confluence in the Bransfield and Gerlache straits (between the coastal Peninsula and South Shetland Islands). As the whole Southern Ocean, the Antarctic Peninsula is generally enriched in macronutrients (nitrate and phosphate) as a result of three main factors: high nutrient concentrations in deep water, deep winter mixing, and micronutrient limitation (particularly iron) that prevents nutrient depletion. Nitrate concentration from 23 to 36 μM and phosphate concentrations from 1.8 to 2.7 μM have been measured in different areas of the Antarctic Peninsula (Serebrennikova and Fanning, 2004). The Southern Ocean is considered as one of the largest high nutrient-low chlorophyll (HNLC) areas, that is, relatively low algal biomass is found despite high nitrate and phosphate availability (Minas et al., 1986). This phytoplankton constrain is most probably due to limitation by light (Mitchell et al., 1991) or micronutrients such as iron (Martin et al., 1990; de Baar et al., 1995). By contrast, the coastal zone of the Antarctic Peninsula, where water is enriched with iron from land contact or from upwelling along shelves and continental slopes, supports high biological richness and productivity. In coastal waters off Palmer station (Anvers Island), primary production ranges from 47 to 351 $\text{gC m}^{-2} \text{y}^{-1}$ (mean value 176 $\text{gC m}^{-2} \text{y}^{-1}$), and from 219 $\text{gC m}^{-2} \text{y}^{-1}$ in the continental shelf of Antarctic Peninsula to a range between 37 and 110 $\text{gC m}^{-2} \text{y}^{-1}$ in oceanic Antarctic waters, and it is worth to note that, in contrast to lower latitude oceans, this productivity is achieved only during the ice-free period (Huntley et al., 1991). The ice-retreat period starts by September and it extends until the end of March-April, and the distributions and dynamics of biological communities are closely linked to the dynamics of ice sheets (Dierssen et al., 2002; Constable et al., 2003). While zooplankton communities, particularly Antarctic krill *Euphasia superba*, graze on algal communities associated to ice during winter (Nicol, 2006), the seasonal ice melting, which supplies iron and other nutrients to the water surface, creates a stable surface layer (Smith and Nelson, 1985), that usually supports dense ice-edge phytoplankton blooms with associated bacteria.

· Mediterranean Sea

The Mediterranean Sea is a semi-enclosed sea surrounded by Europe, Africa and Asia, with a surface of $2.5 \times 10^6 \text{ km}^2$ and mean depth of 1500 m. It repre-

sents 0.7% of the ocean surface and 0.3% of the ocean volume. Despite its small volume, it supports thermohaline circulation and dense water formation processes which can be representative of a real ocean for circulation climatological studies (Bethoux et al., 1999). The main input of water to the Mediterranean Sea comes from the surface water from the Atlantic Ocean, depleted in nutrients, which flows into the Mediterranean Sea through the strait of Gibraltar compensating the outflow of nutrient-enriched Mediterranean deep waters. In addition to the inputs from the Atlantic Ocean, the phosphorus, nitrogen, and silica inputs to the semi-enclosed Mediterranean come from continental weathering and wet and dry atmospheric deposition. All these inputs, however, do not prevent the oligotrophic status of this ecosystem. In addition, contrasting to the general consideration that nitrogen is the primary limiting nutrient in the ocean (Tyrrell and Law, 1997), the Mediterranean Sea appears to be limited by phosphorus, being this limitation particularly accurate in the easternmost basin (Thingstad et al., 2005). The phosphorus limitation is well evidenced by a nitrate (N) vs. phosphate (P) ratio of about 22 (McGill, 1963), compared to about 16 for the world's oceans (Redfield, Ketchum & Richards, 1963). This ratio also increases from western to eastern basins of the Mediterranean Sea, ranging from 16 to 22 in the Western Mediterranean (Bethoux et al. 1998) to around 24 to 29 in the Eastern Mediterranean (Krom et al. 1991). This limitation can be explained by fast N fixation rates (Bethoux and Copinmontegut, 1986) or selective phosphate precipitation due to inputs of iron-containing dust from the Sahara (Krom et al. 1991), and limits both primary production (Bonin et al., 1989; Zohary and Robarts, 1998; Psarra et al., 2005) and bacteria (Sala et al., 2002; Pinhassi et al., 2006). The systems exhibits primary productivity ranging from 86-232 gC m⁻² y⁻¹ in the Northwestern Mediterranean (Marty and Chiaverini, 2002) to 59-80 gC m⁻² y⁻¹ in the Eastern Mediterranean (Psarra et al., 2000).

· North Sea

The North Sea (NS) is a large, shallow, semi-enclosed sea, limited by the Scandinavian straits Skagerrak and Kattegat in the East, and the English Channel in the West, and with a mean depth of 90m. The sea opens to the Atlantic Ocean in the North but the most significant inputs are received from rivers and from the Baltic Sea. (Ducrotoy et al., 2000). In the last years, the high anthropogenic pressure has caused detrimental effects on the North Sea ecosystems, such as eutrophication or accumulation of toxic substances (Joint and Pomroy, 1993).

The Eastern coastal area of the North Sea (German and Danish bights, from 53° N to 57°N and from 6° E to 9° E (ICES, 1983), with a mean depth of 30m), is particularly influenced by river discharge, with freshwater inputs of 32 km³ y⁻¹ (Ducrottoy et al., 2000) specially from Elbe and Weser rivers. Temperature in this area ranges from around 5°C during winter to 15°C during summer, with salinity values around 29 ‰ and nutrient concentration show averages from 10 to 40 μM of nitrate and from 0.1 to 1 μM of phosphate (Raabe et al., 1997; Radach, 1998). In this area, the primary productivity shows a mean value of 261 gC m⁻² y⁻¹ (Joint and Pomroy, 1993), with > 8 μg l⁻¹ of chl *a* near spring (Joint and Pomroy, 1993).

2. SAMPLING PROTOCOLS

Sampling in the Antarctic Peninsula was carried out during late spring and summer 2004 and 2005 in the two ICEPOS oceanographic cruises. The first cruise took place from January 14th to February 9th 2004 aboard R/V 'Las Palmas' and 12 stations were selected with 4-5 depths each, from surface waters to 150m (Fig. m.1). These stations covered three transects, from Livingston Island to (I) Decep-

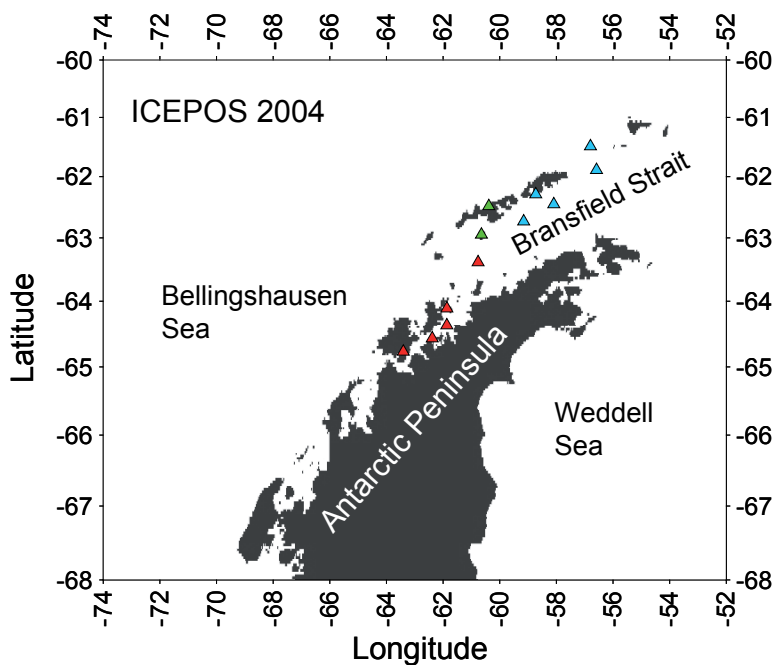


Figure m.1. Location of the stations sampled during ICEPOS 2004 cruise. The three transects from Livingston Island are represented using different symbols. Green: Transect to Deception Island. Red: Transect to Anvers Island. Blue: Transect to King George Island.

Table m.1. Physical and biological parameters (average and ranges) for the study area in the Southern Ocean during ICEPOS 2004 merging all data (total) or separated in geographical areas (Deception Island and transits to Anvers and King George Islands) or depths (upper mixed layer (UML) or below mixed layer (BML)). bdl= below detection limit. na= not analyzed.

Variable	Total (*)			Deception			Anvers			King George		
	Total (*)	UML	BML	UML	BML	UML	BML	UML	BML	UML	BML	
Temperature (°C)	1.02 (-1.02-2.18)	1.33 (0.89-2.18)	0.01 (-1.02-0.81)	1.27 (0.93-1.65)	-0.19	1.42 (0.92-2.18)	0.47 (0.11-0.81)	1.23 (0.89-1.48)	-0.58 (-1.02-0.47)			
Salinity (PSU)	34.0 (33.6-34.7)	34.0 (33.6-34.7)	34.3 (34.1-34.4)	33.9	34.1	33.9 (33.6-34.0)	34.3 (34.1-34.4)	34.1 (34.0-34.7)	34.3 (34.2-34.4)			
DOC (µM)	68 (43-108)	70 (43-108)	57 (44-107)	60 (55-69)	49 (49-50)	72 (44-107)	58 (47-107)	68 (43-108)	55 (44-81)			
Chl a (µg l ⁻¹)	0.63 (bdl-1.13)	0.73 (0.38-1.13)	0.18 (bdl-0.45)	5.92 (5.04-7.18)	0.71 (0.42-1.00)	0.61 (0.38-0.99)	0.30 (0.04-0.45)	0.84 (0.52-1.13)	0.08 (bdl-0.31)			
BA (x10 ⁵ cell ml ⁻¹)	3.1 (1.03-6.13)	3.39 (1.60-6.13)	1.72 (1.03-2.64)	8.57 (8.00-8.95)	na	3.14 (2.28-4.60)	1.87 (1.32-2.50)	3.58 (1.60-6.13)	1.56 (1.03-2.64)			

(*) Excluding data from DI

tion Island, (2) Anvers Island, and (3) King George Island. In the first transect, two stations were sampled, inside Port Foster in Deception Island (a semi-enclosed bay with high surface chl *a* concentration (Table m.1), and in coastal waters near Livingstone Island. The stations located in the transits to Anvers Island and to King George Island showed, respectively, warmer and less saline waters (likely influenced by Bellingshausen Sea) and colder and more saline waters (likely influenced by Weddell Sea).

The second cruise took place aboard R/V 'Hespérides' from January 26th to February 26th, 2005. We selected 18 stations along the eastern Bellingshausen Sea, Bransfield and Gerlache straits and the Western Weddell Sea (Fig. m.2). At each station, 5-6 depths were sampled, from surface waters to below deep chlorophyll maximum (DCM). The stations located in Bellingshausen Sea (stations #1-7) were characterized by shallow mixed layers (from 20 to 50m) and increases in temperature below the mixed layer depth. The stations located in Antarctic Strait and Weddell Sea (stations #8-12, hereafter referred as Weddell Sea stations) were characterized by colder and more saline waters, mixed vertical profiles, and high chl *a* concentration (Table m.2). In addition, surrounding ice platelets were

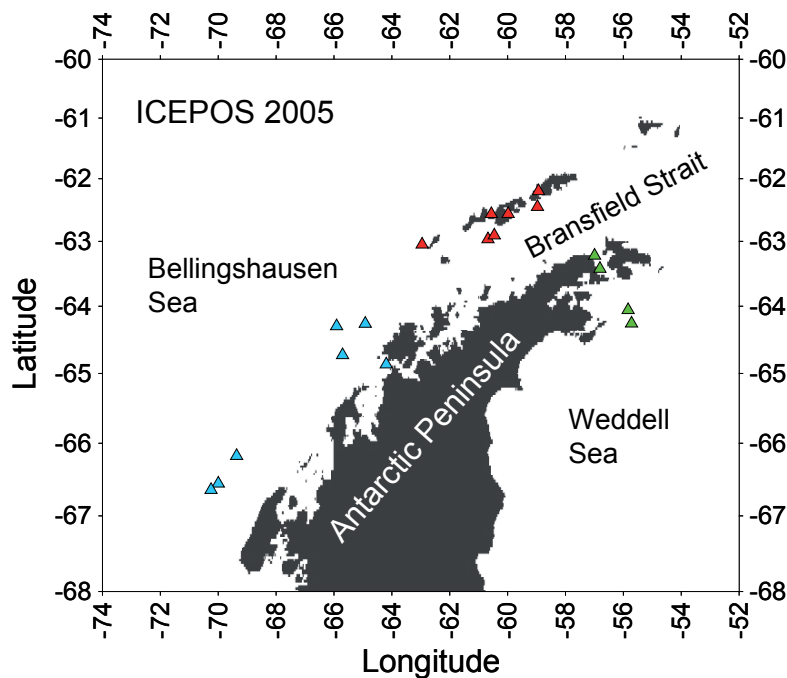


Figure m.2. Location of the stations sampled during ICEPOS 2005 cruise. The three study areas are represented using different colors. Blue: Bellingshausen Sea stations. Green: Weddell Sea stations. Red: Bransfield Strait stations.

Table m.2. Physical and biological parameters (average and ranges) for the study area in the Southern Ocean ICEPOS 2005 merging all data (total) or separated in geographical areas (Bellingshausen Sea, Weddell Sea and Bransfield Strait) or depths (upper mixed layer (UML) or below mixed layer (BML)).

Variable	Total		Bellingshausen Sea		Weddell Sea		Bransfield Strait	
	Total	UML	BML	UML	BML	UML	BML	UML
Temperature (°C)	0.45 (-1.57-1.56)	0.58 (-1.09-1.56)	0.24 (-1.57-1.30)	1.27 (0.77-1.51)	-0.09 (-1.57-1.30)	-0.70 (-1.09--1.48)	1.41 (1.29-1.56)	0.78 (0.33-1.29)
Salinity (‰)	34.0 (33.2-34.6)	34.0 (33.2-34.5)	34.1 (33.7-34.6)	33.5 (33.2-33.8)	34.1 (33.2-34.5)	34.3 (33.9-34.5)	33.9 (33.8-34.0)	34.1 (33.9-34.4)
DOC (µM)	55 (44-75)	56 (49-75)	54 (44-67)	54 (45-62)	52 (44-58)	57 (49-77)	56 (48-65)	56 (47-67)
Chl <i>a</i> (µg l ⁻¹)	1.55 (0.01-5.36)	2.15 (0.25-5.36)	0.54 (0.01-2.24)	1.21 (0.55-2.19)	0.29 (0.01-1.27)	1.98 (0.25-4.71)	2.95 (0.99-5.36)	0.91 (0.10-2.24)
BA (x10 ⁵ cell ml ⁻¹)	7.15 (0.57-17.6)	8.66 (1.55-17.6)	4.84 (0.57-13.9)	6.13 (1.55-16.2)	3.41 (0.57-7.78)	7.99 (3.45-16.6)	12.25 (5.78-17.6)	8.35 (5.04-13.9)
BP (ng C l ⁻¹ h ⁻¹)	30.8 (0.16-218)	41.9 (2.0-218)	12.06 (0.16-12.39)	26.8 (2.0-55.0)	8.45 (0.16-46.1)	55.7 (8.27-218)	36.20 (16.3-51.4)	17.55 (3.90-9.67)



Image m.3.

present in these waters (see image m.1). Finally, the stations situated along the Bransfield strait showed higher variability characterized by a deeper mixed layer (from 70 to 100m), or homogeneous profiles in stations #13 (in the coast of King George Island) and #15 (inside Foster Bay in Deception Island). Values of physical and biological variables in the study area are shown in Table m.2.

Water was collected using a Niskin bottle with external spring (12 l) during ICEPOS 2004 and a Sea Bird™ rosette sampler (24 Niskin bottles, 12 l each) attached to a conductivity-temperature-depth (CTD) system during ICEPOS 2005. Samples were taken for chromophoric dissolved organic matter (CDOM) characterization, transparent exopolymer particles (TEP), dissolved mono- and polysaccharides (DMCHO and DPCHO), and dissolved organic carbon (DOC) concentration, chlorophyll *a* (chl *a*), bacterial abundance (BA) and bacterial production (BP).

Data were analyzed merged or separated according to geographical areas or depths. The areas were separated as described above (3 areas during ICEPOS 2004 and 3 areas during ICEPOS 2005). Waters were also separated according to depth criteria in waters within and below the upper mixed layer. The mixed layer depth (MLD) was estimated considering a gradient of temperature higher than $0.1\text{ }^{\circ}\text{C m}^{-1}$ after visualizing vertical temperature profiles obtained with the CTD system.

Sampling in the Mediterranean Sea was performed during May 2007, in the context of Thresholds research project, aboard the Spanish R/V 'García del Cid'. A total of 24 sampling stations were conducted within a transit from Barcelona to Alexandria (Fig m.3). In this case, discrete geographical areas were not differentiated. The vertical profiles showed a similar pattern in all stations, with generally shallow mixed layers (between 4m in stations # 14 and 15, to 29 m in station # 6) and variable deep chlorophyll maximum (DCM). The DCM was situated below the upper mixed layer, and ranged from 40-50m in the Western Mediterranean, to 140 m in the Eastern Mediterranean, close to Alexandria.

Data were not separated by geographical areas. However, data were separated in three subsets, corresponding to waters within the upper mixed layer, data below the upper mixed layer but within the euphotic layer, and data below the euphotic layer. The MLD was calculated following the same criteria as for SO

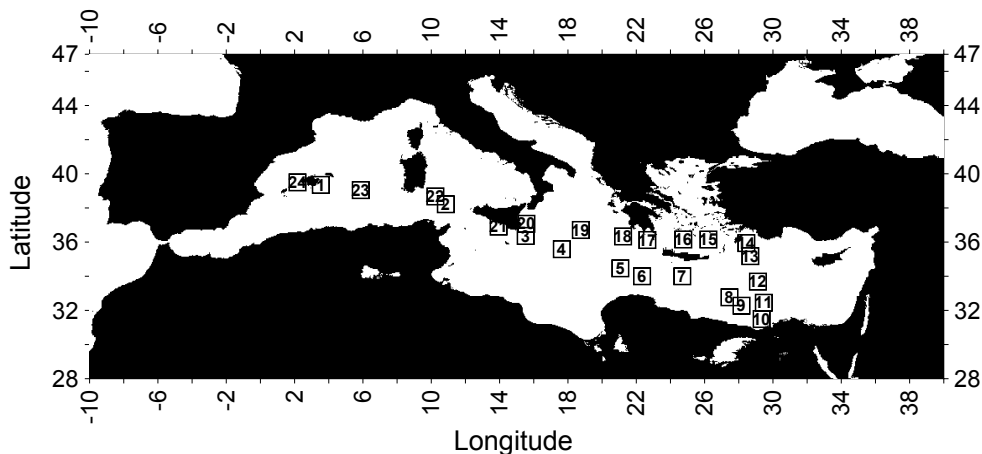


Figure m.3. Location of the stations sampled during Thresholds II cruise in the Mediterranean Sea.

Table m.3. Physical and biological parameters (Average and ranges) in the Mediterranean Sea during Thresholds II merging all data (total) or separated in or depths (upper mixed layer (UML), below mixed layer (BML) but within the euphotic layer and below euphotic layer. bdl= below detection limit.

Variable	Total	UML	BML Euphotic	Below Euphotic
Temperature	16.6 (13.2-21.6)	19.4 (17.6-21.6)	16.4 (13.9-19.6)	15.2 (13.2-16.9)
Salinity (PSU)	38.6 (37.2-39.5)	38.4 (37.1-39.3)	38.6 (37.2-39.5)	38.8 (37.9-39.2)
DOC (μM)	78 (43-142)	86 (64-123)	80 (58-142)	70 (43-129)
Chl <i>a</i> ($\mu\text{g l}^{-1}$)	0.16 (bdl-1.78)	0.07 (0.03-0.13)	0.28 (0.02-1.78)	0.06 (bdl-0.31)
BA ($\times 10^5$ cell ml^{-1})	5.04 (0.54-15.7)	4.92 (0.53-12.4)	6.29 (3.20-15.7)	3.42 (0.76-7.88)
BP ($\text{ng C l}^{-1} \text{ h}^{-1}$)	12.1 (0.28-60.9)	14.3 (1.63-26.3)	16.9 (3.32-60.9)	4.11 (0.28-8.55)

samples, and the euphotic layer depth was estimated as that receiving 1% of photosynthetically active radiation and was situated between 50 and 140 m.

Six representative depths from surface to 200m, including the deep chlorophyll maximum (DCM) were chosen, and water was collected using a Sea Bird™ rosette sampler (12 Niskin bottles, 12 liter each) attached to a CTD system. Samples were taken for CDOM, TEP, DMCHO, DPCHO, DOC, chl *a*, BA and BP.

Sampling in the North Sea was carried out during a transit from Helgoland (Island located at the German bight at 70km north to the main land, 54° 10N, 7° 53E) to Bremerhaven (53° 32N, 8° 34 E), North Germany, aboard the R/V 'Utörn' in September 30th 2005 (Fig i.4). Vertical profiles were sampled using a Niskin bottle (5 depths from 0 to 35 m for st #1, 3 depths from 5 to 15 m for st #2). Water was collected in clean 10 liter plastic carboys for further processing, within hours, in the Alfred Wegener Institute laboratory.

Samples were taken for CDOM, TEP, DMCHO, DPCHO, DOC and BA. DOC concentration showed a mean value of 139 μM and BA averaged 11.7×10^5 cell ml^{-1} . Temperature and salinity data, as well as chl *a*, was not determined in these stations.

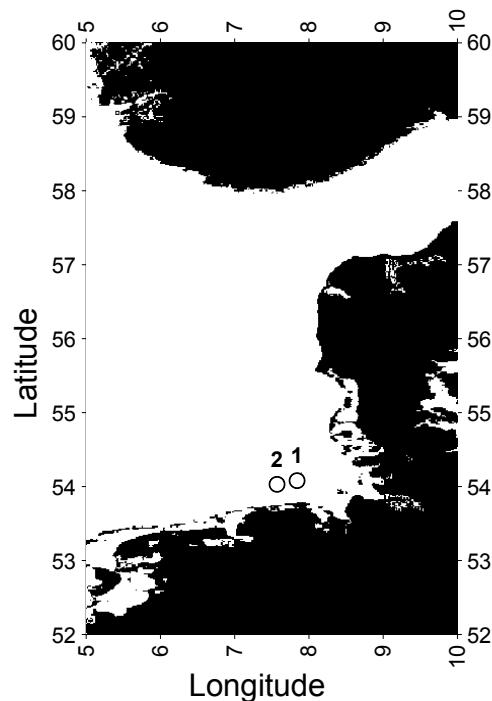


Figure m.4. Location of the stations sampled in the German Bight of the North Sea.

3. CHEMICAL AND BIOLOGICAL ANALYSES

· Chromophoric dissolved organic matter (CDOM)

CDOM optical characterization was analyzed by direct measurements of filtered water absorption. Samples were filtered by pre-combusted (450°C, > 3hours) glass-fiber filters (Whatman GF/F, nominal pore size 0.7 µm) and stored in sterile polypropylene flasks at 4°C in the dark until analysis (within hours to days). For Southern Ocean and Mediterranean Sea samples, MilliQ water was filtered and stored in parallel.

The filtrates were measured in 10-cm quartz cuvettes using a Shimadzu UV-2401 PC spectrophotometer (Southern Ocean and Mediterranean Sea samples) and a Varian Cary-Win 4000 UV-Vis spectrophotometer (North Sea samples). Absorbance scans from 200 or 250 to 700 nm were performed at 1nm intervals, a baseline with MilliQ water (North Sea samples) or MilliQ water filtered and treated as a sample (Southern Ocean and Mediterranean Sea samples) was subtracted, and the internal backscattering was corrected by subtracting the absorbance at a long wavelength (700 nm). The measurements of filtered MilliQ water showed detectable absorbance (0.011 absorbance units at 325 nm and 0.007 absorbance units at 443 nm).

Two reference wavelengths (325nm and 443 nm) were used to express as Napierian absorption coefficients (a_{325} and a_{443}) in m^{-1} using the following equation (Miller 1998):

$$a_{325,443} = \frac{2.303A_{325,443}}{l}$$

where l is the optical path length in m. We selected 325 nm as a representative wavelength within the UVA spectrum (Nelson and Siegel, 2002), and 443 nm was selected to be comparable to satellite measurements.

Molar absorption coefficients, surrogate of CDOM quality, were calculated dividing the absorption coefficients at 325 nm and 443 nm by the DOC concentration in mM.

The spectral slopes (S_{uv}) were calculated by a standard linear regression of the ln-transformed data from 290 nm to 400nm (Green and Blough, 1994). These measurements which showed values below the detection limit in wavelengths within the selected visible range were discarded.

· Transparent Exopolymer Particles (TEP)

TEP concentrations were determined using the colorimetric method proposed by Passow and Alldredge (1995). TEP are stained with Alcian Blue (copper-phthalocyanin with four methylene-tetramethylcisonium chloride side chains), a hydrophilic cationic dye that complexes with anionic carboxyl or half ester-sulfate groups of “acidic” polysaccharides.

TEP were analyzed in fresh (Mediterranean and North Seas) or fixed (Southern Ocean) samples. Fixation was performed with 0.2 filtered formalin (1% final concentration), and fixed samples were stored in 250 ml polyethylene flasks the dark until analysis.

Samples (200-250 ml for natural samples, 20-100 ml for experiments, were filtered onto polycarbonate filters (0.4 μm , 25mm \varnothing , Millipore for Southern Ocean samples, Poretics for Mediterranean and North Seas samples). Filters were subsequently stained with 0.5 ml of a 0.02% solution of Alcian Blue (Sigma) in 0.06% acetic acid, left stain for a few seconds, and rinsed with milliQ water to eliminate excess dye. Stained filters were then frozen at -20°C until extraction.

To perform the extraction, filters were unfrozen and placed in clean 20 ml glass or polypropylene flasks, and 5 ml of 80% sulfuric acid was added. Filters were let extract for 2-3 hours, shaking 2-3 times to enhance extraction, and, finally, absorbance was read at 787nm in 1 cm disposable cuvettes. Replicate or triplicate filter blanks were also analyzed in every batch of samples using empty stained filters.

The alcian blue solution was calibrated using Xantan Gum (XG), and TEP were expressed in $\mu\text{g XG eq l}^{-1}$. Four to 5 known volumes of the XG solution were filtered onto pre-weighted polycarbonate filters and weighted again to determine the exact concentration of the XG solution. Another similar set of filters

were stained and analyzed as described above to get the correspondence between weight and absorption. The calibration factor (f_x) was calculated according to this expression:

$$f_x = W[(est_{787} - C_{787}) \times V_{st}^{-1}]^{-1}$$

where W is the concentration of the XG solution ($\mu\text{g l}^{-1}$), est_{787} is the absorption of the extract at 787nm, C_{787} is the absorption of the blank, and V_{st} is the filtered volume (l). TEP concentration was expressed in $\mu\text{g Gum Xanthan (XG)}$ equivalents per litre and in carbon units using the conversion factor of $0.75 \mu\text{gC XG } \mu\text{eq l}^{-1}$ proposed by Engel and Passow (2001). The detection limit of the method is $2.2 \mu\text{g XG eq l}^{-1}$ and the coefficient of variation is 13%.

· Dissolved Monosaccharides (DMCHO) and polysaccharides (DPCHO)

Samples for DMCHO and DPCHO analysis were filtered onto pre-combusted GF/F filters and stored frozen (-20°C) in sterile polypropylene flasks (Southern Ocean and Mediterranean Sea samples) or in pre-combusted glass scintillation vials (North Sea samples). The analysis of DMCHO and DPCHO was performed following the spectrophotometric method proposed by Myklestad et al. (1997). This technique consists of the submission of monosaccharides to an oxidation reaction at alkaline pH. During this reaction, Fe^{3+} is reduced to Fe^{2+} which is subsequently determined using the chromogen 2,4,6-tripyridyl-s-triazin (TPTZ). TPTZ gives violet color that is determined colorimetrically at 595nm. Polysaccharides are previously degraded to monosaccharides after the hydrolysis of the glycosidic bonds. Hydrolysis was performed acidifying with 1N HCl and incubating the samples for one hour at 150°C . Then, they were neutralized with 1N NaOH prior to spectrophotometric analysis.

As all reagents are photosensitive, light incidence was minimized the whole procedure (preparation of reagents and sample analysis) covering the reagents flasks with aluminum foil, and using amber glass test tubes or alternatively covering them with aluminum foil or placing them inside opaque boxes. All glassware was acid-washed and combusted (500°C , > 2 hours).

Calibration curves were prepared every two days with desiccated d-glucose at 0.25, 0.5, 1.0 and 2.0 mg l⁻¹, equivalent to 8.33, 16.67, 33.33 and 66.67 μmol C l⁻¹ respectively. The detection limit of the method is 0.4 μmol C l⁻¹ and the coefficient of variation is 7%.

· Dissolved Organic Carbon concentration

Samples for dissolved organic carbon (DOC) analyses were collected after filtration through pre-combusted Whatman GF/F filters into pre-combusted 10 ml glass ampoules, acidified with phosphoric acid (final pH < 2), sealed and stored at 4°C until analysis. DOC was analyzed by High-Temperature Catalytic Oxidation on a Shimadzu TOC-5000A. Standards of 44 - 45 μmol C l⁻¹ and 2 μmol C l⁻¹, provided by D.A. Hansell and Wenhao Chen (Univ. of Miami), were used to assess the accuracy of the measurements.

· Chlorophyll *a*

Chlorophyll *a* concentration (chl *a*) was determined fluorometrically by filtering 50 ml sub-samples through Whatman GF/F filters, extracted in 90% acetone for c.a. 24 hours in the dark and refrigerated conditions. The fluorescence of the extracts was read in a calibrated Turner Design fluorometer (Parsons et al., 1984).

The pigment-specific absorption (a_{ph}) was estimated from chl *a* concentration in μg l⁻¹ using the following expression (Bricaud et al., 1995):

$$a_{\text{ph}}(443) = 0.04 \times \text{Chl } a^{0.668}$$

Phytoplankton carbon content (phyto-C) was estimated from chl *a* concentration using a conversion factor of 40 μgC μg chl *a*⁻¹ proposed by Banse (1977).

· Bacterial Abundance

Total bacterial abundance in Southern Ocean samples during 2004 and North Sea samples was determined by epifluorescence microscopy after staining with the fluorochrome 4'-6-diamino-2-phenylindol (DAPI) (Porter and Feig, 1980). Samples

Material and Methods

(10-15 ml) were fixed with 0.2 µm filtered and neutralized formaldehyde (2% final concentration) and stored at 4°C until their processing (within days (North Sea samples) to two months (Southern Ocean 2004 samples). DAPI stain was added to 3-10 ml samples at a final concentration of 1 µg ml⁻¹ and let stain for 15 minutes in the dark. Samples were then filtered onto black 0.2 µm polycarbonate filters (Millipore) with low pressure (100 mm Hg), and the filters were placed in microscope slides using immersion oil of low fluorescence. A minimum of 300 cells were counted per sample using epifluorescence microscopy.

Bacterial abundance was obtained by the expression (Jones, 1979):

$$BA \text{ (cell ml}^{-1}\text{)} = \frac{Y \cdot A}{a \cdot V}$$

where Y is the average cell number by reticule, A is the filtration area (mm²); a is the reticule area (mm²) and V is the sample volume (ml).

Samples corresponding to Southern Ocean during 2005 and Mediterranean Sea were determined using flow cytometry (del Giorgio et al., 1996; Gasol and Del Giorgio, 2000). Samples (4 ml) were fixed with paraformaldehyde (Southern Ocean samples) and a mixture of paraformaldehyde and glutaraldehyde (Mediterranean Sea samples) to 1% final concentration, let fix for 30 minutes in the dark, deep freeze in liquid nitrogen, and stored at -20° C or -70°C until analysis (within hours up to two days). Samples were then thawed, 200 to 400 µl of sample were placed in plastic cytometry tubes, and 4 µl of 5 µmol l⁻¹ SYTO13 (Molecular Probes) diluted in dimethyl sulfoxide was added to 5 to 10 µmol l⁻¹ final concentration. Samples were incubated for 10 minutes in the dark, and 5 µl of a solution of yellow-green 0.92 µm Polysciences latex beads were added as an internal standard. After staining, samples were run through a Becton & Dickinson FACScalibur™ flow cytometer fitted with a laser emitting at 488 nm. Fluorescent filters and detectors used were the standard equipment, with green fluorescence collected in the FL1 channel, orange fluorescence collected in the FL2 channel, and red fluorescence collected in the FL3 channel. All parameters were collected as logarithmic signals. Samples were run at low speed and data were acquired in log mode until 10000 events were acquired. Bacteria were detected by their signature in bivariate plots of Side scatter (SSC) vs. FL1 (green fluorescence). The beads solution was sonicated (10 min) before being added to the sample. Its con-

centration was calibrated using TruCounts (Becton Dickinson). A standard solution of known abundance was used for Southern Ocean samples (twice during the cruise) and by direct enumeration of the beads using epifluorescence microscopy for Mediterranean Sea samples (once every two days). The coefficient of variation between measurements was 18%.

Cell concentration was determined using the following expression:

$$BA \text{ (cell ml}^{-1}\text{)} = \frac{C_{\text{beads}} \cdot V_{\text{beads}}}{V \text{ (sample + beads)}} \times \frac{N_{\text{cells}}}{N_{\text{beads}}}$$

Where C is the concentration of the beads, V is volume (ml) and N is the number of detected events (cells or beads).

Bacterial carbon content (bact-C) was estimated from bacterial abundance using the conversion factor of 20 fgC cell⁻¹ (Lee and Fuhrman, 1987)

· Bacterial Production

Bacterial production was determined following the centrifugation method proposed by Smith and Azam (1992). Samples (1.5 ml) were placed in microcentrifugation tubes. Then, a known volume of L-[4,5-³H] leucine was added as follows:

- Southern Ocean 2004 samples: 10 µl of ³H Leucine (MP Biomedicals). Specific activity: 59.5 Ci/mmol. Final concentration: 56 nM
- Southern Ocean 2005 samples: 10 µl of ³H Leucine (MP Biomedicals). Specific activity: 63.3 Ci/mmol. Final concentration: 52.7 nM
- Mediterranean Sea samples: 5 µl of ³H Leucine (Amersham). Specific activity: 162 Ci/mmol. Final concentration: 28.8 nM

Two to three replicates were always taken. Samples were incubated at 2°C in the Southern Ocean and 20°C in the Mediterranean Sea for 2 to 5 hours, and

Material and Methods

the incubation was stopped adding 0.3 ml of 50% Trichloroacetic Acid (TCA). One to two blanks per sample were also conducted in parallel. For sample blanks, 0.3 ml of 50% TCA was added before starting the incubations.

Samples were then stored refrigerated until their processing. Southern Ocean 2004 and Mediterranean Sea samples were processed in the laboratory within weeks to two months. For SO 2005, samples were immediately processed on board.

The sample tubes were centrifuged (10 min, 14000 rpm) and aspirated. Then, the tubes were washed with 1.5 of 5% TCA, vortexed, and centrifuged again. Then 1.5 ml of scintillation cocktail (Ecoscint) was added, the tubes were placed in scintillation vials, and radioassayed in a liquid scintillation counter (Beckman)

We determined uptaken leucine into protein using the following expression:

$$\text{nmol leu}^{-1} \text{ h}^{-1} = \frac{\text{dpm} / V.t}{2.2 \times 10^6 \times S.A.}$$

Where dpm are disintegrations per minute, V is the sample volume (l), t is the incubation time (h) and S.A is the specific activity of the tritiated leucine.

We used a conversion factor from leucine to carbon incorporation of 1.5 kg C mol leu⁻¹, which represents a standard assuming no isotope dilution (Simon and Azam, 1989).

REFERENCES

- BANSE, K. (1977) Determining the carbon to chlorophyll *a* of natural phytoplankton. *Marine Biology*. 41: 199–212.
- BETHOUX, J.P. and G. COPINMONTEGUT (1986) Biological fixation of atmospheric Nitrogen in the Mediterranean Sea. *Limnology and Oceanography*. 31: 1353-1358.
- BETHOUX, J.P., B. GENTILI, P. MORIN, E. NICOLAS, C. PIERRE and D. RUIZ-PINO (1999) The Mediterranean Sea: a miniature ocean for climatic and environmental studies and a key for the climatic functioning of the North Atlantic. *Progress in Oceanography*. 44: 131-146.
- BONIN, D.J., M.C. BONIN and T. BERMAN (1989) Experimental evidence of nutrients limiting the production of microneoplankton and ultraplankton in the coastal waters of the Eastern Mediterranean Ocean (Haifa, Israel). *Aquatic Sciences*. 51: 129-152.
- BRICAUD, A., M. BABIN, A. MOREL and H. CLAUSTRE (1995) Variability in the chlorophyll-specific absorption coefficients of natural phytoplankton - analysis and parameterization. *Journal of Geophysical Research-Oceans*. 100: 13321-13332.
- CALDEIRA, K. and P.B. DUFFY (2000) The role of the Southern Ocean in uptake and storage of anthropogenic carbon dioxide. *Science*. 287: 620-622.
- CONSTABLE, A.J., S. NICOL and P.G. STRUTTON (2003) Southern Ocean productivity in relation to spatial and temporal variation in the physical environment. *Journal of Geophysical Research-Oceans*. 108.
- DE BAAR, H.J.W., J.T.M. DE JONG, D.C.E. BAKKER, B.M. LOSCHER, C. VETH, U. BATHMANN and V. SMETACEK (1995) Importance of iron for plankton blooms and carbon dioxide drawdown in the Southern Ocean. *Nature*. 373: 412-415.
- DELGIORGIO, P., D.F. BIRD, Y.T. PRAIRIE and D. PLANAS (1996) Flow cytometric determination of bacterial abundance in lake plankton with the green nucleic acid stain SYTO 13. *Limnology and Oceanography*. 41: 783-789.
- DIERSSEN, H.M., R.C. SMITH and M. VERNET (2002) Glacial meltwater dynamics in coastal waters west of the Antarctic peninsula. *Proceedings of the National Academy of Sciences of the United States of America*. 99: 1790-1795.
- DUCKLOW, H.W., K. BAKER, D.G. MARTINSON, L.B. QUETIN, R.M. ROSS, R.C. SMITH, S.E. STAMMERJOHN, M. VERNET and W. FRASER (2007) Marine pelagic ecosystems: The West Antarctic Penin-

I Material and Methods

- sula. *Philosophical Transactions of the Royal Society B-Biological Sciences*. 362: 67-94.
- DUCROTOY, J.-P., M. ELLIOTT and V.N.D. JONGE (2000) The North Sea. *Marine Pollution Bulletin*. 41: 5-23.
- ENGEL, A. and U. PASSOW (2001) Carbon and nitrogen content of transparent exopolymer particles (TEP) in relation to their Alcian Blue adsorption. *Marine Ecology-Progress Series*. 219: 1-10.
- GASOL, J.M. and P.A. DEL GIORGIO (2000) Using flow cytometry for counting natural planktonic bacteria and understanding the structure of planktonic bacterial communities. *Scientia Marina*. 64: 197-224.
- GREEN, S.A. and N.V. BLOUGH (1994) Optical absorption and fluorescence properties of chromophoric dissolved organic matter in natural waters. *Limnology and Oceanography*. 39: 1903-1916.
- GURNEY, K.R., R.M. LAW, A.S. DENNING, P.J. RAYNER, D. BAKER, P. BOUSQUET, L. BRUHWILER, Y.H. CHEN, P. CIAIS, S. FAN, I.Y. FUNG, M. GLOOR, M. HEIMANN, K. HIGUCHI, J. JOHN, T. MAKI, S. MAKSYUTOV, K. MASARIE, P. PEYLIN, M. PRATHER, B.C. PAK, J. RANDERSON, J. SARMIENTO, S. TAGUCHI, T. TAKAHASHI and C.W. YUEN (2002) Towards robust regional estimates of CO₂ sources and sinks using atmospheric transport models. *Nature*. 415: 626-630.
- HUNTLEY, M., D.M. KARL, P. NIILER and O. HOLM-HANSEN (1991) Research on Antarctic coastal ecosystem rates (RACER): an interdisciplinary field experiment. *Deep-Sea Research Part a-Oceanographic Research Papers*. 38: 911-941.
- ICES (1983) Flushing times in the North Sea. *Cooperative Research Report* 123.
- JOINT, I. and A. POMROY (1993) Phytoplankton biomass and production in the Southern North Sea. *Marine Ecology-Progress Series*. 99: 169-182.
- JONES, J.C. (1979) A guide to methods for estimating microbial numbers and biomass in freshwater. *FBA Scientific Publication*. 39.
- LEE, S. and J.A. FUHRMAN (1987) Relationships between biovolume and biomass of naturally derived marine bacterioplankton. *Applied and Environmental Microbiology*. 53: 1298-1303.
- MARTIN, J.H., R.M. GORDON and S.E. FITZWATER (1990) Iron in Antarctic waters. *Nature*. 345: 156-158.
- MARTY, J.C. and J. CHIAVERINI (2002) Seasonal and interannual variations in phytoplankton production at DYFAMED time-series station, northwestern Medi-

- terranean Sea. Deep-Sea Research Part II-Topical Studies in Oceanography. 49: 2017-2030.
- MINAS, H.J., M. MINAS and T.T. PACKARD (1986) Productivity in upwelling areas deduced from hydrographic and chemical fields. *Limnology and Oceanography*. 31: 1182-1206.
- MITCHELL, B.G., E.A. BRODY, O. HOLM-HANSEN, C. MCCLAIN and J. BISHOP (1991) Light limitation of phytoplankton biomass and macronutrient utilization in the Southern Ocean. *Limnology and Oceanography*. 36: 1662-1677.
- MYKLESTAD, S., E. SKANOY and S. HESTMANN (1997) A sensitive and rapid method for analysis of dissolved mono- and polysaccharides in seawater. *Marine Chemistry*. 56: 279-286.
- NELSON, N.B. and D.A. SIEGEL (2002) Chromophoric DOM in the open ocean. *In*: D. A. Hansell and C. A. Carlson (eds.) *Biogeochemistry of marine dissolved organic matter*. Academic Press, San Diego.
- NICOL, S. (2006) Krill, currents, and sea ice: *Euphausia superba* and its changing environment. *Bioscience*. 56: 111-120.
- OPPENHEIMER, M. (1998) Global warming and the stability of the West Antarctic Ice Sheet. *Nature*. 393: 325-332.
- PARSONS, T.R., Y. MAITA and C.M. LALLI (1984) *A manual of chemical and biological methods for sea water analysis*. Pergamon Press, Oxford.
- PASSOW, U. and A.L. ALLDREDGE (1995) A dye-binding assay for the spectrophotometric measurement of transparent exopolymer particles (TEP). *Limnology and Oceanography*. 40: 1326-1335.
- PINHASSI, J., L. GOMEZ-CONSARNAU, L. ALONSO-SAEZ, M.M. SALA, M. VIDAL, C. PEDROS-ALIO and J.M. GASOL (2006) Seasonal changes in bacterioplankton nutrient limitation and their effects on bacterial community composition in the NW Mediterranean Sea. *Aquatic Microbial Ecology*. 44: 241-252.
- PORTER, K.G. and Y.S. FEIG (1980) The use of DAPI for identifying and counting aquatic microflora. *Limnology and Oceanography*. 25: 943-948.
- PSARRA, S., A. TSELEPIDES and L. IGNATIADIS (2000) Primary productivity in the oligotrophic Cretan Sea (NE Mediterranean): seasonal and interannual variability. *Progress in Oceanography*. 46: 187-204.
- PSARRA, S., T. ZOHARY, M.D. KROM, R.F.C. MANTOURA, T. POLYCHRONAKI, N. STAMBLER, T. TANAKA, A. TSELEPIDES and T.F. THINGSTAD (2005) Phytoplankton response to a Lagrangian

- phosphate addition in the Levantine Sea (Eastern Mediterranean). *Deep-Sea Research Part II-Topical Studies in Oceanography*. 52: 2944-2960.
- RAABE, T.U., U.H. BROCKMANN, C.D. DURSELEN, M. KRAUSE and H.J. RICK (1997) Nutrient and plankton dynamics during a spring drift experiment in the German Bight. *Marine Ecology-Progress Series*. 156: 275-288.
- RADACH, G. (1998) Quantification of long-term changes in the German Bight using an ecological development index. *Ices Journal of Marine Science*. 55: 587-599.
- SALA, M.M., F. PETERS, J.M. GASOL, C. PEDRÓS-ALIÓ, C. MARRASÉ and D. VAQUÉ (2002) Seasonal and spatial variations in the nutrient limitation of bacterioplankton growth in the northwestern Mediterranean. *Aquatic Microbial Ecology*. 27: 47-56.
- SARMIENTO, J.L., T.M.C. HUGHES, R.J. STOUFFER and S. MANABE (1998) Simulated response of the ocean carbon cycle to anthropogenic climate warming. *Nature*. 393: 245-249.
- SEREBRENNIKOVA, Y.M. and K.A. FANNING (2004) Nutrients in the Southern Ocean GLOBEC region: variations, water circulation, and cycling. *Deep-Sea Research Part II-Topical Studies in Oceanography*. 51: 1981-2002.
- SIMON, M. and F. AZAM (1989) Protein content and protein synthesis rates of planktonic marine bacteria. *Marine Ecology-Progress Series*. 51: 201-213.
- SMETACEK, V. and S. NICOL (2005) Polar ocean ecosystems in a changing world. *Nature*. 437: 362-368.
- SMITH, D.C. and F. AZAM (1992) A simple economical method for measuring bacterial protein synthesis rates in seawater using ³H leucine. *Marine Microbiology: Food Webs*. 6: 107-114.
- SMITH, R.C. and S.E. STAMMERJOHN (2001) Variations of surface air temperature and sea-ice extent in the western Antarctic Peninsula region *Annals of Glaciology*, Vol 33, vol. 33. Int Glaciological Soc, Cambridge. pp. 493-500.
- SMITH, W.O. and D.M. NELSON (1985) Phytoplankton bloom produced by a receding ice edge in the Ross Sea - Spatial coherence with the density field. *Science*. 227: 163-166.
- TAKAHASHI, T., S.C. SUTHERLAND, C. SWEENEY, A. POISSON, N. METZL, B. TILBROOK, N. BATES, R. WANNINKHOF, R.A. FEELY, C. SABINE, J. OLAFSSON and Y. NOJIRI (2002) Global sea-air CO₂ flux based on climatological surface ocean pCO₂, and seasonal biological and temperature effects. *Deep-Sea Research Part II-Topical Studies in Oceanography*. 49: 1601-1622.

THINGSTAD, T.F., M.D. KROM, R.F.C. MANTOURA, G.A.F. FLATEN, S. GROOM, B. HERUT, N. KRESS, C.S. LAW, A. PASTERNAK, P. PITTA, S. PSARRA, F. RASSOULZADEGAN, T. TANAKA, A. TSELEPIDES, P. WASSMANN, E.M.S. WOODWARD, C.W. RISER, G. ZODIATIS and T. ZOHARY (2005) Nature of phosphorus limitation in the ultraoligotrophic Eastern Mediterranean. *Science*. 309: 1068-1071.

TYRRELL, T. and C.S. LAW (1997) Low nitrate: Phosphate ratios in the global ocean. *Nature*. 387: 793-796.

VAUGHAN, D.G., G.J. MARSHALL, W.M. CONNOLLEY, C. PARKINSON, R. MULVANEY, D.A. HODGSON, J.C. KING, C.J. PUDSEY and J. TURNER (2003) Recent rapid regional climate warming on the Antarctic Peninsula. *Climatic Change*. 60: 243-274.

WEBB, D.J. and N. SUGINOHARA (1997) Vertical Mixing in the ocean. *Nature*. 409.

ZOHARY, T. and R.D. ROBARTS (1998) Experimental study of microbial P limitation in the eastern Mediterranean. *Limnology and Oceanography*. 43: 387-395.



Chapter 1:
Chromophoric dissolved organic matter in marine ecosystems:
distribution and controlling factors.

Ortega-Retuerta, E., Pulido-Villena, E., Agustí, S., Duarte, C.M., and Reche, I.

Abbreviated title: CDOM distribution in marine ecosystems



INTRODUCTION

Chromophoric dissolved organic matter (CDOM) is one of the main factors that control solar radiation attenuation in the water column. This contribution is significant (about one half of total non-water absorption at 443nm) even in those areas with extremely low CDOM, and shows geographical patterns, with an increase in high latitude oceans (Siegel et al., 2002; Siegel et al., 2005). Below the deep chlorophyll maximum, CDOM is the dominant factor for light attenuation (up to 100%, Coble, 2007).

The perception of CDOM has evolved over time, from being considered as a refractory fraction of DOM formed essentially by slow-cycling compounds mostly of terrestrial origin (Williams, 1971) to a fraction of contemporary origin and short residence times (Amon and Benner, 1994; Santschi et al., 1995; Opsahl and Benner, 1998).

In the past, several attempts have been done to use CDOM absorbance or fluorescence as a proxy of DOC concentration (Blough and del Vecchio, 2002). However, a significant relationship between these parameters has been only found in coastal areas (Vodacek et al., 1997; Ferrari, 2000), where both DOC and CDOM are mostly of terrestrial origin (such as river inputs) and controlled by the mixing with oceanic waters. Terrestrial CDOM is not always confined to the vicinity of the coast, but in areas with a large river discharge it can extend widely offshore (Blough et al., 1993; Hu et al., 2004) and it has been proposed as a tracer for river inputs (Blough et al., 1993; Murphy et al., 2008).

In open ocean areas, far from terrestrial influence, an uncoupling or even a near-inverse relationship between DOC and CDOM is generally observed both in temporal dynamics (Nelson et al., 1998) and in depth profiles (Hansell, 2002). Therefore, these two pools of organic carbon are governed by different sources and sinks or are formed and recycled at different timescales. In open ocean areas, where phytoplankton is the main responsible of all fixed carbon, chlorophyll *a* (chl *a*) and CDOM distribution and dynamics are expected to be linked (Carder et al., 1989), and, indeed, satellite images have shown that CDOM distribution at a global scale mirrors that of chl *a* (Siegel et al., 2002). However, several studies have outlined a spatial and temporal uncoupling of these two variables. Nelson et al. (1998) observed CDOM maxima in the Sargasso sea during spring stratification above the deep chlorophyll maximum (DCM), coinciding with maxima of bacterial activity. They proposed that CDOM is not directly produced by phytoplankton but it is a byproduct of bacterial activity.

On the other hand, lower CDOM in the upper mixed layer than in deeper waters (Chen and Bada, 1992; Nelson et al., 1998; Twardowski and Donaghay, 2001) suggests that photobleaching (the loss of absorbance due to the reaction of solar radiation with CDOM) could be a major sink. The combination of high incident sunlight and shallow mixed layers make central gyres and tropical areas to have very low CDOM near the surface, increasing towards the poles, where high CDOM is apparently a result of a lower sunlight dose over year and deeper mixed layers (Siegel et al., 2002).

Despite satellite observations of ocean color have provided global CDOM distribution patterns (Siegel et al., 2002), field studies on CDOM distribution and dynamics are still lacking. Particularly, the studies on CDOM distribution in the Southern Ocean are limited and confined to the Australian sector (Clementson et al., 2001) and Ross Sea (Barbini et al., 2003; Misic et al., 2006), being scarce the available information on CDOM in the Antarctic peninsula area (but see Patterson, 2000). Similarly, CDOM distributions in the Mediterranean Sea are limited and usually confined to coastal areas as the Rhone river plume (Babin et al., 2003) or Thyrrenian Sea (Seritti et al., 1998; Vignudelli et al., 2004). By contrast, in the North Sea, and particularly in the German Bight area, there is more information about CDOM distribution (Obernosterer and Herndl, 2000; Stedmon et al., 2000). Indeed, the first works on CDOM or “yellow substance” in open waters were carried out in the Baltic and North Seas (Jerlov, 1953; Kalle, 1966).

In this chapter, we describe CDOM geographical and vertical patterns (usually upon the first 200 m) in the three study areas: 1) around Antarctic Peninsula in the Southern Ocean, 2) a transit from West to East in the Mediterranean Sea, and 3) two coastal stations in the German North Sea. In addition, we explored the relationship between CDOM and DOC, as well as other physical and biological factors potentially controlling CDOM distribution in these study areas.

MATERIAL AND METHODS

The sampling protocols and physical, chemical and biological analyses (chromophoric dissolved organic matter, salinity, dissolved organic carbon, chl *a*, bacterial abundance and bacterial production) were detailed in the general section of methods.

The percentage of CDOM with respect to pigment absorption at 443nm ($\%a_{\text{cdom}}(443)$) was determined using the following expression:

$$\%a_{\text{cdom}}(443) = \frac{a_{\text{cdom}}(443)}{a_{\text{ph}}(443) + a_{\text{cdom}}(443)} \times 100$$

where $a_{\text{cdom}}(443)$ is the CDOM absorption coefficient at 443nm and $a_{\text{ph}}(443)$ is the pigment-specific absorption at 443nm.

To determine the controlling factors of CDOM distribution, simple regression analyses were performed. Data were log-transformed to fit the regression assumptions of normality and homogeneity of variances when needed. Data were analyzed as a single data set, and separated into different subsets of data according to geographical areas (Southern Ocean) or depths (Mediterranean Sea).

RESULTS

CDOM in the Southern Ocean showed similar average values in 2004 and 2005. The a_{325} values ranged from below the detection limit to 2.17 m^{-1} (mean value 0.39 m^{-1}) during ICEPOS 2004, and from undetectable to 0.76 m^{-1} (mean value 0.34 m^{-1}) during ICEPOS 2005. The a_{443} values ranged from undetectable to 0.76 m^{-1} (mean value 0.13 m^{-1}) during 2004, and from undetectable to 0.23 m^{-1} (mean value 0.12 m^{-1}) during 2005 (Table 1.1). Around 20-25% of the measurements were below the detection limit at 443 nm. In 2004, the highest CDOM (a_{325}) was observed inside Foster Bay in Deception Island (mean value 1.30 m^{-1} , Table 1.1) and near Livingston Island (0.98 m^{-1}), whereas the lowest values were detected during the transit to King George Island (0.18 m^{-1}). In 2005, the highest a_{325} values were observed within the photic layer of the stations situated in Weddell Sea (0.50 m^{-1} , st #9 and #10) and stations located at a higher latitude than the polar circle in Bellingshausen Sea (0.54 m^{-1} , st #2 and #3), while the lowest values were detected in stations situated in Bransfield strait (0.10 m^{-1} , st #17 and #18).

CDOM vertical profiles were diverse (Fig. 1.1). In 5 of 12 stations in 2004 and in 10 of 18 stations in 2005, higher CDOM values were observed in deep waters (below 100m) than in the upper layer. This deep CDOM increase was

Table 1.1. Average values and ranges of absorption coefficients at 325 and 443 nm (m^{-1}) and spectral slopes ($\times 10^{-3} \text{ nm}^{-1}$) in the six study areas of the Southern Ocean. bdl= below detection limit.

	$a_{325} \text{ (m}^{-1}\text{)}$	$a_{443} \text{ (m}^{-1}\text{)}$	$S_{uv} \text{ (}\times 10^{-3} \text{ nm}^{-1}\text{)}$
	Mean (range)	Mean (range)	Mean (range)
Total	0.36 (bdl – 2.17)	0.11 (bdl – 0.76)	12.9 (9.8 – 22.9)
Deception Island (2004)	1.30 (0.73 – 2.17)	0.46 (0.25- 0.76)	10.8 (10.3 – 11.4)
Anvers I. transit (2004)	0.41 (0.09– 1.28)	0.13 (bdl – 0.46)	16.6 (10.6 – 22.2)
King George I. transit (2004)	0.18 (bdl – 0.26)	0.05 (bdl – 0.14)	14.8 (10.7-22.9)
Bellingshausen Sea (2005)	0.41 (0.22– 0.66)	0.14 (bdl – 0.23)	11.8 (9.8 – 13.3)
Weddell Sea (2005)	0.44 (0.19 – 0.76)	0.10 (bdl – 0.15)	12.3 (11.1 – 15.2)
Bransfield strait (2005)	0.23 (bdl – 0.57)	0.06 (bdl – 0.19)	12.5 (10.6 – 14.7)

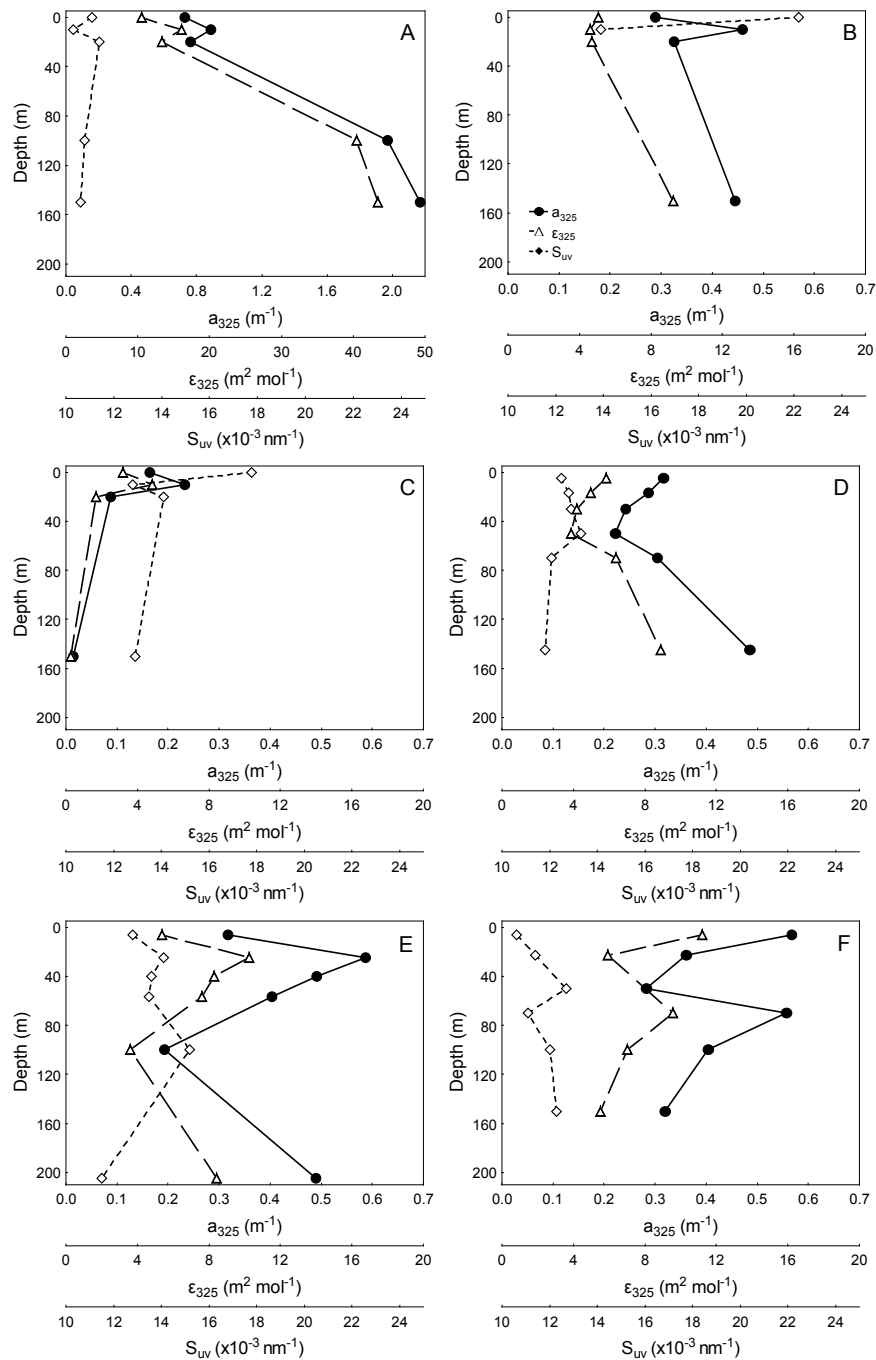


Figure 1.1. Vertical profiles of absorption coefficient at 325 nm (a_{325} , m^{-1} , filled circles), molar absorption coefficient at 325 (ϵ_{325} , $m^2 mol^{-1}$, open triangles) and spectral slopes (S_{uv} , $\times 10^{-3} nm^{-1}$, open diamonds) in six representative locations situated in Deception Island (A), the transit to Anvers Island (2004, B) and the transit to King George island (C) sampled in 2004, and Eastern Bellingshausen Sea (st #4, D) and Western Weddell Sea (st #10, E) and Bransfield Strait (st #12, F) sampled during 2005. Note the different scale for a_{325} and ϵ_{325} in Deception Island (A).

more accurate inside Deception Island (Fig. 1.1A), and in the stations situated in Bellingshausen Sea (st #1-7, Fig 1.1D), where the highest CDOM values were found below the mixed layer. By contrast, CDOM showed higher values within the euphotic layer than below it in the transit to King George Island in 2004 (Fig 1.1C) and in the Weddell Sea area in 2005 (Fig. 1.1E). In the Bransfield Strait in 2005, no consistent vertical patterns were observed (Fig. 1.1F).

Molar absorption coefficients at 325nm (ϵ_{325}) ranged between 0.27 and 43.37 $\text{m}^2 \text{mol}^{-1}$ (mean value 6.40 $\text{m}^2 \text{mol}^{-1}$) at 325nm and from undetectable to 15.22 $\text{m}^2 \text{mol}^{-1}$ (mean value 1.99 $\text{m}^2 \text{mol}^{-1}$) at 443nm (ϵ_{443}) in 2004. In 2005, molar absorption coefficients showed mean values of 5.95 $\text{m}^2 \text{mol}^{-1}$ at 325nm and 2.07 $\text{m}^2 \text{mol}^{-1}$ at 443nm. Molar absorption coefficients were highest in Deception Island in 2004 (mean value 24.8 $\text{m}^2 \text{mol}^{-1}$, Fig. 1.2), and lowest in the transit to King George Island (Fig. 1.2), both in 2004. The vertical profiles of molar absorption coefficients generally tracked those of absorption coefficients (Fig. 1.1).

The spectral slopes (S_{uv}) ranged from 9.8 to 22.9 $\times 10^{-3} \text{nm}^{-1}$ and were higher in 2004 (15.0 $\times 10^{-3} \text{nm}^{-1}$) than in 2005 (12.2 $\times 10^{-3} \text{nm}^{-1}$, Table 1.1, Fig. 1.1). The lowest spectral slopes were observed in Deception Island in 2004 and in Bellingshausen Sea in 2005 (Table 1.1).

The pigment-specific absorption at 443nm (a_{ph443}) ranged from 0.002 m^{-1} to 0.149 m^{-1} (mean value 0.044 m^{-1}). The $\%a_{cdom}(443)$ averaged 69 and 68% in

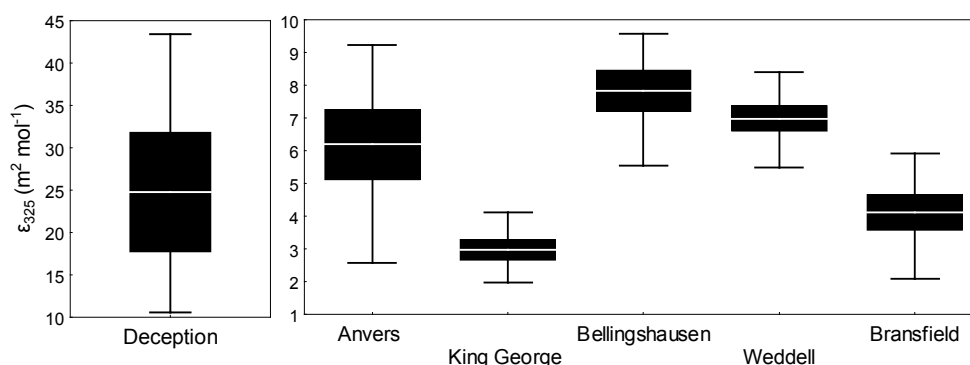


Figure 1.2. Molar absorption coefficients at 325nm (ϵ_{325} , $\text{m}^2 \text{mol}^{-1}$) in the five sampled areas during 2004 and 2005. Lines= Mean values. Boxes= Standard Error and whiskers= non-outlier ranges. Note the different scale for Deception Island.

2004 and 2005 respectively, and ranged from 60% in the eastern area (King George Transit, Weddell Sea and Bransfield strait) to 80% in the western area (Anvers Island transit and Bellingshausen Sea). The $\%a_{\text{cdom}}(443)$ showed a higher percentage in waters below the mixed layer than within it (Fig. 1.3).

CDOM and DOC were not correlated in any study areas ($p > 0.05$). In 2004, no significant relationships were obtained between CDOM (a_{325} , a_{443}) and salinity, chl *a* and bacterial abundance and production in the transit to Anvers Island. In the stations of the transit to King George Island, a_{325} was significant and positively correlated to chl *a* ($r^2 = 0.29$, $p < 0.05$, $n=20$). In the Bellingshausen Sea in 2005,

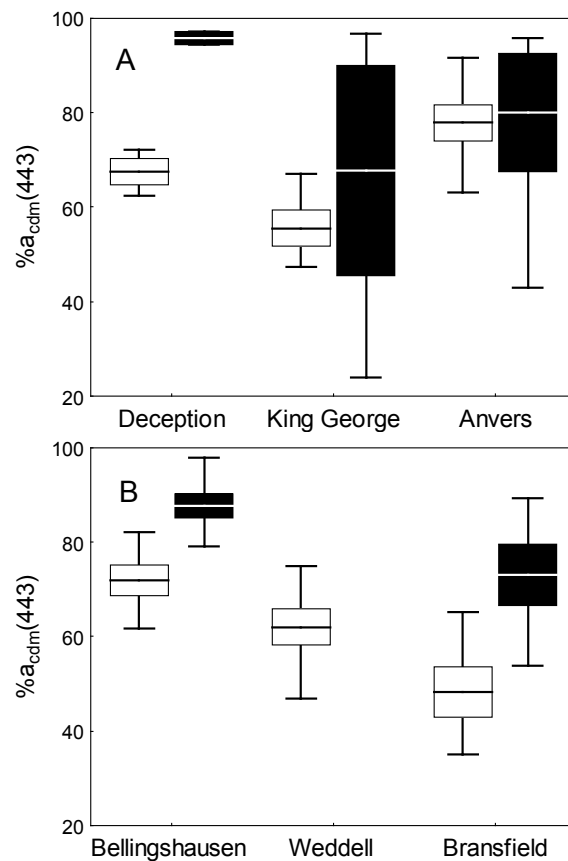


Figure 1.3. Percentage of CDOM absorption at 443nm respect to total non-water absorption in the upper (white boxes) and below (black boxes) the mixed layer in the five sampled areas during 2004 (A) and 2005 (B). Lines= Mean values. Boxes= Standard Error and whiskers= non-outlier ranges. Note: As the stations located in the Weddell Sea area were vertically mixed, only one bar, corresponding to data within the upper mixed layer, is shown.

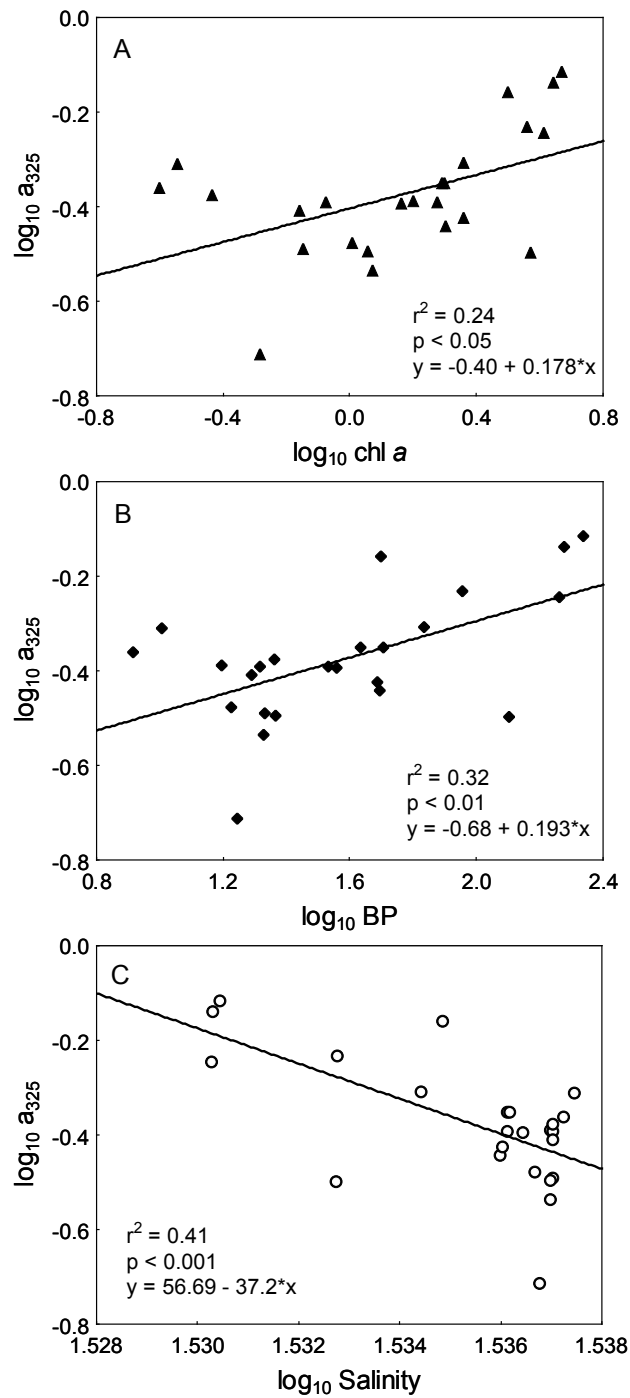


Figure 1.4. Log-log Scatterplots between chl *a* ($\mu\text{g l}^{-1}$), BP ($\mu\text{g C l}^{-1} \text{h}^{-1}$) and salinity (PSU) and a_{325} (m^{-1}) in the Weddell Sea area of the Southern Ocean (2005, stations #8-11).

significant negative relationships were observed only between a_{325} and chl a ($r^2 = 0.18$, $p < 0.01$, $n=38$) and BP ($r^2 = 0.11$, $p < 0.05$, $n=38$). By contrast, in the Weddell Sea area, positive relationships were observed between a_{325} and both chl a ($r^2 = 0.24$, $p < 0.05$, $n=23$, Fig. 1.4A) and BP ($r^2 = 0.32$, $p < 0.01$, $n=24$, Fig. 1.4B), but not with BA. Salinity was significant and negatively correlated to a_{325} and showed the highest explained variance ($r^2 = 0.41$, $p < 0.001$, $n=22$, Fig. 1.4C). Finally, no significant relationships were observed between CDOM and salinity, chl a and bacterial parameters in the stations situated along Bransfield strait.

The a_{325} values in the Mediterranean Sea ranged from undetectable to 0.38 m^{-1} (mean value 0.11 m^{-1} , Table 1.2), with 25% of measurements below the detection limit, and a_{443} values ranged from undetectable to 0.11 (mean value 0.03 m^{-1} , Table 1.2), with 75% of measurements below the detection limit at 443nm.

CDOM showed a variable geographical distribution (Fig. 1.5). Both a_{325} and a_{443} were the highest in the stations situated in the Southern Aegean Sea (st #13-15, Fig. 1.6D) and the lowest in stations near Alexandria (#9 to #12, Fig. 1.6C).

In most stations (17 of 24), CDOM in the upper layer was lower than below it (Fig. 1.6). CDOM peaks coincided with the chlorophyll a maxima (9 stations) and bacterial production maxima (8 stations).

Table 1.2. Average values and ranges of absorption coefficients at 325 and 443 nm (m^{-1}) in waters situated in the upper mixed layer, below the upper mixed layer but within the euphotic layer, and below the euphotic layer of the Mediterranean Sea. bdl = below detection limit

	$a_{325} \text{ (m}^{-1}\text{)}$	$a_{443} \text{ (m}^{-1}\text{)}$	$S_{uv} \text{ (}\times 10^{-3} \text{ nm}^{-1}\text{)}$
	Mean (range)	Mean (range)	Mean (range)
Total	0.11 (bdl – 0.38)	0.03 (bdl – 0.11)	15.6 (11.1- 23.7)
Upper Mixed Layer	0.11 (bdl – 0.32)	0.02 (bdl – 0.08)	16.9 (13.2 – 23.7)
Euphotic Layer	0.16 (bdl – 0.38)	0.03 (bdl – 0.11)	15.3 (12.0 – 20.5)
Below Euphotic Layer	0.13 (bdl – 0.30)	0.03 (bdl – 0.11)	15.4 (11.1 – 20.5)

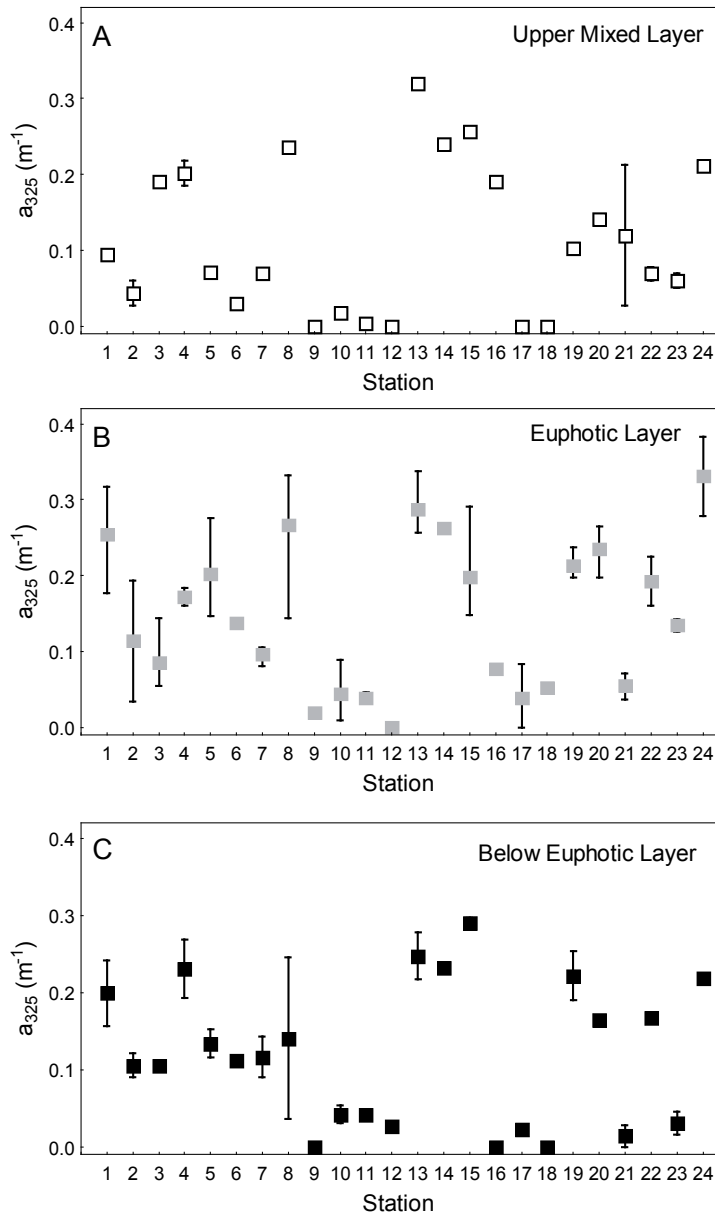


Figure 1.5. Mean and non-outlier ranges of a_{325} (m^{-1}) in the different study stations of the Mediterranean Sea within the upper mixed layer (white squares, A), below upper ML but within the euphotic layer (grey squares, B) and below the euphotic layer (black squares, C)

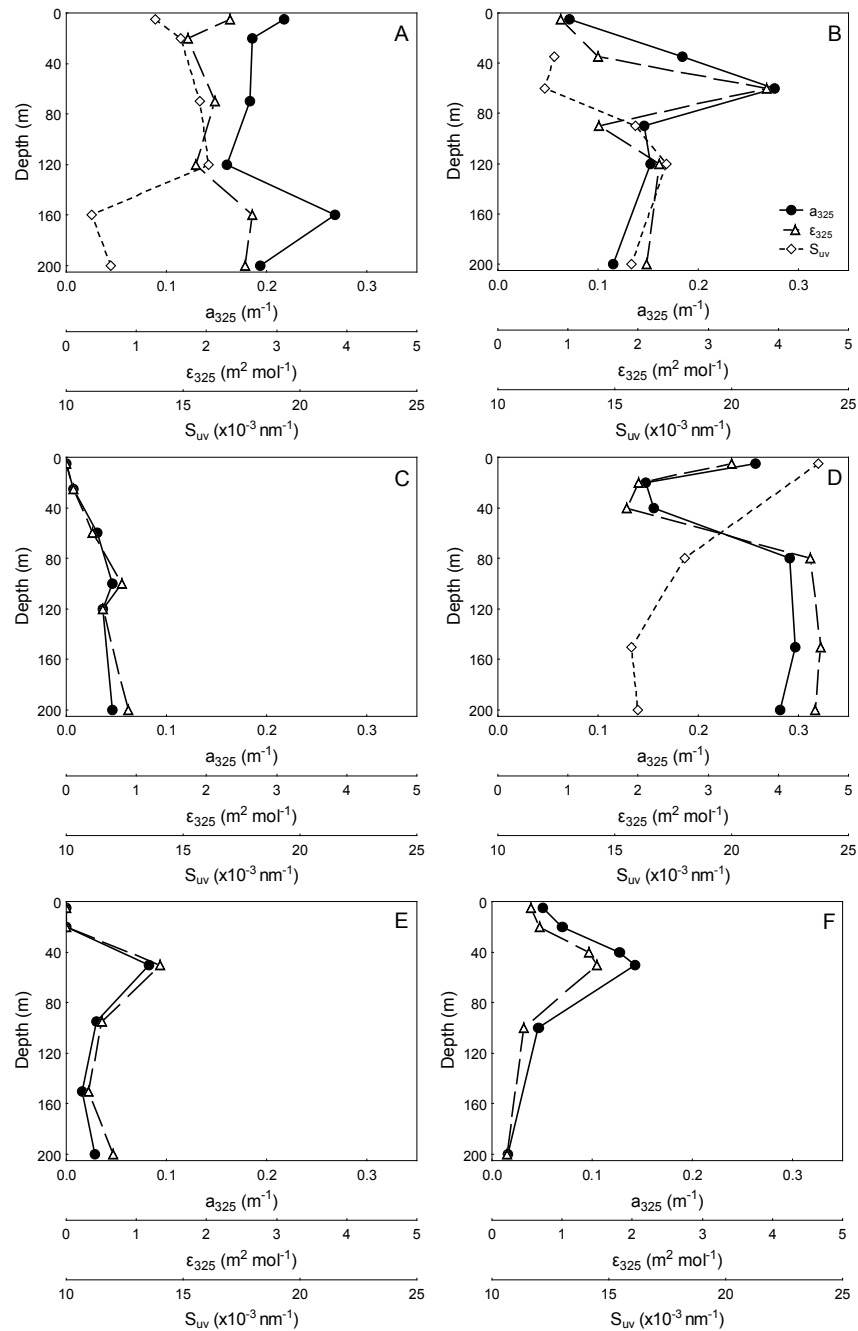


Figure 1.6. Vertical profiles of absorption coefficient at 325 nm (a_{325} , m^{-1} , filled circles), molar absorption coefficient at 325 (ϵ_{325} , $\text{m}^2 \text{mol}^{-1}$, open triangles) and spectral slopes (S_{uv} , $\times 10^{-3} \text{nm}^{-1}$, open diamonds) in six representative locations situated near Sicily Island (st #4, A), in the central Mediterranean (st #5, B), in the Eastern Mediterranean near Alexandria (st #11, C), in the Aegean Sea near Rhodes Island (st #15, D), below the Greek Peninsula (st #17, E) and near Balear Islands (st #23, F). In panels C, D and F, the spectral slopes were not determined as CDOM absorption was below the detection limit at wavelengths $< 400\text{nm}$.

Molar absorption coefficients averaged $1.83 \text{ m}^2 \text{ mol}^{-1}$ at 325 nm and $0.38 \text{ m}^2 \text{ mol}^{-1}$ at 443nm, and ranged from undetectable to 5.49 and $1.42 \text{ m}^2 \text{ mol}^{-1}$ respectively. Like the absorption coefficients, the highest values were observed in stations #13 to #15 and the lowest in stations #9 to #12 (Fig. 1.7).

The spectral slopes (S_{uv}) averaged $15.6 \times 10^{-3} \text{ nm}^{-1}$. However, 55 of 122 spectra were below the detection limit at wavelengths below 400nm, and were excluded from the average calculations. Spectral slopes were generally higher in the upper mixed layer than below it (Table 1.2).

The pigment-specific absorption at 443nm (a_{ph443}) ranged from $0.6 \times 10^{-3} \text{ m}^{-1}$ to 0.059 m^{-1} . The $\%a_{cdom}(443)$ was on average 35% and ranged from 0.14 to 97%. This contribution was lower within the euphotic layer (25%) than below it (53%), and was highest in stations situated around Sicily (#3, #4, #5 and #19, mean value 49%).

We did not find any significant relationships between CDOM (a_{325} or a_{443}) and salinity, chl *a*, BA and BP merging all data or discriminating into depths ($p > 0.05$). However, a weak but significant relationship was observed between a_{325} and DOC in waters within the euphotic layer ($r^2 = 0.11$, $p < 0.05$, $n=42$).

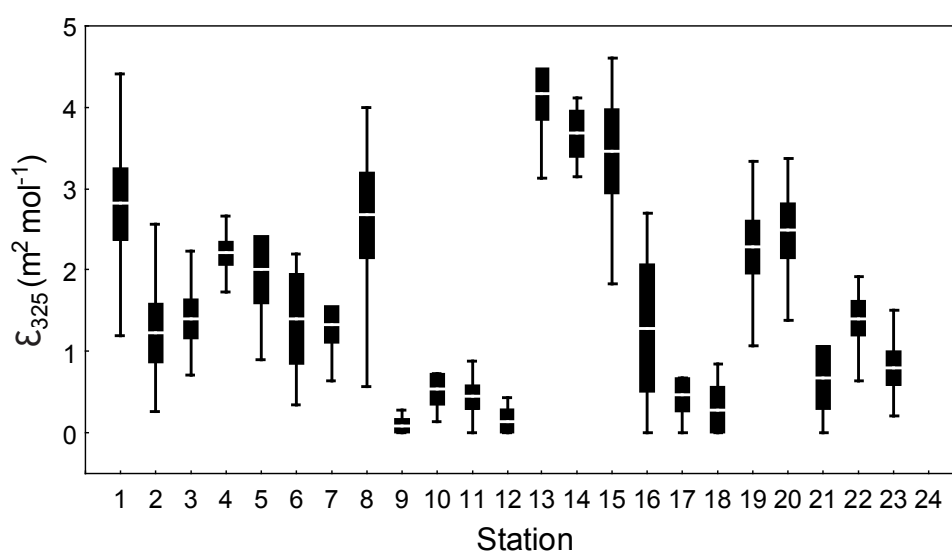


Figure 1.7. Molar absorption coefficients at 325nm (ϵ_{325} , $\text{m}^2 \text{ mol}^{-1}$) averaged over vertical profiles in the study stations of the Mediterranean Sea. Lines= Mean values. Boxes= Standard Error and whiskers= non-outlier ranges.

CDOM DISTRIBUTION IN THE NORTH SEA.

In the two sampled stations in the North Sea, a_{325} ranged from 1.60 to 1.85 (mean value of 1.72 m^{-1}) and a_{443} ranged from 0.27 to 0.43 m^{-1} (mean value 0.33 m^{-1}). CDOM showed homogeneous vertical profiles and similar values in both stations. Molar absorption coefficients at 325 nm (ϵ_{325}) ranged from 11.27 to $12.67 \text{ m}^2 \text{ mol}^{-1}$ (mean value $11.98 \text{ m}^2 \text{ mol}^{-1}$) while ϵ_{443} ranged from 1.81 to $2.12 \text{ m}^2 \text{ mol}^{-1}$ (mean value $1.94 \text{ m}^2 \text{ mol}^{-1}$). The spectral slopes (S_{uv}) showed an average value of $17.7 \times 10^{-3} \text{ nm}^{-1}$ and ranged from 17.1 to $20.7 \times 10^{-3} \text{ nm}^{-1}$.

DISCUSSION

In this chapter we have described generally higher CDOM values in the Antarctic Peninsula area than in the Mediterranean Sea.

The selection of different methodological approaches (absorbance vs. fluorescence) or different reference wavelengths (e.g. 375 nm, (Bricaud et al., 1981), 325 nm (Nelson et al., 1998) or 350 nm (Ferrari, 2000)) make CDOM data hardly comparable (Table 1.3).

CDOM in the Antarctic Peninsula area was generally higher in this study than the reported in the literature for the Australasian sector of the Southern Ocean (Clementson et al., 2001) in the Ross Sea (Barbini et al., 2003) or subantarctic areas (Howard-Williams et al., 1995) (Table 1.3). However, a_{325} values reported in our study are not substantially higher than the reported for the western Antarctic Peninsula area by Patterson (2000). Also other variables, such as chl *a* or bacterial abundance and production showed relatively high values, suggesting a productive status of the ecosystem.

Respect to the Mediterranean Sea, the published studies on CDOM are confined to coastal sites as the river Rhone plume or Gulf of Lions (Ferrari, 2000), Northern Adriatic Sea (Babin et al., 2003) or Northern Thyrrhenian Sea. CDOM values reported in those works are generally higher than CDOM in our study (Table 1.3).

Table 1.3. Values of CDOM absorption coefficients (average or ranges) previously reported in the literature in the study systems.

Study area	Wavelength (nm)	a_{CDOM} (m^{-1})	Reference
Southern Ocean			
Antarctic Peninsula	443	0.11 (bdl – 0.76)	this study
Western Ant. Pen.	320	0.19 (0.13-0.77)	Patterson (2000)
Australasian Sector	443	0.019-0.099	Clementson et al. (2001)
Ross Sea	400	0.031-0.120	Barbini et al. (2003)
Subantarctic	443	0.027-0.033	Howard-Williams et al. (1995)
Mediterranean Sea			
Barcelona-Alexandria	443	0.03 (bdl – 0.11)	this study
Thyrrhenian Sea	355	0.27 (0.13-0.36)	Seritti et al. (1998)
Gulf of Lions	350	0.061-0.274	Ferrari (2000)
NW Mediterranean	443	0.0114-0.0251	Babin et al. (2003)
Eastern Mediterranean	412	0.06	Oubelkheir et al. (2005)
North Sea			
German Bight	443	0.33 (0.27-0.43)	this study
German Bight	380	1.50	Højerslev et al. (1996)
Dutch North Sea	365	0.640	Obernosterer and Herndl (2000)
Danish North Sea	375	0.290-0.894	Stedmon et al. (2000)
German-Baltic transition	440	0.227	Lund-Hansen (2004)
English Channel	375	0.82	Vantrepotte et al. (2007)

In the North Sea stations, taking in consideration that different reference wavelengths were selected, CDOM was consistent with previous data in the transition between North Sea and Baltic Sea (Stedmon et al., 2000; Lund-Hansen, 2004) the English channel (Vantrepotte et al., 2007), adjacent to the Elbe river (Obernosterer and Herndl, 2000) or the coastal German waters (Højerslev et al., 1996) (Table 1.3).

The spectral slopes were generally lower in the Southern Ocean than in the Mediterranean Sea (12.9 and $15.6 \times 10^{-3} \text{ nm}^{-1}$ respectively). In both systems the spectral slopes were surprisingly in the lowest range usually found for oceanic areas (generally from 14 to $25 \times 10^{-3} \text{ nm}^{-1}$) (Bricaud et al., 1981; Nelson and Siegel, 2002; Blough and del Vecchio, 2002) and lower than the obtained in this study for coastal North Sea waters (average value $17.7 \times 10^{-3} \text{ nm}^{-1}$). However, different analytical factors can interfere in the slopes determination, such as the procedure used to compute slopes values, the range of wavelengths chosen to calculate slopes (Coble, 2007), or the baseline correction applied (Babin et al., 2003). In our case, a baseline of GF/F-filtered MilliQ water was subtracted to the sample spectra in Southern Ocean and Mediterranean Sea samples, but not in North Sea samples.

CDOM vertical profiles were very heterogeneous among the Southern Ocean study areas (Bellingshausen Sea, Weddell Sea, Bransfield strait). In the literature, also variable CDOM vertical distributions have been reported, from high CDOM in surface waters (Misic et al., 2006) to low CDOM concentrations within the first 200-300 m (Wedborg et al., 1998; Yamashita et al., 2007).

The absence of strong relationships between CDOM and the biological and physical studied parameters underlines the complexity of CDOM dynamics at this scale. In the Western Antarctic peninsula area (the transit to Anvers Island in 2004, Bellingshausen Sea stations in 2005) CDOM was not apparently driven by organisms or salinity changes. The vertical distribution, with particularly high CDOM below the upper mixed layer, suggests that CDOM can be dominated by physical forces. In these stations, with well-stratified waters columns and shallow mixed layers, the upper mixed layer is depleted in CDOM likely due to photobleaching losses. In waters below the mixed layer, high CDOM can be explained, in addition to the absence of photobleaching, by the influence of relatively warm waters from the Antarctic circumpolar current, which act as a source of nutrients

(Smith et al., 1999; Garcia et al., 2002). In Weddell Sea stations, where water was collected in areas surrounded by ice platelets, the negative relationship between CDOM and salinity suggests the role of ice melting as a source of CDOM, either directly or indirectly through the growth of algae and bacterial activity associated to nutrient release during ice melting. The influence of Weddell Sea water can also be responsible for the weak but significant relationship between CDOM and chl *a* in the transit to King George Island in 2004.

In the Mediterranean Sea, CDOM geographical distributions reflect general productivity patterns in the area. Hence, the highest CDOM was observed in the stations between Greek Islands, where also the highest chl *a* and BP values were observed, whereas the lowest CDOM was observed in the less productive stations around Alexandria. Indeed, a positive relationship between a_{325} and BP is observed when averaging vertical profiles of all stations ($r^2 = 0.29$, $p < 0.01$, $n=24$), and CDOM peaks below the upper mixed layer, coincident with maximum values of either chl *a* or bacterial production, suggest a biological source of CDOM. On the other hand, the lowest CDOM values generally observed in the upper mixed layer (17 of 24 stations) is consistent with previous studies in the Mediterranean Sea (Obernosterer et al., 1999) and in other areas (Chen and Bada, 1992; Nelson et al., 1998). This low CDOM in the upper mixed layer, added to higher spectral slopes than below it, is likely due to photobleaching, which would play a significant role controlling CDOM vertical distribution in the area.

The percentage of CDOM with respect to pigment-specific absorption was significantly higher in the Southern Ocean (68%) than in the Mediterranean Sea (35%), which agrees with the global trend of %CDOM increasing toward the poles (Clementson et al., 2001; Siegel et al., 2002). The contribution of detrital particles to the total non water absorption was not considered in our calculations, and although it is generally low (< 10%, Siegel et al., 2002) its contribution in the Antarctic Peninsula area appears to be higher than in other areas (see chapter 4) and, thus, the contribution of CDOM to the total non-water would be lower than the reported in this chapter. However, the observed values highlight CDOM as a key contributor to non-water light absorption, with particular significance in Southern Ocean waters.

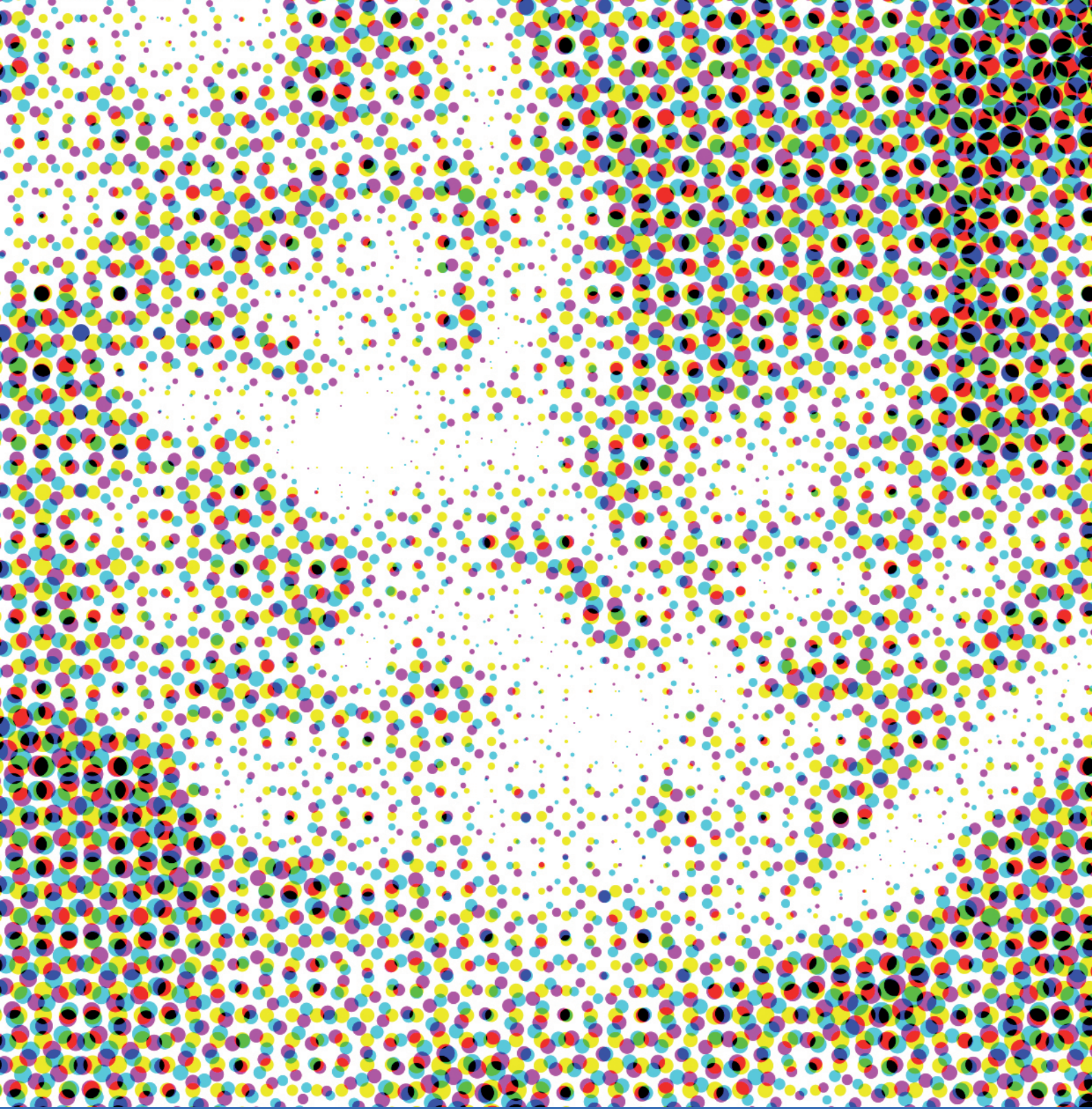
REFERENCES

- AMON, R.M.W. and R. BENNER (1994) Rapid cycling of high-molecular-weight dissolved organic matter in the ocean. *Nature*. 369 549-552.
- BABIN, M., D. STRAMSKI, G.M. FERRARI, H. CLAUSTRE, A. BRICAUD, G. OBOLENSKY and N. HOEPFFNER (2003) Variations in the light absorption coefficients of phytoplankton, nonalgal particles, and dissolved organic matter in coastal waters around Europe. *Journal of Geophysical Research-Oceans*. 108.
- BARBINI, R., F. COLAO, R. FANTONI, G.M. FERRARI, A. LAI and A. PALUCCI (2003) Application of a lidar fluorosensor system to the continuous and remote monitoring of the Southern Ocean and Antarctic Ross Sea: results collected during the XIII and XV Italian oceanographic campaigns. *International Journal of Remote Sensing*. 24: 3191-3204.
- BLOUGH, N.V. and R. DELVECCHIO (2002) Chromophoric DOM in the coastal environment. *In*: D. A. Hansell and C. A. Carlson (eds.) *Biogeochemistry of Marine Dissolved Organic Matter*. Academic Press, San Diego. pp. 547– 578.
- BLOUGH, N.V., O.C. ZAFIRIOU and J. BONILLA (1993) Optical absorption spectra of waters from the Orinoco River outflow: terrestrial input of colored organic matter to the Caribbean. *Journal of Geophysical Research-Oceans*. 98: 2271-2278.
- BRICAUD, A., A. MOREL and L. PRIEUR (1981) Absorption by dissolved organic matter of the sea (yellow substance) in the UV and visible domains. *Limnology and Oceanography*. 26: 43-53.
- CARDER, K.L., R.G. STEWARD, G.R. HARVEY and P.B. ORTNER (1989) Marine humic and fulvic-acids: their effects on remote sensing of ocean chlorophyll. *Limnology and Oceanography*. 34: 68-81.
- CHEN, R.F. and J.L. BADA (1992) The fluorescence of dissolved organic matter in seawater. *Marine Chemistry*. 37: 191-221.
- CLEMENTSON, L.A., J.S. PARSLAW, A.R. TURNBULL, D.C. MCKENZIE and C.E. RATHBONE (2001) Optical properties of waters in the Australasian sector of the Southern Ocean. *Journal of Geophysical Research-Oceans*. 106: 31611-31625.
- COBLE, P.G. (2007) Marine optical biogeochemistry: The chemistry of ocean color. *Chemical Reviews*. 107: 402-418.
- FERRARI, G.M. (2000) The relationship between chromophoric dissolved organic matter and dissolved organic carbon in

- the European Atlantic coastal area and in the West Mediterranean Sea (Gulf of Lions). *Marine Chemistry*. 70: 339-357.
- GARCÍA, M.A., C.G. CASTRO, A.F. RÍOS, M.D. DOVAL, G. ROSON, D. GOMIS and O. LÓPEZ (2002) Water masses and distribution of physico-chemical properties in the Western Bransfield Strait and Gerlache Strait during Austral summer 1995/96. *Deep-Sea Research Part II-Topical Studies in Oceanography*. 49: 585-602.
- HANSELL, D.A. (2002) DOC in the Global Ocean Carbon Cycle *In*: D. A. Hansell and C. A. Carlson (eds.) *Biogeochemistry of marine dissolved organic matter*. Academic Press, San Diego.
- HØJERSLEV, N.K., N. HOLT and T. AARUP (1996) Optical measurements in the North Sea-Baltic Sea transition zone. I. On the origin of the deep water in the Kattegat. *Continental Shelf Research*. 16: 1329-1342.
- HOWARD-WILLIAMS, C., R. DAVIES-COLLEY and W.F. VINCENT (1995) Optical properties of the coastal and oceanic waters off South Island, New Zealand: Regional variation. *New Zealand Journal of Marine and Freshwater Research*. 29: 589-602.
- HU, C.M., E.T. MONTGOMERY, R.W. SCHMITT and F.E. MULLER-KARGER (2004) The dispersal of the Amazon and Orinoco River water in the tropical Atlantic and Caribbean Sea: Observation from space and S-PALACE floats. *Deep-Sea Research Part II-Topical Studies in Oceanography*. 51: 1151-1171.
- JERLOV, N.G. (1953) Influence of suspended and dissolved matter on the transparency of sea water. *Tellus*. 5: 59-65.
- KALLE, K. (1966) The problem of gelbstoff in the Sea. *Oceanography and Marine Biology: Annual Reviews*. 4: 91-104.
- LUND-HANSEN, L.C. (2004) Diffuse attenuation coefficients $K_d(\text{PAR})$ at the estuarine North Sea-Baltic Sea transition: time-series, partitioning, absorption, and scattering. *Estuarine, Coastal and Shelf Science*. 61: 251-259.
- MISIC, C., M. CASTELLANO, N. RUGGIERI and P. POVERO (2006) Dissolved organic matter characterization and temporal trends in Terra Nova Bay (Ross Sea, Antarctica). *Estuarine Coastal and Shelf Science*. 70: 405-414.
- MURPHY, K.R., C.A. STEDMON, T.D. WAITE and G.M. RUIZ (2008) Distinguishing between terrestrial and autochthonous organic matter sources in marine environments using fluorescence spectroscopy. *Marine Chemistry*. 108: 40-58.
- NELSON, N.B. and D.A. SIEGEL (2002) Chromophoric DOM in the open ocean. *In*: D. A. Hansell and C. A. Carlson (eds.)

- Biogeochemistry of marine dissolved organic matter. Academic Press, San Diego.
- NELSON, N.B., D.A. SIEGEL and A.F. MICHAELS (1998) Seasonal dynamics of colored dissolved material in the Sargasso Sea. *Deep-Sea Research Part I-Oceanographic Research Papers*. 45: 931-957.
- OBERNOSTERER, I. and G.J. HERNDL (2000) Differences in the optical and biological reactivity of the humic and nonhumic dissolved organic carbon component in two contrasting coastal marine environments. *Limnology and Oceanography*. 45: 1120-1129.
- OBERNOSTERER, I., B. REITNER and G.J. HERNDL (1999) Contrasting effects of solar radiation on dissolved organic matter and its bioavailability to marine bacterioplankton. *Limnology and Oceanography*. 44: 1645-1654.
- OPSAHL, S. and R. BENNER (1998) Photochemical reactivity of dissolved lignin in river and ocean waters. *Limnology and Oceanography*. 43: 1297-1304.
- OUBELKHEIR, K.J., H. CLAUSTRE, A. SCIAN-DRA and M. BABIN (2005) Bio-optical and biogeochemical properties of different trophic regimes in oceanic waters. *Limnology and Oceanography*. 50: 1795-1809.
- PATTERSON, K.W. (2000) Contribution of chromophoric dissolved organic matter to attenuation of ultraviolet radiation in three contrasting coastal areas. PhD. University of California Santa Barbara, Santa Barbara.
- SANTSCHI, P.H., L.D. GUO, M. BASKARAN, S. TRUMBORE, J. SOUTHON, T.S. BIANCHI, B. HONEYMAN and L. CIFUENTES (1995) Isotopic evidence for the contemporary origin of high molecular weight organic matter in oceanic environments. *Geochimica et Cosmochimica Acta*. 59: 625-631.
- SERITTI, A., D. RUSSO, L. NANNICINI and R. DEL VECCHIO (1998) DOC, absorption and fluorescence properties of estuarine and coastal waters of the Northern Tyrrhenian Sea. *Chemical Speciation and Bioavailability*. 10: 95-106.
- SIEGEL, D.A., S. MARITORENA and N.B. NELSON (2005) Independence and interdependencies among global ocean color properties: Reassessing the bio-optical assumption. *Journal of Geophysical Research-Oceans*. 110.
- SIEGEL, D.A., S. MARITORENA, N.B. NELSON, D.A. HANSELL and M. LORENZIKAYSER (2002) Global distribution and dynamics of colored dissolved and detrital organic materials. *Journal of Geophysical Research-Oceans*. 107.

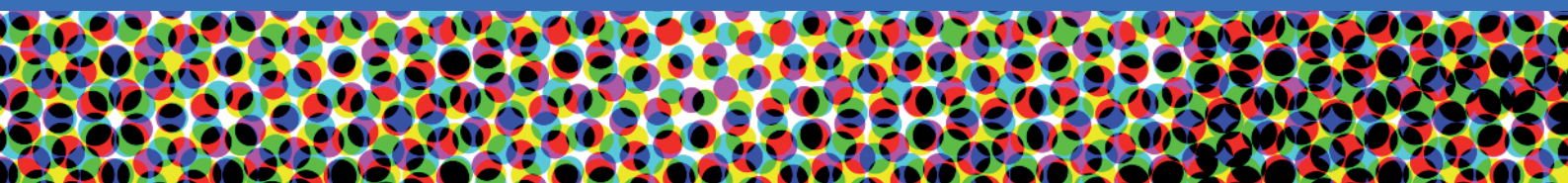
- SMITH, D.A., E.E. HOFMANN, J.M. KLINCK and C.M. LASCARA (1999) Hydrography and circulation of the west Antarctic Peninsula continental shelf. *Deep-Sea Research Part I-Oceanographic Research Papers*. 46: 925-949.
- STEDMON, C.A., S. MARKAGER and H. KAAS (2000) Optical properties and signatures of chromophoric dissolved organic matter (CDOM) in Danish coastal waters. *Estuarine Coastal and Shelf Science*. 51: 267-278.
- TWARDOWSKI, M.S. and P.L. DONAGHAY (2001) Separating in situ and terrigenous sources of absorption by dissolved materials in coastal waters. *Journal of Geophysical Research-Oceans*. 106: 2545-2560.
- VANTREPOTTE, V., C. BRUNET, X. MERIAUX, E. LECUYER, V. VELLUCCI and R. SANTER (2007) Bio-optical properties of coastal waters in the Eastern English Channel. *Estuarine Coastal and Shelf Science*. 72: 201-212.
- VIGNUDELLI, S., C. SANTINELLI, E. MURRU, L. NAINNICINI and A. SERITTI (2004) Distributions of dissolved organic carbon (DOC) and chromophoric dissolved organic matter (CDOM) in coastal of the northern Tyrrhenian Sea (Italy). *Estuarine Coastal and Shelf Science*. 60: 133-149.
- VODACEK, A., N.V. BLOUGH, M.D. DEGRANDPRE, E.T. PELTZER and R.K. NELSON (1997) Seasonal variation of CDOM and DOC in the Middle Atlantic Bight: Terrestrial inputs and photooxidation. *Limnology and Oceanography*. 42: 674-686.
- WEDBORG, M., M. HOPPEMA and A. SKOOG (1998) On the relation between organic and inorganic carbon in the Weddell Sea. *Journal of Marine Systems*. 17: 59-76.
- WILLIAMS, P.M. (1971) The distribution and cycling of organic matter in the ocean. *In*: S. D. Faust and J. V. Hunter (eds.) *Organic compounds in the aquatic environment*. Dekker New York. pp. 145-163.
- YAMASHITA, Y., A. TSUKASAKI, T. NISHIDA and E. TANOUE (2007) Vertical and horizontal distribution of fluorescent dissolved organic matter in the Southern Ocean. *Marine Chemistry*. 106: 498-509.



Chapter 2:
**Role of photoreactions on chromophoric dissolved organic
matter dynamics in marine ecosystems and further influence
on bacterioplankton.**

Ortega-Retuerta, E., Pulido-Villena, E., Duarte, C.M., and Reche, I.

Abbreviated title: CDOM photoreactivity in marine ecosystems



INTRODUCTION

Chromophoric dissolved organic matter (CDOM) has a strong impact in the cycling of carbon and other elements acting as a primary reactant of sunlight-mediated processes. The absorption of solar radiation by CDOM leads to the formation of singlet excited state species ($^1\text{DOM}^*$) that subsequently decay through different photochemical pathways (Mopper and Kieber, 2000). One of these processes is the degradation of organic compounds into smaller molecules (Kieber et al., 1989; Mopper et al., 1991), which involves a loss of absorbance (Kouassi and Zika, 1992; de Haan, 1993; Skoog et al., 1996) known as photobleaching. Several experimental studies have reported a CDOM absorbance decay higher than 50% in terms of days, frequently associated to increases in the spectral slope (Whitehead et al., 2000; Del Vecchio and Blough, 2002). Alternatively, the sunlight-mediated transformation of organic compounds such as fatty acids or triglycerides into humic-like substances, termed photohumification, has been proposed as a key process in the open ocean (Kieber et al., 1997). Finally, the photooxidation of CDOM into inorganic forms such as carbon monoxide or dioxide and dissolved inorganic carbon (DIC), known as photomineralization, is considered an important pathway of DOC removal from the ocean (Valentine and Zepp, 1993; Miller and Zepp, 1995), although global estimates of photomineralization rates are highly variable, from 0.1 to 12 Tg year⁻¹ (Nelson and Siegel, 2002). CDOM photoreactivity, that is, its susceptibility to react with sunlight and vary its optical properties will be a function of its chemical composition, origin (terrestrial vs marine), diagenetic status (fresh vs aged), and the environmental conditions where carbon is dissolved (Reche et al., 1999; Bertilsson and Tranvik, 2000; Osburn et al., 2001).

The complex reactions between CDOM and sunlight alter its availability as bacterial substrate. The photoproduction of small and low molecular weight compounds from refractory organic matter can enhance (Lindell et al., 1995; Moran and Zepp, 1997; Reche et al., 1998) or reduce (Tranvik and Kokalj, 1998; Obernosterer et al., 2001) its bioavailability. The net effect of DOM photoreactions on bacterial growth depends on its intrinsic properties, on the availability of other limiting substrates, or on the chemical environment (Reche et al., 1998; Ortega-Retuerta et al., 2007). Therefore, DOM enriched in aromatic and aliphatic compounds derived from terrestrial sources or deep waters, which are considered refractory for bacterial processing, can be transformed by solar radiation into more bioavailable substrate. Conversely, if DOM is initially formed by freshly algal-derived organic compounds, more labile for bacterioplankton, then solar radiation can alter it into more biorefractory compounds (Benner and Biddanda, 1998; Obernosterer et al., 1999b; Tranvik and Bertilsson, 2001).

In the present chapter, we experimentally determined CDOM photoreactivity in waters with contrasting chemical and optical properties and assessed its significance for in situ CDOM dynamics. In addition, we analyzed the influence of photoproducts on bacterial growth in the particular case of the Southern Ocean.

MATERIAL AND METHODS

CDOM PHOTOREACTIVITY EXPERIMENTS

To determine CDOM photoreactivity in the study systems we set up an experimental design that is illustrated in Figure 2.1. Seawater was initially filtered through pre-rinsed 0.2 µm nitrocellulose filters (Millipore) to exclude most bacteria. Quartz flasks (50 ml)(UV treatments) and Black-tape covered borosilicate flasks (50ml) (control treatments) were filled and incubated in parallel. A set of experimental bottles were sequentially taken over the incubation for CDOM characterization (see image 2.1).

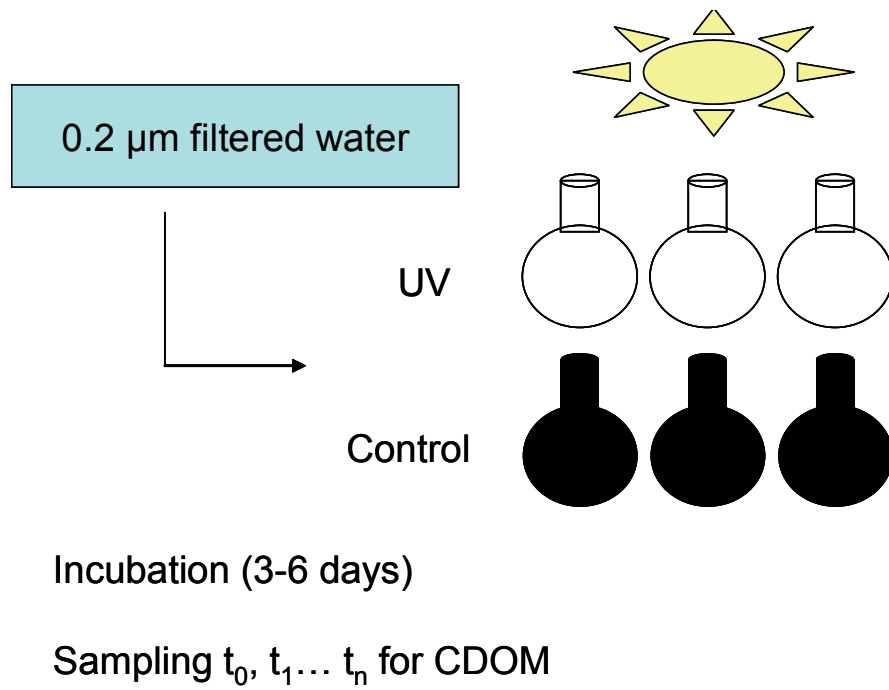


Figure 2.1. Experimental design to determine CDOM photoreactivity in the study systems.

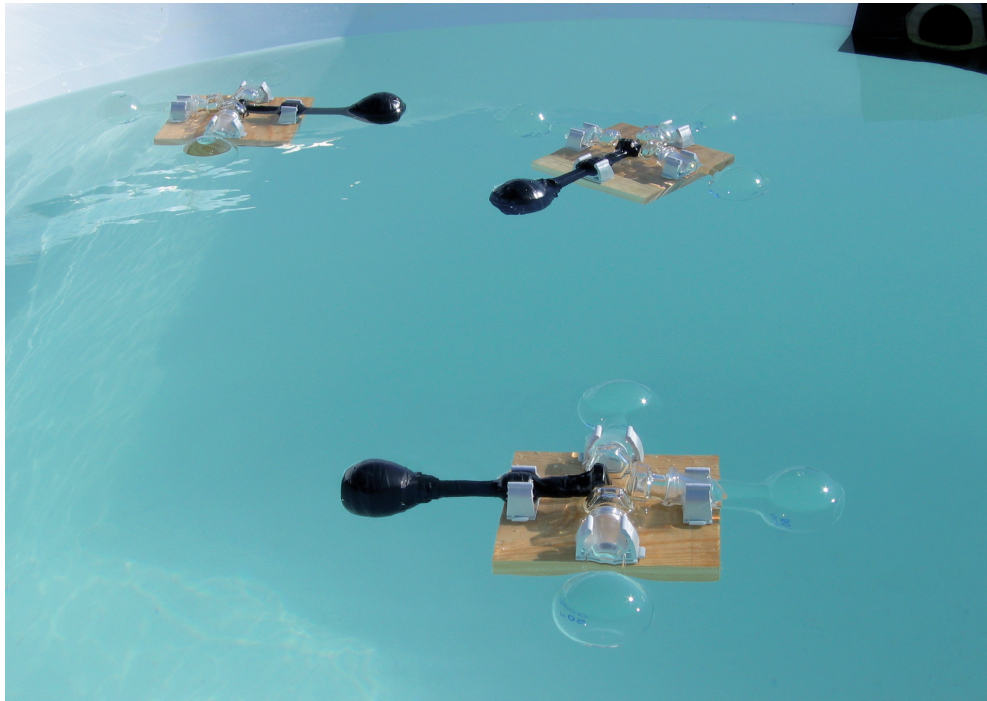


Image 2.1. Photoreactivity experiment performed in Livingston Island (Southern Ocean).

Table 2.1. Selected locations for the photoreactivity experiments performed in the Southern Ocean: in situ DOC concentration, chlorophyll *a*, and bacterial abundance, and optical properties (a_{325} , a_{443} and slopes from 290 to 400nm) at initial time. bdl= below detection limit, nd= not determined.

Exp	Sampling Area	Location	Depth	a_{325} (m^{-1})	a_{443} (m^{-1})	S_{uv} ($\times 10^{-3} nm^{-1}$)	DOC (μM)	Chl <i>a</i> ($\mu g l^{-1}$)	BA ($\times 10^5$ cell ml^{-1})
1	Deception Island	62° 57' S 60° 39' W	0m	0.77	0.20	13.9	69.0	5.03	7.99
2	Livingston Island	63° 24' S 60° 23' W	0m	1.97	0.71	10.6	75.3	0.71	4.33
3	Livingston Island	63° 24' S 60° 23' W	50m	0.72	0.23	12.3	70.5	0.64	3.80
4	Anvers Island	64° 35' S 63° 24' W	0m	0.40	0.12	13.4	44.5	0.73	2.27
5	Anvers Island	64° 35' S 63° 24' W	150m	0.78	0.25	12.4	54.9	0.35	2.50
6	Bellingshausen S.	66° 34' S 69° 60' W	DCM (40m)	0.10	bdl	32.9	nd	0.64	2.25
7	Weddell Sea	64° 16' S 55° 43' W	DCM (80m)	0.57	0.14	12.5	nd	4.42	12.5

Table 2.2. Selected locations for the photoreactivity experiments performed using Mediterranean Sea waters: in situ DOC concentration, chlorophyll *a*, and bacterial abundance; and optical properties (a_{325} , a_{443} and slopes from 290 to 400nm) at initial time. bdl= below detection limit. nd= not determined.

Exp	Sampling Area	Location	Depth	a_{325} (m^{-1})	a_{443} (m^{-1})	S_{uv} ($\times 10^{-3} nm^{-1}$)	DOC (μM)	Chl <i>a</i> ($\mu g l^{-1}$)	BA ($\times 10^5$ cell ml^{-1})
1	St #2	38° 14' N 10° 52' E	200m	0.06	bdl	nd	60.0	bdl	1.4
2			DCM	0.15	bdl	nd	76.0	1.15	5.6
3	St #15	36° 09' N 26° 13' E	200m	0.18	0.04	14.8	65.3	0.06	3.2
4			DCM	0.28	0.08	13.7	62.4	0.62	8.9

CDOM PHOTOREACTIVITY IN THE SOUTHERN OCEAN

Five experiments were performed during ICEPOS 2004 (experiments # 1 to 5) and two experiments during ICEPOS 2005 (experiments # 6 and 7).

Water for the experiments during ICEPOS 2004 was selected from three different locations (near Livingston Island, Deception Island and Anvers Island), two depths, surface (experiments # 1, 2 and 4) and below the euphotic layer (50 m for Livingstone Island, 150m for Anvers Island, experiments # 3 and 5). Table 2.1 shows the location and the field properties of CDOM for each experiment. During ICEPOS 2005, two experiments were performed using waters from the deep chlorophyll maximum (DCM) from two locations in the Bellingshausen Sea (station #2) and in the Weddell Sea (station #9) (experiments # 6 and 7, Table 2.1).

Water for the experiments was incubated for 3 to 6 days in the surface of temperature-controlled water baths under natural sunlight conditions. These water baths were located at Juan Carlos I Spanish base during ICEPOS 2004 (image 2.1) and in the stern deck of R/V 'Hespérides' during ICEPOS 2005.

Incident solar radiation was monitored using a PUVR 2500 Biospherical Instruments Meter. When direct data were not available, incident radiation data were provided by the NSF UV Monitoring Network, operated by Biospherical Instruments Inc. under a contract from the United States National Science Foundation's Office of Polar Programs via Raytheon Polar Services Company. When both datasets were available, the coefficient of variation was around 14% between both measurements.

CDOM PHOTOREACTIVITY IN THE MEDITERRANEAN SEA

We performed 4 experiments in the Mediterranean Sea using water from two different locations, in the western Mediterranean (station #2) and in the Aegean Sea (station #15). Two depths were selected in each station (200m and DCM). Table 2.2 shows the locations and field properties of CDOM for the experiments.

Water was incubated for up to three days in the stern deck of R/V 'García del Cid' under natural sunlight conditions. Samples for bacterial abundance (flow cytometry) were also taken to control their potential growth. In the second set

of experiments (exps # 3 and 4, with Aegean Sea waters) the incubation was stopped at the second day as several experimental bottles were accidentally opened and emptied.

In this case, only an integrated measurement over the whole spectrum, ($W m^{-2}$) of incident radiation was monitored during the course of the experiments. Photoreactivity rates were only calculated in time units.

CDOM PHOTOREACTIVITY IN THE NORTH SEA

Two experiments were performed using North Sea waters from station #1 at 5 m and station #2 at 5 m. Table 2.3 shows the locations and field properties of CDOM for the experiments. Water was incubated inside water baths in the laboratory roof for three days under natural solar conditions in the first experiment, whereas water was incubated in a culture room using artificial PAR and UVB lamps for three days with a light regime of 16 hours light/8 hours dark and a constant temperature of 15°C in the second experiment. Samples for bacterial abundance (epifluorescence microscopy) were also taken to control their potential growth.

During these experiments, incident radiation was monitored using integrated radiation sensors for UVB (integrated radiation from 300 to 320 nm, $kJ m^{-2}$), UVA (integrated radiation from 320 to 400 nm, $kJ m^{-2}$), and PAR (integrated radiation from 400 to 700 nm, $\mu E cm^{-2} s^{-2}$). Photoreactivity rates were calculated in time units.

Table 2.3. Selected locations for the photoreactivity experiments performed using North Sea waters: in situ DOC concentration, chlorophyll *a*, and bacterial abundance; and optical properties (a_{325} , a_{443} and slopes from 290 to 400nm) at initial time. bdl= below detection limit. nd= not determined.

Exp	Sampling Area	Location	Depth	a_{325} (m^{-1})	a_{443} (m^{-1})	S_{uv} ($\times 10^{-3} nm^{-1}$)	DOC (μM)	Chl <i>a</i> ($\mu g l^{-1}$)	BA ($\times 10^5$ cell ml^{-1})
1	St #1	54° 08' N 7° 54' E	5m	1.33	0.16	19.2	145	nd	13.2
2	St #2	54° 03' N 7° 57' E	5m	1.41	0.17	19.4	140	nd	12.5

DATA ANALYSIS

To test for significant differences between treatments over time in each experiment, repeated measures ANOVA tests were applied. This analysis is useful for experiments where there may be a within-subject effect (incubation time) and a between-subjects effect (UV radiation).

Photoreactivity rates (k_λ) at 325 and 443 nm were expressed in time units (eq. 1) and in sunlight dose units (only for Southern Ocean experiments, eq. 2) (Reche et al., 2000), assuming second order decay kinetics (Reche et al. 1999):

$$k_\lambda(\text{d}^{-1}) = \frac{\ln \frac{a_{\lambda n}}{a_{\lambda 0}}}{t} \quad (1)$$

$$k_\lambda((\text{kJm}^2)^{-1}) = \frac{\ln \frac{a_{\lambda n}}{a_{\lambda 0}}}{Dn} \quad (2)$$

where λ is 325 or 443 nm, $a_{\lambda 0}$ and $a_{\lambda n}$ are absorption coefficients at the initial and final time of incubation, Dn is the cumulative sunlight dose at 320nm and 400nm in kJ m^{-2} and t is time in days. Sunlight doses at 320 and 400 nm were chosen as they were the available data of incident radiation with the closest wavelengths to the selected reference wavelengths for CDOM characterization (325nm and 443nm).

CDOM absorption half lives (time to reduce a 50% the initial absorption coefficients by photobleaching, eq. 3) or duplication times (time or increment a 100% the initial absorption coefficients by photohumification, eq. 4) in days units were calculated as:

$$\text{half life } (hl_\lambda) = \frac{\ln(0.5)}{k_\lambda(\text{d}^{-1})} \quad (3)$$

$$\text{duplication time } (dt_\lambda) = \frac{1}{k_\lambda(\text{d}^{-1})} \quad (4)$$

EFFECTS OF CDOM PHOTOPRODUCTS ON BACTERIOPLANKTON

In the Southern Ocean, we evaluated the effects of CDOM photoproducts on bacterioplankton. Four re-growth cultures were performed using waters from two locations (Deception and Livingston Islands) and two depths (surface and below the photic layer).

A scheme of the experimental design is shown in Figure 2.2. Water was initially filtered through glass fiber filters (Whatman GF/F, nominal pore size 0.7 μm). This procedure removed a large fraction of *in situ* bacteria (87-89 %) and all bacterivores and phytoplankton (visual examination).

Each experiment consisted in two treatments: Control and photoproducts. Water for the photoproducts treatments was placed in 1 liter quartz bottles in the surface of a circulating water bath under natural solar radiation for 27 to 31 hours, corresponding to a total PAR of 5391.2 $\mu\text{E}/\text{cm}^2$ and a total UV at 320nm of 753 $\text{kJ}/\text{cm}^2 \text{ nm}$. Water for control treatments was maintained in the dark for the same time period. Each treatment was conducted by triplicate. After the irradiation in the photoproducts treatments, re-growth cultures were set up. Samples were taken at the initial time for CDOM characterization. All treatments were subsequently inoculated (10% of total volume) with non light-exposed filtered water to avoid the use of bacteria with potential UV-damage. Re-growth cultures were incubated for 100-120 hours in 250 ml sterilized glass flasks in the dark at ambient temperature (around 2° C). Aliquots from each treatment and replicate were sequentially taken approximately every 24h to determine BA (epifluorescence microscopy) and BP. Flagellate growth was also checked at each time.

Differences in BA and BP between treatments over time in each experiment were tested using repeated measures ANOVA.

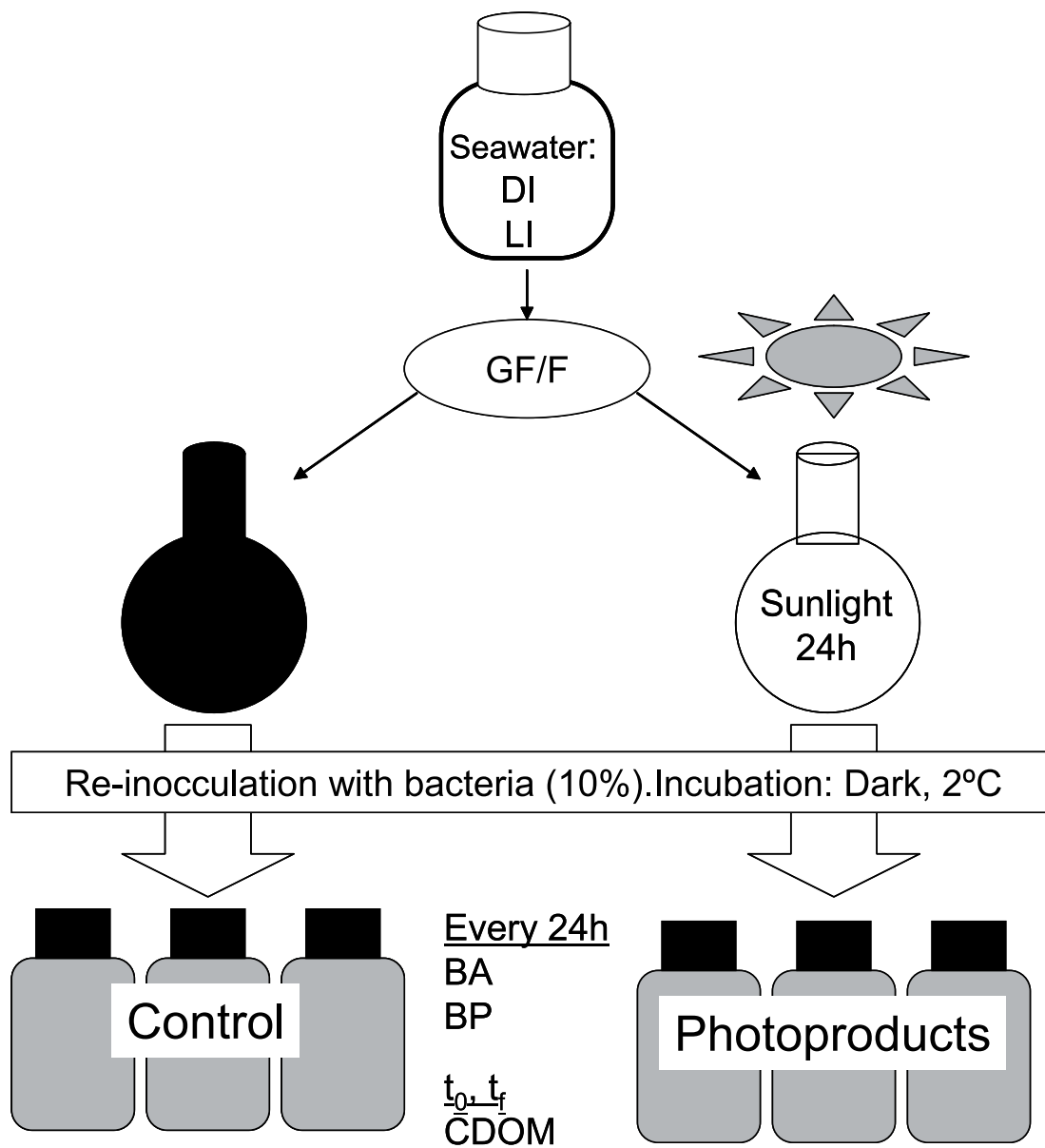


Figure 2.2. Experimental design to determine the effect of CDOM photoproducts on bacterial growth in the Southern Ocean using water from Deception Island (DI) and Livingston Island (LI).

RESULTS

Photoreactivity experiments yielded both photobleaching and photohumification and changes (increase or decrease in absorption coefficients) were generally consistent over the whole spectra (Fig. 2.3).

CDOM PHOTOREACTIVITY IN THE SOUTHERN OCEAN

The CDOM photoreactivity experiments performed using Southern Ocean waters showed CDOM net losses at 325nm and 443nm over the incubation time in UV treatments in 5 experiments (Fig. 2.4A-B), and increases or no changes in UV treatments in two experiments (# 3 and 6, Fig. 2.4C). Changes in CDOM in the dark treatments were also detected in the experiments. In particular, in all the experiments with CDOM decreases in UV treatments, CDOM also decreased,

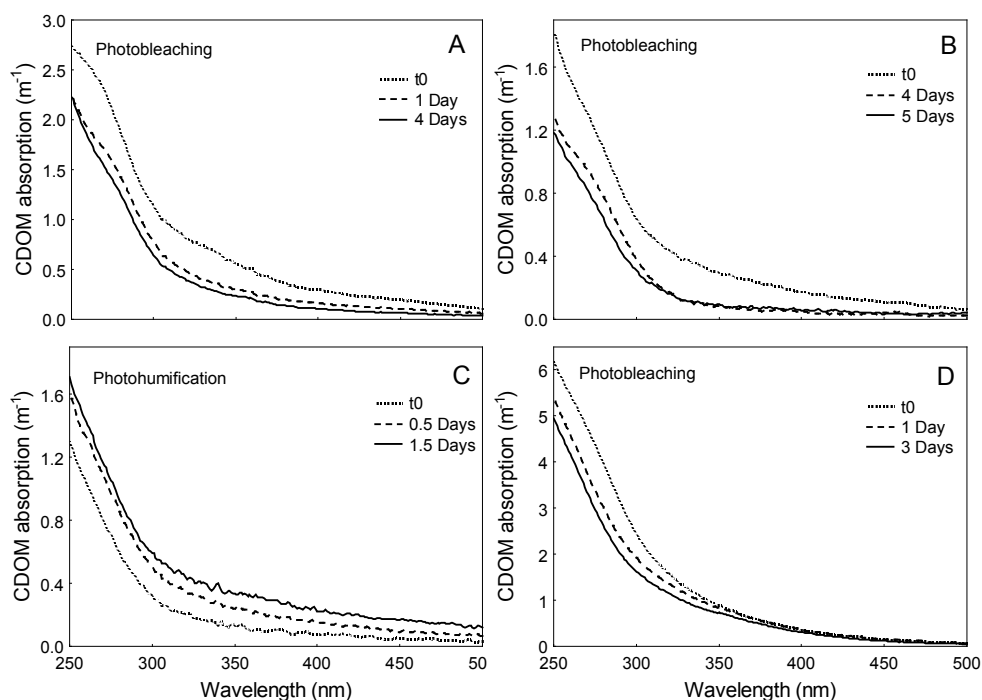


Figure 2.3. Changes in the CDOM spectra from 250 to 500 nm at initial (dotted line), intermediate (dashed line) and final (solid line) times in several experiments. Experiment # 1 and # 4 of the Southern Ocean: Deception Island 0m (A), and Anvers Island 0m (B); experiment # 3 of the Mediterranean Sea, st #15 200m (C) and experiment # 2 of the North Sea, st #2 5m (D). Note the different scales in the y axis.

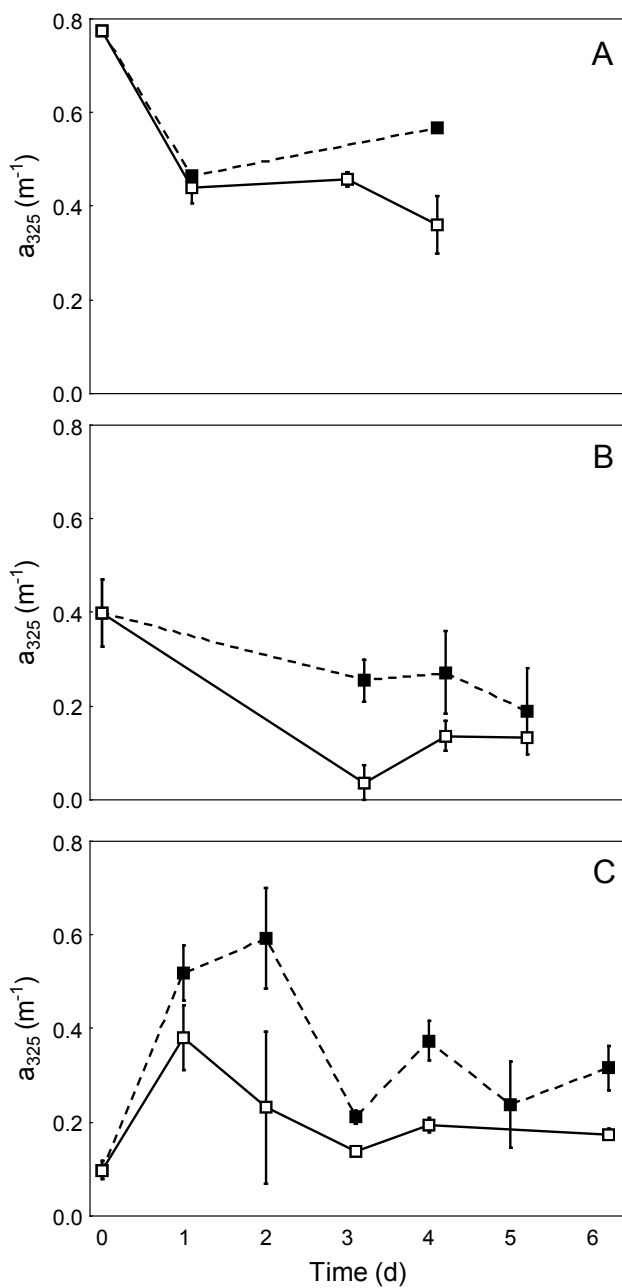


Figure 2.4. Changes in absorption coefficients at 325nm (a_{325} , m^{-1}) over time (days) in experiments # 1 (Deception Island 0m, A), exp # 4 (Anvers Island 0m, B) and exp # 6 (Bellingshausen Sea DCM, C). Open squares= UV treatments. Filled squares= Control treatments. Whiskers= Standard Error.

although less markedly, in control treatments. Differences over time in control vs UV treatments were not significant in any of the experiments (repeated measures ANOVA, $p > 0.05$).

The spectral slopes increased over the incubation time in all experiments where photobleaching was the dominant process (exp # 1, 2, 4, 5 and 7, Fig. 2.5A) whereas slopes decreased in experiments # 3 and 6 (Fig. 2.5B).

The cumulative sunlight doses ranged from 16.4 to 28.4 kJ m^2 at 320nm and from 60.23 to 104.8 kJ m^2 at 400nm. Photobleaching rates (k_{325}) ranged from -0.03 to -0.07 $(\text{kJ m}^2)^{-1}$ and from -0.12 to -0.24 d^{-1} in those experiments with noticeable losses of absorption, corresponding to half lives from 2.6 to 6.6 days (Table 2.4). In the experiments where photohumification was the net process, duplication times ranged from 10.9 to 15.7 days (Table 2.4). Photobleaching rates at 443nm (k_{443}) ranged from -0.009 to -0.017 $(\text{kJ m}^2)^{-1}$ and from -0.119 to -0.323 d^{-1} , corresponding to half lives from 2.3 to 6.4 days in the experiments with photobleaching and duplication times from 4.9 to 10 days in the experiments with photohumification (Table 2.5).

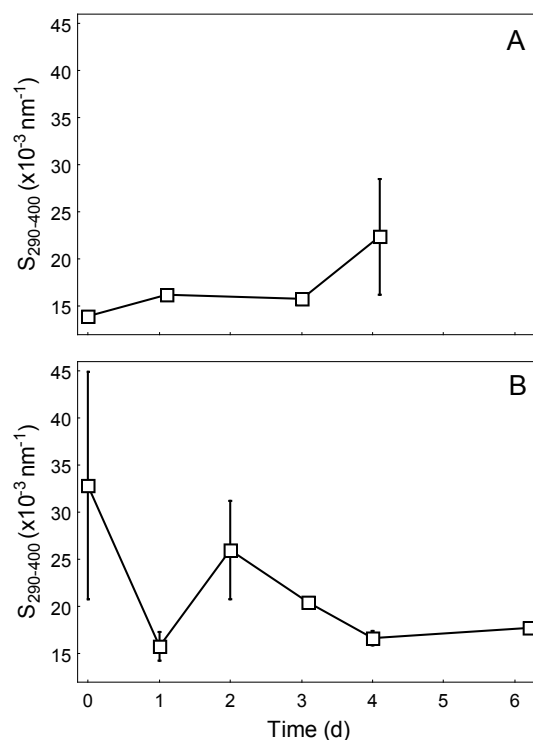


Figure 2.5. Changes in the spectral slopes ($s_{290-400}$) over the incubation time in the UV treatments of experiment 1 (A) and 6 (B). Whiskers= Standard Error.

Table 2.4. Photoreactivity rates (k) (mean \pm standard error) in sunlight dose units ($(\text{kJ m}^{-2})^{-1}$) and in time units (d^{-1}) and half lives (photobleaching) or duplication times (photohumification) (d) at 325 nm determined in the experiments performed with Southern Ocean waters. Standard errors are not included when only one replicate was measured at final time.

Exp	Sampling Area	Depth	Process	k_{325} (kJ/m^2) ⁻¹	k_{325} (d^{-1})	Half life ₃₂₅ (d)	Duplication time ₃₂₅ (d)
1	Deception Island	0m	Photobleaching	-0.03 \pm 0.01	-0.19 \pm 0.05	4.0 \pm 0.9	
2	Livingston Island	0m	Photobleaching	-0.04 \pm 0.01	-0.24 \pm 0.04	2.9 \pm 0.5	
3	Livingston Island	50m	Photohumification	0.01 \pm 0.00	0.07 \pm 0.02		15.7 \pm 4.5
4	Anvers Island	0m	Photobleaching	-0.07 \pm 0.01	-0.18 \pm 0.00	2.6 \pm 0.0	
5	Anvers Island	150m	Photobleaching	-0.07	-0.18	2.6	
6	Bellingshausen S.	DCM (40m)	Photobleaching	0.02 \pm 0.00	0.09 \pm 0.01		10.9 \pm 1.2
7	Weddell Sea	DCM (80m)	Photohumification	-0.05 \pm 0.02	-0.12 \pm 0.04	6.6 \pm 2.2	

Table 2.5. Photoreactivity rates in sunlight dose units (kJ m^{-2})⁻¹ and in time units (d^{-1}) and half lives (photobleaching) and duplication times (photohumification) (d) at 443 nm determined in the experiments with Southern Ocean waters.

Exp	Sampling Area	Depth	Process	k_{443} (kJ/m^2) ⁻¹	k_{443} (d^{-1})	Half life ₄₄₃ (d)	Duplication time ₄₄₃ (d)
1	Deception Island	0m	Photobleaching	-0.009 \pm 0.006	-0.218 \pm 0.155	6.4 \pm 4.6	
2	Livingston Island	0m	Photobleaching	-0.014 \pm 0.003	-0.315 \pm 0.078	2.3 \pm 0.5	
3	Livingston Island	50m	Photohumification	0.005 \pm 0.001	0.103 \pm 0.019	-6.8 \pm 1.2	10.0 \pm 1.8
4	Anvers Island	0m	Photobleaching	-0.017 \pm 0.002	-0.197 \pm 0.021	2.5 \pm 0.5	
5	Anvers Island	150m	Photobleaching	-0.015	-0.174	2.6	
6	Bellingshausen S.	DCM (40m)	Photobleaching	0.013 \pm 0.003	0.215 \pm 0.050		4.9 \pm 1.2
7	Weddell Sea	DCM (80m)	Photohumification	-0.012	-0.119	5.8	

EFFECTS OF CDOM PHOTOPRODUCTS ON BACTERIAL GROWTH

The exposure of CDOM to solar radiation to generate photoproducts resulted in a remarkable CDOM photobleaching (26-50% at 325nm and 63-55% at 443nm) using water from Deception Island, whereas little (4-12% at 325nm) or no CDOM decreases due to photobleaching were observed in waters from Livingston Island (Fig. 2.6).

Bacterial abundance (Fig. 2.7) and bacterial production (Fig. 2.8) were generally higher over the entire course of the experiments performed with waters from Deception Island (exps # 1 and 2) than those performed with waters from Livingston Island (exps # 3 and 4) (Fig. 2.7, 2.8). In experiments # 1 and 2, higher increases in BA (Table 2.6, Fig. 2.7) and BP (Table 2.7, Fig. 2.8) were generally observed in the control treatments than in those with photoproducts (Fig. 2.8). In contrast, no significant differences in BA or BP in control vs photoproducts treatments were observed in experiments 3 and 4 (Table 2.6, 2.7, Fig. 2.7, 2.8).

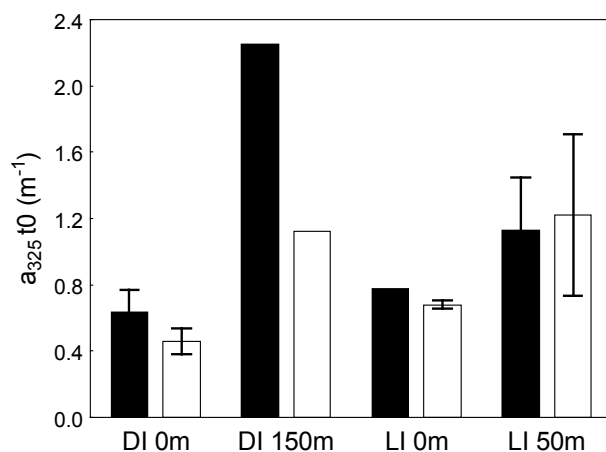


Figure 2.6. Changes in absorption coefficients at 325nm (a_{325} , m^{-1}) in seawater from Deception Island (DI) and Livingston Island (LI) used as a substrate for bacterial re-growth cultures in control (black bars) and photoproducts (white bars) treatments. Whiskers= Standard Error.

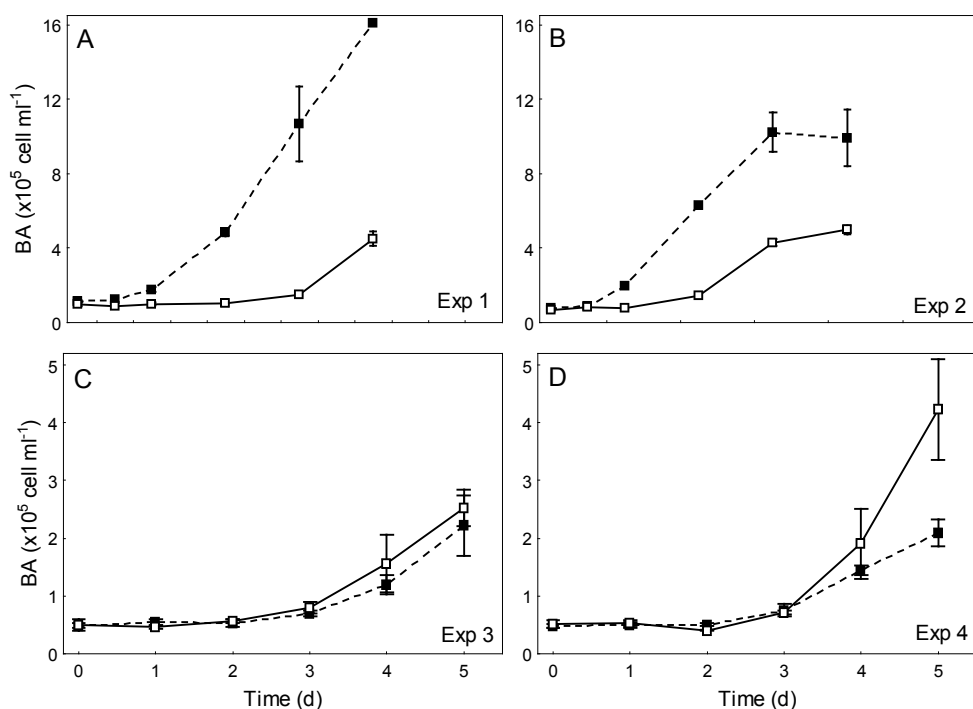


Figure 2.7. Changes in BA ($\times 10^5$ cell ml^{-1}) over time in control (filled squares) and photoproducts (open squares) treatments of each re-growth experiment performed in Deception Island at surface and 150m (A and B) and in Livingston Island at surface and 50m (C and D) during ICEPOS 2004. Whiskers= Standard Error. Note the different scales in the y axis.

Table 2.6. Results of repeated measures ANOVA to test differences in BA over time in control vs photoproducts treatments of the re-growth cultures.

Experiment	Location	Depth	Effect	F	p
1	Deception	Surface	Photoproducts	92.96	< 0.01
			Time * Photop	21.46	< 0.001
2	Deception	Below photic layer	Photoproducts	53.05	< 0.01
			Time * Photop	13.66	< 0.001
3	Livingston	Surface	Photoproducts	0.71	ns
			Time * Photop	0.29	ns
4	Livingston	Below photic layer	Photoproducts	2.57	ns
			Time * Photop	4.70	< 0.01

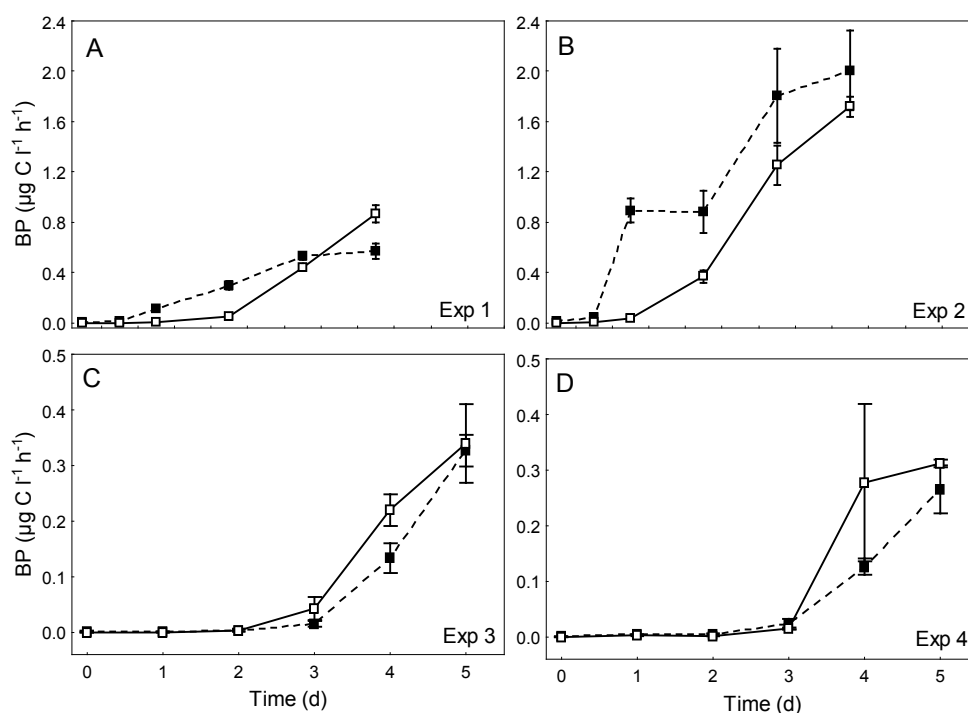


Figure 2.8. Changes in BP ($\mu\text{g C l}^{-1} \text{h}^{-1}$) over time in control (filled squares) and photoproducts (open squares) treatments of each re-growth experiment performed in Deception Island at surface and 150m (A and B) and in Livingston Island at surface and 50m (C and D) during ICEPOS 2004. Whiskers= Standard Error. Note the different scales in the y axis.

Table 2.7. Results of repeated measures ANOVA to test differences in BP over time in control vs photoproducts treatments of the re-growth cultures.

Experiment	Location	Depth	Effect	F	p
1	Deception	Surface	Photoproducts	3.64	ns
			Time * Photop	15.83	< 0.001
2	Deception	Below photic layer	Photoproducts	5.56	ns
			Time * Photop	3.40	< 0.05
3	Livingston	Surface	Photoproducts	2.26	ns
			Time * Photop	0.84	ns
4	Livingston	Below photic layer	Photoproducts	1.42	ns
			Time * Photop	1.06	ns

CDOM PHOTOREACTIVITY IN THE MEDITERRANEAN SEA

In the experiments performed using Mediterranean Sea waters, no consistent changes in CDOM absorption at 325 or 443 nm were detected over time. Changes in CDOM did not follow a clear trend in experiments # 1 and 2, with alternative increases and decreases of absorption (Table 2.8, Fig. 2.9 A). By contrast, net CDOM increases were observed in the UV treatments of experiment # 3 (Fig. 2.9 B) and # 4. In this last experiment, CDOM increases were detected in control and UV treatments but these were significantly higher in the controls (Table 2.8). Bacterial growth was detected in the photoreactivity experiments and was of a similar magnitude (around 10^5 cell ml⁻¹ d⁻¹) in all experiments and treatments.

The spectral slopes were not calculated in experiments # 1 and 2 because values were undetectable at the longest wavelengths of the UV spectrum. In experiments # 3 and 4, spectral slopes decreased over time in the UV treatments (Fig. 2.10).

The cumulative sunlight doses (over the whole solar spectrum) for the incubation times were 129444 kJ m⁻² for experiments 1 and 2 and 51147 kJ m⁻² for experiments 3 and 4.

Photoreactivity rates (k) ranged from 0.09 to 0.56 d⁻¹ for a_{325} and from 0.32 to 0.64 d⁻¹ for a_{443} , leading to duplication times from 0.6 to 35 days (Table 2.9).

Table 2.8. Results of repeated measures ANOVA to test differences over time in UV vs control treatments of the Mediterranean Sea photoreactivity experiments.

Experiment	Sampling Area and Depth	Effect	F	p
1	St #2 200m	UV	0	ns
		Time * UV	0	ns
2	St #2 DCM	UV	1.59	ns
		Time * UV	5.06	ns
3	St #15 200m	UV	699.2	< 0.05
		Time * UV	0.95	ns
4	St #15 DCM	UV	0.61	ns
		Time * UV	7.45	< 0.05

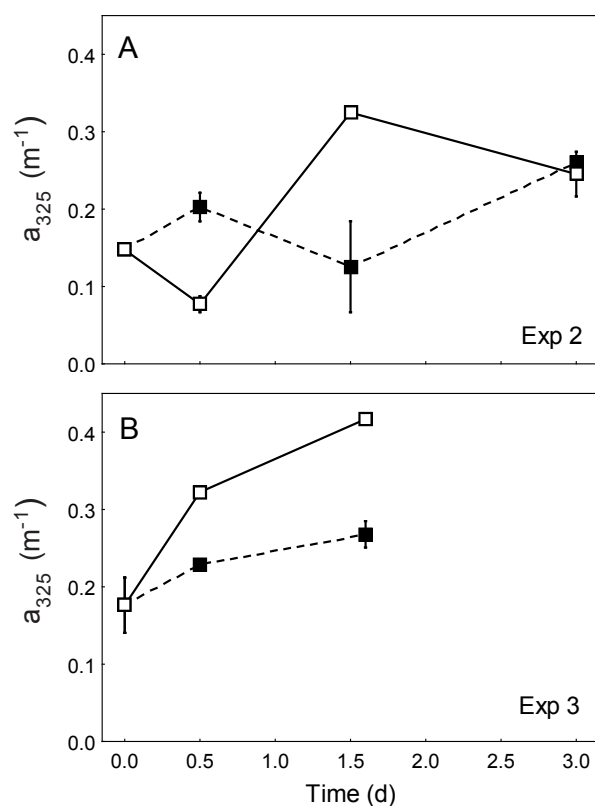


Figure 2.9. Changes in absorption coefficients at 325nm (a_{325} , m^{-1}) over time (days) in the experiments performed using waters from the Mediterranean Sea. Experiments # 2 (st #2 DCM)(A) and exp # 3 (st #15 200m)(B). Open squares= UV treatments. Filled squares= Control treatments. Whiskers= Standard Error.

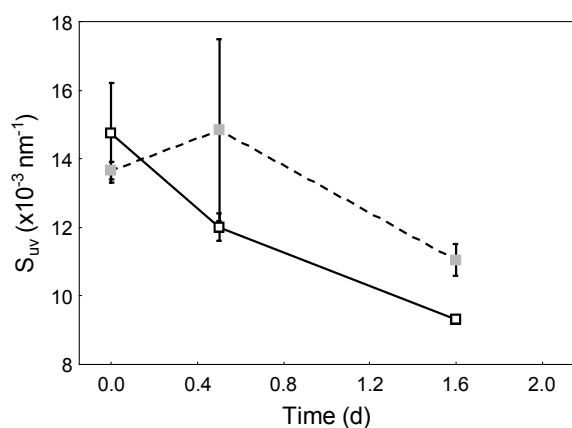


Figure 2.10. Changes in the spectral slopes (S_{uv}) over the incubation time in the UV treatments of experiment # 3 (white squares) and # 4 (grey squares). Whiskers= Standard Error

Table 2.9. Photoreactivity rates in time units (d^{-1}) and half lives (d) at 325 and 443 nm determined in the experiments performed with Mediterranean Sea waters.

Exp	Location	Process	k_{325} (d^{-1})	k_{443} (d^{-1})	Duplication time ₃₂₅ (d)	Duplication time ₄₄₃ (d)
1	St #2 200m	Both	0.11 ± 0.42	1.637	0.6 ± 2.5	0.6
2	St #2 DCM	Both	0.21 ± 0.05	0.544 ± 0.163	5.1 ± 1.2	2.0 ± 0.6
3	St #15 200m	Photo-humification	0.56	0.893	1.8	1.1
4	St #15 DCM	Photo-humification	0.09 ± 0.07	0.321 ± 0.053	34.8 ± 28.6	3.2 ± 0.5

CDOM PHOTOREACTIVITY IN THE NORTH SEA

In the two photoreactivity experiments performed with North Sea waters, significant photobleaching in a_{325} and a_{443} were observed over time in the UV treatments, while no significant changes were detected in the controls (Table 2.10, Fig. 2.11). Bacterial growth was not detected in these experiments. The spectral slopes did not change in experiment # 1 and decreased from t_0 to t_1 in experiment 2 (Fig. 2.12).

The cumulative sunlight doses at UVB, UVA and PAR were 1.14 kJ m^{-2} of UVB, 412 kJ m^{-2} of UVA and $7552 \mu\text{E cm}^{-2}$ of PAR in the roof (exp # 1) and 29.3 kJ m^{-2} of UVB, 1149 kJ m^{-2} of UVA and $2916 \mu\text{E cm}^{-2}$ of PAR in the culture room (exp # 2). The photobleaching rates were -0.072 and -0.103 d^{-1} at 325nm and -0.020 and -0.104 at 443nm, which corresponded to half lives from 3.7 to 10.2 days (Table 2.11).

Table 2.10. Results of repeated measures ANOVA to test differences over time in control vs UV treatments of the North Sea photoreactivity experiments.

Experiment	Location	Effect	F	p
1	St #1 5m	UV	11.26	< 0.05
		Time * UV	7.52	< 0.01
2	St #2 5m	UV	36.0	< 0.05
		Time * UV	11.38	< 0.01

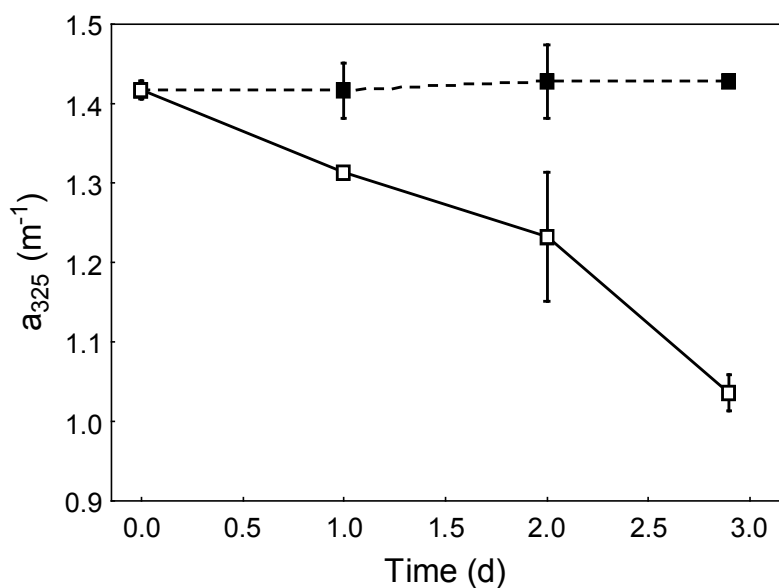


Figure 2.11. Changes in absorption coefficients at 325nm (a_{325} , m^{-1}) over time (days) in one photoreactivity experiment performed using water from North Sea. Experiment # 2 (st #2 at 5m). Open squares= UV treatment. Filled squares= Control treatment. Whiskers= Standard Error.

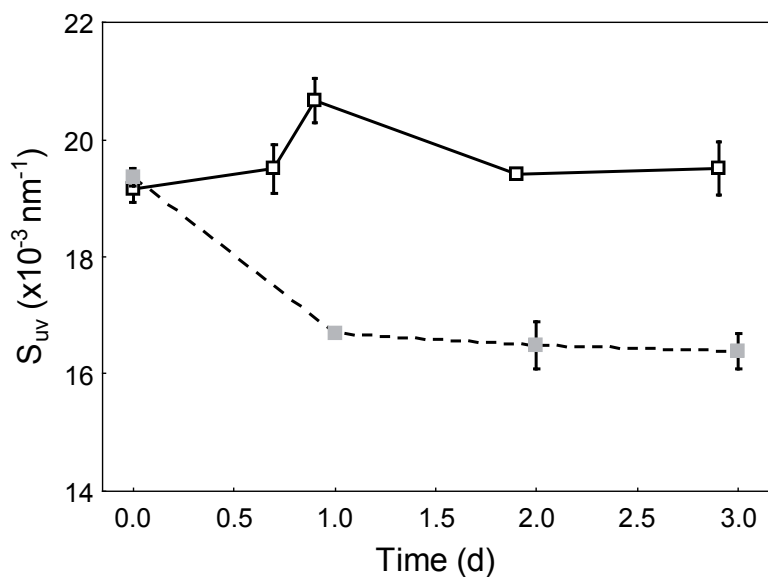


Figure 2.12. Changes in the spectral slopes (S_{uv}) over the incubation time in the UV treatments of experiment # 1 (white squares) and # 2 (grey squares). Whiskers= Standard Error.

Table 2.11. Photoreactivity rates in time units (d⁻¹) and half lives (d) at 325 and 443 nm determined in the experiments performed with North Sea waters.

Exp	Location	Process	k_{325} (d ⁻¹)	k_{443} (d ⁻¹)	Half life ₃₂₅ (d)	Half life ₄₄₃ (d)
1	St #1 5m	Photobleaching	-0.072 ± 0.011	-0.020 ± 0.032	10.2 ± 1.8	3.7 ± 9.5
2	St #2 5m	Photobleaching	-0.104 ± 0.007	-0.104 ± 0.030	6.7 ± 1.4	7.3 ± 1.7

DISCUSSION

The photoreactivity experiments performed illustrate the complexity of CDOM photoreactions in marine systems. We observed the two processes, photobleaching and photohumification of CDOM, with perceptible CDOM changes within days. The most common pattern was net CDOM photobleaching in those areas with high CDOM (North Sea and most areas in the Southern Ocean) and a net photohumification in those experiments performed using waters with low initial CDOM (Bellingshausen Sea in the Southern Ocean and Mediterranean Sea). However, these changes were not consistent over the different experiments in the three study areas.

CDOM PHOTOREACTIVITY IN THE SOUTHERN OCEAN

We observed a significant CDOM photobleaching over time in 5 of 7 experiments, and photobleaching rates were in the range of a few days. These results are consistent with previous experimental studies in this ecosystem that reported significant CDOM photodegradation in less than 24 hours (Kieber and Mopper, 1995; Obernosterer et al., 2001; Bertilsson et al., 2004). Consequently, this process could explain the lower CDOM values found in surface waters (Clementson et al., 2001; Misic et al., 2006). Photobleaching losses involved an increase in the spectral slopes, consistent with previous works (Del Vecchio and Blough, 2002). Although we observed some changes in CDOM over incubation time also in control treatments, we generally detected more accentuated decreases in the

UV treatments. In those experiments where photobleaching was not noticeable (experiments 3 and 6) this fact could be explained by different reasons, such as that CDOM from these sites were apparently resistant to photobleaching or, alternatively, the sunlight dose received was not enough to induce this process. Photobleaching resistance can be related to DOM residence time in the photic layer (Ortega-Retuerta et al., 2007). Finally, in experiment # 7, performed using waters from Bellingshausen Sea, although a net increase of CDOM was observed in both UV and control treatments, this increase in absorption was lower in the light treatment, so light was likely causing CDOM photobleaching at some extent. Although in situ irradiance measurements were not available for this experiment, cloudy days during the incubation could yield lower cumulative sunlight doses.

The increases in CDOM observed, generally starting after three days (e.g. experiments # 4 and 5) can be attributed to bacteria that could be generating CDOM, but this contribution cannot be confirmed as bacterial growth was not checked in these experiments.

EFFECT OF CDOM PHOTOPRODUCTS ON BACTERIOPLANKTON IN THE SOUTHERN OCEAN

The exposure of DOM to solar radiation before setting up re-growth experiments yielded contrasting bacterial responses to the presence of photoproducts. Photoproducts had a negative short-term effect on bacterial abundance and production in both experiments performed using Deception Island waters (Table 2.6, 2.7, Figs 2.7, 2.8). These results suggest a negative effect of photoproducts to bacteria at this short timescale, probably due to the existence of toxic byproducts (reactive oxygen species) (Blough and Zepp, 1995). These compounds cause a delay on the start of the exponential growth phase. However, due to the short residence times of reactive oxygen species (Blough and Zepp, 1995), the negative short-term effect of photoproducts may be compensated at a longer time. Indeed, higher BP was observed at time 5 in one of the experiments (see Fig. 2.8).

By contrast, in the experiments performed using Livingston Island waters (# 3 and 4), the lack of clear photobleaching or photohumification resulted in the absence of significantly different responses of bacterioplankton. The substrate used for these experiments is likely both photochemical and biologically recalcitrant, which was also suggested by the lower increases in BP and BA than in the ex-

periments # 1 and 2. These last results (exp # 3 and 4) are consistent with previous experimental studies in the area (Bertilsson et al., 2004) while Obernosterer et al. (2001) showed a negative effect within the first 24 hours.

CDOM PHOTOREACTIVITY IN THE MEDITERRANEAN SEA

In this ecosystem, the dominant process was CDOM photohumification, contrasting to those performed in the Southern Ocean and in the North Sea. In Mediterranean Sea waters, photobleaching has been suggested in field studies (Momzikoff et al., 1994; Obernosterer et al., 1999a) and confirmed experimentally using mesopelagic waters from the strait of Gibraltar and Aegean Sea (Obernosterer et al., 1999b). However, like in this study, no significant photobleaching has been observed in waters from the chlorophyll maximum in the same area (Obernosterer et al., 1999b) or in the Northern Adriatic Sea (Obernosterer and Herndl, 2000).

These experimental results contrast to the vertical pattern observed in the field (see chapter 1), where lower CDOM concentration were found within the upper mixed layer than below it. Waters from this area likely have an autochthonous origin, with a high contribution of low-molecular weight compounds (Obernosterer and Herndl, 2000) with low chromophoricity. Moreover, the Mediterranean Sea is submitted to an intense and frequent solar regime, in contrast to the Southern Ocean where solar irradiance is restricted to the austral summer; so waters from Mediterranean Sea have been likely submitted to previous photobleaching which preclude us to determine photobleaching rates. In addition to photohumification, the increases in CDOM can be partially due to the growth of bacteria in the experiments.

CDOM PHOTOREACTIVITY IN THE NORTH SEA

The photoreactivity experiments performed with North Sea waters revealed a significant photobleaching in three days in both experiments, consistent with the literature (Obernosterer and Herndl, 2000), although photobleaching was not accompanied by an increase in the slopes. The lower photobleaching coefficients detected in North Sea waters than in the Southern Ocean can be due to the lower cumulative sunlight doses received in the North Sea experiments, representative of a less intense radiation regime at this latitude.

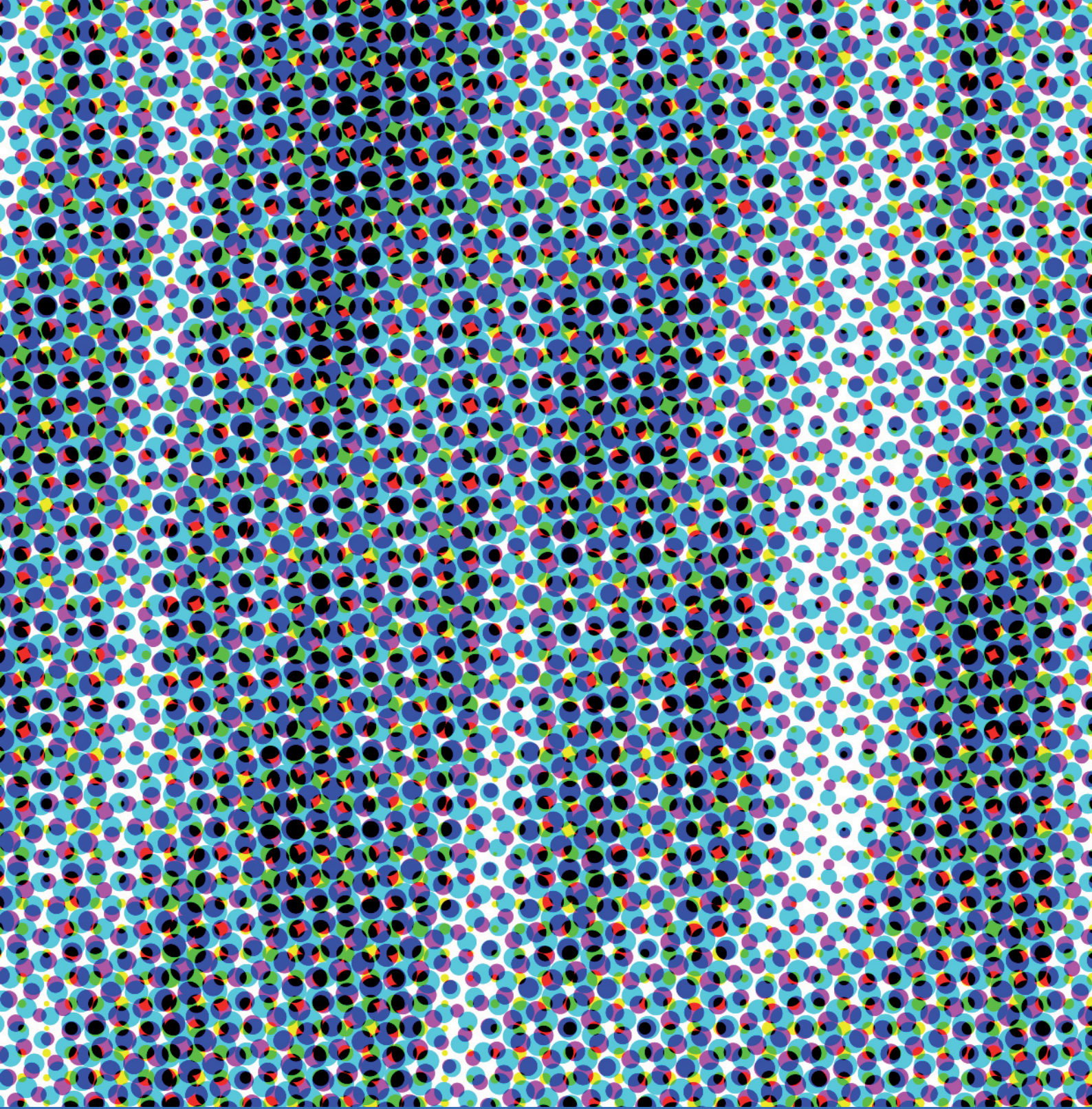
Overall, in this chapter we have underscored the photoreactive nature of CDOM in the different marine ecosystems and, consequently, the key role of solar radiation on CDOM dynamics. Photobleaching could be acting as a sink of CDOM within days in waters with initially high CDOM values, explaining the lower CDOM values found in many upper layers. Alternatively, photohumification could represent a source of CDOM in clear waters at similar timescales. These two processes likely occur simultaneously in the field. In addition, CDOM photobleaching could result in a short-term reduction of bacterioplankton growth, likely due to the liberation of byproducts such as reactive oxygen species.

REFERENCES

- BENNER, R. and B. BIDDANDA (1998) Photochemical transformations of surface and deep marine dissolved organic matter: Effects on bacterial growth. *Limnology and Oceanography*. 43: 1373-1378.
- BERTILSSON, S., P. CARLSSON and W. GRANÉLI (2004) Influence of solar radiation on the availability of dissolved organic matter to bacteria in the Southern Ocean. *Deep-Sea Research Part II-Topical Studies in Oceanography*. 51: 2557-2568.
- BERTILSSON, S. and L.J. TRANVIK (2000) Photochemical transformation of dissolved organic matter in lakes. *Limnology and Oceanography*. 45: 753-762.
- BLOUGH, N.V. and R.G. ZEPP (1995) Reactive Oxygen Species in natural waters. *In*: C. S. Foote, J. S. Valentine, A. Greenberg and J. F. Liebman (eds.) *Chemistry*, vol. 5. Blackie, London. pp. 280-335.
- CLEMENTSON, L.A., J.S. PARLOW, A.R. TURNBULL, D.C. MCKENZIE and C.E. RATHBONE (2001) Optical properties of waters in the Australasian sector of the Southern Ocean. *Journal of Geophysical Research-Oceans*. 106: 31611-31625.
- DE HAAN, H. (1993) Solar UV-Light Penetration and Photodegradation of Humic Substances in Peaty Lake Water. *Limnology and Oceanography*. 38: 1072-1076.
- DEL VECCHIO, R. and N.V. BLOUGH (2002) Photobleaching of chromophoric dissolved organic matter in natural waters: kinetics and modeling. *Marine Chemistry*. 78: 231-253.
- KIEBER, D.J., J. MCDANIEL and K. MOPPER (1989) Photochemical source of biological substrates in seawater: implications for carbon cycling. *Nature*. 341: 637-639.
- KIEBER, D.J. and K. MOPPER (1995) Photochemistry of Antarctic waters during the 2004 austral summer. *Antarctic Journal of the United States*. 30: 150-151.
- KIEBER, R.J., L.H. HYDRO and P.J. SEATON (1997) Photooxidation of triglycerides and fatty acids in seawater: Implication toward the formation of marine humic substances. *Limnology and Oceanography*. 42: 1454-1462.
- KOUASSI, A.M. and R.G. ZIKA (1992) Light-Induced destruction of the absorbency property of dissolved organic matter in seawater. *Toxicological and Environmental Chemistry*. 35: 195-211.
- LINDELL, M.J., W. GRANÉLI and L.J. TRANVIK (1995) Enhanced bacterial growth

- in response to photochemical transformation of dissolved organic matter. *Limnology and Oceanography*. 40: 195-199.
- MILLER, W.L. and R.G. ZEPP (1995) Photochemical production of dissolved inorganic carbon from terrestrial organic matter - significance to the oceanic organic-carbon cycle. *Geophysical Research Letters*. 22: 417-420.
- MISIC, C., M. CASTELLANO, N. RUGGIERI and P. POVERO (2006) Dissolved organic matter characterisation and temporal trends in Terra Nova Bay (Ross Sea, Antarctica). *Estuarine Coastal and Shelf Science*. 70: 405-414.
- MOMZIKOFF, A., S. DALLOT and G. GONDRY (1994) Distribution of seawater fluorescence and dissolved flavins in the Almeria-Oran front (Alboran Sea, Western Mediterranean Sea). *Journal of Marine Systems*. 5: 361-376.
- MOPPER, K. and D.J. KIEBER (2000) Marine photochemistry and its impact on carbon cycling *In*: S. de Mora, S. Demers and M. Vernet (eds.) *The Effects of UV Radiation in the Marine Environment*, vol. 10. Cambridge University Press, Cambridge. pp. 101-129.
- MOPPER, K., X.L. ZHOU, R.J. KIEBER, D.J. KIEBER, R.J. SIKORSKI and R.D. JONES (1991) Photochemical degradation of dissolved organic carbon and its impact on the oceanic carbon cycle. *Nature*. 353: 60-62.
- MORAN, M.A. and R.G. ZEPP (1997) Role of photoreactions in the formation of biologically labile compounds from dissolved organic matter. *Limnology and Oceanography*. 42: 1307-1316.
- NELSON, N.B. and D.A. SIEGEL (2002) Chromophoric DOM in the open ocean. *In*: D. A. Hansell and C. A. Carlson (eds.) *Biogeochemistry of marine dissolved organic matter*. Academic Press, San Diego.
- OBERNOSTERER, I. and G.J. HERNDL (2000) Differences in the optical and biological reactivity of the humic and nonhumic dissolved organic carbon component in two contrasting coastal marine environments. *Limnology and Oceanography*. 45: 1120-1129.
- OBERNOSTERER, I., G. KRAAY, E. DE RANITZ and G.J. HERNDL (1999a) Concentrations of low molecular weight carboxylic acids and carbonyl compounds in the Aegean Sea (Eastern Mediterranean) and the turnover of pyruvate. *Aquatic Microbial Ecology*. 20: 147-156.
- OBERNOSTERER, I., B. REITNER and G.J. HERNDL (1999b) Contrasting effects of solar radiation on dissolved organic matter and its bioavailability to marine bacterioplankton. *Limnology and Oceanography*. 44: 1645-1654.

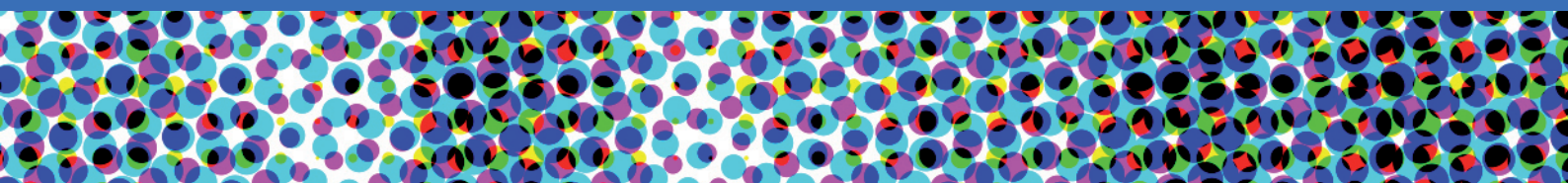
- OBERNOSTERER, I., R. SÉMPÉRE and G.J. HERNDL (2001) Ultraviolet radiation induces reversal of the bioavailability of DOM to marine bacterioplankton. *Aquatic Microbial Ecology*. 24: 61-68.
- ORTEGA-RETUERTA, E., E. PULIDO-VILLENA and I. RECHE (2007) Effects of dissolved organic matter photoproducts and mineral nutrient supply on bacterial growth in mediterranean inland waters. *Microbial Ecology*. 54: 161-169.
- OSBURN, C.L., H.E. ZAGARESE, D.P. MORRIS, B.R. HARGREAVES and W.E. CRAVERO (2001) Calculation of spectral weighting functions for the solar photobleaching of chromophoric dissolved organic matter in temperate lakes. *Limnology and Oceanography*. 46: 1455-1467.
- RECHE, I., M.L. PACE and J.J. COLE (1998) Interactions of photobleaching and inorganic nutrients in determining bacterial growth on colored dissolved organic carbon. *Microbial Ecology*. 36: 270-280.
- RECHE, I., M.L. PACE and J.J. COLE (1999) Relationship of trophic and chemical conditions to photobleaching of dissolved organic matter in lake ecosystems. *Biogeochemistry*. 44: 259-280.
- RECHE, I., M.L. PACE and J.J. COLE (2000) Modeled effects of dissolved organic carbon and solar spectra on photobleaching in lake ecosystems. *Ecosystems*. 3: 419-432.
- SKOOG, A., M. WEDBORG and E. FOGELQVIST (1996) Photobleaching of fluorescence and the organic carbon concentration in a coastal environment. *Marine Chemistry*. 55: 333-345.
- TRANVIK, L. and S. KOKALJ (1998) Decreased biodegradability of algal DOC due to interactive effects of UV radiation and humic matter. *Aquatic Microbial Ecology*. 14: 301-307.
- TRANVIK, L.J. and S. BERTILSSON (2001) Contrasting effects of solar UV radiation on dissolved organic sources for bacterial growth. *Ecology Letters*. 4: 458-463.
- VALENTINE, R.L. and R.G. ZEPP (1993) Formation of carbon monoxide from the photodegradation of terrestrial dissolved organic carbon in natural waters. *Environmental Science & Technology*. 27: 409-412.
- WHITEHEAD, R.F., S. DE MORA, S. DEMERS, M. GOSSELIN, P. MONFORT and B. MOSTAJIR (2000) Interactions of ultraviolet-B radiation, mixing, and biological activity on photobleaching of natural chromophoric dissolved organic matter: A mesocosm study. *Limnology and Oceanography*. 45: 278-291.



Chapter 3:
**Chromophoric dissolved organic matter generation by
bacterioplankton and Antarctic krill in the Southern Ocean and
Mediterranean Sea.**

Ortega-Retuerta, Frazer, T.K., Duarte, C.M., and Reche, I.

Abbreviated title: CDOM generation by bacteria and krill



INTRODUCTION

Dynamics of chromophoric dissolved organic matter (CDOM) in the open ocean, where land inputs have a minimal influence, reflect the net balance between local sources and sinks. Biological generation of CDOM is likely an important source of optically labile compounds in the open ocean (Nelson et al., 2004; Steinberg et al., 2004; Nieto-Cid et al., 2006). However, there are few studies that have quantified the rates of biologically generated CDOM. Phytoplankton are the dominant sources of organic carbon in the open ocean, but the generation of CDOM appears to occur indirectly as a consequence of further bacterial processing of algal exudates (Nelson et al., 1998; Rochelle-Newall and Fisher, 2002; Cammack et al., 2004) or through photoalteration of this DOM released by algae (Kieber et al., 1997; Rontani, 1998; Reche et al., 2001). CDOM may also be generated directly through extracellular release by prokaryotes (Nelson et al., 2004; Steinberg et al., 2004), zooplankton excretion (Steinberg et al., 2004; Urban-Rich et al., 2006) and coral reefs (Boss and Zaneveld, 2003).

Bacterioplankton can regulate DOM composition through the selective consumption of labile compounds and subsequent release of humic-like (chromophoric) substances (Tranvik, 1993; Kawasaki and Benner, 2006) that are generally biorefractory. The production of this material, that can represent a similar or even higher proportion than new bacterial biomass generation, can comprise a significant proportion of total DOM pool extending its residence time in the water column with obvious consequences for carbon cycling (Brophy and Carlson, 1989;

Ogawa et al., 2001). CDOM generation by bacterial DOM processing appears to be dependent on several factors such as substrate quality, bacterial growth stage (exponential vs stationary phase), previous photochemical transformations, and/or nitrogen availability (Kramer and Herndl, 2004; Nelson et al., 2004; Biers et al., 2007). In addition, its persistence and optical properties appear to be very variable, and the contribution of CDOM generated by bacteria to CDOM dynamics is poorly understood and explored.

In the Southern Ocean, Antarctic krill (*Euphasia superba*) often forms large swarms that are associated to ice boundaries (Brierley and Watkins, 2000). These organisms play a pivotal role in the Antarctic food web as they are both consumers and preys, and also control primary production and recycling processes (Smetacek and Nicol, 2005; Nicol, 2006; Tovar-Sanchez et al., 2007). Thus, their influence on optical properties of organic matter and carbon cycling in the area are feasible and should be also considered. Although heterotrophic organisms such as zooplankton or protozoans also generate CDOM (Steinberg et al., 2004; Urban-Rich et al., 2006), published data on CDOM generation by euphausiids in seawater are scarce and not species-specific (Steinberg et al., 2004).

In this chapter, we experimentally determined the magnitude and optical quality of CDOM generated by bacterioplankton in the Southern Ocean and Mediterranean Sea, using different substrates (Southern Ocean, with and without photoproducts) or locations (Mediterranean Sea), and by Antarctic krill *Euphasia superba* also in the Southern Ocean. In addition, we assessed the potential contribution of these agents to CDOM dynamics in the study areas.

MATERIAL AND METHODS

BACTERIAL CDOM GENERATION IN THE SOUTHERN OCEAN

To quantify bacterial CDOM generation in the Southern Ocean, we applied the same experimental design as explained in chapter 2 to study the effects of DOM photoproducts on bacteria in 2004. Briefly, 8 re-growth cultures were set up with GF/F filtered water from two different locations and depths (Deception and Livingston Islands, and waters from the surface and below the euphotic layer). As solar radiation can affect the structural conformation of dissolved organic matter and modify its bioreactivity (Moran and Zepp, 1997), we also assessed the potential changes in bacterial CDOM generation associated with the presence of photoproducts by including a treatment with photoproducts for each location and depth. Samples were taken for CDOM characterization at the beginning and end of each re-growth culture.

BACTERIAL CDOM GENERATION IN THE MEDITERRANEAN SEA.

To quantify CDOM biogeneration by bacterioplankton in the Mediterranean Sea, eight bacterial re-growth experiments were set up in triplicate (Fig 3.1). Water was selected from two locations (stations #2 and #15) and depths (200 m and the deep chlorophyll maximum (DCM), situated at 40 and 80m respectively). In chapter 2 are resumed the field dissolved organic carbon, chlorophyll *a* and bacterial abundance values for each experiment (Table 2.2).

Water was initially filtered by glass fiber filters (Whatman GF/F, nominal pore size $\sim 0.7 \mu\text{m}$), to eliminate all phytoplankton and heterotrophic consumers. To prevent the growth of a biased and unrepresentative bacterial community due to filtration (Gasol and Morán, 1999), water was subsequently inoculated with unfiltered water from the same location (10% of final volume).

Re-growth cultures were set up in triplicate in 250 ml sterilized glass flasks, inside a recirculating water bath at surface seawater temperature (17-22 °C) and in the dark (flasks were covered with opaque plastic bags). Two different treatments were included for each experiment: one treatment including natural bacteria (Bact.) and one treatment were Sodium azide (0.02 % final concentration) was

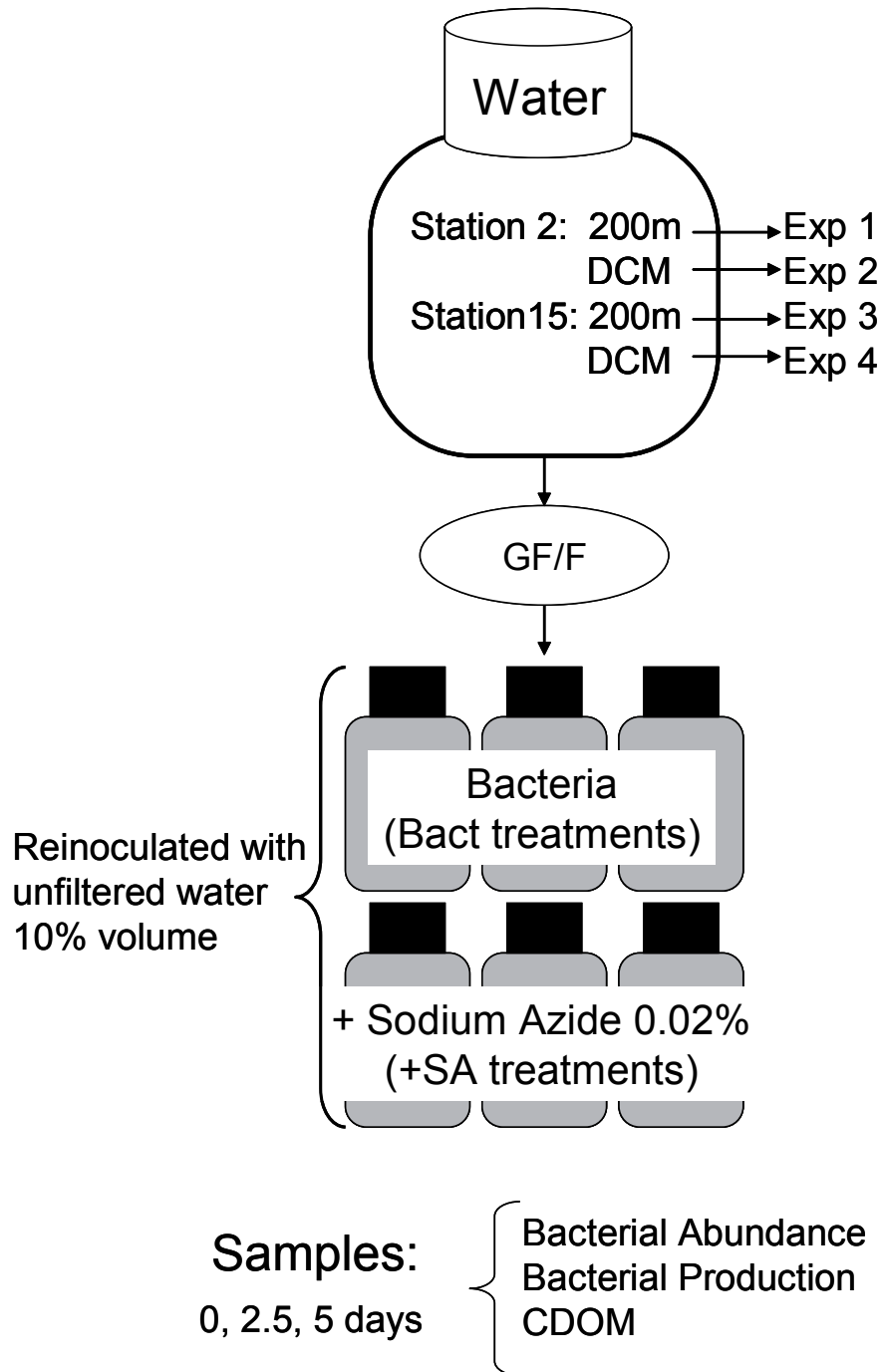


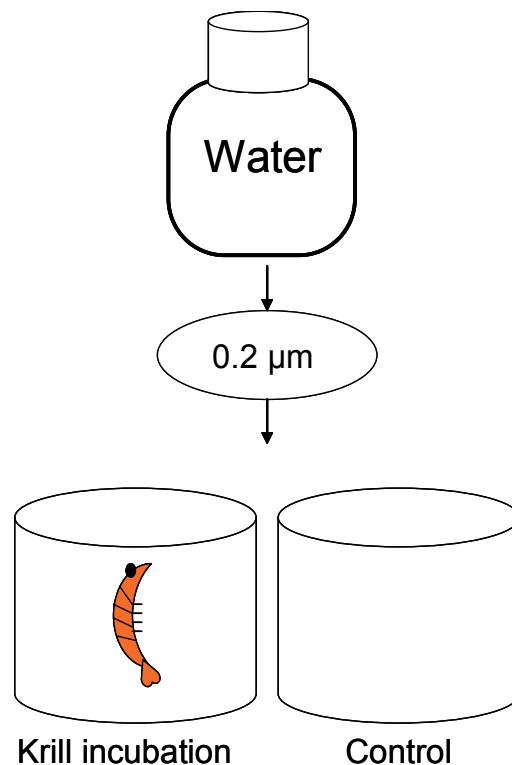
Figure 3.1. Experimental design to quantify bacterial CDOM generation in the Mediterranean Sea.

added to control treatments to inhibit bacterial growth (+SA). The additions of Sodium Azide were repeated every 3 days.

Samples were taken at the beginning and after 2.5 (t₁) and 5 (t₂) days for CDOM characterization, bacterial abundance (BA) and bacterial production (BP).

KRILL CDOM GENERATION EXPERIMENTS IN THE SOUTHERN OCEAN

We performed 15 simple incubations in 4 sets to characterize and quantify CDOM released by Antarctic krill, *Euphasia superba*. Adult krill were collected west of Anvers Island during January 2004 and maintained in large-volume, flow-through aquaria at Palmer Station prior to transport and experimentation at Juan Carlos I Station. For each incubation, individual krill were placed in 1-l glass jars pre-filled with 0.7 l of 0.2 µm filtered seawater to minimize bacterial influence (Fig 3.2). Replicate controls with 0.2 µm filtered seawater and without krill additions



Sampling t₀ and t_f (12-24h) for CDOM

Figure 3.2. Experimental design to quantify krill CDOM generation in the Southern Ocean.

were incubated in parallel. Incubations were carried out for 12 to 24 hours at ambient light and temperature conditions. Samples for CDOM characterization were taken at the beginning and end of each experiment. To assess the potential growth of bacteria attached to krill or non-excluded by 0.2 μm -filtration during the incubations, we set up another experiment subject to the same conditions, and took samples for bacterial abundance and production at the beginning and after 24h.

DETERMINATION OF BIOGENERATION RATES

We calculated daily CDOM increases (Δa_λ , $\text{m}^{-1}\text{d}^{-1}$) in all bacterial and krill experiments as follows:

$$\Delta a_\lambda = \frac{a_{\lambda f} - a_{\lambda 0}}{t}$$

where λ is the reference wavelength (nm), a_λ is the absorption coefficient (m^{-1}), f is the final time, 0 is the initial time, and t is the incubation time in days. The reference wavelengths (λ) were 325 and 443 nm.

To compare these CDOM increases among the different treatments and experiments, we calculated the percentage of Δa_λ (d^{-1}) using the following expression:

$$\% \Delta a_\lambda = \frac{\Delta a_\lambda}{\Delta a_0} \times 100$$

where λ is the reference wavelength (325 or 443 nm), Δa_λ is the daily CDOM increase ($\text{m}^{-1}\text{d}^{-1}$), a_λ is the absorption coefficient (m^{-1}), and 0 is the initial time.

We determined “experimental bacterial CDOM generation rates” ($\text{m}^{-1} \text{d}^{-1}$ per BA, BP or cell-sp BP units) using linear regressions to relate $\Delta a_{325,443}$ to mean bacterial abundance (BA), bacterial production (BP) and cell-specific bacterial production (cell-sp BP) of each re-growth treatment. We forced the regression line to pass through the origin to avoid the effects of a high CDOM background. In the experiments performed using Mediterranean Sea waters, we considered only the

first interval of the experiments (from t_0 to t_1) since CDOM generation by bacteria is highest within 2-3 days, likely coinciding with the exponential growth phase (Nelson et al., 2004; Biers et al., 2007). To extrapolate these experimental rates to “field CDOM bacterial generation rates” ($\text{m}^{-1} \text{d}^{-1}$) we used average BA and BP values determined in the Southern Ocean and Mediterranean Sea.

We expressed “experimental krill CDOM generation rates” per organism and liter, as daily increases in $a_{325,443}$ ($\text{m}^{-1} \text{d}^{-1}$) subtracting the changes in CDOM per day in the controls without krill additions, and extrapolating to a density of one organism per liter correcting by the volume used in the incubations (0.7 l). To extrapolate the experimental rates to “field CDOM biogeneration by krill” ($\text{m}^{-1} \text{d}^{-1}$), we used krill abundance data from the literature. We used an average krill density in spring-summer seasons in Antarctic waters between 1977 and 1996 of 77.8 individual/1000 m^3 (Loeb et al., 1997), and a krill density within swarms of 1000 individual m^{-3} (Brierley and Watkins, 2000).

We estimated CDOM duplication times attributable to bacterioplankton or to krill in the study areas relating field data of $a_{325,443}$ in the Antarctic Peninsula and Mediterranean Sea (chapter 1) to the field CDOM generation rates derived from the experiments. We used the following equation:

$$\text{field CDOM}_{\lambda} \text{ duplicate time (d)} = \frac{\text{field CDOM}_{\lambda} \text{ (m}^{-1}\text{)}}{\text{field CDOM}_{\lambda} \text{ generation rates (m}^{-1} \text{d}^{-1}\text{)}}$$

where λ are the reference wavelengths (nm).

RESULTS

BACTERIAL CDOM GENERATION IN THE SOUTHERN OCEAN

The exposure of water to incident solar radiation to generate photoproducts for bacterial CDOM generation experiments yielded site-specific differences (see chapter 2).

At the conclusion of the incubation periods, increases in a_{325} and a_{443} absorption coefficients were found in all bacterial re-growth cultures, irrespective of site, depth, or treatment imposed (Table 3.1). However, the magnitude of CDOM daily increase ($\Delta a_{325,443}$) was highly variable depending on the initial conditions of each incubation. CDOM daily increases ($\Delta a_{325,443}$ $\text{m}^{-1} \text{d}^{-1}$) were comparatively higher in the re-growth cultures with photoproducts than in those where photoproducts were absent, except for those incubations involving water collected at 50 m from the Livingston Island site. The values of Δa_{325} ranged from 0.049 to 0.375 $\text{m}^{-1} \text{d}^{-1}$ and Δa_{443} ranged from 0.015 to 0.142 $\text{m}^{-1} \text{d}^{-1}$ (Table 3.1). The percentage of generated CDOM with respect to the initial absorption ($\% \Delta a_{325,443}$) showed a similar pattern.

Table 3.1. Daily CDOM increases at 325 and 443 nm ($\text{m}^{-1} \text{d}^{-1}$) and relative percentage with respect to initial absorption at 325 and 443 nm (d^{-1}) in all bacterial re-growth experiments. No Ph: Treatments without photoproducts. Ph: Treatments with photoproducts.

Location	Depth	Treatment	Δa_{325} ($\text{m}^{-1} \text{d}^{-1}$)	Δa_{443} ($\text{m}^{-1} \text{d}^{-1}$)	$\% \Delta a_{325}$ (d^{-1})	$\% \Delta a_{443}$ (d^{-1})
Deception	0m	No Ph	0.056	0.023	8.9	13.8
		Ph	0.099	0.048	21.6	76.9
	150m	No Ph	0.265	0.099	11.8	13.3
		Ph	0.375	0.142	33.4	43.3
Livingston	0m	No Ph	0.126	0.056	16.2	23.1
		Ph	0.148	0.052	21.8	22.4
	50m	No Ph	0.172	0.057	15.2	14.8
		Ph	0.049	0.015	4.0	3.8

In addition to the quantitative differences in CDOM generation observed in the different re-growth cultures, the spectral shape of bacterial generated CDOM also differed markedly. In the incubations carried out with water collected near Deception Island, where marked CDOM photobleaching was detected prior to the onset of the re-growth cultures (see Fig 2.6 in chapter 2), the CDOM spectra generated by bacteria showed distinctive peaks between 290-295 nm in the treatments with photoproducts. In comparison, the treatments without photoproducts exhibited the characteristic negative exponential shape (Fig. 3.3A). In the experiments performed using water from Livingston Island, where photobleaching was negligible, all CDOM spectra generated by bacteria were similar, approaching a negative exponential function (Fig. 3.3B). The spectral slopes of bacterial generated CDOM from 290 to 400 nm (S_{uv}) ranged from 7.8 to 12.6 $\times 10^{-3} \text{ nm}^{-1}$ and were higher in the experiments with deep waters (150 or 50 m). Similar spectral slopes were observed in treatments with and without photoproducts.

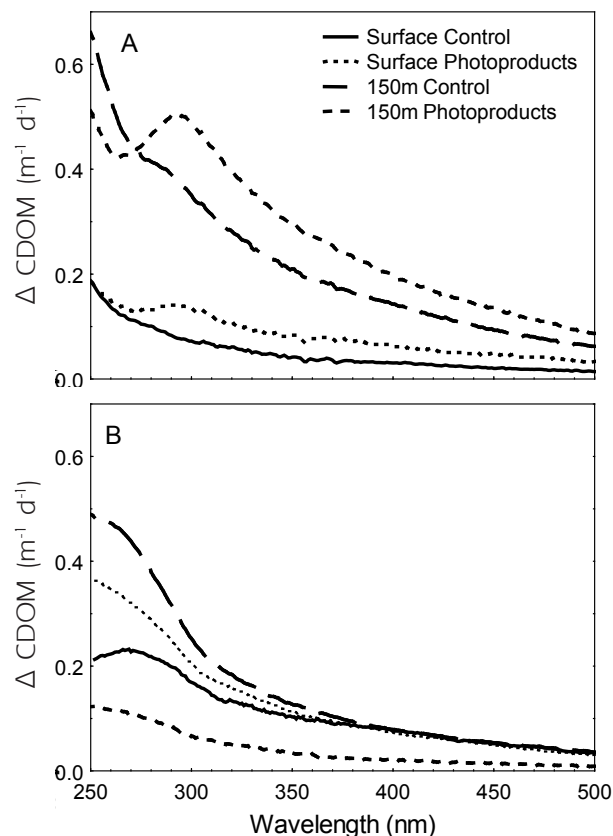


Figure 3.3. Bacterial generated CDOM spectra from 250 nm to 500 nm (final – initial per day) in the different treatments using Deception Island waters (A) and Livingston Island waters (B) of the Southern Ocean.

Daily CDOM increases were related to average BP and cell-specific BP in the incubations (Fig. 3.4), but not to BA. The slopes of the regression lines passing through the origin were not significantly different from the regression lines with the intercept and were used as estimates of bacterial CDOM generation rates (Table 3.2). An extrapolation of these experimental rates ($\Delta a_{325,443}$ per unit of BP or cell-specific BP) to field BP and cell-specific BP average values yielded estimates of field CDOM generation rates of 10.2 and $4.3 \times 10^{-3} \text{ m}^{-1} \text{ d}^{-1}$ at 325 nm and 3.8 and $1.7 \times 10^{-3} \text{ m}^{-1} \text{ d}^{-1}$ at 443 nm (Table 3.2). These CDOM generation rates lead to CDOM duplication times of 31 to 78 days (Table 3.2).

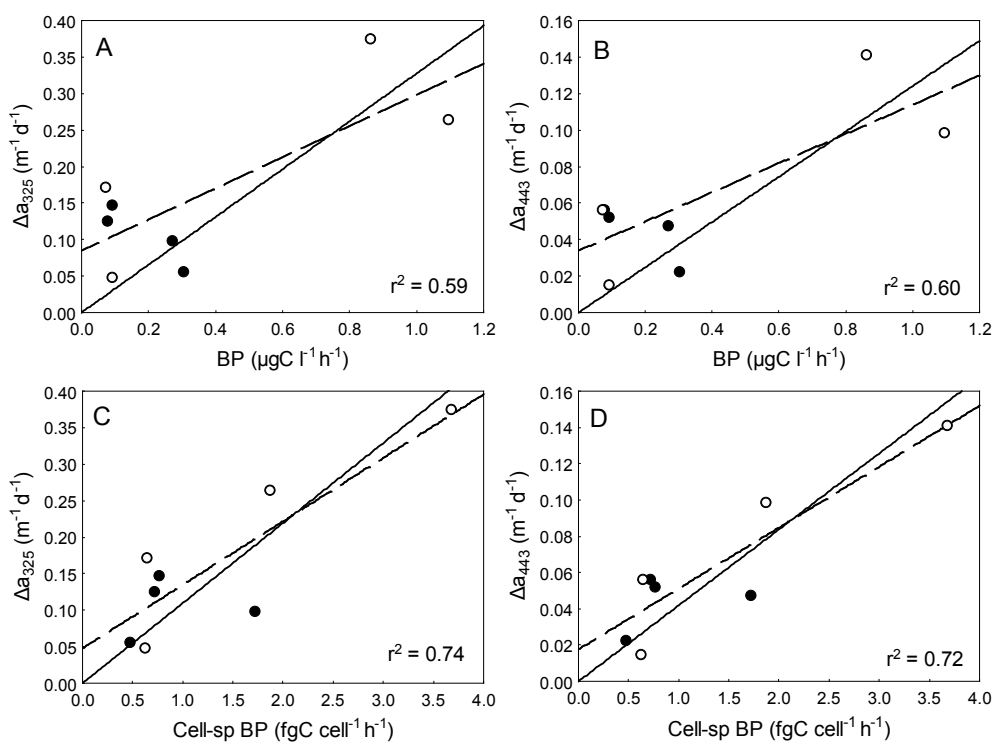


Figure 3.4. Relationships between Δa_{325} or Δa_{443} in all re-growth experiments and mean BP (A and B) and mean cell-specific BP (C and D). Open circles: Treatments with photoproducts. Filled circles: Treatments without photoproducts. Solid lines represent the regression lines passing through the origin, and dashed lines represent the regression lines with the intercept. In no cases the two equations were significantly different ($p > 0.05$). The slopes of the solid lines represent the experimental bacterial CDOM generation rates ($\text{m}^{-1} \text{ d}^{-1}$ per $\mu\text{gC l}^{-1} \text{ h}^{-1}$ or per $\text{fgC cell}^{-1} \text{ h}^{-1}$, see Table 3.2)

Table 3.2. Bacterial CDOM generation rates of absorption at 325 nm and 443 nm obtained experimentally and calculated from BP ($\text{m}^{-1} \text{d}^{-1}$ per $\mu\text{g C l}^{-1} \text{h}^{-1}$), and from cell-specific BP ($\text{m}^{-1} \text{d}^{-1}$ per $\text{fg C cell}^{-1} \text{h}^{-1}$), field bacterial CDOM generation rates at 325 and 443 nm ($\text{m}^{-1} \text{d}^{-1}$) estimated for field conditions in the Southern Ocean, and CDOM duplication times (d).

	BP	Cell-sp BP
Experimental a_{325} generation rate ($\text{m}^{-1} \text{d}^{-1}$ per $\mu\text{g C l}^{-1} \text{h}^{-1}$ or per $\text{fg C cell}^{-1} \text{h}^{-1}$)	0.3275	0.1097
Experimental a_{443} generation rate ($\text{m}^{-1} \text{d}^{-1}$ per $\mu\text{g C l}^{-1} \text{h}^{-1}$ or per $\text{fg C cell}^{-1} \text{h}^{-1}$)	0.1241	0.0419
Field Δa_{325} ($\times 10^{-3} \text{ m}^{-1} \text{d}^{-1}$)	10.2	4.3
Field Δa_{443} ($\times 10^{-3} \text{ m}^{-1} \text{d}^{-1}$)	3.8	1.7
Field a_{325} duplication time (d)	33	78
Field a_{443} duplication time (d)	31	72

BACTERIAL CDOM GENERATION IN THE MEDITERRANEAN SEA

Bacteria increased both in abundance and production in all experiments and treatments (Fig 3.5). The addition of SA did not prevent completely bacterial growth, but inhibited it partially yielding to lower BA and BP (repeated measures ANOVA, Table 3.3, Fig. 3.5). Increases in BA and BP in the cultures were generally highest in the experiment with water from st#2 and higher when using DCM waters respect to the use of 200m waters. The addition of Sodium Azide yielded abnormally high absorbance at wavelengths below 300nm, but no difference was observed between bact and +SA treatments at longer wavelengths, including 325nm and 443 nm.

Increases in a_{325} and a_{443} absorption coefficients were detected in all bacterial re-growth cultures and treatments in the Mediterranean Sea. CDOM daily increases were highly variable, ranging from 0.022 to 0.172 $\text{m}^{-1} \text{d}^{-1}$ for a_{325} and from 0.003 to 0.027 $\text{m}^{-1} \text{d}^{-1}$ for a_{443} (Table 3.4). Daily increases in CDOM were generally higher in the first set of experiments (performed using waters from station #2) than in the second one (performed using waters from station #15), and higher at the first interval of the experiments (from t_0 to t_1), than at the second interval (from t_1 to t_2). The percentage of generated CDOM ($\% \Delta a_{325,443}$) ranged from 4.4 to 106 % for a_{325} and from 11 to 106% for a_{443} (Table 3.4).

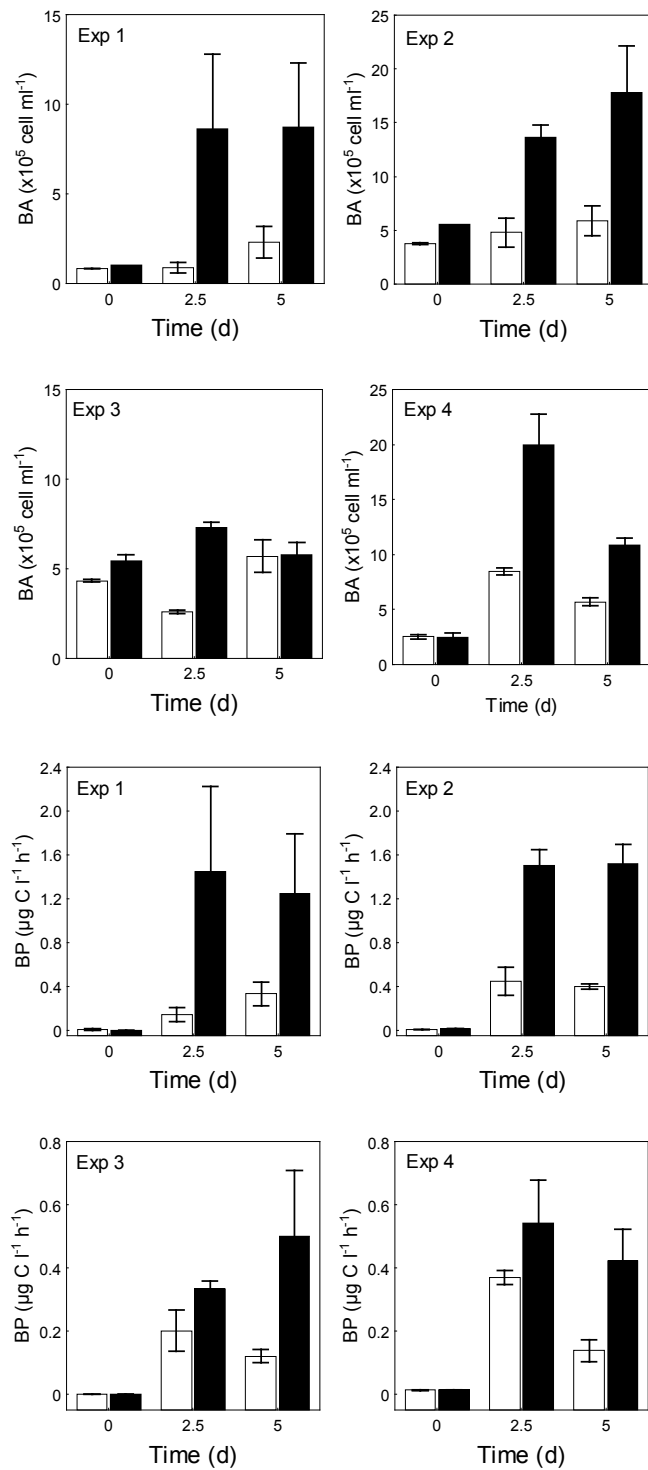


Figure 3.5. Changes in BA (top panels) and BP (bottom panels) over the course of the re-growth cultures performed in the four experiments. White bars: +SA treatments. Black bars: Bact. treatments. Whiskers= Standard Errors. Note the different y-axis scales.

Table 3.3. Results of the repeated measures ANOVA to study differences in bacterial abundance (BA) and production (BP) over the incubation time in bact. and +SA treatments of Mediterranean Sea experiments. ns= not significant.

Variable	Exp. #	Effect	F	p level
BA	1	Sodium Azide	68.02	< 0.05
		Time * SA	0.95	ns
	2	Sodium Azide	17.11	ns (=0.05)
		Time * SA	2.50	ns
	3	Sodium Azide	17.22	ns (=0.05)
		Time * SA	29.70	< 0.01
	4	Sodium Azide	32.91	< 0.05
		Time * SA	30.00	< 0.05
BP	1	Sodium Azide	10.06	< 0.05
		Time * SA	1.20	ns
	2	Sodium Azide	130.73	< 0.01
		Time * SA	15.25	< 0.01
	3	Sodium Azide	2.27	ns
		Time * SA	1.78	ns
	4	Sodium Azide	1.08	ns
		Time * SA	1.40	ns

The spectral shape of the generated CDOM spectra in bact. treatments showed a negative exponential with a slight peak at 290-295 nm (Fig 3.6). The spectral slopes from 290 to 400 nm (S_{uv}) of bacterial generated CDOM in those treatments ranged from 16.7 to 21.5 $\times 10^{-3}$ nm⁻¹.

A significant relationship was observed only between Δa_{325} and Δa_{443} and average BP during the first interval of the experiments from t0 to t1 (Fig 3.7), but not with BA or cell-sp BP. The slopes of the regression lines between Δa_{325} and Δa_{443} and average BP were used as bacterial CDOM generation rates in the Mediterranean Sea and are presented in Table 3.5. When these rates were extrapolated to field BP values in the Mediterranean Sea, estimates of field CDOM generation rates of 4.5 and 0.9 ($\times 10^{-3}$ m⁻¹ d⁻¹) were obtained, that suggested CDOM duplication times of 29.8 and 30.2 days at 325 and 443 nm respectively.

Table 3.4. Daily CDOM increases at 325 and 443 nm ($\text{m}^{-1} \text{d}^{-1}$), relative percentage with respect to initial absorption at 325 and 443 nm (d^{-1}), and daily increases in BA ($\times 10^8 \text{ cell l}^{-1} \text{d}^{-1}$) and BP ($\mu\text{g C l}^{-1} \text{h}^{-1} \text{d}^{-1}$) in all re-growth cultures in the Mediterranean Sea. bdl= below detection limit.

Location	Depth	Treatment	Δa_{325} ($\text{m}^{-1} \text{d}^{-1}$)	Δa_{443} ($\text{m}^{-1} \text{d}^{-1}$)	% Δa_{325} (d^{-1})	% Δa_{443} (d^{-1})	ΔBA ($\times 10^8 \text{ cell l}^{-1} \text{d}^{-1}$)	ΔBP ($\mu\text{g C l}^{-1} \text{h}^{-1} \text{d}^{-1}$)
St #2	200m	+SA	0.071	0.011	32.2	23.2	0.30	0.07
		Bact	0.083	0.012	50.5	28.1	1.56	0.25
	DCM	+SA	0.129	0.027	60.0	84.1	0.43	0.08
		Bact	0.172	0.019	49.9	14.4	2.49	0.31
St #15	200m	+SA	0.040	0.009	24.5	106.7	0.26	0.02
		Bact	0.022	0.003	4.4	11.7	0.06	0.10
	DCM	+SA	0.040	0.007	16.0	30.5	0.60	0.03
		Bact	0.090	0.021	106.6	bdl	1.56	0.08

Table 3.5. Bacterial CDOM generation rates of absorption at 325 nm obtained experimentally and calculated from BP ($\text{m}^{-1} \text{d}^{-1}$ per $\mu\text{g C l}^{-1} \text{h}^{-1}$), field bacterial CDOM generation rates at 325 and 443 nm ($\text{m}^{-1} \text{d}^{-1}$) estimated for field conditions in the Mediterranean Sea, and CDOM duplication times (d).

Absorption coefficient	a_{325}	a_{443}
Experimental CDOM Generation rate ($\text{m}^{-1} \text{d}^{-1}$ per $\mu\text{g C l}^{-1} \text{h}^{-1}$)	0.3721	0.0739
Field ΔCDOM ($\times 10^{-3} \text{ m}^{-1} \text{d}^{-1}$)	4.5	0.89
Field CDOM duplication time (d)	29.8	30.2

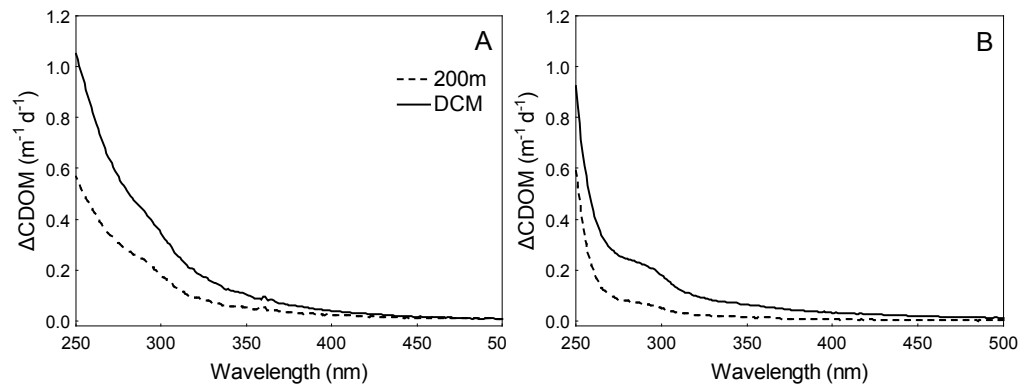


Figure 3.6. Bacterial generated CDOM spectra from 250 nm to 500 nm (final – initial per day) in the different bact. treatments of experiments 1 and 2 (st #2, A) and 3 and 4 (st #15, B).

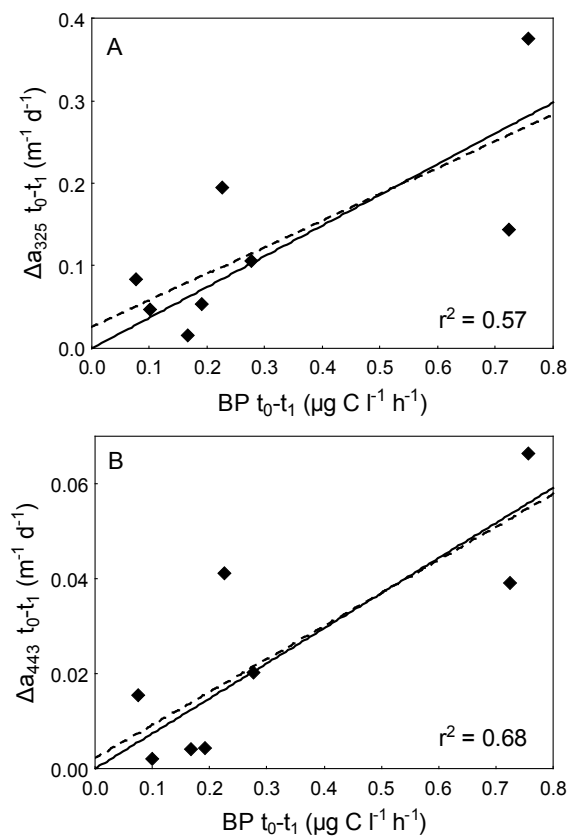


Figure 3.7. Relationships between mean BP and Δa_{325} (A) or Δa_{443} (B) in the first interval (from t_0 to t_1) of all re-growth experiments performed with Mediterranean Sea waters. Solid lines represent the regression lines passing through the origin, and dashed lines represent the regression lines with the intercept. In no cases the two equations were significantly different ($p > 0.05$). The slopes of the solid lines represent the experimental bacterial CDOM generation rates in the Mediterranean Sea ($m^{-1} d^{-1}$ per $\mu g C l^{-1} h^{-1}$, see Table 3.5)

KRILL CDOM GENERATION IN THE SOUTHERN OCEAN

Increases in CDOM were detected in most incubations (12 of 15) using adult krill. In those incubations where an increase in CDOM was observed, Δa_{325} ranged from 0.132 to 1.535 $\text{m}^{-1} \text{d}^{-1}$ and Δa_{443} ranged from 0.043 to 0.524 $\text{m}^{-1} \text{d}^{-1}$ (Table 3.6). The shapes of the CDOM spectra generated by krill tended to exhibit the characteristics of a negative exponential with higher absorption coefficients at shorter wavelengths (Fig. 3.8).

To assess the potential effect of bacterial growth on CDOM generation in the krill incubations and, then, to correct the values of CDOM generated and attributed exclusively to krill, we monitored BP and BA in parallel. BP showed an hourly increase of 0.0086 $\mu\text{g C l}^{-1} \text{h}^{-1}$ and BA showed an hourly increase of 656 cell ml^{-1} that yield an hourly increase of cell sp BP of 0.23 $\text{fg C cell}^{-1} \text{h}^{-1}$. Thus,

Table 3.6. Daily CDOM increases at 325 and 443nm ($\text{m}^{-1} \text{d}^{-1}$) and percentages of CDOM increase at 325 and 443nm (d^{-1}) in all krill incubations (Inc #). Horizontal lines separate different sets of incubations.

Inc #	$\Delta a_{325} (\text{m}^{-1} \text{l}^{-1} \text{d}^{-1})$	$\Delta a_{443} (\text{m}^{-1} \text{l}^{-1} \text{d}^{-1})$	$\% \Delta a_{325} (\text{d}^{-1})$	$\% \Delta a_{443} (\text{d}^{-1})$
1	-1.348	-0.403	-119	-107
2	-1.299	-0.432	-95	-92
3	-1.114	-0.385	-138	-130
4	0.651	0.229	45	44
5	0.360	0.115	25	22
6	0.192	0.043	13	8
7	0.540	0.150	37	29
8	0.646	0.315	64	101
9	1.059	0.453	119	161
10	0.132	0.122	14	42
11	0.496	0.084	137	60
12	1.535	0.524	509	785
13	0.593	0.264	157	310
14	0.302	0.132	71	115
15	0.655	0.185	154	130

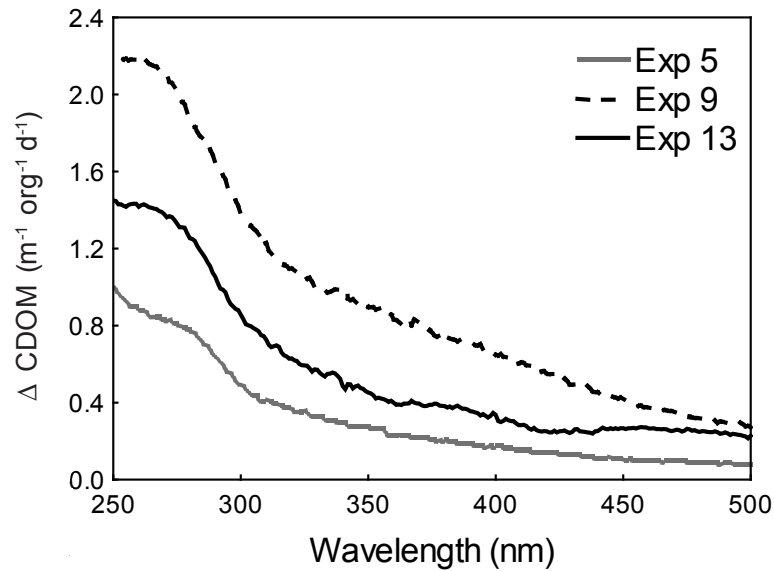


Figure 3.8. Krill generated CDOM spectra (daily CDOM increases, normalized by daily changes in the control treatments) in three representative krill incubations (numbers 5, 9 and 13; see also Table 3.6).

even using the most conservative index ($\Delta a_{325,443}$ corrected for potential bacterial contributions due to cell-sp BP in the Southern Ocean), two thirds (10 of the 15 incubations) still showed CDOM daily increases at a_{325} and a_{443} .

Biogeneration rates by krill, after corrections for potential CDOM bacterial contributions and extrapolated to a density of one organism per liter, are shown in Table 3.7. These rates ranged from 0.357 to 0.403 $\text{m}^{-1} \text{d}^{-1}$ for a_{325} and from 0.117 to 0.147 $\text{m}^{-1} \text{d}^{-1}$ for a_{443} . Extrapolating krill CDOM generation rates to field data, we estimated field Δa_{325} from 0.027 to 0.031 $\times 10^{-3} \text{m}^{-1} \text{d}^{-1}$ and field Δa_{443} from 0.009 to 0.011 $\times 10^{-3} \text{m}^{-1} \text{d}^{-1}$, considering average krill densities around Antarctic Peninsula of 77.8 individuals in 1000 m^3 (Loeb et al. 1997) (Table 3.7). The application of these average CDOM generation values to the study area would yield a CDOM duplication time of years. Considering 1000 organisms per cubic meter as an average density of krill swarms (Brierley and Watkins 2000), field CDOM generation would be analogous to the experimentally determined krill CDOM generation rates ($\Delta a_{325,443}$ per org l^{-1}), and would imply CDOM duplication times from 0.29 to 1.03 days (Table 3.7).

Table 3.7. Krill generation rates ($\text{m}^{-1} \text{d}^{-1}$ per org l^{-1}), estimated field CDOM generation rates by krill at 325 and 443 nm ($\text{m}^{-1} \text{d}^{-1}$), and field CDOM duplication times within swarms (d). Krill CDOM generation rates were corrected by potential bacterial contributions due to BP (first column) and cell-specific BP (second column) in the Southern Ocean.

Correction Factor for bacterial contribution to CDOM	BP	cell-sp BP
Krill a_{325} generation rate	0.403	0.357
Krill a_{443} generation rate	0.147	0.117
Field Δa_{325} ($\times 10^{-3} \text{ m}^{-1} \text{ d}^{-1}$)	0.031	0.027
Field Δa_{443} ($\times 10^{-3} \text{ m}^{-1} \text{ d}^{-1}$)	0.011	0.009
Field a_{325} duplication time (d) within swarms	0.29	0.34
Field a_{443} duplication time (d) within swarms	0.82	1.03

DISCUSSION

Bacterial generation of CDOM was evident in all bacterial re-growth experiments and confirms the potential role of bacteria as a CDOM source in both the Southern Ocean and the Mediterranean Sea. Previous work based on field observations of seasonal CDOM dynamics, geographical distribution (Nelson et al., 1998; Sasaki et al., 2005; Yamashita et al., 2007) and changes in bacterial abundance within phytoplankton cultures or mesocosms (Rochelle-Newall et al., 1999; Rochelle-Newall and Fisher, 2002) had inferred this linkage. Recently bacterial CDOM generation have been experimentally confirmed (Nelson et al., 1998; Cammack et al., 2004; Kramer and Herndl, 2004; Nieto-Cid et al., 2006). However, quantitative bacterial CDOM generation rates are hardly comparable among these studies as different analytical approaches (absorbance vs. fluorescence, different reference wavelengths) were employed. The percentages of CDOM increase (d^{-1}) reported herein are consistent, or even higher in some cases (e.g. experiments 1 and 2 in the Mediterranean Sea), than values reported by Nelson et al. (2004) for bacterial production rates during exponential growth phase.

In the Southern Ocean, despite the consistent CDOM bacterial generation obtained in the experiments, the magnitude and quality of bacterial generated CDOM was different depending on the presence/absence of photoproducts as a substrate. In those treatments where marked photobleaching was evident (in-

cubations carried out with water collected near Deception Island) CDOM generation was greater, suggesting that photoaltered CDOM is more susceptible to further bacterial processing. In addition, bacterial generated CDOM from photoaltered DOM exhibited a distinct spectral shape, with maximum absorbance at 290-295nm, providing additional insight into the nature of the transformations. This particular spectral shape might be attributed to the selective growth of specific bacterial subpopulations, or to unique properties of the DOM. Indeed, Deception Island is a semi-enclosed bay with high chl *a* levels where DOM is likely to be of recent algal origin and, thus, likely more photo- and bioreactive. On the other hand, the lack of significant CDOM photobleaching observed in waters from Livingston Island is possibly attributable to the more refractory nature of DOM or to the lower cumulative sunlight dose received in the photoproducts treatments of Livingston Island experiments. There was a similar response in bacterial generated CDOM generation in all treatments irrespective of the presence/absence of photoproducts and showed more typical negative exponential absorption spectra.

In the case of the experiments performed using water from the Mediterranean Sea, all generated CDOM spectra showed negative exponential spectra (Fig. 3.6). Generally higher spectral slopes of bacterial generated CDOM than in Southern Ocean experiments were detected. These results suggest that the shape of bacterial CDOM spectra could be influenced by site-specific factors such as the composition of the bacterial community, or the organic and inorganic substrate quality, including the presence of photoproducts.

Despite the spectral shape can be influenced by specific factors, we demonstrate in this chapter a direct link between bacterial activity (bacterial production in the Southern Ocean and Mediterranean Sea, and cell-specific bacterial production in the Southern Ocean) and the magnitude of CDOM generation, irrespective of initial CDOM or mineral nutrient concentration or the presence or absence of photoproducts. This novel finding suggests an active role of bacteria in the generation of CDOM that would result in consistent values of CDOM duplication times in both study areas. However, in the Southern Ocean, cell-specific bacterial production was calculated as an average of bacterial production per cell which assumes an equal contribution of all individuals and bacterial subpopulations to BP. This assumption is certainly violated when applied to a field scenario (see Lebaron et al., 2001; Longnecker et al., 2005) and extrapolation of our rates to field conditions warrant some caution.

Extrapolating experimental bacteria CDOM generation rates to the field predicts a CDOM duplication time of around 30 days considering average BP values in the Antarctic Peninsula area and in the Mediterranean Sea, and up to 78 days considering average cell-specific BP values in the Antarctic Peninsula. However, in areas where high BP values are observed (e.g., in the western Weddell Sea during ice-free periods, or the western Mediterranean Sea) CDOM duplication times of about 7 to 10 days are possible. Thus, we have demonstrated that bacteria can generate significant amounts of CDOM on a short (i.e. less than a week) timescale. The impact of bacteria on CDOM dynamics will depend on the persistence of the bacterial generated CDOM in the environment, which can range from labile material, consumed or degraded in a few days (Nelson et al., 2004; Biers et al., 2007), to refractory (Brophy and Carlson, 1989; Ogawa et al., 2001), depending on nitrogen availability (Biers et al., 2007) and the susceptibility of the material to further photochemical transformations (Kramer and Herndl, 2004).

Our results provide the first evidence for the potential of Antarctic krill, *Euphasia superba*, to contribute to the CDOM pool in the Southern Ocean. Previous studies have reported the release of CDOM and fluorescent DOM by different zooplankton species (Steinberg et al., 2004; Urban-Rich et al., 2006) indicating that these organisms could be responsible for unique CDOM and fluorescent DOM signatures. In this study, the shape of CDOM spectra generated by krill showed a maximum below 300 nm. This finding is consistent with a previous report of CDOM excretion by euphasiids (Steinberg et al., 2004). However, not all krill incubations showed CDOM production. In fact, one complete set of incubations (experiments 1 to 3; see Table 3.6) indicated a decrease in CDOM. This suggests that CDOM production by Antarctic krill is likely dependent on other factors, such as ambient conditions and the nutritional status of the organisms, which deserve further attention. Indeed, in the aforementioned set of incubations, abnormally high background levels of CDOM at time 0 were observed (data not shown) which could have masked the krill contribution.

The relevance of estimating the potential contributions of Antarctic krill to CDOM dynamics is underscored by their status as a keystone species in the Southern Ocean; krill are both important grazers (Ross et al., 1998) and preferential prey for most higher-order consumers, including seals, penguins, whales and seabirds (Croxall et al., 1999; Everson et al., 1999), while they affect biogeochemical cycling as well (Tovar-Sanchez et al., 2007). Accordingly, CDOM duplication

times attributable to krill would be generally an order of magnitude longer than CDOM attributable to bacteria when considering average seasonal krill densities in waters around the Antarctic Peninsula (Loeb et al., 1997). Whereas this could suggest a minor role of krill on CDOM dynamics, these organisms can form large swarms with hundreds to thousands of organisms per cubic meter (Brierley and Watkins, 2000). In these conditions, CDOM duplication times would be shorter than a day (Table 3.7). Therefore, an intense CDOM signal is expected in association with krill swarms or areas recently occupied by krill swarms. As krill activity releases large amounts of labile organic carbon, ammonium and other limiting elements as phosphate or iron (Quetin et al., 1994; Tovar-Sanchez et al., 2007), krill activity could greatly stimulate bacterioplankton growth, fueling further bacterial CDOM generation.

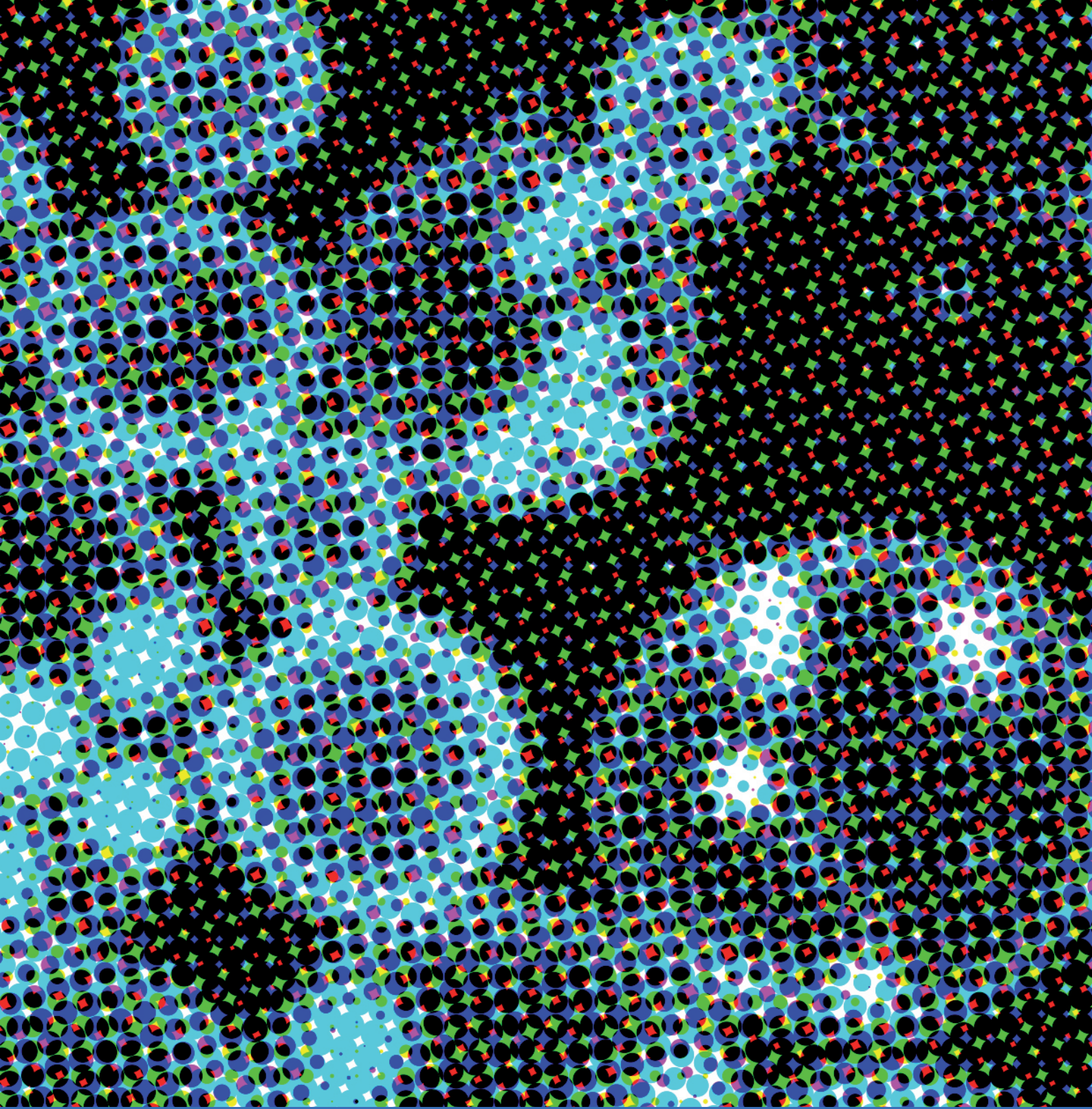
Overall, our findings highlight the potential significance of bacteria in the generation of CDOM in the Southern Ocean and Mediterranean Sea, and the relevance of Antarctic krill swarms in CDOM dynamics. CDOM duplication times from days (considering CDOM in krill swarms) to months (considering bacterial activity) or years (considering average krill densities) in these areas underscore the reactive nature of CDOM.

REFERENCES

- BIERS, E.J., R.G. ZEPP and M.A. MORAN (2007) The role of nitrogen in chromophoric and fluorescent dissolved organic matter formation. *Marine Chemistry*. 103: 46-60.
- BOSS, E. and J.R.V. ZANEVELD (2003) The effect of bottom substrate on inherent optical properties: Evidence of biogeochemical processes. *Limnology and Oceanography*. 48: 346-354.
- BRIERLEY, A.S. and J.L. WATKINS (2000) Effects of sea ice cover on the swarming behaviour of Antarctic krill, *Euphausia superba*. *Canadian Journal of Fisheries and Aquatic Sciences*. 57: 24-30.
- BROPHY, J.E. and D.J. CARLSON (1989) Production of biologically refractory dissolved organic carbon by natural seawater microbial populations. *Deep-Sea Research A: Oceanographic research papers*. 36: 497-507.
- CAMMACK, W.K.L., J. KALFF, Y.T. PRAIRIE and E.M. SMITH (2004) Fluorescent dissolved organic matter in lakes: Relationships with heterotrophic metabolism. *Limnology and Oceanography*. 49: 2034-2045.
- CROXALL, J.P., K. REID and P.A. PRINCE (1999) Diet, provisioning and productivity responses of marine predators to differences in availability of Antarctic krill. *Marine Ecology-Progress Series*. 177: 115-131.
- EVERSON, I., G. PARKES, K.H. KOCK and I.L. BOYD (1999) Variation in standing stock of the mackerel icefish *Champsocephalus gunnari* at South Georgia. *Journal of Applied Ecology*. 36: 591-603.
- GASOL, J.M. and X.A.G. MORÁN (1999) Effects of filtration on bacterial activity and picoplankton community structure as assessed by flow cytometry. *Aquatic Microbial Ecology*. 16: 251-264.
- KAWASAKI, N. and R. BENNER (2006) Bacterial release of dissolved organic matter during cell growth and decline: Molecular origin and composition. *Limnology and Oceanography*. 51: 2170-2180.
- KIEBER, R.J., L.H. HYDRO and P.J. SEATON (1997) Photooxidation of triglycerides and fatty acids in seawater: Implication toward the formation of marine humic substances. *Limnology and Oceanography*. 42: 1454-1462.
- KRAMER, G.D. and G.J. HERNDL (2004) Photo- and bioreactivity of chromophoric dissolved organic matter produced by marine bacterioplankton. *Aquatic Microbial Ecology*. 36: 239-246.

- LEBARON, P., P. SERVAIS, H. AGOGUÉ, C. COURTIES and F. JOUX (2001) Does the high nucleic acid content of individual bacterial cells allow us to discriminate between active cells and inactive cells in aquatic systems? *Applied and Environmental Microbiology*. 67: 1775-1782.
- LOEB, V., V. SIEGEL, O. HOLMHANSEN, R. HEWITT, W. FRASER, W. TRIVELPIECE and S. TRIVELPIECE (1997) Effects of sea-ice extent and krill or salp dominance on the Antarctic food web. *Nature*. 387: 897-900.
- LONGNECKER, K., B.F. SHERR and E.B. SHERR (2005) Activity and phylogenetic diversity of bacterial cells with high and low nucleic acid content and electron transport system activity in an upwelling ecosystem. *Applied and Environmental Microbiology*. 71: 7737-7749.
- MORAN, M.A. and R.G. ZEPP (1997) Role of photoreactions in the formation of biologically labile compounds from dissolved organic matter. *Limnology and Oceanography*. 42: 1307-1316.
- NELSON, N.B., C.A. CARLSON and D.K. STEINBERG (2004) Production of chromophoric dissolved organic matter by Sargasso Sea microbes. *Marine Chemistry*. 89: 273-287.
- NELSON, N.B., D.A. SIEGEL and A.F. MICHAELS (1998) Seasonal dynamics of colored dissolved material in the Sargasso Sea. *Deep-Sea Research Part I-Oceanographic Research Papers*. 45: 931-957.
- NICOL, S. (2006) Krill, currents, and sea ice: *Euphausia superba* and its changing environment. *Bioscience*. 56: 111-120.
- NIETO-CID, M., X.A. ALVAREZ-SALGADO and F.F. PÉREZ (2006) Microbial and photochemical reactivity of fluorescent dissolved organic matter in a coastal upwelling system. *Limnology and Oceanography*. 51: 1391-1400.
- OGAWA, H., Y. AMAGAI, I. KOIKE, K. KAISER and R. BENNER (2001) Production of refractory dissolved organic matter by bacteria. *Science*. 292: 917-920.
- QUETIN, L.B., R.M. ROSS and A. CLARKE (1994). In: S. El-Sayed (ed.) *Southern Ocean Ecology: The BIOMASS perspective*. Cambridge University Press, Cambridge. pp. 161-184.
- RECHE, I., E. PULIDO-VILLENA, J.M. CONDE-PORCUNA and P. CARRILLO (2001) Photoreactivity of dissolved organic matter from high-mountain lakes of Sierra Nevada, Spain. *Arctic Antarctic and Alpine Research*. 33: 426-434.
- ROCHELLE-NEWALL, E.J. and T.R. FISHER (2002) Production of chromophoric dissolved organic matter fluorescence

- in marine and estuarine environments: an investigation into the role of phytoplankton. *Marine Chemistry*. 77: 7-21.
- ROCHELLE-NEWALL, E.J., T.R. FISHER, C. FAN and P.M. GLIBERT (1999) Dynamics of chromophoric dissolved organic matter and dissolved organic carbon in experimental mesocosms. *International Journal of Remote Sensing*. 20: 627-641.
- RONTANI, J.F. (1998) Photodegradation of unsaturated fatty acids in senescent cells of phytoplankton: photoproduct structural identification and mechanistic aspects. *Journal of Photochemistry and Photobiology A-Chemistry*. 114: 37-44.
- ROSS, R.M., L.B. QUETIN and K.L. HABERMAN (1998) Interannual and seasonal variability in short-term grazing impact of *Euphausia superba* in nearshore and offshore waters west of the Antarctic Peninsula. *Journal of Marine Systems*. 17: 261-273.
- SASAKI, H., T. MIYAMURA, S. SAITOH and J. ISHIZAKA (2005) Seasonal variation of absorption by particles and colored dissolved organic matter (CDOM) in Funka Bay, southwestern Hokkaido, Japan. *Estuarine Coastal and Shelf Science*. 64: 447-458.
- SMETACEK, V. and S. NICOL (2005) Polar ocean ecosystems in a changing world. *Nature*. 437: 362-368.
- STEINBERG, D.K., N.B. NELSON, C.A. CARLSON and A.C. PRUSAK (2004) Production of chromophoric dissolved organic matter (CDOM) in the open ocean by zooplankton and the colonial cyanobacterium *Trichodesmium* spp. *Marine Ecology-Progress Series*. 267: 45-56.
- TOVAR-SÁNCHEZ, A., C.M. DUARTE, S. HERNÁNDEZ-LEÓN and S.A. SAÑUDO-WILHELMY (2007) Krill as a central node for iron cycling in the Southern Ocean. *Geophysical Research Letters*. 34.
- TRANVIK, L.J. (1993) Microbial transformations of labile organic matter into humic-like matter in seawater. *FEMS Microbiology Ecology*. 12: 177-183.
- URBAN-RICH, J., J.T. MCCARTY, D. FERNÁNDEZ and J.L. ACUÑA (2006) Larvaceans and copepods excrete fluorescent dissolved organic matter (FDOM). *Journal of Experimental Marine Biology and Ecology*. 332: 96-105.
- YAMASHITA, Y., A. TSUKASAKI, T. NISHIDA and E. TANOUE (2007) Vertical and horizontal distribution of fluorescent dissolved organic matter in the Southern Ocean. *Marine Chemistry*. 106: 498-509.



Chapter 4:
**Dynamics of Chromophoric dissolved and detrital organic matter
(CDM) using remote sensing in the Southern Ocean:
data validation, temporal dynamics, and global warming implication.**

Ortega-Retuerta, E., Siegel, D.V., Duarte, C.M., and Reche, I.

Abbreviated title: CDM dynamics using remote sensing

INTRODUCTION

Earth remote sensing is defined as the use of electromagnetic radiation to acquire information about the ocean, land and atmosphere without being in physical contact with the object (Martin, 2002). The use of remote sensing in Earth sciences, and particularly in oceanography, involves enormous advantages as it covers broader areas of the ocean and longer temporal series than ship measurements of geophysical parameters. Indeed, satellites with sun-synchronous orbits can view every square kilometer of cloud-free ocean every 48 hours, providing a variety of geophysical parameters such as ocean color, sea surface temperature, altimetry or wind speed and directions with near global coverage and small time intervals.

From the first ocean remote sensing satellite launched in the 70's to date, there are a growing number of ocean satellite missions provided by different countries (e.g. the US coastal zone color scanner (CZCS), the Japanese Earth Resources satellite (SAR), the European Medium Resolution Imaging Spectrometer (MERIS) or the joint missions JASON-1 altimeter or Tropical Rainfall Measuring Mission (TRMM), that reflect the increasing interest in ocean remote sensing both for scientific and economical applications.

All satellite sensors measure electromagnetic radiation at different wavelengths in the ultraviolet, visible, infrared and microwave spectra. The use of a specific wavelength by a satellite sensor is dependent on the geophysical parameter to be measured (Fig. 4.1).

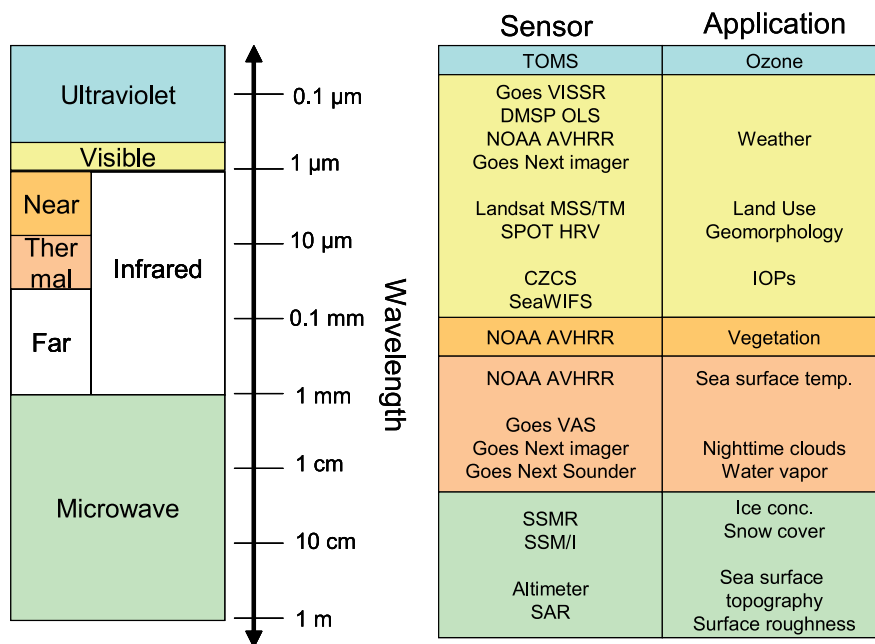


Figure 4.1. List of satellite sensors, the wavelength range used, and the geophysical variable retrieved with each sensor.

Specifically, satellite sensors for ocean color are passive sensors that detect remote upwelling radiance (Fig. 4.2). The measured radiance originates from sunlight that passes through the atmosphere, then is reflected, absorbed, and scattered by the different constituents in the ocean, and is transmitted back through the atmosphere to the satellite sensor. These sensors measure total radiance (L_t), normalized to the solar irradiance, at discrete wavelengths (bands) in the visible and near-infrared portions of the solar spectrum.

Currently there are 8 satellite instruments for ocean color observation and, among them, the most used are the US instruments Sea-viewing Wide Field-of-view Sensor (SeaWiFS), launched in the spacecraft SeaStar 1997 (<http://oceancolor.gsfc.nasa.gov/SeaWiFS/>), and Moderate Resolution Imaging Spectroradiometer (MODIS) (<http://modis.gsfc.nasa.gov/>), launched in the spacecrafts TERRA in 1999 and AQUA in 2002. Although the primary purpose of satellite ocean color measurement was to estimate chlorophyll *a* (chl *a*) (O'Reilly et al., 1998; IOCG, 2006), the retrieval of inherent optical properties (IOPs) can represent a tool for estimating biogeochemical parameters in the oceans (IOCG, 2006), such as diffuse attenuation coefficients (Kirk, 1984; Lee et al., 2005; Oubelkheir et al., 2006),

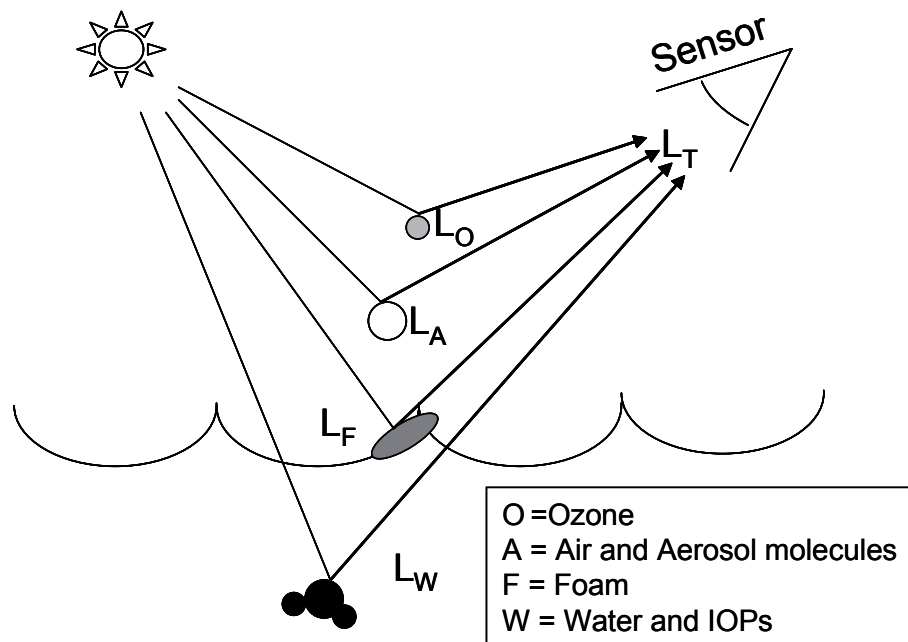


Figure 4.2. Major contributors to total radiance (L_T) measured by a passive ocean color sensor.

particulate organic carbon (Stramski et al., 1999; Pabi and Arrigo, 2006) or water mass classification (Arnone and Parsons, 2004).

SeaWiFS and MODIS satellite sensors measure upwelling radiance in 8 discrete bands or wavelengths (Table 4.1, Fig. 4.3). The combination of data within these bands, along with the use of different algorithms, allows retrieving the different geophysical products. For instance, 443, 510 and 551 nm are used for chlorophyll determinations, and 412 and 443 nm for the detection of CDOM and detrital organic matter (Table 4.1).

From the total radiance measured by the satellite sensors in the visible spectrum (L_T), at most 10% comes from the ocean and is referred as water-leaving radiance (L_w). L_w is defined as the radiance that exits the ocean in a non-attenuating atmosphere and the sun at zenith (Gordon and Voss, 1999) and is affected by the scattering and absorption of ocean water and its main constituents, known as inherent optical properties, (IOPs). The rest is attenuated by different components in the atmosphere such as ozone attenuation, radiances associated with sun glint and foam, and the Rayleigh and aerosol path radiances.

Table 4.1. Wavelengths of all bands from SeaWiFS and MODIS sensors and the main purpose for each wavelength.

Band	Center λ (nm) SeaWiFS	Center λ (nm) MODIS	Purpose
1	412	412	CDOM and detritus
2	443	443	CDM- pigment
3	490	488	Pigment algorithm
4	510	531	Pigment algorithm
5	555	551	Pigment algorithm
6	670	667	Atmospheric correction
7	765	748	Atmospheric correction
8	865	869	Atmospheric correction

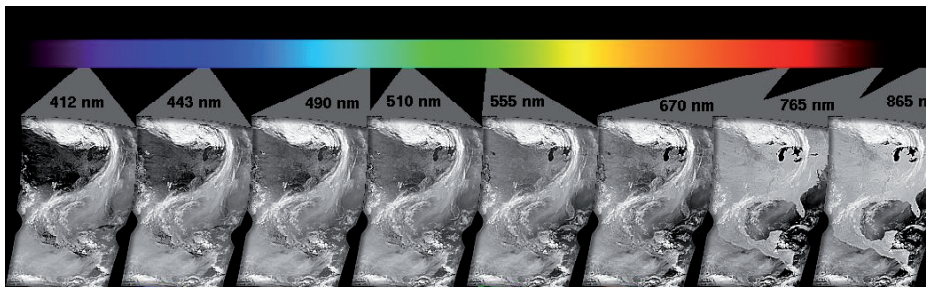


Figure 4.3. The eight SeaWiFS wavelength bands (extracted from NASA ocean color web, <http://oceancolor.nasa.gov/SEAWIFS>).

Traditionally, ocean color imagery has been processed in two sequential steps. First, water-leaving radiance (L_w), is retrieved from the total radiance received by the satellite (L_r) sensor (Fig. 4.2). For that purpose, an atmospheric correction algorithm is applied to remove all other radiances (L_o , L_A , L_F) that are contributing to the signal (Gordon and Wang, 1994; Gordon, 1997). Second, L_w is used in bio-optical algorithms to extract the biogeochemical variables, e.g. chlorophyll concentration or chromophoric dissolved organic matter (CDOM) absorption (O'Reilly et al., 1998; Maritorena et al., 2002).

The atmospheric correction algorithm for SEAWIFS measures the spectral variation in L_T in the near-infrared spectral region, where L_w is negligible, to assess the aerosol's contribution to the reflectance in the visible wavelengths (Gordon and Wang, 1994). This algorithm can provide L_w with the desired accuracy as long as the aerosol is weakly absorbing, but the presence of strongly absorbing aerosols, e.g., aerosols from anthropogenic sources or mineral dust, include an error that affects the determination of IOPs (Gordon et al., 1997), particularly for those retrieved at shorter wavelengths (i. e. 412 or 443 nm) such as CDOM (Siegel et al., 2005).

Once the atmospheric contribution is corrected, there are two kinds of bio-optical algorithms employed to retrieve biogeochemical parameters from satellite observations of L_w : empirical and semianalytic algorithms. The empirical algorithms (e.g. the OC4.v4 algorithm developed by the NASA Ocean Biology Processing Group), are derived from direct relationships between coincident satellite and ship observations of water leaving radiance (L_w) and chlorophyll concentration. By contrast, the semianalytic algorithms, such as GSM01 (abbreviation of Garver, Siegel & Maritorena), combine theoretical models of the relation of L_w to the ratio of absorption to backscatter with empirical models of the dependence of absorption and backscatter on IOPs.

The empiric algorithms only yield chl *a* values and assume that the major optically-active components of the ocean surface covary with chl *a* in a predictable manner. This assumption is not always valid. By contrast, the semi analytic algorithms discriminate the relative contribution of the different non-water optical constituents (i.e. chl *a* and other pigments, CDOM and detrital organic matter (CDM), and particle backscattering coefficients).

In Antarctic waters, in particular, global empiric algorithms generally underestimate chlorophyll concentration (Mitchell and Holmhanzen, 1991; Dierssen and Smith, 2000; Marrari et al., 2006). The proposed reasons for this discrepancy are low chlorophyll specific absorption (Mitchell and Holmhanzen, 1991; Dierssen and Smith, 2000), low backscattering of particles (Dierssen and Smith, 2000), different approaches used for estimating chl *a* (Marrari et al., 2006) or different composition of the algal community (Arrigo et al., 1998). As empiric algorithms use a fixed relation between L_w and chl *a*, different optical properties in this region with respect to the global ocean may account for this error. In this sense,

a significant source of error is the ratio and covariance between chlorophyll *a* and chromophoric dissolved organic matter. This ratio is known to differ in high latitude waters respect to other areas (Siegel et al., 2002).

The GSM01 model was optimized using a large global *in situ* data set that consisted mostly of offshore oceanic waters with very few stations from eutrophic waters (Siegel et al., 2002; Gregg and Casey, 2004; Siegel et al., 2005), and recent attempts have been done to optimize the model for local uses (Kudela and Chavez, 2004; Magnuson et al., 2004; Kostadinov et al., 2007). The robustness of the model, however, has not yet been corroborated for Southern Ocean waters, where inherent optical properties (IOPs) can differ from those used to tune the GSM01 model.

Despite satellite chl *a* measurements have been repeatedly used in Southern Ocean studies (Reynolds et al., 2001; Gregg and Casey, 2004; Moore and Doney, 2006), to date there are no published works using remote sensing CDM data. In general, global satellite CDM images mirror the major large-scale circulation systems. The combination of high cumulative sunlight doses and shallow mixed layers make central gyres tropical areas to have very low CDM near the surface, whereas this concentration increases towards the poles, where high CDM values are observed and apparently result of a combination of reduced cumulative sunlight doses and deep mixed layers (Siegel et al., 2002).

In this thesis chapter two main objectives were addressed: First, we validated the GSM01 (hereafter referred as GSM) algorithm to retrieve CDM data in the Antarctic Peninsula area using field data. Second, we used GSM data of CDM to assess geographical variability and temporal dynamics of CDM in this area, and we explored the potential driving factors.

MATERIAL AND METHODS

VALIDATION OF GSM DATA OF CDM WITH FIELD CDOM DATA

To validate of CDM data obtained by satellite observations using the GSM model with field CDOM data, we used three different datasets:

1. CDOM data corresponding to austral summers of 1997, 1998 and 1999 obtained from the Palmer Long Term Ecological Research (PalTER) dataset (<http://pal.lternet.edu/>). The Palmer LTER site is centered in the US station Palmer, in Anvers Island ($64^{\circ}40' S$ $64^{\circ}03' W$). The dataset covers a grid situated west of the Antarctic Peninsula that extends over a region of 900 km^2 with sampling points spaced every 20 km in parallel with the peninsula (Fig. 4.4). Specifically, CDOM data were provided by Dr. Karen Patterson. CDOM was measured from filtered samples (polycarbonate filters, $0.2 \mu\text{m}$) using 10cm pathlength quartz cuvettes in a Perkin-Elmer Lambda 6 spectrophotometer (Patterson, 2000).

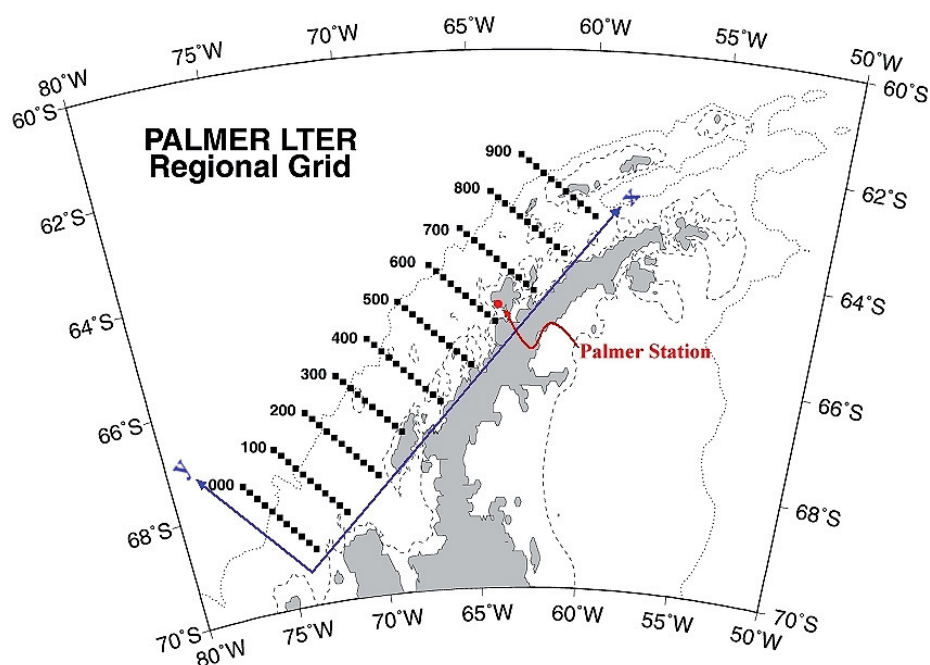


Figure 4.4. Geographical location of Palmer LTER regional grid. The Peninsula grid uses station 600.040 just off Palmer Station as the center point to a Universal Transverse Mercator projection parallel to the Antarctic Peninsula.

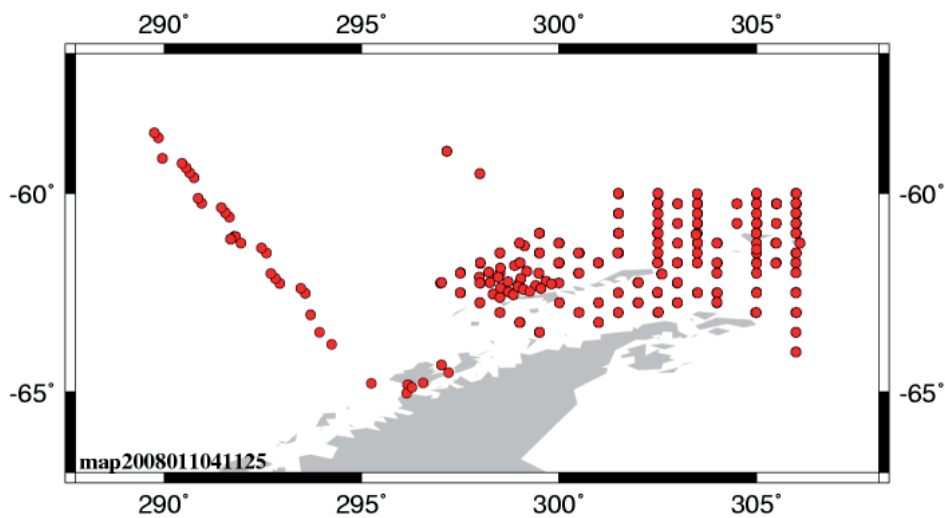


Figure 4.5. Example of sampling stations during AMLR cruise (February-March 2002).

2. CDOM data corresponding to 2000, 2001 and 2002 were obtained from de SeaBass archive, which is an *in situ* oceanographic and atmospheric dataset maintained by the NASA OBPG (Ocean Biology Processing Group, <http://seabass.gsfc.nasa.gov/>) created to support regular scientific analyses (satellite data product validation, algorithm development and other scientific goals), such as bio-optical data for validation of SeaWiFS and MODIS data and generated with both voluntary and funded data contributions from investigators worldwide. The specific data used here corresponded to AMLR cruises (PI Dr. Greg Mitchell) during February-March 2000, 2001 and 2002 along Gerlache Strait and South Shetland Islands (Fig. 4.5). CDOM was measured from filtrate samples according to the standard protocols (Pegau et al., 2003)
3. CDOM dataset corresponding to 2004 and 2005 were obtained by us during ICEPOS cruises and analyzed as it has been described in the general methods section.

Data of detrital absorption ($a_d(443)$) were also available for Palmer LTER and AMLR. Measurements of a_d were performed filtering samples through GF/F filters and subsequent spectrophotometrical measurements of absorption.

Satellite a_{cdm} (443) data were obtained from SeaWiFS data from 1997 to 2002 and from merged (SeaWiFS + MODIS) data from 2002 to 2005 corresponding to GSM products on 9x9 km grids in daily and monthly averages (<http://www.icesc.ucsb.edu/OCisD/>). Briefly, The GSM semi-analytical ocean color model algorithm is based on the relationship between water-leaving radiance (L_w) and the IOPs, which are decomposed into absorption by phytoplankton (a_{ph}), chromophoric dissolved and detrital organic matter (a_{cdm}) and pure water (a_w), and backscattering of water (b_{bw}) and particles (b_{bp}) as expressed in the following equation:

$$L_{wN}(\lambda) = \left(\frac{tF_0(\lambda)}{n_{\text{sw}}^2} \right) \sum_{m=1}^2 g_m \left\{ \frac{b_{\text{bw}}(\lambda) + \text{BBP} \left(\frac{\lambda_0}{\lambda} \right)^\eta}{b_{\text{bw}}(\lambda) + \text{BBP} \left(\frac{\lambda_0}{\lambda} \right)^\eta + a_w(\lambda) + \text{Chl}_{\text{a}_{\text{ph}}}^*(\lambda) + \text{CDM} \exp[-S(\lambda - \lambda_0)]} \right\}^m$$

where BBP (particulate backscattering) chl (chlorophyll *a*) and CDM (chromophoric dissolved and detrital matter) are the parameters to be retrieved.

Values of backscattering ($b_{\text{bw}}(\lambda)$) and absorption ($a_w(\lambda)$) coefficients for pure water, optical closure constants (g_m), downwelling irradiance at the top-of-the-atmosphere ($F_0(\lambda)$, the air-sea transmission factor (t), and the real part of the seawater index of refraction (n_{sw}) are known. Terms for the chlorophyll specific phytoplankton absorption spectrum, $a_{\text{ph}}^*(\lambda)$, and spectral slopes for the particulate backscattering coefficient (η) and chromophoric dissolved and detrital matter (S) were specified through by tuning the model against a large field data set (Maritorena et al., 2002).

GSM and field data match-ups were validated following the protocol described in Bailey and Werdell (2006). Since satellite navigation may be not accurate for a single pixel, GSM data were obtained from a 3x3 pixel grid centered in the location of the field data point. We only used GSM data with more than 4 pixels with valid data. Data from all valid pixels in the 3x3 matrix were averaged and compared with the corresponding field data points.

SPATIAL DISTRIBUTION AND TEMPORAL DYNAMICS OF CDM AROUND THE ANTARCTIC PENINSULA

To evaluate spatial and temporal variability of CDM and its potential drivers, maps of satellite data corresponding to the Antarctic Peninsula area (from 55 to 70° S and from 50 to 80° W) were clipped from the GSM database. ASCII files (360 x 240 pixel grids of 9x9 km pixels) for daily and monthly CDM data and png images were created using IDL software.

To examine CDM temporal dynamics we selected five contrasting locations (Fig. 4.6). Locations 1 and 2 are situated in offshore waters west of the Antarctic Peninsula, locations 3 and 4 are situated along the coastline in the Bransfield strait region, and location 5 is situated in the Weddell Sea (Table 4.2).

We calculated the contribution of CDM to the total non-water absorption in all the selected locations using the following expression:

$$\%CDM = \frac{a_{\text{cdm}}(443)}{a_{\text{ph}}(443) + a_{\text{cdm}}(443)}$$

where $a_{\text{ph}}(443)$ is the pigment absorption (m^{-1}), calculated from chl a using this equation (Bricaud et al., 1995):

$$a_{\text{ph}}(443) = 0.04 \times \text{chl } a^{0.668}$$

To evaluate interannual variability in CDM dynamics we calculated monthly CDM anomalies using the following expression:

$$\text{CDM Anomaly (\%)} = \frac{a_{\text{cdm}}(443)_a - \overline{a_{\text{cdm}}(443)}_a}{\overline{a_{\text{cdm}}(443)}_a} \times 100$$

Where $a_{\text{cdm}}(443)_a$ is monthly CDM in a single month and $\overline{a_{\text{cdm}}(443)}_a$ is the average CDM for the same month over all years (1997-2005). Positive values represent higher CDM concentration than usual and vice versa.

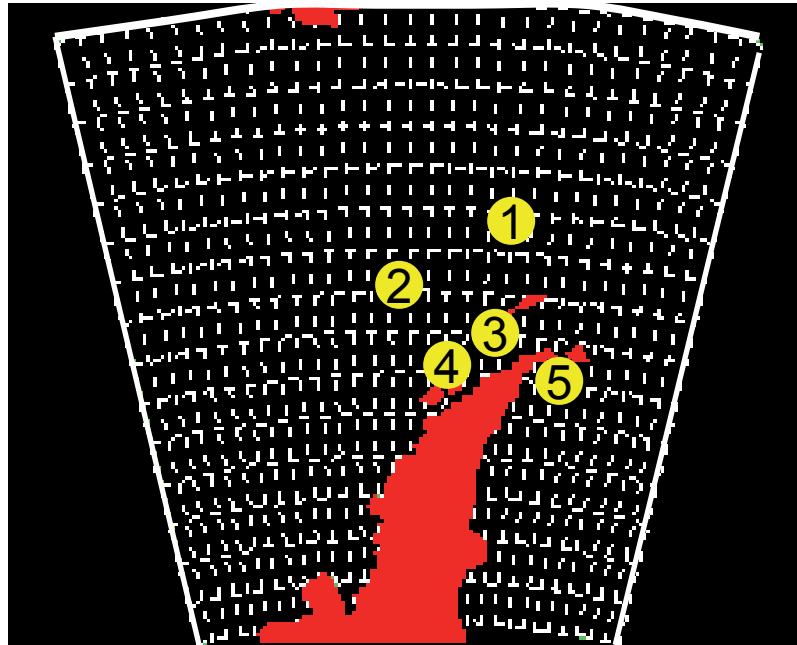


Figure 4.6. Geographical locations of selected areas to study temporal CDM dynamics around the Antarctic Peninsula. Geographical coordinates and main geophysical properties are detailed in Table 4.2.

Table 4.2. Geographical coordinates (latitude and longitude) and means of (a_{443}), m^{-1}), chl a ($\mu\text{g l}^{-1}$), SST ($^{\circ}\text{C}$) and PAR ($\text{E m}^2 \text{d}^{-1}$) for the five selected locations.

Location	1	2	3	4	5
Lat ($^{\circ}$)	-60	-62	-62.7	-63.5	-64
Lon ($^{\circ}$)	-59	-65	-59	-62	-56.5
Mean a_{443}	0.013	0.014	0.022	0.022	0.036
Mean chlorophyll a	0.11	0.13	0.29	0.28	0.65
Mean sea surface temperature	na	1.88	0.91	0.71	-0.01
Mean photosynthetically active radiation	26.1	25.0	27.9	22.6	26.1

SPATIAL AND TEMPORAL DRIVERS OF CDM IN THE ANTARCTIC PENINSULA

We used satellite data of different geophysical variables from different sources to evaluate the potential controlling factors of CDM distribution and dynamics. Chl *a* data were also obtained from SeaWiFS (1997-2002) or merged (2002-2005) GSM products (<http://www.icess.ucsb.edu/OCisD/>). Sea surface temperature (SST) data were obtained from NOAA/NASA AVHRR Pathfinder Global 9km daily SST Products averaged over monthly periods (http://podaac.jpl.nasa.gov/DATA_CATALOG/avhrr.html). Photosynthetically active radiation (PAR) satellite data (level 3, $E\ m^{-2}\ d^{-1}$) from SeaWiFS, were obtained from the NASA's Ocean Color database (http://oceancolor.gsfc.nasa.gov/DOCS/seawifs_par_wfigs.pdf). Ice extent data, as average monthly extent (km^2) for the Bellingshausen-Admunsen and Weddell sectors of the Southern Ocean, were obtained by Nimbus-7 SMMR and DMSP SSM/I passive microwave data from the National Snow and Ice Data Center (Boulder, Colorado USA) (<http://nsidc.org/data/>). Antarctic Oscillation Index (AAO, also known as southern annular mode (SAM) monthly values were obtained from the Climate Prediction Center of the NOAA's National Weather Service (http://www.cpc.noaa.gov/products/precip/CWlink/daily_ao_index/aao/aao.shtml) AAO is defined as the difference of zonal mean sea level pressure between 40°S and 65°S and it is used as an objective index to monitor and measure the atmospheric circulation condition in high southern latitudes. AAO positive anomaly values are associated with a lowering of geopotential heights over Antarctica and an increasing strength of the westerlies over the subpolar Southern Ocean (Thompson and Solomon, 2002) with consequences for ice extent and sea surface temperature (Hall and Visbeck, 2002; Kwok and Comiso, 2002).

RESULTS

VALIDATION OF GSM CDM DATA WITH FIELD CDOM DATA

From the 142 available field data points, only 15 valid field-satellite comparisons (match-ups) were obtained with GSM satellite data. From the ICEPOS data no valid match-ups were obtained, whereas only one match-up corresponded to Palmer LTER data and the resting 14 from AMLR cruises.

The results of the comparison between field $a_{\text{cdom}}(443)$ and satellite GSM $a_{\text{cdm}}(443)$ data showed good correspondence ($r^2 = 0.70$), with a slope value higher than 1 (slope = 1.25 ± 0.23) (Fig. 4.7). The detrital absorption $a_d(443)$, determined in Palmer and AMLR datasets, contributed a mean 19% to the field $a_{\text{cdm}}(443)$. When comparing $a_d(443) + a_{\text{cdom}}(443)$ together with GSM $a_{\text{cdm}}(443)$, a better fit was achieved, with a $r^2 = 0.74$ and a slope value of 1.01 ± 0.16 (Fig. 4.7).

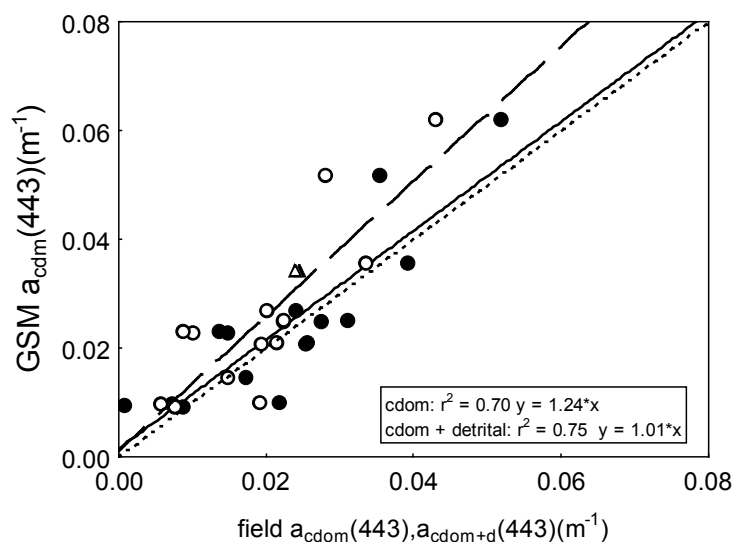


Figure 4.7. Results of direct comparisons between field $a_{\text{cdom}}(443)$ and GSM satellite $a_{\text{cdm}}(443)$ (open symbols, dashed line) and between field $a_{\text{cdom}} + a_d(443)$ and GSM satellite $a_{\text{cdm}}(443)$ (continuous line, filled symbols). Circles = data from AMLR cruises (SeaBass database). Triangles = Palmer LTER data.

SPATIAL DISTRIBUTION AND TEMPORAL DYNAMICS OF CDM IN THE ANTARCTIC PENINSULA

The use of GSM satellite data allowed visualizing the geographical distribution of monthly CDM averages in the Antarctic Peninsula area during ice-free periods (from September-October to March-April). The use of monthly averages instead of daily or weekly data permitted to obtain higher spatial coverage of valid data.

In general, higher CDM was observed near the coastline or in zones with recent ice melting, particularly in Marguerite Bay (Southwestern Antarctic peninsula), in the Western Weddell Sea below the Antarctic strait, along the Peninsula coastline, and near South Shetland Islands in the Bransfield strait. (Fig. 4.8).

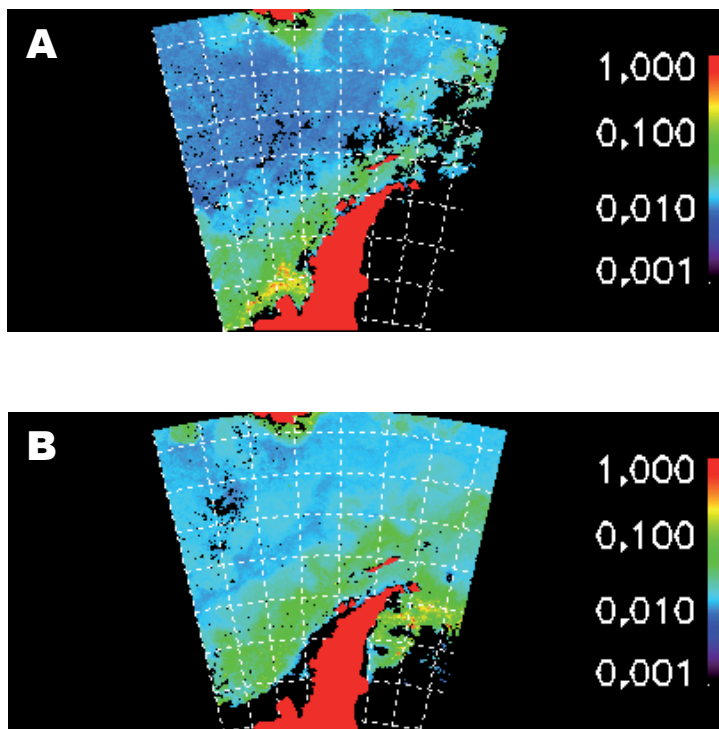


Figure 4.8. Maps of CDM ($a_{\text{cdm}}(443)$, m^{-1}) in the Antarctic Peninsula area during February 2001 and 2002, showing patches of high CDM in Marguerite Bay, in the Western Antarctic Peninsula (A), and near the ice boundary in the Western Weddell Sea (B). Black areas represent locations with no valid data over the entire month. Wide black areas at the bottom of the figures represent zones covered by ice.

At the beginning of the ice-free period (October-November) CDM was more homogeneously distributed along the study area. The $a_{\text{cdm}}(443)$ values were lower than 0.1 m^{-1} at all locations. However, as the austral summer progressed, we observed a more contrasting CDM geographical pattern. In February-March, $a_{\text{cdm}}(443)$ reached absorption up to 1 m^{-1} in areas near the coastline, and adjacent to the ice edge (Fig. 4.9). This pattern from homogenous to patchy pictures, although variable in absolute concentrations, was consistent in all studied ice-free periods.

In location 5 (situated near the ice boundary in the Wedell Sea) we found the highest CDM values (mean $a_{\text{cdm}}(443) = 0.036 \text{ m}^{-1}$), while in locations 1 and 2 (situated in open waters) CDM values were, comparatively, lower (mean $a_{\text{cdm}}(443) = 0.013 \text{ m}^{-1}$).

In locations 1 and 2 maximum CDM values were observed in the austral spring months (around November-December). In contrast, highest CDM was observed during the austral summer (January-March) in locations 3, 4 and 5 (Fig. 4.10). The seasonal amplitude was also variable among locations. CDM values

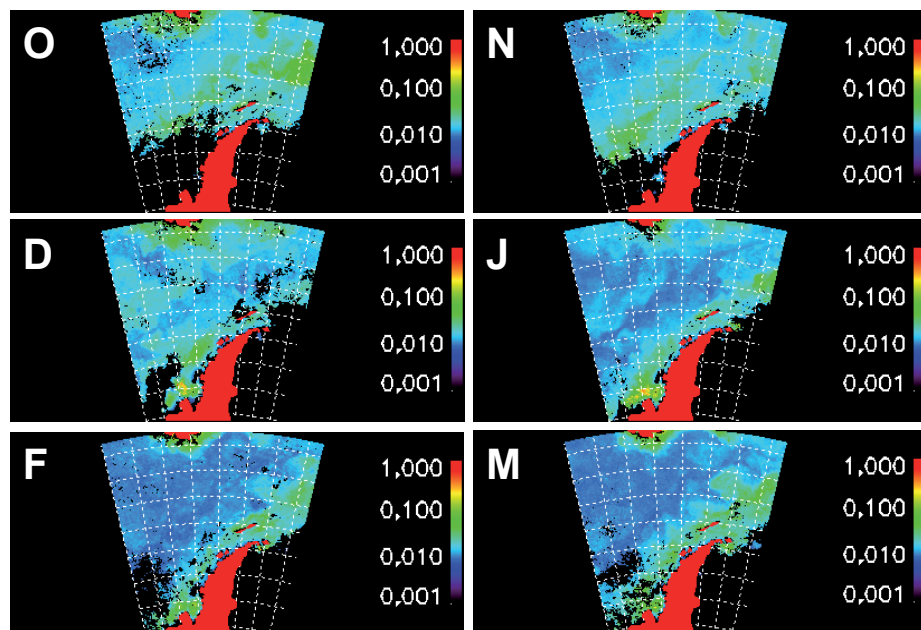


Figure 4.9. Maps of CDM ($a_{\text{cdm}}(443)$ m^{-1}) in the Antarctic Peninsula area during 2003-2004 period (from October (O) to March (M)). Black areas represent locations with no valid data over the entire month. Wide black areas at the bottom of the figures represent zones covered by ice.

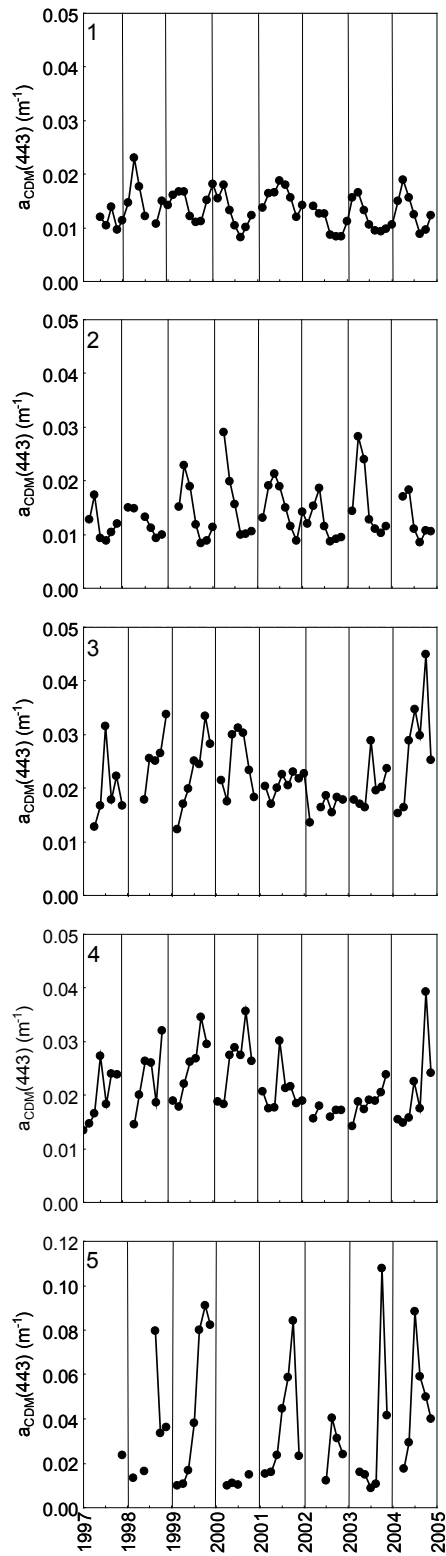


Figure 4.10. Temporal patterns of monthly $a_{\text{cdm}}(443)$ during the study ice-free periods (1997 to 2005) in the five selected locations. Note location 5 has a different y-axis scale.

oscillated seasonally in a range of $\pm 0.007 \text{ m}^{-1}$ to $\pm 0.010 \text{ m}^{-1}$ between maxima and minima in stations 1, 2, 3 and 4. By contrast, seasonal amplitude in location 5 was higher, ranging $\pm 0.046 \text{ m}^{-1}$ (Fig. 4.10)

The contribution of CDM to non-water absorption at 443nm (%CDM) averaged 57.7% and ranged from 40.5% to 72.6% in the study locations. This percentage was quite constant, although a decreasing trend with latitude was observed (mean %CDM was highest at locations 1 and 2 (57.1%) and lowest at location 5 (55.6%)). Respect to seasonal variations, in locations 3, 4 and 5 a %CDM was consistently maximum at the beginning of the ice-free periods, decreased in the middle (by November-December) and increased again at the end (Fig. 4.11). In locations 1 and 2 this seasonal pattern was less evident. In location 1, %CDM tended to decrease along with the summer, while in location 2 the seasonal pattern was not repetitive over the different study periods (Fig. 4.11).

The determination of CDM anomaly patterns let us to observe interannual variability, which was also variable among locations. Locations 1 and 2 (situated farther to the coastline) showed a relatively homogenous anomaly pattern, close to 0. Locations inside Bransfield Strait (3 and 4) ranged within $\pm 40\%$ of average values and showed a cyclic pattern of CDM anomaly (Fig. 4.12), where negative anomalies from 1997 to 1999 and from 2002 to 2004 alternated with positive anomalies from 2000 to 2001 and in 2005. Finally, location 5, situated in the western Weddell Sea, showed highest CDM anomalies (within $\pm 100\%$), and although the temporal pattern was quite irregular, positive anomalies were observed in the same periods as in locations 3 and 4, being highest in 2005.

SPATIAL AND TEMPORAL DRIVERS OF CDM IN THE ANTARCTIC PENINSULA

The correlation analyses between CDM and chl *a*, SST, PAR and ice extent in the different selected locations showed significant and positive relationships between CDM and chl *a* in all locations. Additionally, SST was weakly or unrelated to CDM, being only positively related inside Bransfield strait (location 3). CDM and PAR were positively correlated only in the Southern locations (3, 4 and 5), and this correlation was particularly high in the Weddell Sea (Table 4.3). Finally, in the locations situated nearer the ice boundary layer (4 and 5) CDOM was negatively correlated to ice extent, while this correlation was positive in locations 1 and 2 (Table 4.3)

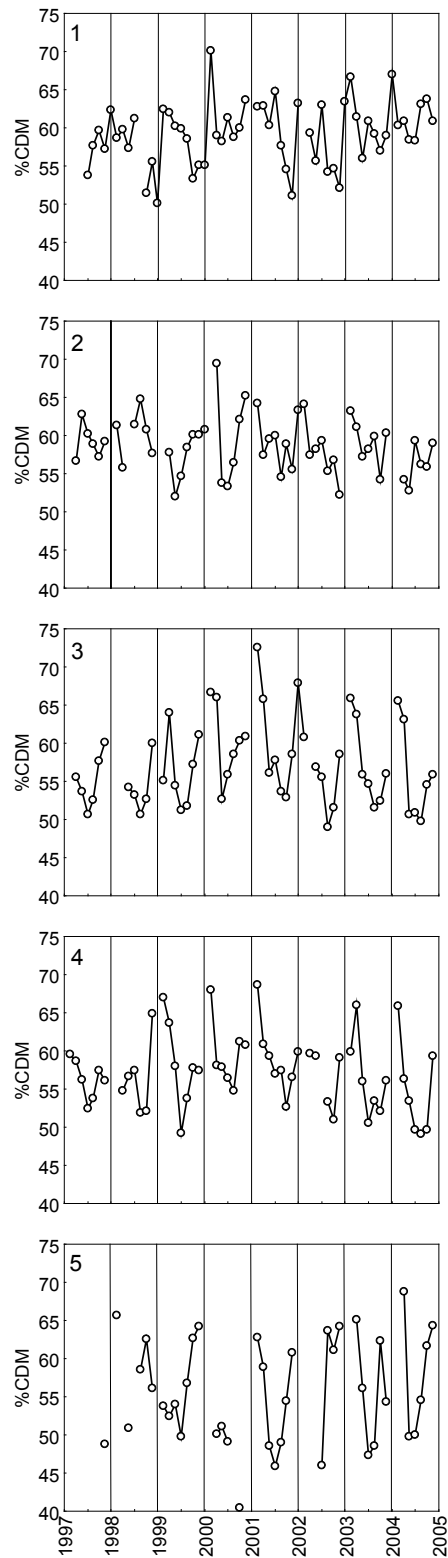


Figure 4.11. Temporal patterns of the contribution of CDM to the total non-water absorption (%CDM) during the study ice-free periods (1997 to 2005) in the five selected locations.

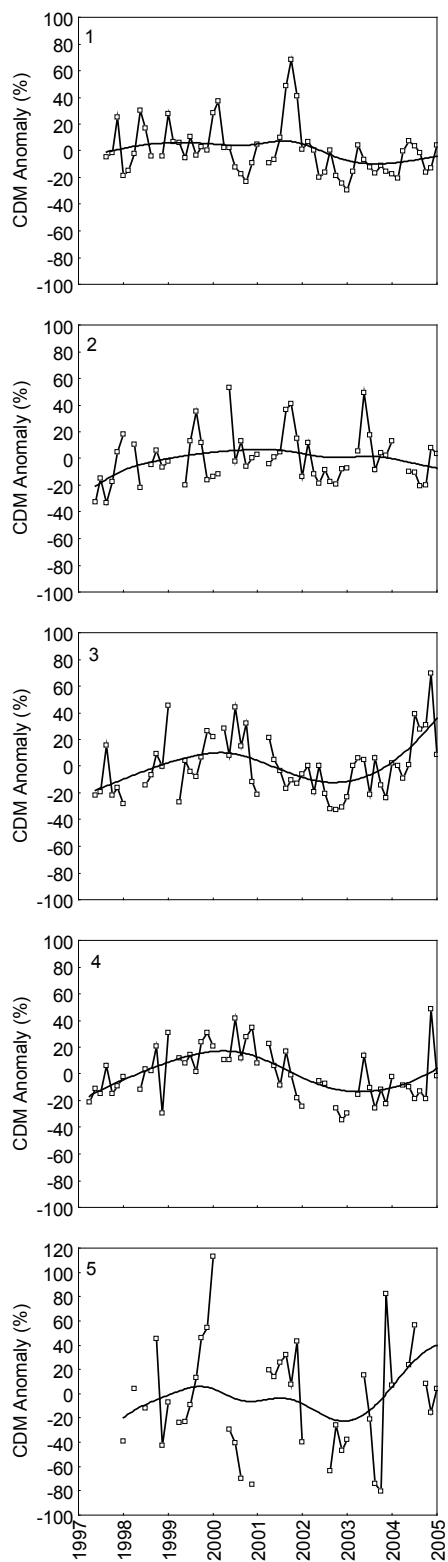


Figure 4.12. Temporal patterns of monthly CDM anomalies along 1997 to 2005 ice-free periods in the five study locations.

Table 4.3. Temporal patterns of the contribution of CDM to the total non-water absorption (%CDM) during the study ice-free periods (1997 to 2005) in the five selected locations.

Location	1	2	3	4	5
Chl a	0.79*	0.87*	0.89*	0.83*	0.91*
SST		-0.21	0.37*	-0.27	-0.02
Ice extent	0.63*	0.79*	-0.24	-0.36*	-0.60*
PAR	-0.12	0.15	0.39*	0.27*	0.68*

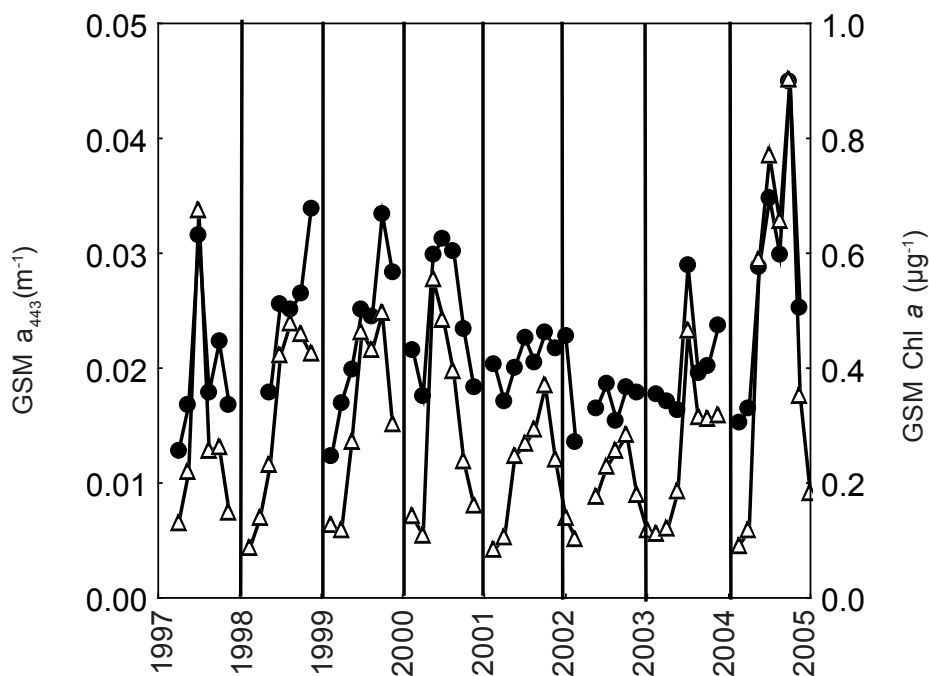


Figure 4.13. Temporal trends of monthly CDM (Brown circles) and chl a (Green circles) in location 3 over all studied ice-free periods.

Table 4.4. Results of correlation analyses between CDM anomalies and chlorophyll a (chl a), and Antarctic Oscillation Index (AAO). Asterisks represent significant correlations at $p < 0.05$.

Location	1	2	3	4	5
Chl a	0.70*	0.42*	0.61*	0.48*	0.75*
AAO	0.32*	0.36*	-0.02	0.25	0.11

CDM and chl *a* followed synchronous dynamics (Fig. 4.13) and a lag time between both variables was not detected after lagged correlation analyses ($p > 0.05$). This lag time between chl *a* and CDM was not observed in any study locations and years. Chl *a* and CDM also coincided geographically, which could be visualized when comparing monthly satellite images of CDM and chl *a* (Fig. 4.14).

Likewise, CDM anomaly was correlated to chl *a* in all locations (Table 4.4), and this anomaly was related to AAO in locations 1 and 2 (Table 4.4) but not significantly correlated to SST, PAR and ice extent at any locations. The oscillation of the AAO index showed a similar pattern that CDM anomaly. Periods with positive CDM anomalies roughly corresponded to positive AAO and vice versa, except from spring and summer 2000-2001. In station 5, although we did not obtain significant correlations, similar trends between CDM anomaly and AAO could be observed (Fig. 4.15).

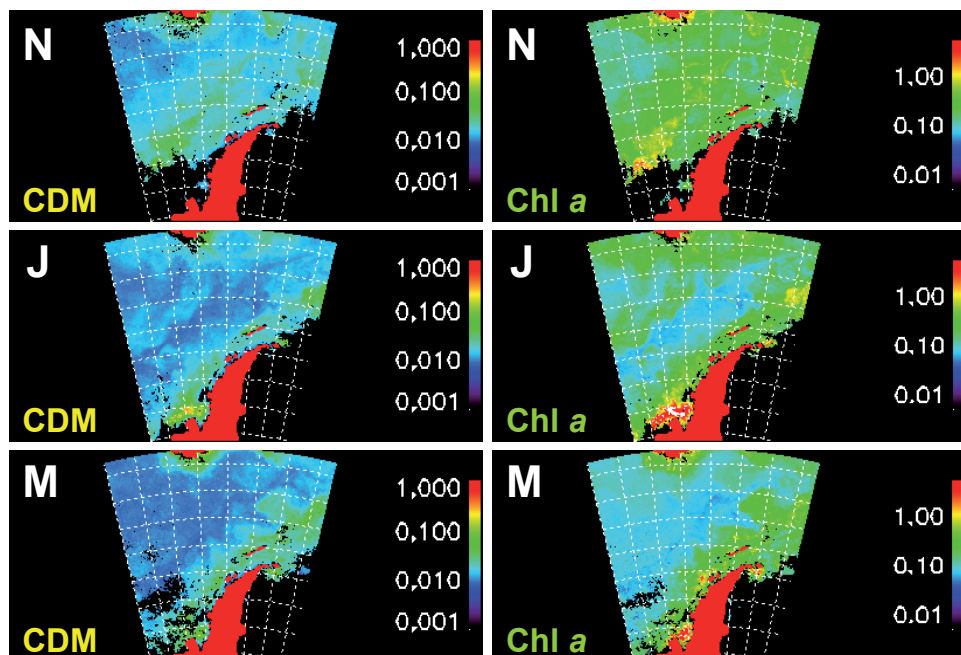


Figure 4.14. Maps of CDM ($a_{\text{cdm}}(443)$, m^{-1} , first column) and chl *a* ($\mu\text{g l}^{-1}$, second column) in the Antarctic Peninsula area in November (N), January (J) and March (M) 2003-2004.

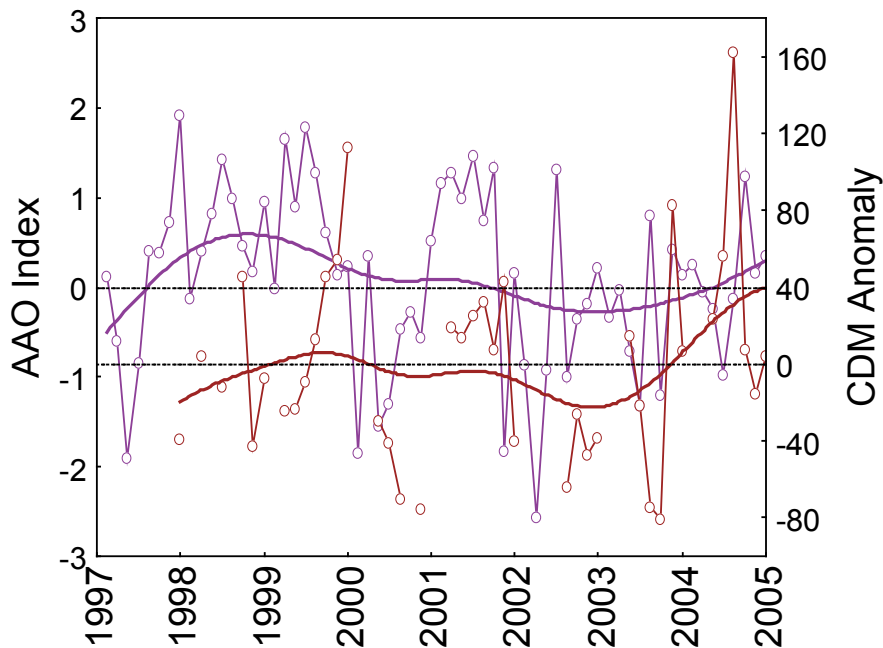


Figure 4.15. Monthly mean of AAO Index during the study ice-free periods (source: http://www.cpc.noaa.gov/products/precip/CWlink/daily_ao_index/aao/aao_index.htm, purple line) and CDM anomaly pattern in location 5 (brown line)

DISCUSSION

VALIDATION OF GSM CDM DATA WITH FIELD CDOM DATA

The validity of the GSM algorithm in the Antarctic Peninsula was confirmed in this study as significant comparisons between field and satellite (GSM model) were obtained. Indeed, the GSM Model, optimized for global open ocean waters, has also reported satisfactory results when applied to more optically complex coastal waters (Kudela and Chavez, 2004; Kostadinov et al., 2007).

The slope of the regression line between field $a_{\text{cdom}}(443)$ and GSM $a_{\text{cdm}}(443)$ was higher than the regression lines obtained globally (Siegel et al., 2002; Siegel et al., 2005). The comparative analysis was made between field CDOM (0.2 μm filtered water) and satellite CDM data which also includes detrital organic matter. The higher slope values for the $a_{\text{cdom}}(443)$ -GSM $a_{\text{cdm}}(443)$ that those reported by

Siegel et al. (2002) for the global ocean suggest a higher contribution of detrital particles to CDM absorption in this particular area. This contribution averaged a 20%, in contrast to a mean 12% in the Sargasso Sea (Siegel et al., 2005). This higher contribution could be caused by ice meltwater during austral summer, that has a noticeable influence from the ice edge to waters up to 100 km offshore, and particles releasing “glacial flour” during ice melting cause an increasing turbidity in the water (Dierssen et al., 2002). Indeed, if the comparison includes field detrital absorption ($a_d(443)$) the obtained slope value is 1, confirming the validity of the GSM algorithm for CDM retrievals in the area (Fig. 4.7).

The higher contribution of detrital particles to the CDM signal can affect the percentage of CDM to the optical signal of water-leaving radiance (L_w). The contribution of CDM respect to non-water absorption in this area was on average 58%, higher than the reported for the global ocean (51.1%, Siegel et al., 2002). Therefore, CDM appears to have a greater contribution than chl *a* to the optical signal of L_w . This higher contribution of CDM relative would lead to an overestimation of chl *a* when empirical algorithms are used. Empirical algorithms assume a fixed relationship between the contribution of phytoplankton and CDM absorption to the signal. This contrasts with what it is actually observed in Southern Ocean waters (Mitchell and Holmhansen, 1991; Dierssen and Smith, 2000; Marrari et al., 2006), that is, a general underestimation of satellite chl *a* estimations compared to shipboard measurements. Hence, the contribution of CDM fails in explaining these biases, which are more likely due to other reasons such as different pigment-specific absorption (Mitchell and Holmhansen, 1991; Dierssen and Smith, 2000), phytoplankton composition (Arrigo et al., 1998), or methodology (Marrari et al., 2006).

SPATIAL DISTRIBUTION AND TEMPORAL DYNAMICS OF CDM IN THE ANTARCTIC PENINSULA

The processed images exemplified that CDM was not homogeneously distributed over the study area. As austral summer advances, more and more patches of higher CDM were detected in coastal areas and zones with recent ice melting. This general pattern was repeatedly observed in all the study ice-free periods, although the amount of ice existing at the end of the season, as well as the specific areas with higher ice retreat (e.g. Marguerite Bay vs Weddell Sea, Fig. 4.8) was variable among the different periods. Likewise, the study of CDM anomalies

in the different locations revealed that CDM dynamics in certain areas are driven not only by seasonal drivers but also by non-seasonal forcings such as the variation in the Antarctic oscillation (AAO) index.

As terrestrial influence on DOM cannot be associated to factors such as river discharge, CDM patches in the coastal areas or the ice edge indicates that they are mostly originated by snow and glacial ice melting from land or to sea ice retreat, so ice would be acting as a direct or indirect source of CDM. Indeed, in the locations situated near the coastline of the Peninsula or the ice edge showed higher seasonal averages and amplitudes in comparison to offshore locations. In those locations, a negative correlation between ice extent and CDM was observed. However, total monthly ice extent is a rude estimate of the existing ice retreat rates in every pixel, and in this sense further work is needed to accurately estimate the magnitude of CDM attributable to ice melting dynamics.

In contrast to the role of ice affecting CDM distribution, no significant relationship was observed between CDM and SST. Temperature is a primary controlling factor of all metabolic processes (Nedwell, 1999; Boyd, 2002) and, thus, it could regulate biological CDOM generation and consumption processes. However, the low relationships observed between SST and CDM dynamics suggest that temperature appears not to be a major driver of CDM in this region.

In the case of PAR radiation, as previously reported in chapters 1 and 2, photobleaching losses represent an important sink of CDOM in the ocean surface (Vodacek et al., 1997; Nelson et al., 1998). Since PAR radiation appears to contribute significantly to CDOM photobleaching at 440nm (Reche et al., 2000), a negative correlation between PAR and CDOM could be expected. In contrast, these two variables were positively correlated in the locations situated at higher latitudes. This fact could be partly due to an indirect effect of CDOM generation through an enhancement of primary production by PAR in these higher latitudes with light limitation (Mitchell et al., 1991; Boyd, 2002).

Unlike the non-significant or weak relationships between SST or PAR and CDM dynamics, the relationship between CDM and chl *a* was very robust. A coincidence in CDM and chl *a* was observed both in spatial distributions and also in temporal (seasonal and interannual) dynamics (based in monthly data). This consistency is apparently contradictory to the results reported in chapter 1, where

simultaneous field observations of chl *a* and CDOM over the Antarctic Peninsula were not correlated. To explain this temporal correspondence between chl *a* and CDM we propose two hypothesis. One plausible explanation is that phytoplankton act as a source of CDM which is only detectable at these temporal and spatial scales. In the Southern Ocean, most organic carbon has an ultimate algal source. The complexity of CDOM cycling, along with different renovation times of chl *a* and CDOM, can lead to non significant relationships at shorter spatial and temporal scales, as we observed with field data (chapter 1). From the results showed in this chapter, we cannot determine whether the source of CDM by phytoplankton is direct (exudates or dead cells) or indirect through a subsequent microbial processing or humification. In both cases, the correspondence between chl *a* and CDM at monthly scales suggests that the processes converting algal DOM into CDOM should happen at a timescale of less than a month. In chapter 3 we proposed CDOM duplication times attributable to bacteria within months, so CDM dynamics may be not only due to bacterial processing but have a combined source of direct algal release and indirect CDOM generation by bacteria and other organisms such as krill.

The second reason to explain the synchrony between chl *a* and CDM dynamics is the common response of both variables to external forces. In this sense, high CDM values have been consistently observed in areas with recent ice retreat or in zones adjacent to the coastline (see figures 4.8 and 4.9). Indeed, the annual advance and retreat of sea ice together with glacial meltwater dynamics are the major physical determinant of spatial and temporal changes in the structure and function of the Antarctic marine ecosystem (Dierssen et al., 2002; Ducklow et al., 2007). Sea ice and snow melting can provide macronutrients and also limiting micronutrients which were incorporated into the ice during its formation or accumulated as dust in the snow cover (Smetacek and Nicol, 2005). Therefore, an accumulation of chromophoric compounds in the ice or snow and its subsequent release during ice and snow melting would not be surprising. Although to date there are no published data, D.N. Thomas (personal comm.) measured high CDOM values in ice cores from the Atlantic section of the Southern Ocean, with $a_{\text{cdom}}(440)$ in the bottom of the ice cores ranging from 0.92 to 7.60 m^{-1} (mean 4.15 m^{-1}). In addition, the provision of macro and micronutrients and a shallow surface layer associated to ice and snow melting can also supply enhance algal bloom development.

The two-fold effect of ice melting releasing CDOM and promoting algal growth allow us to propose a combined effect of the two explanations described above. First, CDM dynamics would be affected directly by ice melting. Second, the growth of algae associated to this ice retreat, along with the communities of algae and bacteria associated to the underside of ice, would “seed” the waters when this ice melts. This algal growth could be fueling bacterial communities and krill swarms, which are demonstrated to be net sources of CDOM (Rochelle-Newall and Fisher, 2002; Nelson et al., 2004; Steinberg et al., 2004)see chapter 3). The seasonal changes in %CDM in the locations situated closer to the ice edge (locations 3, 4 and 5), support this hypothesis. The %CDM increases as the austral summer advances suggests a more retarded response of CDM than chl *a*. Therefore, the dynamics of sea ice and glacial snow could have a cascading effect that yield to an ultimate regulation of CDM in the region, both directly and indirectly promoting the development of different biological communities that have a significant role in CDOM generation (Fig. 4.16).

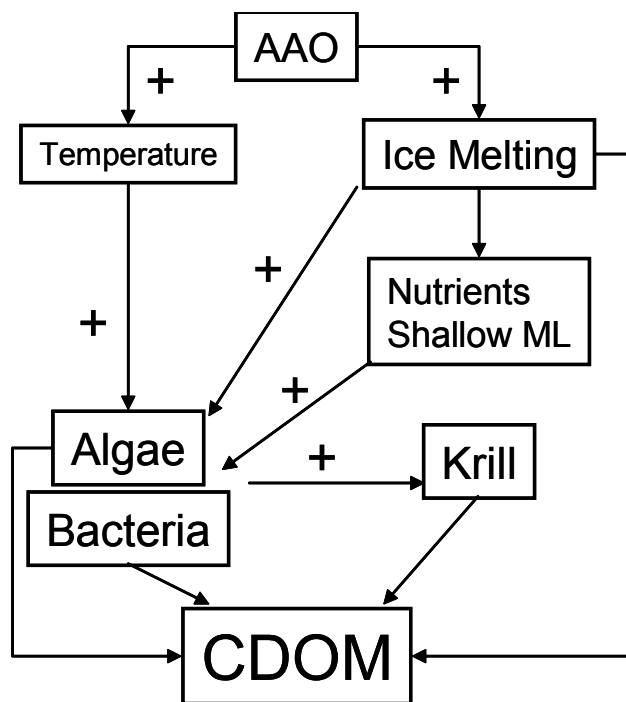


Figure 4.16. Scheme of principal processes affecting CDOM dynamics in the Antarctic Peninsula.

The Antarctic Peninsula is one of the most vulnerable areas to global change, with a warming rate that exceeds any other observed globally (Vaughan et al., 2003; Clarke et al., 2007). This influence involves a significant decreasing trend in the magnitude of ice extent and in the duration of winter ice. That is, the ice cap retreats earlier in the season and starts to grow later (Clarke et al., 2007; Ducklow et al., 2007) that could lead to an increase in average and seasonal amplitude of CDM.

The observed warming over Antarctic Peninsula and its subsequent ice retreat appears to be a consequence of the increasing trend of the AAO index in the last years due mostly to photochemical ozone losses (Thompson and Solomon, 2002). In this sense, oscillations in the AAO index also appear to have an effect in CDM anomaly patterns (Table 4.4, Fig. 4.15). A positive AAO index lead to abnormally increases of CDM and vice versa. Positive anomalies of the AAO index have been associated to warmer surface temperatures and higher ice retreat in the Antarctic Peninsula area (Comiso, 2000; Kwok and Comiso, 2002; Lovenduski and Gruber, 2005) and also have been related to higher chl *a* concentrations in the region (Lovenduski and Gruber, 2005). Under this scenario, the increase of AAO index and its consequences on physical variables such as ice extent and duration will have an evident effect on CDM concentrations altering their seasonal and interannual dynamics.

To conclude, we have demonstrated in the first section of the chapter the reliability of the GSM algorithm to retrieve CDM concentrations from satellite observations in the Antarctic Peninsula. The contribution of detrital particles to the CDM signals, higher than that observed in other ocean areas, can result in a higher contribution of CDM to the non-water absorption that would ultimately result in low accuracy of empiric algorithms to retrieve chl *a* data from SeaWiFS and MODIS satellite observations in the Antarctic Peninsula. The demonstrated precision of the GSM algorithms to retrieve CDM in the study area allowed us to study temporal geographical CDM dynamics around the Antarctic Peninsula. From these determinations we can conclude that seasonal CDM dynamics in the Antarctic Peninsula are strongly dependent on the seasonal retreat and advance of the ice cap, while interannual variation can be related to climatic forces such as the Antarctic Oscillation. The geographical and temporal synchrony of chl *a* suggest a significant role of primary producers in long-term dynamics of CDM, which could be direct or indirect through the fueling of heterotrophic communities such as bacteria and krill populations.

REFERENCES

- ARNONE, R.A. and A.R. PARSONS (2004) Real-time use of ocean color remote sensing for coastal monitoring. *In*: R. L. Miller, C. E. DelCastillo and B. A. McKee (eds.) *Remote Sensing of the Coastal Environments*. Kluwer academic, Dordrecht, The Netherlands.
- ARRIGO, K.R., D.H. ROBINSON, D.L. WORTHEN, B. SCHIEBER and M.P. LIZOTTE (1998) Bio-optical properties of the southwestern Ross Sea. *Journal of Geophysical Research-Oceans*. 103: 21683-21695.
- BAILEY, S.W. and P.J. WERDELL (2006) A multi-sensor approach for the on-orbit validation of ocean color satellite data products. *Remote Sensing of Environment*. 102: 12-23.
- BOYD, P.W. (2002) Environmental factors controlling phytoplankton processes in the Southern Ocean. *Journal of Phycology*. 38: 844-861.
- BRICAUD, A., M. BABIN, A. MOREL and H. CLAUSTRE (1995) Variability in the chlorophyll-specific absorption-coefficients of natural phytoplankton - analysis and parameterization. *Journal of Geophysical Research-Oceans*. 100: 13321-13332.
- CLARKE, A., N.M. JOHNSTON, E.J. MURPHY and A.D. ROGERS (2007) Introduction. *Antarctic ecology from genes to ecosystems: the impact of climate change and the importance of scale*. *Philosophical Transactions of the Royal Society B-Biological Sciences*. 362: 5-9.
- COMISO, J.C. (2000) Variability and trends in Antarctic surface temperatures from in situ and satellite infrared measurements. *Journal of Climate*. 13: 1674-1696.
- DIERSSEN, H.M. and R.C. SMITH (2000) Bio-optical properties and remote sensing ocean color algorithms for Antarctic Peninsula waters. *Journal of Geophysical Research-Oceans*. 105: 26301-26312.
- DIERSSEN, H.M., R.C. SMITH and M. VERNET (2002) Glacial meltwater dynamics in coastal waters west of the Antarctic peninsula. *Proceedings of the National Academy of Sciences of the United States of America*. 99: 1790-1795.
- DUCKLOW, H.W., K. BAKER, D.G. MARTINSON, L.B. QUETIN, R.M. ROSS, R.C. SMITH, S.E. STAMMERJOHN, M. VERNET and W. FRASER (2007) Marine pelagic ecosystems: The West Antarctic Peninsula. *Philosophical Transactions of the Royal Society B-Biological Sciences*. 362: 67-94.

- GORDON, H.R. (1997) Atmospheric correction of ocean color imagery in the Earth Observing System era. *Journal of Geophysical Research-Atmospheres*. 102: 17081-17106.
- GORDON, H.R., T. DU and T.M. ZHANG (1997) Remote sensing of ocean color and aerosol properties: resolving the issue of aerosol absorption. *Applied Optics*. 36: 8670-8684.
- GORDON, H.R. and K.J. VOSS (1999) MODIS normalized water-leaving radiance. *In: N. G. S. F. Center (ed.) MODIS Algorithm Theoretical Basis Document ATMD MOD-17*, Greenbelt, MD.
- GORDON, H.R. and M.H. WANG (1994) Retrieval of water-leaving radiance and aerosol optical-thickness over the oceans with SeaWiFS - a preliminary algorithm. *Applied Optics*. 33: 443-452.
- GREGG, W.W. and N.W. CASEY (2004) Global and regional evaluation of the SeaWiFS chlorophyll data set. *Remote Sensing of Environment*. 93: 463-479.
- HALL, A. and M. VISBECK (2002) Synchronous variability in the Southern hemisphere atmosphere, sea ice, and ocean resulting from the Annular Mode. *Journal of Climate*. 15: 3043-3057.
- IOCG (2006) Remote sensing of inherent optical properties: fundamentals, tests of algorithms, and applications, vol. 5. IOCG, Darmouth, Canada.
- KIRK, J.T.O. (1984) Dependence of relationship between inherent and apparent optical-properties of water on solar altitude. *Limnology and Oceanography*. 29: 350-356.
- KOSTADINOV, T.S., D.A. SIEGEL, S. MARI-TORENA and N. GUILLOCHEAU (2007) Ocean color observations and modeling for an optically complex site: Santa Barbara Channel, California, USA. *Journal of Geophysical Research-Oceans*. 112.
- KUDELA, R.M. and F.P. CHAVEZ (2004) The impact of coastal runoff on ocean color during an El Nino year in Central California. *Deep-Sea Research Part II-Topical Studies in Oceanography*. 51: 1173-1185.
- KWOK, R. and J.C. COMISO (2002) Spatial patterns of variability in antarctic surface temperature: Connections to the Southern Hemisphere Annular Mode and the Southern Oscillation. *Geophysical Research Letters*. 29: 1705-1709.
- LEE, Z.P., K.P. DU and R. ARNONE (2005) A model for the diffuse attenuation coefficient of downwelling irradiance. *Journal of Geophysical Research-Oceans*. 110.
- LOVENDUSKI, N.S. and N. GRUBER (2005) Impact of the Southern Annular Mode

- on Southern Ocean circulation and biology. *Geophysical Research Letters*. 32.
- MAGNUSON, A., L.W. HARDING, M.E. MALLONEE and J.E. ADOLF (2004) Bio-optical model for Chesapeake Bay and the Middle Atlantic Bight. *Estuarine Coastal and Shelf Science*. 61: 403-424.
- MARITORENA, S., D.A. SIEGEL and A.R. PETERSON (2002) Optimization of a semi-analytical ocean color model for global-scale applications. *Applied Optics*. 41: 2705-2714.
- MARRARI, M., C.M. HU and K. DALY (2006) Validation of SeaWiFS chlorophyll a concentrations in the Southern Ocean: A revisit. *Remote Sensing of Environment*. 105: 367-375.
- MARTIN, S. (2002) *An introduction to ocean remote sensing*. Cambridge University Press, Cambridge.
- MITCHELL, B.G., E.A. BRODY, O. HOLM-HANSEN, C. MCCLAIN and J. BISHOP (1991) Light limitation of phytoplankton biomass and macronutrient utilization in the Southern Ocean. *Limnology and Oceanography*. 36: 1662-1677.
- MITCHELL, B.G. and O. HOLM-HANSEN (1991) Biooptical properties of Antarctic Peninsula waters - Differentiation from temperate ocean models. *Deep-Sea Research Part a-Oceanographic Research Papers*. 38: 1009-1028.
- MOORE, J.K. and S.C. DONEY (2006) Remote sensing observations of ocean physical and biological properties in the region of the Southern Ocean Iron Experiment (SOFEX). *Journal of Geophysical Research-Oceans*. 111.
- NEDWELL, D.B. (1999) Effect of low temperature on microbial growth: lowered affinity for substrates limits growth at low temperature. *FEMS Microbiology Ecology*. 30: 101-111.
- NELSON, N.B., C.A. CARLSON and D.K. STEINBERG (2004) Production of chromophoric dissolved organic matter by Sargasso Sea microbes. *Marine Chemistry*. 89: 273-287.
- NELSON, N.B., D.A. SIEGEL and A.F. MICHAELS (1998) Seasonal dynamics of colored dissolved material in the Sargasso Sea. *Deep-Sea Research Part I-Oceanographic Research Papers*. 45: 931-957.
- O'REILLY, J.E., S. MARITORENA, B.G. MITCHELL, D.A. SIEGEL, K.L. CARDER, S.A. GARVER, M. KAHRU and C. MCCLAIN (1998) Ocean color chlorophyll algorithms for SeaWiFS. *Journal of Geophysical Research-Oceans*. 103: 24937-24953.
- OUBELKHEIR, K., L.A. CLEMENTSON, I.T. WEBSTER, P.W. FORD, A.G. DEKKER, L.C. RADKE and P. DANIEL (2006) Using inherent optical properties to investigate

- te biogeochemical dynamics in a tropical macrotidal coastal system. *Journal of Geophysical Research-Oceans*. 111.
- PABI, S. and K.R. ARRIGO (2006) Satellite estimation of marine particulate organic carbon in waters dominated by different phytoplankton taxa. *Journal of Geophysical Research-Oceans*. 111.
- PATTERSON, K.W. (2000) Contribution of chromophoric dissolved organic matter to attenuation of ultraviolet radiation in three contrasting coastal areas. University of California Santa Barbara, Santa Barbara.
- PEGAU, S., J.V.R. ., B. ZANEVELD., G. MITCHELL, J.L. MUELLER, M. KAHRU, J. WIELAND, MALGORZAT and M. STRAMSKA (2003) *Inherent Optical Properties: Instruments, characterizations, field measurements and data analysis protocols*, vol. IV. NASA.
- RECHE, I., M.L. PACE and J.J. COLE (2000) Modeled effects of dissolved organic carbon and solar spectra on photobleaching in lake ecosystems. *Ecosystems*. 3: 419-432.
- REYNOLDS, R.A., D. STRAMSKI and B.G. MITCHELL (2001) A chlorophyll-dependent semianalytical reflectance model derived from field measurements of absorption and backscattering coefficients within the Southern Ocean. *Journal of Geophysical Research-Oceans*. 106: 7125-7138.
- ROCHELLE-NEWALL, E.J. and T.R. FISHER (2002) Production of chromophoric dissolved organic matter fluorescence in marine and estuarine environments: an investigation into the role of phytoplankton. *Marine Chemistry*. 77: 7-21.
- SIEGEL, D.A., S. MARITORENA and N.B. NELSON (2005) Independence and interdependencies among global ocean color properties: Reassessing the bio-optical assumption. *Journal of Geophysical Research-Oceans*. 110.
- SIEGEL, D.A., S. MARITORENA, N.B. NELSON, D.A. HANSELL and M. LORENZIKAYSER (2002) Global distribution and dynamics of colored dissolved and detrital organic materials. *Journal of Geophysical Research-Oceans*. 107.
- SMETACEK, V. and S. NICOL (2005) Polar ocean ecosystems in a changing world. *Nature*. 437: 362-368.
- STEINBERG, D.K., N.B. NELSON, C.A. CARLSON and A.C. PRUSAK (2004) Production of chromophoric dissolved organic matter (CDOM) in the open ocean by zooplankton and the colonial cyanobacterium *Trichodesmium spp.* *Marine Ecology-Progress Series*. 267: 45-56.

STRAMSKI, D., R.A. REYNOLDS, M. KAHRU and B.G. MITCHELL (1999) Estimation of particulate organic carbon in the ocean from satellite remote sensing. *Science*. 285: 239-242.

THOMPSON, D.W.J. and S. SOLOMON (2002) Interpretation of recent Southern Hemisphere climate change. *Science*. 296: 895-899.

VAUGHAN, D.G., G.J. MARSHALL, W.M. CONNOLLEY, C. PARKINSON, R. MULVANEY, D.A. HODGSON, J.C. KING, C.J. PUDSEY and J. TURNER (2003) Recent rapid regional climate warming on the Antarctic Peninsula. *Climatic Change*. 60: 243-274.

VODACEK, A., N.V. BLOUGH, M.D. DEGRANDPRE, E.T. PELTZER and R.K. NELSON (1997) Seasonal variation of CDOM and DOC in the Middle Atlantic Bight: Terrestrial inputs and photooxidation. *Limnology and Oceanography*. 42: 674-686.



Chapter 5: **Uncoupled distribution of transparent exopolymer particles and dissolved carbohydrates in the Southern Ocean.**

Ortega-Retuerta, E., Pulido-Villena, E., Agustí, S., Duarte, C.M., and Reche, I.

Abbreviated title: TEP and dissolved carbohydrates in the Southern Ocean



INTRODUCTION

The importance of transparent exopolymer particles (TEP) dynamics has received considerable attention in the last few years as they are a significant component of the sedimentary flux in marine ecosystems (Passow, 2002b). Transparent exopolymer particles were described for the first time in a diatom culture, and their origin was proposed to be dissolved polysaccharide exudates, released copiously by phytoplankton and bacteria, that would spontaneously assemble to form these particles (Alldredge et al., 1993). Thereafter, phytoplankton cells have traditionally been considered to be the major source of both TEP and their precursors in marine ecosystems (Passow and Alldredge, 1994; Passow, 2002a; Passow, 2002b); and it has been well evidenced that exponentially-growing diatoms can excrete significant amounts of TEP precursors (Alldredge et al., 1993; Passow, 2002a) or TEP directly via sloughing and lysis of senescent colonies (Hong et al., 1997). Other organisms, such as macroalgae (Thornton, 2004), or zooplankton (Passow and Alldredge, 1999; Prieto et al., 2001) have also been described as secondary sources of TEP. However, the interaction between bacterioplankton and TEP still remains unclear, and appear to be more complex than hitherto thought, since bacteria can either generate (Stoderegger and Herndl, 1998; Passow, 2002a) or degrade (Grossart and Simon, 1998) TEP (see chapter 6), or influence algal release of TEP (Grossart, 1999).

TEP geographical distribution reflect prevalently the trophic status of the system, rather than presenting regional differences, so higher TEP concentrations

are usually found in coastal systems within the photic layer (Passow, 2002b). Most studies on TEP have described their formation and dynamics either under experimental conditions (Passow, 2000; Sugimoto et al., 2007) or during phytoplankton blooms (Hong et al., 1997; Ramaiah et al., 2001; Huertas et al., 2005). By contrast, little is known about TEP distribution under non-bloom conditions, and particularly scarce is the published information about TEP distributions in the Southern Ocean (but see Passow et al., 1995; Hong et al., 1997; Corzo et al., 2005), where sedimentary carbon fluxes affect the air-sea exchange of CO₂ on a global scale (Marinov et al. 2006). In addition, although the formation of TEP from dissolved precursor material has been experimentally demonstrated (Mopper et al., 1995; Zhou et al., 1998; Passow, 2000), the published studies describing TEP and dissolved mono and polysaccharides simultaneously in the field are particularly scant (Bhaskar and Bhosle, 2006).

In this chapter, two main objectives were addressed. First, we described the spatial distribution of TEP and dissolved carbohydrates (DMCHO and DPCHO) in the Antarctic Peninsula area of the Southern Ocean. Second, we explored the relationships between TEP and their dissolved precursors and chlorophyll *a* and bacterial abundance and bacterial production.

MATERIAL AND METHODS

The sampling protocols and chemical and biological analyses of dissolved monosaccharides (DMCHO), dissolved polysaccharides (DPCHO), transparent exopolymer particles (TEP), chlorophyll *a* (chl *a*), bacterial abundance (BA) and bacterial production (BP) are detailed in the general section of methods. DMCHO, DPCHO and TEP in the Southern Ocean were only determined during ICEPOS 2005.

To explore the potential controlling factors on TEP distributions, we tested the relationship between TEP, DMCHO, DPCHO, chl *a* concentration and bacterial abundance and production using regression and multiple regression analyses. Data were log-transformed when needed to fit the regression assumptions of normality and homogeneity of variances. Averages were calculated merging all data or separating into different layers, over and below the mixed layer depth (MLD), as described in the general methods section.

RESULTS

DMCHO concentration ranged from undetectable to $12.6 \mu\text{mol C l}^{-1}$ (mean $4.3 \mu\text{mol C l}^{-1}$), while DPCHO ranged from undetectable to $21.0 \mu\text{mol C l}^{-1}$, with an average concentration of $8.6 \mu\text{mol C l}^{-1}$ (Table 5.1). DMCHO concentrations were higher in the Bellingshausen Sea and Bransfield strait than in the Weddell Sea. However, DPCHO concentrations did not differ significantly among the different areas (Table 5.1). On the other hand, similar average DMCHO concentrations were observed over the upper several 200m, while the concentration of DPCHO was slightly higher in waters of the upper mixed layer than below the MLD (Table 5.2). DMCHO and DPCHO were inversely correlated ($p < 0.001$, Fig. 5.1) although the vertical profiles of DMCHO and DPCHO did not show a coupled pattern across the different stations or areas (Fig. 5.2). Together, dissolved carbohydrates (DMCHO+DPCHO) accounted for 23% of the total DOC pool. This percentage was very consistent across the different geographical areas studied (Table 5.1, Fig. 5.3A) and over and below the MLD (Table 5.2).

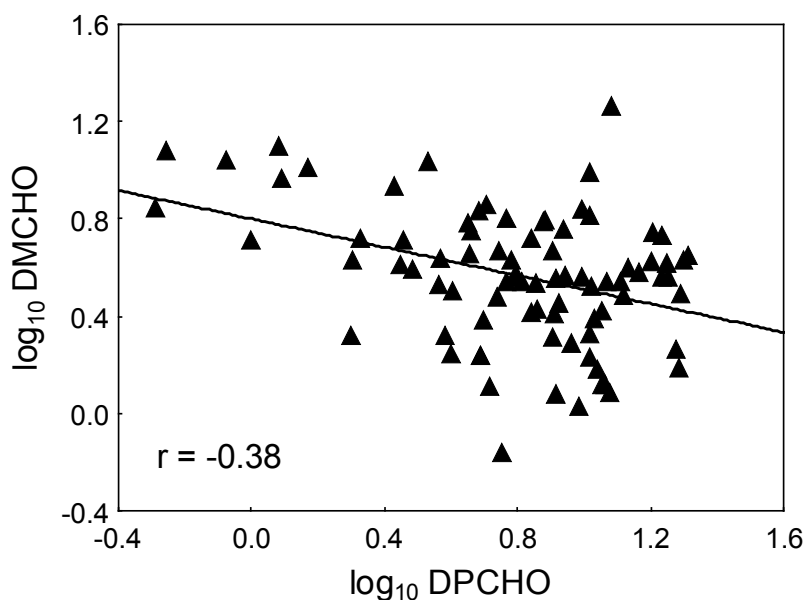


Figure 5.1. Scatterplot between DPCHO and DMCHO (log-log, $\mu\text{mol C l}^{-1}$). r = correlation coefficient.

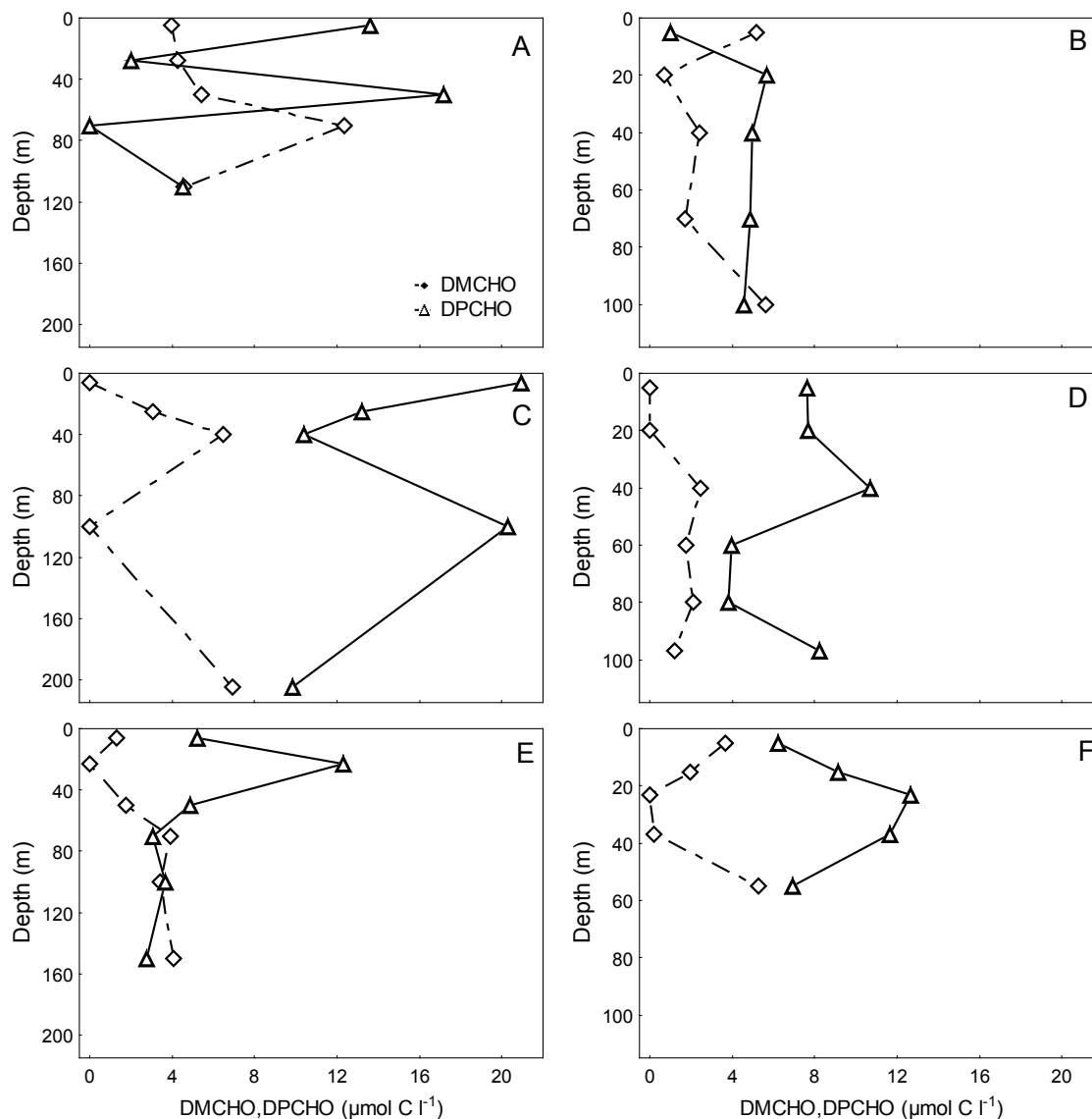


Figure 5.2. Vertical profiles of DMCHO and DPCHO ($\mu\text{mol C l}^{-1}$) in six representative deep (left column) and shallow (right column) locations situated in the three geographical areas of the Southern Ocean: Bellingshausen Sea (stations #3 and #7, A-B), Weddell Sea (stations #10 and #8, C-D) and Bransfield strait (stations #12 and #15, E-F). Note the different depth scales.

Table 5.1. Mean and ranges of dissolved monosaccharides (DMCHO, $\mu\text{mol C l}^{-1}$), dissolved polysaccharides (DPCHO, $\mu\text{mol C l}^{-1}$), percentage of total carbohydrates (DTCHO) relative to DOC, transparent exopolymer particles (TEP, $\mu\text{g XG eq l}^{-1}$), carbon content of TEP ($\mu\text{g TEP-C l}^{-1}$), TEP/chl *a* ($\mu\text{g XG eq } \mu\text{g chl } a^{-1}$), TEP/BA (fg XG cell^{-1}) and percentage of TEP-C with respect to phytoplankton-C and bacterial-C determined in the three geographical areas of the Southern Ocean.

	All data	Bellingshausen Sea	Weddell Sea	Bransfield Strait
	Mean (ranges)	Mean (ranges)	Mean (ranges)	Mean (ranges)
DMCHO	4.3 (0-12.6)	4.5 (0-12.3)	2.8 (0-6.9)	4.7 (0-12.6)
DPCHO	8.6 (0-21.0)	8.8 (0-21.0)	9.5 (2.0-21.0)	7.9 (0-20.6)
%DTCHO/DOC	23.4 (11.5-57.2)	23.4 (11.9-43.1)	24.1 (11.5-57.2)	24.6 (11.9-48.1)
TEP	15.4 (0-48.9)	14.3 (0-33.8)	16.3 (0.6-48.9)	15.8 (0-35.8)
TEP-C	11.6 (0-36.7)	10.8 (0-25.3)	12.2 (0.5-36.7)	10.8 (0-25.3)
TEP/chl <i>a</i>	40.9 (0-1492)	84.2 (0-1492)	9.8 (1.2-28.4)	15.0 (3.0-18.0)
TEP/BA	31.3 (1.0-244.9)	47.4 (2.5-244.9)	17.5 (1.0-41.2)	18.4 (4.5-52.8)
%TEP-C/Phyto-C	71.2 (0-2796.0)	157.8 (3.5-2796)	18.4 (2.1-53.2)	24.6 (0.8-202.5)
%TEP-C/Bact-C	117.4 (0-918.2)	177.6 (9.2-918.2)	65.7 (3.8-154.4)	68.9 (16.9-197.9)

Table 5.2. Mean and ranges of dissolved monosaccharides (DMCHO, $\mu\text{mol C l}^{-1}$), dissolved polysaccharides (DPCHO, $\mu\text{mol C l}^{-1}$), percentage of total carbohydrates (DTCHO) relative to DOC, transparent exopolymer particles (TEP, $\mu\text{g XG eq l}^{-1}$), carbon content of TEP ($\mu\text{g TEP-C l}^{-1}$), and percentage of TEP-C relative to phytoplankton-C and bacterial-C determined merging all data or above and below mixed layer depth (MLD) of the Southern Ocean.

	Over MLD	Below MLD
	Mean (ranges)	Mean (ranges)
DMCHO	3.9 (0-12.6)	5.0 (0.1-12.3)
DPCHO	9.6 (0.5-21.0)	6.9 (0-17.9)
% DTCHO/DOC	24.9 (11.5-57.2)	20.3 (11.9-43.1)
TEP	17.9 (0-48.9)	8.5 (0-27.4)
TEP-C	13.4 (0-36.7)	7.8 (0-20.6)
%TEP-C/Phyto-C	20.1 (0-81.2)	175.0 (0-2796.0)
%TEP-C/Bact-C	97.7 (0-408.0)	150.5 (0-918.2)

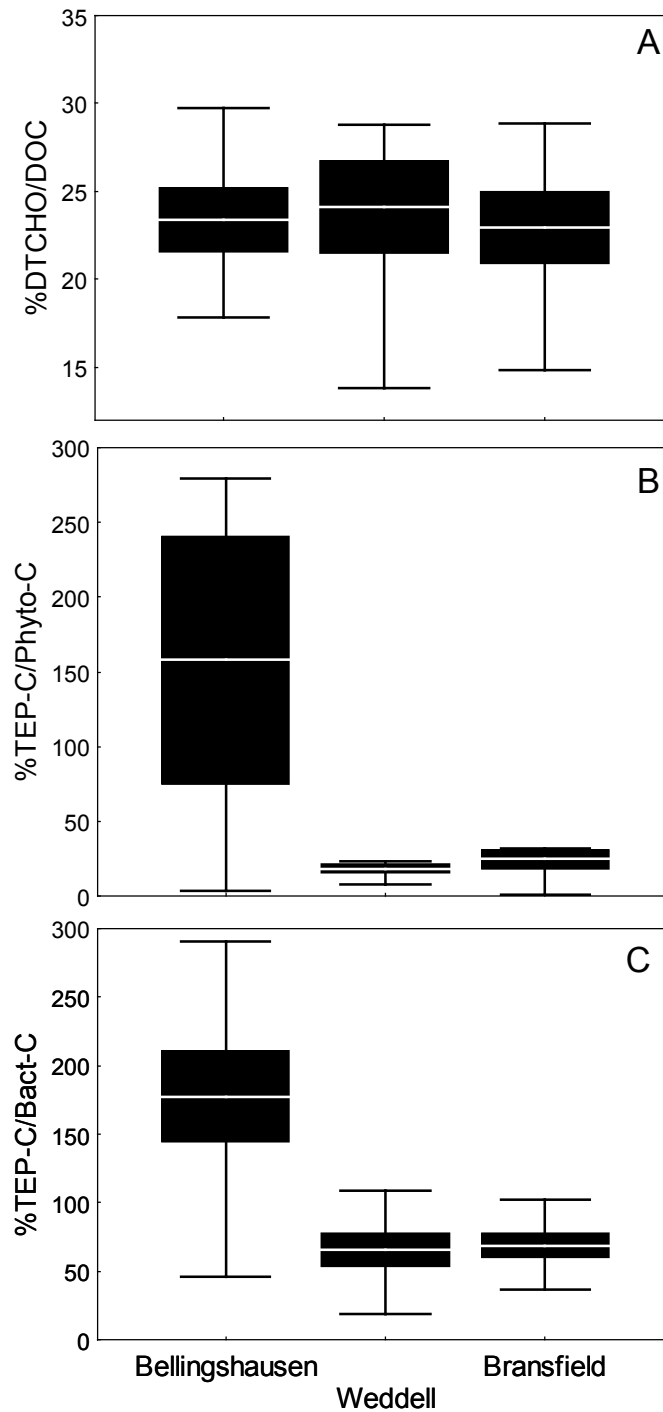


Figure 5.3. Mean (white line) percentage of DMCHO and DPCHO with respect to DOC (A) and mean % of TEP-C with respect to phytoplankton C (B) and bacterial-C (C) in the three geographical areas of the Southern Ocean: Bellingshausen Sea (stations #1-7), Weddell Sea (stations #8-11) and Bransfield Strait (stations #12-18). Boxes= Standard Error. Whiskers=not-outlier extremes.

DMCHO and DPCHO concentrations were independent ($p > 0.05$) of DOC concentration, chl *a*, BA and BP. No significant relationships ($p > 0.05$) was observed between DMCHO and DPCHO and TEP concentration, if either the merged or individual data sets were used (Table 5.3). Separation into geographical areas or horizons showed no correlations either.

TEP concentration ranged from undetectable values to $48.9 \mu\text{g XG eq l}^{-1}$ (Table 5.1). Mean TEP concentrations did not differ significantly ($p > 0.05$) between the different areas (Table 5.1), and were maximal in the deep chlorophyll maximum of Weddell Sea stations ($48.9 \mu\text{g XG eq l}^{-1}$, st #9) and inside Foster Bay of Deception Island ($33.6 \mu\text{g XG eq l}^{-1}$, st #15, Fig. 5.4F).

TEP concentrations were generally higher within the upper mixed layer, with a mean value of $17.9 \mu\text{g XG eq l}^{-1}$, than below the MLD ($8.5 \mu\text{g XG eq l}^{-1}$, Table 5.2). Vertical profiles generally tracked those of chl *a* and bacteria, showing a decreasing pattern with depth in the upper mixed layer (11 of 18 stations, Fig. 5.4A-C), and some exceptional stations with homogeneous profiles or irregular vertical patterns (e.g. st #8 in Antarctic Sound, Fig. 5.4D, st#12 in Bransfield Strait, Fig. 5.4E, or st #15 in Deception Island, Fig. 5.4F). TEP concentration increased slightly in waters below 100 m in 10 of the 18 stations examined (Fig. 5.4A-D).

The highest TEP concentrations were found in the stations with the highest chl *a*, BP and BA (st #9 in Weddell Sea or st #15 at Port Foster in Deception island), but the highest TEP/chl *a*, TEP/BP and TEP/BA ratios were located in Bellingshausen Sea (st #1 to #7) (Table 5.1). These ratios were also higher below the mixed layer than in the upper layer (Table 5.2). In terms of carbon units, TEP concentrations ranged from 0 to $36.7 \mu\text{g TEP-C l}^{-1}$ (Table 5.1), representing 20% and 175% of phytoplankton-C above and below the MLD respectively, and 97% and 150% of bacterial-C. Unlike the uniformity in the percentage of dissolved carbohydrates to total DOC across geographical areas (Fig. 5.3A), TEP-C normalized to phytoplankton-C or to bacterial-C was considerably higher in Bellingshausen area than in the two other areas (Table 5.1, Fig. 5.3B-C).

TEP concentration was significant and positively related to chl *a* if data from all depths was considered ($\log_{10}(\text{TEP}) = 0.38 \cdot \log_{10}(\text{chl } a) + 1.08$, $r^2 = 0.24$, $p < 0.001$, $n = 86$). This relationship varied considering data over and below the MLD, being significantly related within the upper mixed layer but not significant below the MLD (Table 5.3). Significant and positive relationships were found between

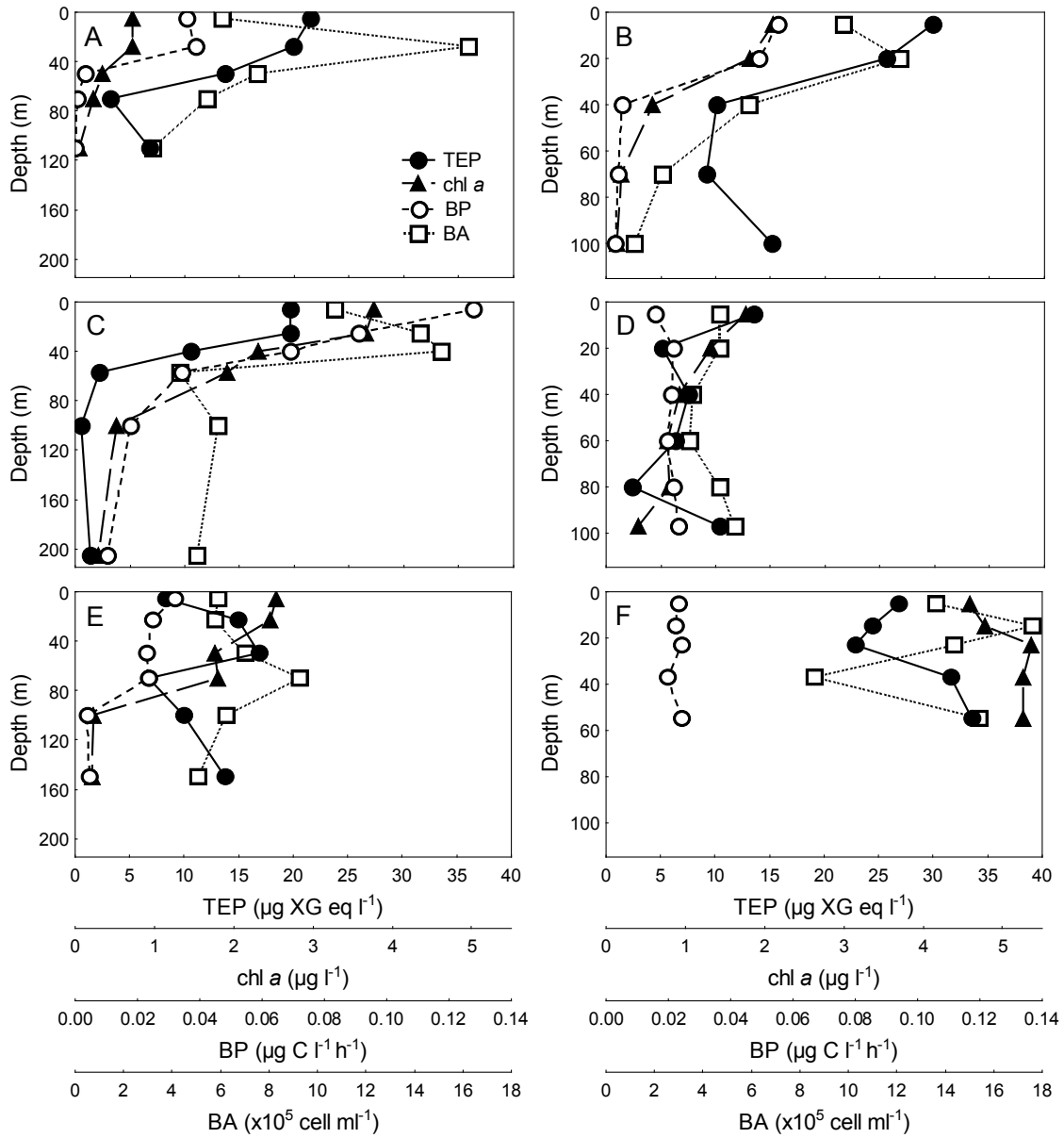


Figure 5.4. Vertical profiles of TEP ($\mu\text{g XG eq l}^{-1}$), chl a ($\mu\text{g l}^{-1}$), bacterial production ($\mu\text{g C l}^{-1} \text{h}^{-1}$), and bacterial abundance ($\times 10^5 \text{ cell ml}^{-1}$) in the same stations as showed in Figure 5.2.

TEP and BP and BA as well (Table 5.3). The TEP-BP relationship was significant both within and below the mixed layer, and that between TEP and BA was significant only within the mixed layer (Table 5.3). We calculated partial correlation coefficients to explore the relative contribution of each parameter to determine TEP concentration. The results showed that chl *a* was the best regressor of TEP concentration in waters above the MLD, while BP was the best regressor of TEP concentration below MLD (Table 5.4).

Table 5.3. Results of the regression analyses performed between TEP and different variables in the Southern Ocean (all variables were \log_{10} transformed). SE= Standard Error r^2 = explained variance p level = level of significance ns = not significant.

Dependent Var	Independent Var	Intercept	Slope \pm SE	r^2	p level
Over MLD					
TEP	DTCHO ($\mu\text{mol C l}^{-1}$)	1.46	-0.28 ± 0.27	0.02	ns
	Chl <i>a</i> ($\mu\text{g l}^{-1}$)	0.98	0.64 ± 0.13	0.27	<0.001
	BP ($\mu\text{g C l}^{-1} \text{h}^{-1}$)	0.49	0.43 ± 0.14	0.12	<0.01
	BA (cell ml^{-1})	-2.26	0.58 ± 0.22	0.13	<0.05
Below MLD					
TEP	DTCHO ($\mu\text{mol C l}^{-1}$)	0.64	-0.74 ± 0.56	0.07	ns
	Chl <i>a</i> ($\mu\text{g l}^{-1}$)	0.97	0.18 ± 0.15	0.07	n.s.
	BP ($\mu\text{g C l}^{-1} \text{h}^{-1}$)	0.64	0.32 ± 0.10	0.24	<0.01
	BA (cell ml^{-1})	-1.08	0.35 ± 0.24	0.08	ns

Table 5.4. Results of partial coefficients obtained in multiple regression between TEP vs. chl *a*, bacterial production and bacterial abundance over and below the upper mixed layer depth of the Southern Ocean. ns = not significant.

Region	Dependent var	Independent var	partial coefficient	p level
Over MLD	TEP	Chl <i>a</i>	0.56	<0.001
		B Production	0.10	ns
		B Abundance	-0.09	ns
Below MLD	TEP	Chl <i>a</i>	-0.16	ns
		B Production	0.55	<0.01
		B Abundance	-0.07	ns

DISCUSSION

The formation of TEP from dissolved carbohydrates has not been described in this chapter as no significant relationships between dissolved carbohydrates and TEP were observed during the study (Table 5.3). Although experimental and modelling studies have demonstrated the formation of TEP from acidic polysaccharide (Mopper et al., 1995; Passow, 2000; Engel et al., 2004), this relationship has not been observed also in previous field studies (Bhaskar and Bhosle, 2006). The spectrophotometric technique used in this study to determine DMCHO and DPCHO gives bulk measurements of both neutral and acidic carbohydrates, whose chemical composition in natural waters appear to be highly variable. However, TEP precursors are rich in acidic polysaccharides, specially deoxysugars and galactose (Mopper et al., 1995; Zhou et al., 1998). The proportion of TEP precursors within the carbohydrate pool is unknown, but likely variable, and only under certain conditions where most polysaccharides are TEP precursors, a significant link between those and TEP may be observed.

The DMCHO and DPCHO concentration ranges found in this study are similar to previously reported for oceanic waters and particularly for Antarctic waters using spectrophotometric techniques (Pakulski and Benner, 1994; Myklestad et al., 1997; van Oijen et al., 2003). However, other studies (Herborg et al., 2001; Kirchmann et al., 2001; Simon and Rosenstock, 2007) have reported lower concentrations in the Ross and Weddell seas. These lower values have been associated with the use of chromatographic techniques, which generally yield lower concentrations than spectrophotometric methods (Panagiotopoulos and Sempéré, 2005) as they measure only neutral carbohydrates in contrast to spectrophotometric methods which measure both neutral and charged ones. Additionally, we report a significant contribution of carbohydrates to the total DOC pool (23%), higher than the reported in previous studies in the same area (16%, Pakulski and Benner, 1994).

The published literature on dissolved carbohydrate distributions in the ocean have reported diverse vertical patterns, from homogeneous concentrations to decreasing concentrations over depth (Pakulski and Benner, 1994; Momzikoff et al., 2004; Wang et al., 2006). In this study, we did not find a common vertical pattern for all the study areas and stations. However, the negative correlation between DMCHO and DPCHO concentration found in our study is consistent

with previous observations (Pakulski and Benner, 1994) and suggests that DM-CHO can be derived in part from the degradation of DPCHO, possibly mediated by bacterial exoenzymes.

TEP values obtained in this study are lower than previously reported for the Southern Ocean (Passow et al., 1995; Hong et al., 1997; Corzo et al., 2005) or for other oceanic areas (Passow and Alldredge, 1995; Passow, 2002b; Engel, 2004; Prieto et al., 2006) (Table 5.5). However, most of the above cited studies were confined to TEP dynamics during phytoplankton blooms or in productive areas, where the concentrations of TEP are expected to be maxima. Indeed, if we attend to the TEP/chl *a* ratio, our data is within the ranges of previously published, particularly for Southern Ocean waters (Table 5.5). Relatively higher TEP/chl *a* and TEP/BA ratios were observed in the stations located at the Bellingshausen Sea (Table 5.1). The TEP/chl *a* ratio is associated with the stage of phytoplankton blooms. In the first stages of a bloom, TEP/chl *a* ratios are usually low, and while the bloom develops nutrient concentrations decline with a subsequent decrease in phytoplankton biomass and, hence, TEP/chl *a* ratios tend to be higher (Corzo et al., 2000). Although no temporal series of chl *a* are available in this study, the lowest TEP/chl *a* ratios were observed in the Weddell Sea, area of recent ice melting, where phytoplankton were likely on the first growth stages. Likewise, TEP/chl *a* is associated to the trophic state of the system, where areas favorable to phytoplankton growth (e.g. with nutrient enrichments) show lower TEP/chl *a* and vice versa (Prieto et al., 2006) as TEP production can represent a pathway of release overconsumed carbon in nutrient-limited waters (Mari et al., 2001) such as the more oligotrophic stations of Bellingshausen Sea.

The contribution of TEP carbon content respect to other significant pools of particulate organic carbon such as phytoplankton-C and bacterial-C is highlighted in our study. The subtle increases of TEP concentration observed in waters below the mixed layer, where TEP could represent a significant fraction of particulate organic carbon (175% of phytoplankton C or 150% of bacterial-C), could be attributed to different non exclusive reasons as: an elevated TEP excretion by phytoplankton and bacteria, a higher stability of polymer particles far from photochemical cracking (Orellana and Verdugo, 2003) or a higher self-assembling rate associated to sedimentation and marine snow formation (Passow et al., 2001).

In this study, TEP showed generally vertical profiles with maxima coincident with peaks of chl *a* within the upper mixed layer. This coupling was verified by

Table 5.5. Average (minimum-maximum) values of TEP ($\mu\text{g TEP-C l}^{-1}$) and TEP/chl *a* ratios ($\mu\text{g XG eq } \mu\text{g chl } a^{-1}$), and equation of chl *a*-TEP relationship ($\log_{10} \mu\text{g l}^{-1}$ vs $\log_{10} \mu\text{g XG eq l}^{-1}$) determined in different studies in the Southern Ocean and other marine areas.

Geographic Area	Depth	Conditions	TEP	TEP/chl <i>a</i>	TEP-chl <i>a</i> relationship	Reference
Southern Ocean						
Antarctic Peninsula	0-200m	non-bloom	15.4 (0-48.9)	40.9 (0-1492)	$y = 0.38x + 1.08$	This study
Anvers Island	surface		207 (10-407)	123 (12-708)	Not related	Passow (pers. comm.)
Ross Sea	0-150m	Bloom. Time serie	308 (0-2800)	89.1	$y = 3.63x + 1.01$	Hong et al. 1997
Bransfield Strait	0-100m	non-bloom	57(0-346)	51.0	$y = 0.32x + 1.63$	Corzo et al. 2005
Gerlache Strait	0-100m	non-bloom	0-283	32.7	$y = 0.67x + 1.52$	Corzo et al. 2005
Drake Passage	0-100m	non-bloom	0-157	29.9	Data not available	Corzo et al. 2005
Other Areas						
Mediterranean Sea	0-200m	non-bloom	21(5-94)	453(0-12386)	$y = 0.17x + 1.43$	This study
Santa Barbara Channel	0-75m	Time serie	197(11-1216)	197(0-6066)	Not related	Passow (pers. comm.)
Friday Harbor	0-20m	Time serie	83(15-159)	31(5-184)	Not related	Passow (pers. comm.)
Northeast Atlantic	10-50m	Different bloom stages	28.5(10-110)	49-104	Not related	Engel 2004
Gulf of Cadiz/Strait of Gibraltar	0-200m	Different bloom stages	25-205	42-2708	$y = 2.14x + 0.20$	Prieto et al. 2006

a significant and positive relationship between TEP and chl *a* in the upper layer (Table 5.3). There is ample evidence that phytoplankton, particularly diatoms, can release high amounts of TEP and dissolved carbohydrates during exponential growth phase or senescence of colonies (Passow and Alldredge, 1994; Passow et al., 1995). However, this evidence is not always supported by significant relationships between chl *a* and TEP in the field (Table 5.5) as TEP release by phytoplankton is rather a function of algal growth rate than chl *a* standing stocks (Waite et al., 1995) and also dependent on factors such as species composition, nutrient availability, light stress or the presence of bacteria. In the SO, the slope of the TEP-chl *a* relationship for the upper layer ($0.64 \pm 0.13 \mu\text{g XG eq } \mu\text{g chl } a^{-1}$) was within the range reported in the literature ($0.65 \pm 0.26 \text{ XG } \mu\text{g XG eq } \mu\text{g chl } a^{-1}$, (Passow, 2002b) and similar to the reported in the Gerlache strait (Table 5.5), and was similar to the slope reported by Corzo et al. (2005) in waters around the same area if we use our merged data (above and below the MLD) (Table 5.5).

The complex link between TEP and bacteria is evidenced by the contrasting relationships between these variables across diverse ocean areas. Some authors (Ramaiah et al., 2000; Passow et al., 2001; Corzo et al., 2005) have reported positive relationships, whereas Passow and Alldredge (1994) and Bhaskar and Bhosle (2006) found negative or no correlations at all. In our study, although a positive relationship was found between TEP and bacterial abundance within the upper mixed layer, the slope of the relationship was lower than the reported in the Corzo et al (2005) study (1.02 ± 0.25 , log-log). The relationship between bacteria and TEP in the upper mixed layer waters appears to be indirect and mediated by phytoplankton (Table 5.4). However, in waters below the MLD a significant relationship was found between TEP and BP. This positive relationship can be due to different non-exclusive explanations. First, an active release of TEP by bacterioplankton (Stoderegger and Herndl, 1999; Passow, 2002a). Second, an enhanced bacterial activity attached to TEP (Herndl, 1988; Grossart and Simon, 1998). Third, a stimulation of the self-assembly of dissolved precursors into TEP driven by bacteria (Sugimoto et al., 2007). Finally, a common response of both bacterial activity and TEP to the presence of dissolved compounds that are both TEP precursors and labile organic substrate for bacteria (Mari and Kiorboe, 1996).

In this study, we reported significant contributions of dissolved carbohydrates and TEP to the dissolved and particulate organic carbon pools respectively in the Southern Ocean. However, these variables were not significantly related in the

field, suggesting considerable complexity in TEP formation and decomposition. In the Southern Ocean, TEP appeared to be weakly controlled by phytoplankton in the upper mixed layer but the TEP/chl *a* ratios differed among regions, in contrast to waters below the mixed layer depth where bacterial activity appears to be the main driver of TEP distributions.

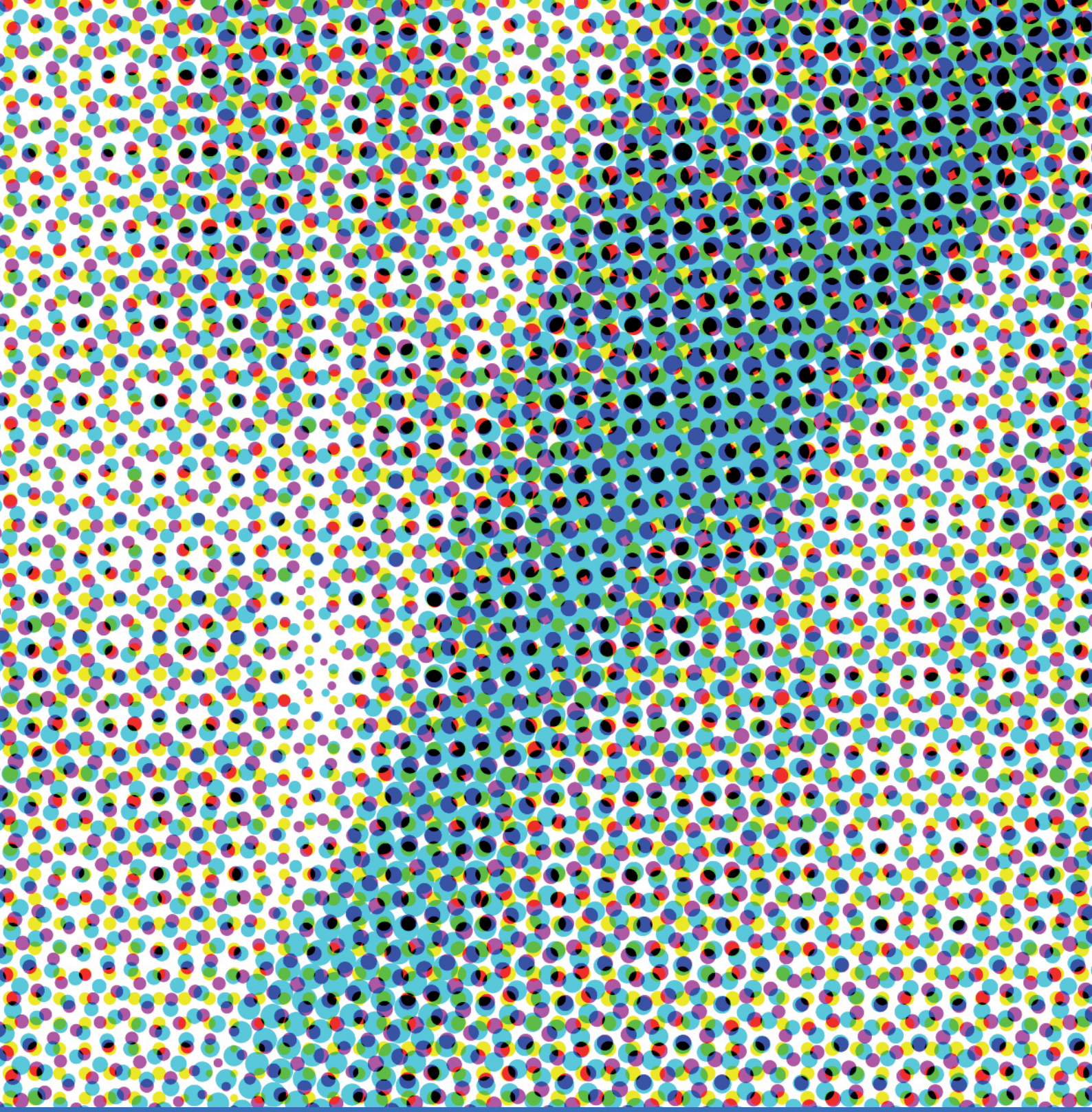
REFERENCES

- ALLDREDGE, A.L., U. PASSOW and B.E. LOGAN (1993) The abundance and significance of a class of large, transparent organic particles in the ocean. *Deep-Sea Research Part I-Oceanographic Research Papers*. 40: 1131-1140.
- BHASKAR, P.V. and N.B. BHOSLE (2006) Dynamics of transparent exopolymeric particles (TEP) and particle-associated carbohydrates in the Dona Paula bay, west coast of India. *Journal of Earth System Science*. 115: 403-413.
- CORZO, A., J.A. MORILLO and S. RODRÍGUEZ (2000) Production of transparent exopolymer particles (TEP) in cultures of *Chaetoceros calcitrans* under nitrogen limitation. *Aquatic Microbial Ecology*. 23: 63-72.
- CORZO, A., S. RODRÍGUEZ-GÁLVEZ, L. LUBIÁN, P. SANGRÁ, A. MARTÍNEZ and J.A. MORILLO (2005) Spatial distribution of transparent exopolymer particles in the Bransfield Strait, Antarctica. *Journal of Plankton Research*. 27: 635-646.
- ENGEL, A. (2004) Distribution of transparent exopolymer particles (TEP) in the northeast Atlantic Ocean and their potential significance for aggregation processes. *Deep-Sea Research Part I-Oceanographic Research Papers*. 51: 83-92.
- ENGEL, A., S. THOMS, U. RIEBESELL, E. ROCHELLE-NEWALL and I. ZONDERVAN (2004) Polysaccharide aggregation as a potential sink of marine dissolved organic carbon. *Nature*. 428: 929-932.
- GROSSART, H.P. (1999) Interactions between marine bacteria and axenic diatoms (*Cylindrotheca fusiformis*, *Nitzschia laevis*, and *Thalassiosira weissflogii*) incubated under various conditions in the lab. *Aquatic Microbial Ecology*. 19: 1-11.
- GROSSART, H.P. and M. SIMON (1998) Bacterial colonization and microbial decomposition of limnetic organic aggregates (lake snow). *Aquatic Microbial Ecology*. 15: 127-140.
- HERBORG, L.M., D.N. THOMAS, H. KENNEDY, C. HAAS and G.S. DIECKMANN (2001) Dissolved carbohydrates in Antarctic sea ice. *Antarctic Science*. 13: 119-125.
- HERNDL, G.J. (1988) Ecology of amorphous aggregations (marine snow) in the Northern Adriatic Sea. II. Microbial density and activity in marine snow and its implication to overall pelagic processes. *Marine Ecology-Progress Series*. 48: 265-275.

- HONG, Y., W.O. SMITH and A.M. WHITE (1997) Studies on transparent exopolymer particles (TEP) produced in the Ross Sea (Antarctica) and by *Phaeocystis antarctica* (Prymnesiophyceae). *Journal of Phycology*. 33: 368-376.
- HUERTAS, E., G. NAVARRO, S. RODRÍGUEZ-GÁLVEZ and L. PRIETO (2005) The influence of phytoplankton biomass on the spatial distribution of carbon dioxide in surface sea water of a coastal area of the Gulf of Cadiz (southwestern Spain). *Canadian Journal of Botany- Revue Canadienne De Botanique*. 83: 929-940.
- KIRCHMANN, D.L., B. MEON, H.W. DUCKLOW, C.A. CARLSON, D.A. HANSELL and G.F. STEWARD (2001) Glucose fluxes and concentrations of dissolved combined neutral sugars (polysaccharides) in the Ross Sea and Polar Front Zone, Antarctica. *Deep-Sea Research Part II-Topical Studies in Oceanography*. 48: 4179-4197.
- MARI, X., S. BEAUVAIS, R. LEMÉE and M.L. PEDROTTI (2001) Non-Redfield C : N ratio of transparent exopolymeric particles in the northwestern Mediterranean Sea. *Limnology and Oceanography*. 46: 1831-1836.
- MARI, X. and T. KIORBOE (1996) Abundance, size distribution and bacterial colonization of transparent exopolymeric particles (TEP) during spring in the Kattegat. *Journal of Plankton Research*. 18: 969-986.
- MOMZIKOFF, A., A. BRINIS, S. DALLOT, G. GONDRY, A. SALIOT and P. LEBARON (2004) Field study of the chemical characterization of the upper ocean surface using various samplers. *Limnology and Oceanography-Methods*. 2: 374-386.
- MOPPER, K., J. ZHOU, K.S. RAMANA, U. PASSOW, H.G. DAM and D.T. DRAPEAU (1995) The role of surface-active carbohydrates in the flocculation of a diatom bloom in a mesocosm. *Deep-Sea Research Part II-Topical Studies in Oceanography*. 42: 47-73.
- MYKLESTAD, S., E. SKANOY and S. HESTMANN (1997) A sensitive and rapid method for analysis of dissolved mono- and polysaccharides in seawater. *Marine Chemistry*. 56: 279-286.
- ORELLANA, M. and P. VERDUGO (2003) Ultraviolet radiation blocks the organic carbon exchange between the dissolved phase and the gel phase in the ocean. *Limnology and Oceanography*. 48: 1618-1623.
- PAKULSKI, D. and R. BENNER (1994) Abundance and distribution of carbohydrates in the ocean. *Limnology and Oceanography-Methods*. 39: 930-940.

- PANAGIOTOPOULOS, C. and R. SEMPÉRÉ (2005) Analytical methods for the determination of sugars in marine samples: A historical perspective and future directions. *Limnology and Oceanography-Methods*. 3: 419-454.
- PASSOW, U. (2000) Formation of transparent exopolymer particles, TEP, from dissolved precursor material. *Marine Ecology-Progress Series*. 192: 1-11.
- PASSOW, U. (2002a) Production of transparent exopolymer particles (TEP) by phyto- and bacterioplankton. *Marine Ecology-Progress Series*. 236: 1-12.
- PASSOW, U. (2002b) Transparent exopolymer particles (TEP) in aquatic environments. *Progress in Oceanography*. 55: 287-333.
- PASSOW, U. and A.L. ALLDREDGE (1994) Distribution, size and bacterial-colonization of transparent exopolymer particles (TEP) in the ocean. *Marine Ecology-Progress Series*. 113: 185-198.
- PASSOW, U. and A.L. ALLDREDGE (1995) A dye-binding assay for the spectrophotometric measurement of transparent exopolymer particles (TEP). *Limnology and Oceanography*. 40: 1326-1335.
- PASSOW, U. and A.L. ALLDREDGE (1999) Do transparent exopolymer particles (TEP) inhibit grazing by the euphausiid *Euphausia pacifica*? *Journal of Plankton Research*. 21: 2203-2217.
- PASSOW, U., W. KOZŁOWSKI and M. VERNET (1995) Palmer LTER: temporal variability of transparent exopolymeric particles in Arthur Harbor during the 1994-95 growth season. *Antarct. J-Review*: 265-266. .
- PASSOW, U., R.F. SHIPE, A. MURRAY, D.K. PAK, M.A. BRZEZINSKI and A.L. ALLDREDGE (2001) The origin of transparent exopolymer particles (TEP) and their role in the sedimentation of particulate matter. *Continental Shelf Research*. 21: 327-346.
- PRIETO, L., G. NAVARRO, A. COZAR, F. ECHEVARRÍA and C.M. GARCÍA (2006) Distribution of TEP in the euphotic and upper mesopelagic zones of the southern Iberian coasts. *Deep-Sea Research Part II-Topical Studies in Oceanography*. 53: 1314-1328.
- PRIETO, L., F. SOMMER, H.N. STIBOR and W. KOEVE (2001) Effects of planktonic copepods on transparent exopolymeric particles (TEP) abundance and size spectra. *Journal of Plankton Research*. 23: 515-525.
- RAMAIAH, N., T. YOSHIKAWA and K. FURUYA (2001) Temporal variations in transparent exopolymer particles (TEP) associated with a diatom spring bloom in a

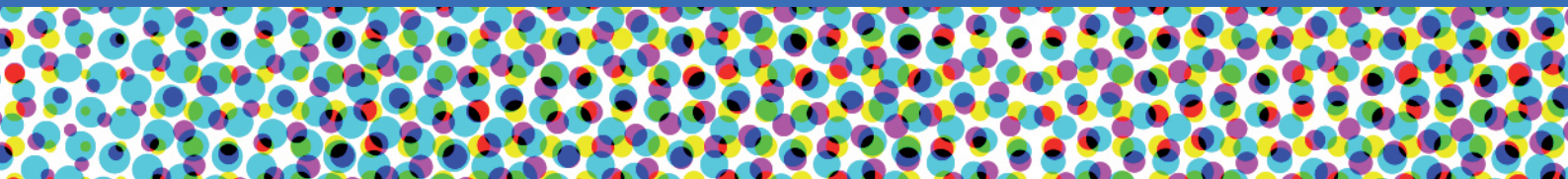
- subarctic ria in Japan. *Marine Ecology-Progress Series*. 212: 79-88.
- SIMON, M. and B. ROSENSTOCK (2007) Different coupling of dissolved amino acid, protein, and carbohydrate turnover to heterotrophic picoplankton production in the Southern Ocean in austral summer and fall. *Limnology and Oceanography*. 52: 85-95.
- STODEREGGER, K. and G.J. HERNDL (1998) Production and release of bacterial capsular material and its subsequent utilization by marine bacterioplankton. *Limnology and Oceanography*. 43: 877-884.
- STODEREGGER, K.E. and G.J. HERNDL (1999) Production of exopolymer particles by marine bacterioplankton under contrasting turbulence conditions. *Marine Ecology-Progress Series*. 189: 9-16.
- SUGIMOTO, K., H. FUKUDA, M.A. BAKI and I. KOIKE (2007) Bacterial contributions to formation of transparent exopolymer particles (TEP) and seasonal trends in coastal waters of Sagami Bay, Japan. *Aquatic Microbial Ecology*. 46: 31-41.
- THORNTON, D.C.O. (2004) Formation of transparent exopolymeric particles (TEP) from macroalgal detritus. *Marine Ecology-Progress Series*. 282: 1-12.
- VAN OIJEN, T., M. VAN LEEUWE and W. GIESKES (2003) Variation of particulate carbohydrate pools over time and depth in a diatom-dominated plankton community at the Antarctic Polar Front. *Polar Biology*. 26: 195-201.
- WAITE, A.M., R.J. OLSON, H.G. DAN and U. PASSOW (1995) Sugar-containing compounds on the cell surfaces of marine diatoms measured using concanavalin A and flow cytometry. *Journal of Phycology*. 31: 925-933.
- WANG, D., S.M. HENRICHS and L. GUO (2006) Distributions of nutrients, dissolved organic carbon and carbohydrates in the western Arctic Ocean. *Continental Shelf Research*. 26: 1654-1667.
- ZHOU, J., K. MOPPER and U. PASSOW (1998) The role of surface-active carbohydrates in the formation of transparent exopolymer particles (TEP) by bubble adsorption of seawater. *Limnology and Oceanography*. 43: 1860-1871.



Chapter 6:
**Role of bacterioplankton on transparent exopolymer
particles formation in the Mediterranean Sea.**

Ortega-Retuerta, E., Duarte, C.M., and Reche, I.

Abbreviated title: TEP generation by bacterioplankton



INTRODUCTION

TEP formation and dynamics in aquatic ecosystems has been traditionally linked to the development of phytoplankton blooms, specially diatoms or *Phaeocystis* sp (Aldredge et al., 1993; Passow, 2002b). However, bacterioplankton are known to be key organisms in organic matter uptake and transformation in aquatic ecosystems (Azam et al., 1983) and they also affect TEP dynamics. The relationship of bacterioplankton with TEP appears to be complex, as they can be interrelated in diverse ways (Fig. 6.1):

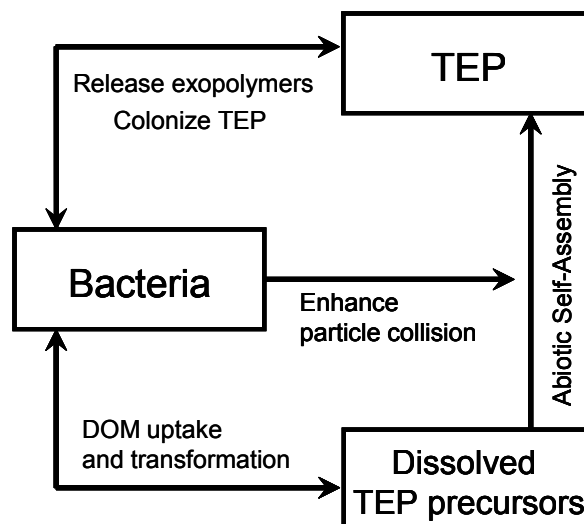


Figure 6.1. Possible pathways relating bacterioplankton and transparent exopolymer particles (TEP) in aquatic ecosystems.

1. Bacteria have the potential to generate TEP. These organisms release high amounts of polysaccharides and TEP as free exopolymers or as capsular material (up to 25% of the respired carbon, Stoderegger and Herndl, 1998) depending on environmental variables such as the turbulence conditions (Stoderegger and Herndl, 1999; Passow, 2002a), the presence of phytoplankton (Grossart et al., 2006) or nutrient availability (Radic et al., 2006). A considerable proportion of bacterioplankton generate capsules as a protection against grazers of toxic substances (Heissenberger et al., 1996b; Stoderegger and Herndl, 1998). Metabolically active bacteria are constantly renewing their polysaccharide capsule (Stoderegger and Herndl, 1998), while inactive or senescent bacteria loose their capsule (Heissenberger et al., 1996a) and can also release their intracellular material, frequently mediated by viral lysis infection (Shibata et al., 1997).
2. Bacteria may induce release of TEP and their precursors by phytoplankton when competing with algae for inorganic nutrients. The more efficient assimilation of nutrients by bacteria than by phytoplankton (Kirchman, 1994; Cotner and Biddanda, 2002) may result in nutrient limitation of algae, which possibly enhances the release of TEP precursors by phytoplankton (Guerrini et al., 1998). Bacteria can also affect bloom aggregation by either colonizing algal cells or by consuming compounds released by algae (Grossart et al. 2006).
3. Bacteria can affect the abiotic formation of TEP from dissolved precursors. Turbulence due to bacterial motility enhance the collisions among particles and colloids, stimulating the assembly and coagulation reactions (Johnson and Kepkay, 1992). Moreover, bacteria can act as nuclei for negatively charged molecules TEP precursors (van Loosdrecht et al., 1989).
4. Bacteria take advantage of TEP, which provide substrate, a stable microhabitat and refuge for them (Passow and Alldredge, 1994; Mari and Kiorboe, 1996), or enhances the efficiency of bacterial exoenzymes (Johnson and Kepkay, 1992), or the availability of nutrients (Kepkay and Johnson, 1988). The proportion of bacteria attached to TEP in seawater is variable, with up to 68% (Alldredge et al., 1993; Passow and Alldredge, 1994; Schuster and Herndl, 1995; Mari and Kiorboe, 1996; Meiners et al., 2004).

Also attachment to particles stimulates bacterial production of exopolymers (Vandevivere and Kirchman, 1993)

5. The self assembly of dissolved material into TEP and their subsequent sedimentation represents an efficient pathway to remove dissolved organic carbon. Hence, it would have an indirect negative effect on bacterioplankton establishing a competition for the utilization of the dissolved substrate (Engel et al., 2004).

All these pathways are non-exclusive and can occur in natural systems at different magnitude and timescales. Thus, the relative importances of the processes governing TEP-bacteria interactions in the natural environment, as well as the fraction of TEP standing stocks and dynamics that can be attributable to bacteria, remain unclear and need further exploration.

In the Mediterranean Sea, the aggregation of DOM into large aggregates including TEP is a frequent phenomenon. This mucilage formation is particularly important in the Northern Adriatic Sea (Vollenweider and Rinaldi, 1995), although it has been described also in other coastal areas (Calvo et al., 1995; Mecozzi et al., 2001). The high N/P ratio of these waters causes phytoplankton to release high amounts of extracellular polymers that exceed bacterial decomposition. The accumulation and further aggregation of this algal-derived material has been proposed as the main pathway of mucilage formation (Obernosterer and Herndl, 1995). However, so far, not all responsible mechanisms, including the specific role of bacteria, have been thoroughly studied.

In this thesis chapter, we studied TEP and dissolved carbohydrates distribution and dynamics in the Mediterranean Sea with a particular focus on the role of bacterioplankton. For that purpose, we first described the geographical distribution of TEP and dissolved carbohydrates, assessed their significance within the organic carbon pool, and explored the potential drivers (dissolved carbohydrates concentration, chlorophyll *a*, bacterial abundance, bacterial production), of TEP variability in the area. Second, we experimentally studied the formation of TEP by bacteria from dissolved material and quantified its contribution on TEP dynamics.

MATERIAL AND METHODS

TEP AND DISSOLVED CARBOHYDRATES DISTRIBUTION IN THE MEDITERRANEAN SEA.

The sampling and analysis protocols in the Mediterranean Sea are detailed in the general section of methods.

We applied correlation analyses to test the relationships between dissolved mono- and polysaccharides (DMCHO and DPCHO) and dissolved organic carbon (DOC), transparent exopolymer particles (TEP) and biological variables (chlorophyll *a* (chl *a*), bacterial abundance (BA) and bacterial production (BP).

To explore the potential controlling factors on TEP distributions, we tested the relationship between TEP, DMCHO, DPCHO, chl *a* concentration and bacterial abundance and production using regression and multiple regression analyses. Data were log-transformed when needed to fit the regression assumptions of normality and homogeneity of variances.

BACTERIAL TEP GENERATION IN THE MEDITERRANEAN SEA

To determine bacterial release of TEP and their dissolved precursors (DMCHO and DPCHO) in the Mediterranean Sea we conducted four experiments applying the same experimental set-up as explained in chapter 3. Briefly, 8 re-growth cultures were set up in triplicate using GF/F filtered water from two locations (stations #2 and #15) and depths (200 m and the deep chlorophyll maximum (DCM), situated at 40 and 80m respectively). The experimental procedure is schematically represented in Fig 6.2. Two different treatments were included for each experiment: one treatment including natural bacteria (Bact.) and one treatment where Sodium azide (0.02 % final concentration) was added to control treatments to inhibit bacterial growth (+SA). Sodium azide does not interfere with TEP coagulation processes (Sugimoto et al., 2007).

Samples for transparent exopolymer particles (TEP), dissolved monosaccharides (DMCHO), dissolved polysaccharides (DPCHO), bacterial abundance (BA) and bacterial production (BP) were taken initially (t0) and after 2.5 days (t1), and 5

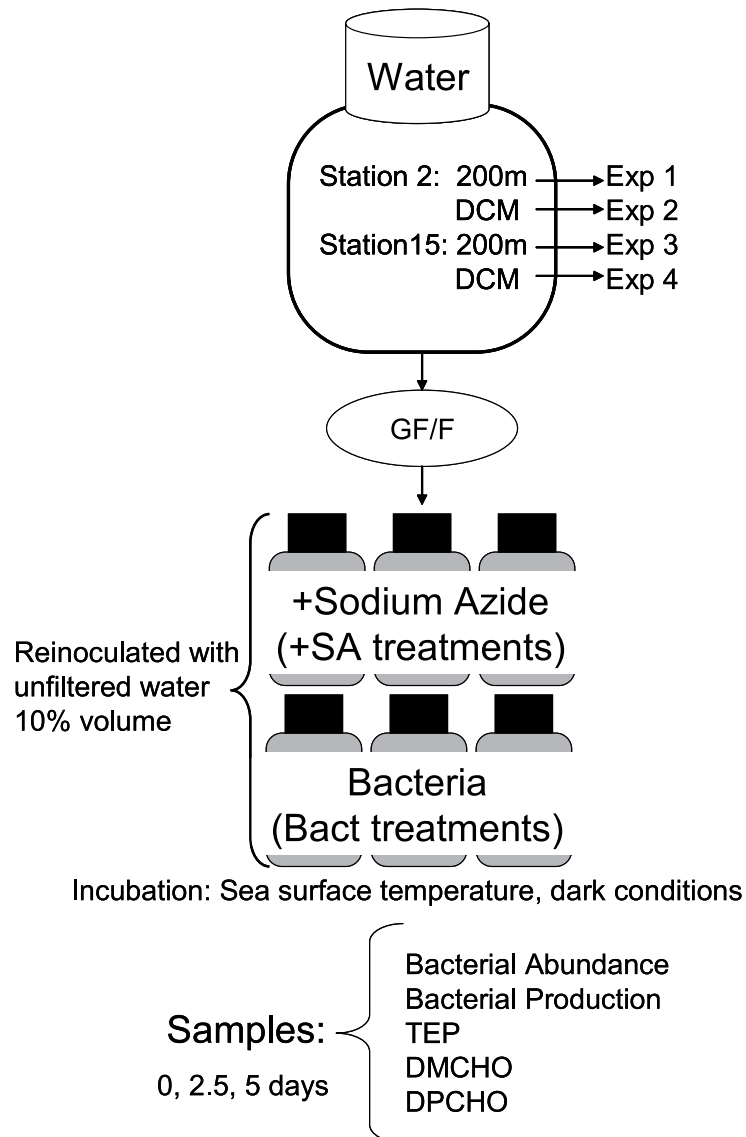


Figure 6.2. Experimental design to evaluate TEP generation by bacterioplankton.

days (t₂) except in experiments 1 and 3, where TEP, DMCHO and DPCHO were only sampled at times t₀ and t₂.

TEP concentrations were expressed in $\mu\text{g XG eq l}^{-1}$ and in carbon units ($\mu\text{g C l}^{-1}$) using the conversion factor of $0.75 \mu\text{g C } \mu\text{g XG eq}^{-1}$ (Engel and Passow, 2001). To compare changes in TEP with those in DMCHO and DPCHO over time, we expressed DMCHO concentrations and DPCHO in $\mu\text{g C l}^{-1}$ in this chapter section.

Daily increases in all variables were calculated using the following expression:

$$\Delta X = \frac{X_{t_f} - X_{t_0}}{t}$$

Where x is the study variable (TEP in $\mu\text{g XG eq l}^{-1}$ or in $\mu\text{g C l}^{-1}$, DMCHO and DPCHO in $\mu\text{g C l}^{-1}$, BA in cell l^{-1} , or BP in $\mu\text{g C l}^{-1} \text{ h}^{-1}$), t_f and t_0 are final and initial time, and t is time in days. Cumulative TEP-C during the course of the experiments, that is, carbon that was accumulated as TEP during the incubations, was calculated as $\text{TEP}_{t_f} - \text{TEP}_{t_0}$ in $\mu\text{g C l}^{-1}$.

Cumulative bacterial production, that is, total amount of carbon taken up by bacteria and incorporated into protein ($\mu\text{g C l}^{-1}$), was calculated from the average BP values in each interval ($\mu\text{g C l}^{-1} \text{ h}^{-1}$) integrated by the incubation time in hours.

Cumulative bacterial biomass during the course of the experiments, that is, carbon accumulated as bacteria during the incubations, was calculated applying a conversion factor of $20 \text{ fg C cell}^{-1}$ (Lee and Fuhrman, 1987) to accumulated BA ($\text{BA}_{t_f} - \text{BA}_{t_0}$).

We related daily increases in TEP (ΔTEP) to daily increases in BA (ΔBA) or BP (ΔBP) by linear regressions. Then we can calculate TEP formation associated to the growth of bacteria (either in abundance or in production).

FIELD EXTRAPOLATION OF BACTERIAL TEP GENERATION

To quantify bacterial TEP formation rates in the experiments in order to extrapolate to field data, we related daily TEP increases ($\mu\text{g XG eq l}^{-1} \text{ d}^{-1}$) with time average BA (cell l^{-1}) and BP ($\mu\text{g C l}^{-1} \text{ h}^{-1}$) in all experiments and treatments. Regression equations were used as experimental TEP formation rates by bacteria ($\mu\text{g XG eq l}^{-1} \text{ d}^{-1}$ per unit of bacterial abundance or bacterial production). We extrapolated these experimental rates to “field TEP formation rates” by bacteria using average data of bacterial abundance ($5.04 \times 10^8 \text{ cell l}^{-1}$) and bacterial production ($0.0121 \mu\text{g C l}^{-1} \text{ h}^{-1}$) determined for the Mediterranean Sea.

We also estimated TEP duplication time attributable to bacteria in the Mediterranean Sea by using average field data of TEP ($21.4 \mu\text{g XG eq l}^{-1}$) and the field TEP formation rate due to bacterial activity:

$$\text{TEP duplication time (d)} = \frac{\text{field TEP}}{\text{field TEP bacterial formation rate}}$$

RESULTS

DISTRIBUTION OF TEP AND DISSOLVED CARBOHYDRATES.

DMCHO in the Mediterranean Sea ranged from undetectable to $9.6 \mu\text{mol C l}^{-1}$ (mean value $2.7 \mu\text{mol C l}^{-1}$), while DPCHO ranged from undetectable to $9.7 \mu\text{mol C l}^{-1}$ (mean value $2.4 \mu\text{mol C l}^{-1}$). In general, DMCHO and DPCHO were higher within the euphotic layer than below it (Table 6.1), but a decrease with depths was observed at some stations (Figure 6.3). An inverse relationship of DMCHO and DPCHO was detected at 12 of 24 stations. DTCHO averaged 6.73% of DOC, ranging from 1.22 to 16.4% (Table 6.1). This percentage was homogenous both geographically and vertically (Table 6.1, Fig. 6.4A).

DMCHO, DPCHO and DTCHO were independent of DOC concentration. DMCHO was negatively correlated to DPCHO ($r = -0.36$, $p > 0.001$, $n = 93$). DTCHO were weakly correlated to chl *a*, bacterial production and abundance, as well as to TEP concentration (Table 6.2), with an explained variance below 10% in all cases.

TEP concentration ranged from 4.5 to $94.3 \mu\text{g XG eq l}^{-1}$ (mean value $21.4 \mu\text{g XG eq l}^{-1}$, Table 6.1). At 11 of 24 stations, TEP concentrations decreased with depths (e.g. st #4 in the central Mediterranean or st #8-13 near Alexandria, Fig. 6.5 A-B), while at others TEP concentrations were minimal at the surface and maxima coincided with peaks of bacterial production (e.g. st #2 or #17, near Sicily, Fig. 6.5 C) or at the combined chl *a* and bacteria peak (e.g. st #5 and #23 in the Western Mediterranean, Fig. 6.5 D). TEP concentration had a fairly constant geographical distribution over the different sampling stations. Highest TEP concentration was observed within the euphotic layer of the stations #13 to #17, situated in the Ae-

Table 6.1. Average and ranges of DMCHO ($\mu\text{mol C l}^{-1}$), DPCHO ($\mu\text{mol C l}^{-1}$), % DTCHO/DOC, TEP ($\mu\text{g XG eq l}^{-1}$), carbon content of TEP ($\mu\text{g TEP-C l}^{-1}$), TEP/chl *a* ($\mu\text{g XG eq } \mu\text{g chl a}^{-1}$) and TEP/BA (fg XG cell^{-1}) and % of TEP-C with respect to phytoplankton-C and bacterial-C determined in the upper mixed layer (UML), below mixed layer but within the euphotic layer (BML-Euphotic L), and below the euphotic layer (B photic L).

	Total	UML	BML-Euphotic L	B Photic L
	Mean (ranges)	Mean (ranges)	Mean (ranges)	Mean (ranges)
DMCHO	2.7 (0-9.6)	2.7 (0-8.9)	3.1 (0-9.6)	2.2 (0-7.7)
DPCHO	2.4 (0-9.7)	3.0 (0-9.5)	2.5 (0-9.7)	1.7 (0-4.4)
%DTCHO/DOC	6.7 (1.2-16.4)	6.8 (2.5 – 16.4)	7.1 (1.4 – 15.4)	6.1 (1.2 – 14.7)
TEP	21.4 (4.5-94.3)	29.2 (19.4-53.1)	26.1 (9.1-94.3)	9.4 (4.5-23.5)
TEP-C	16.0 (3.4-70.7)	21.9 (14.6-31.8)	19.5 (6.8-70.7)	7.1 (3.4-17.6)
TEP/chl <i>a</i>	506 (12.6-12386)	484 (178-1293)	190 (12.6-1329)	947 (41.4-12386)
TEP/BA	50.9 (10.2-404)	80.9 (23.0-404)	44.5 (14.9-164)	37.0 (10.2-199)
% TEP-C/Phyto-C	949 (23.7-23224)	908 (333 -2424)	356 (23.7-2492)	1775 (77.7- 23224)
% TEP-C/Bact-C	191 (38.2-1514)	303 (86.1-1514)	167 (55.7-315)	139 (38.2-745)

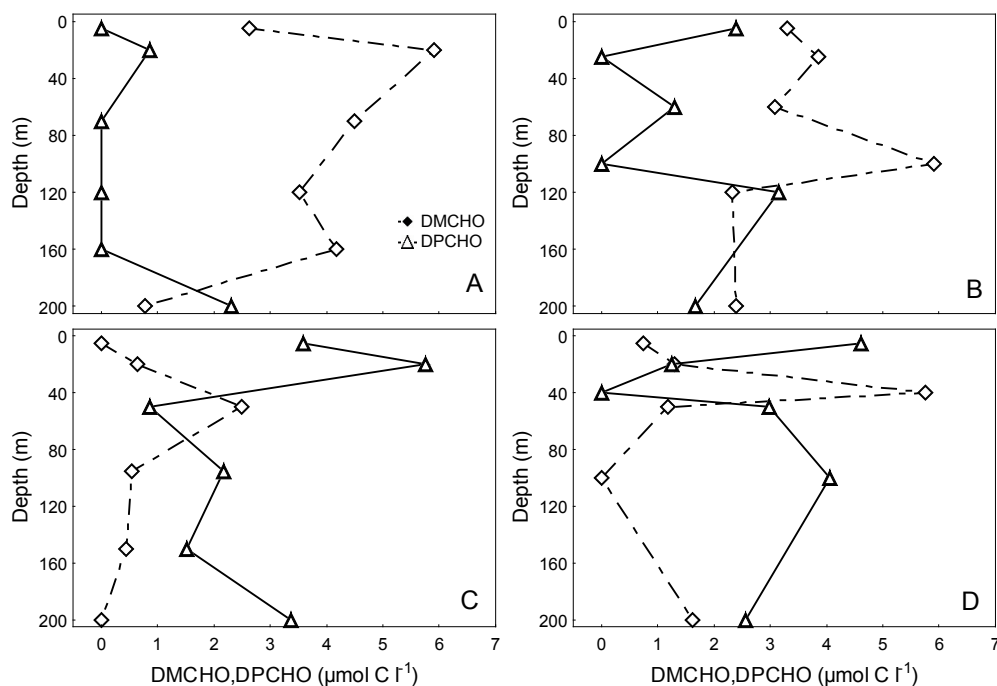


Figure 6.3. Vertical profiles of DMCHO and DPCHO ($\mu\text{mol C l}^{-1}$) in four representative locations in the Mediterranean Sea: st #4, (passed Sicily, A) st #11 (near Alexandria, B), st#17 (near Greece, C) and st#23 (between Sardinia and Balear Islands, D).

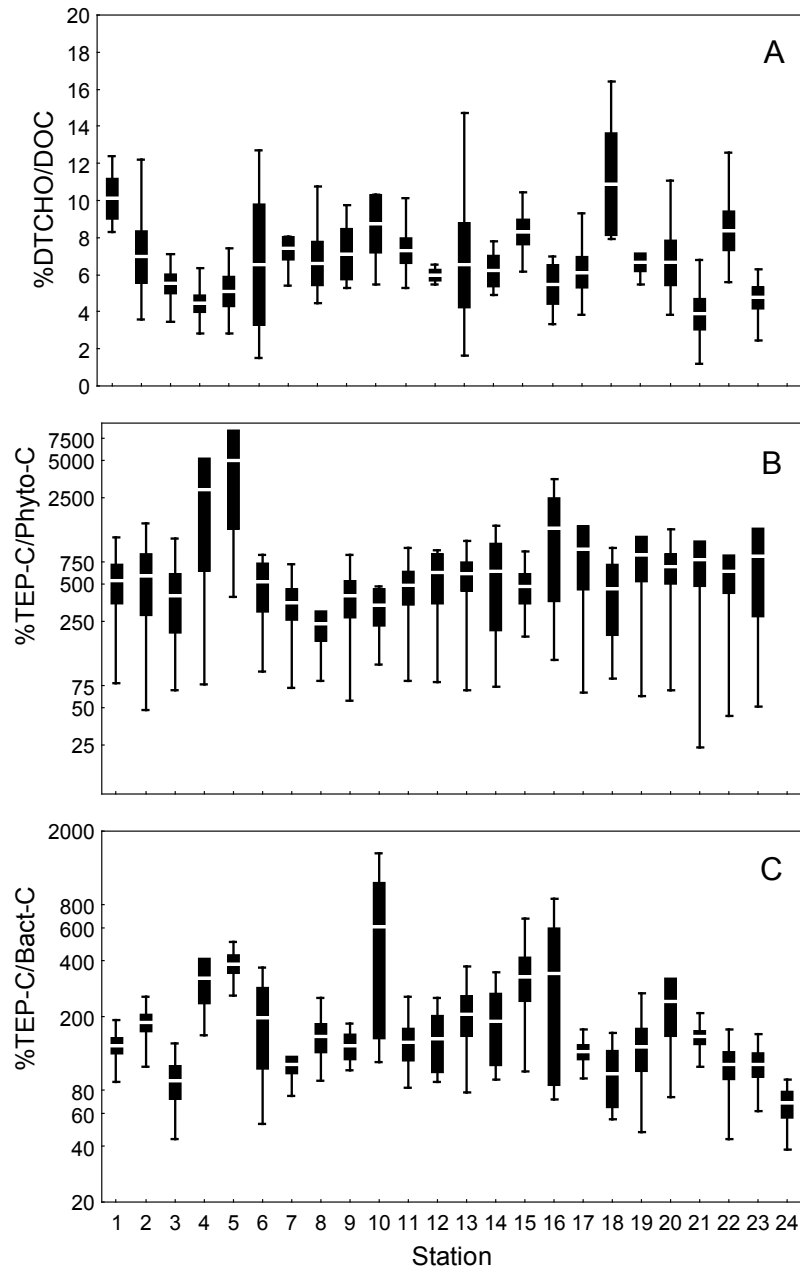


Figure 6.4. Mean percentage of DMCHO and DPCHO with respect to DOC (A) and mean % of TEP-C with respect to phytoplankton C (B) and bacterial-C (C) in all Mediterranean Sea stations. White lines= Mean values. Boxes= Standard Errors. Whiskers= not-outlier extremes. Note that B and C are in log scale.

Table 6.2. Correlation coefficients between DTCHO ($\mu\text{mol C l}^{-1}$) and TEP, chl a concentration and bacterial production (BP) and abundance (BA) in the Mediterranean Sea all (variables were log10 transformed). r = correlation coefficients. p level = level of significance.

Variable	r	p level
TEP ($\mu\text{g XG eq l}^{-1}$)	0.31	<0.001
Chl a ($\mu\text{g l}^{-1}$)	0.25	<0.01
BP ($\mu\text{g C l}^{-1} \text{h}^{-1}$)	0.27	<0.01
BA (cell ml^{-1})	0.21	<0.05

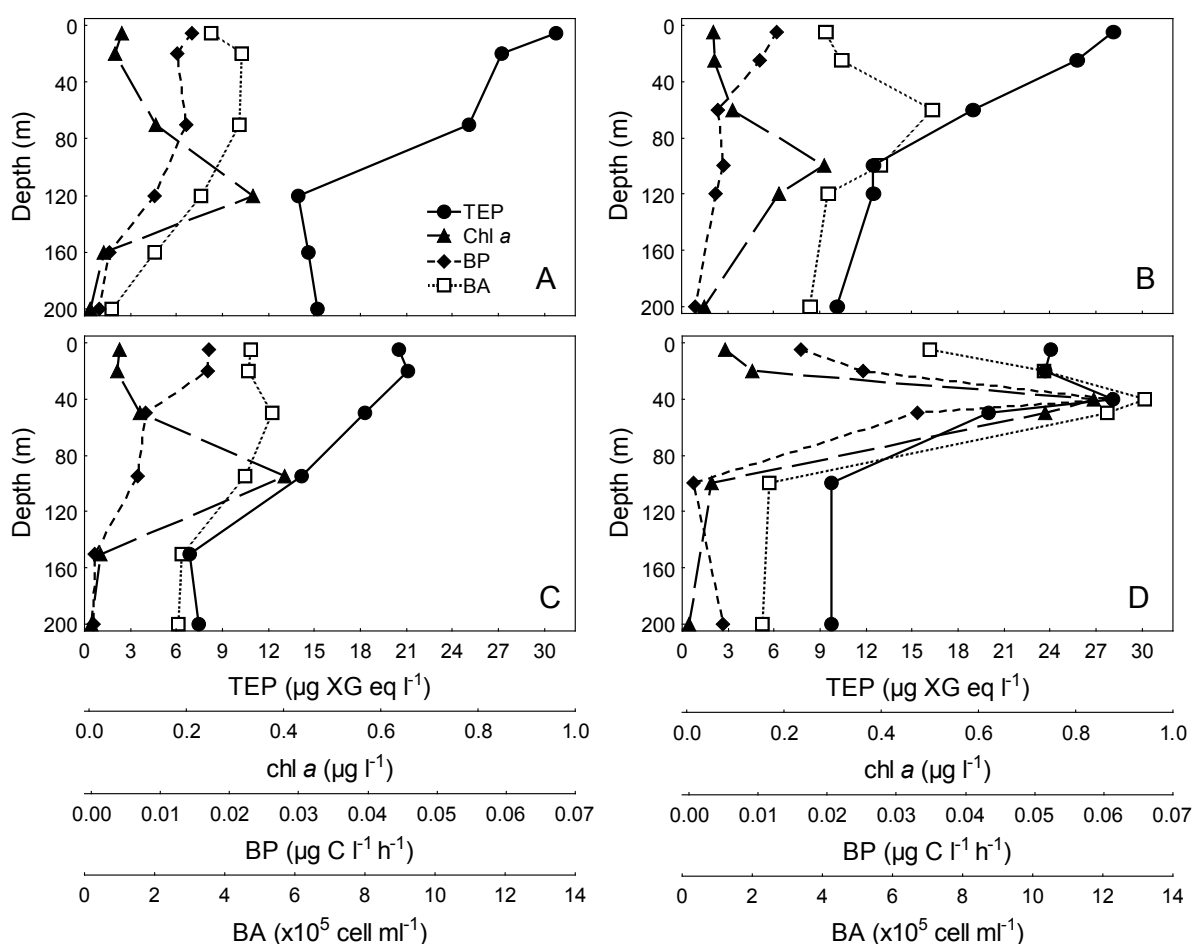


Figure 6.5. Vertical profiles of TEP ($\mu\text{g XG eq l}^{-1}$), chl a ($\mu\text{g l}^{-1}$), bacterial production (BP, $\mu\text{g C h}^{-1} \text{ l}^{-1}$), and bacterial abundance (BA, $\times 10^5 \text{ cell ml}^{-1}$) in four representative locations in the Mediterranean Sea: st #4, (passed Sicily, A) st #11 (near Alexandria, B), st#17 (near Greece, C) and st#23 (between Sardinia and Balear Islands, D).

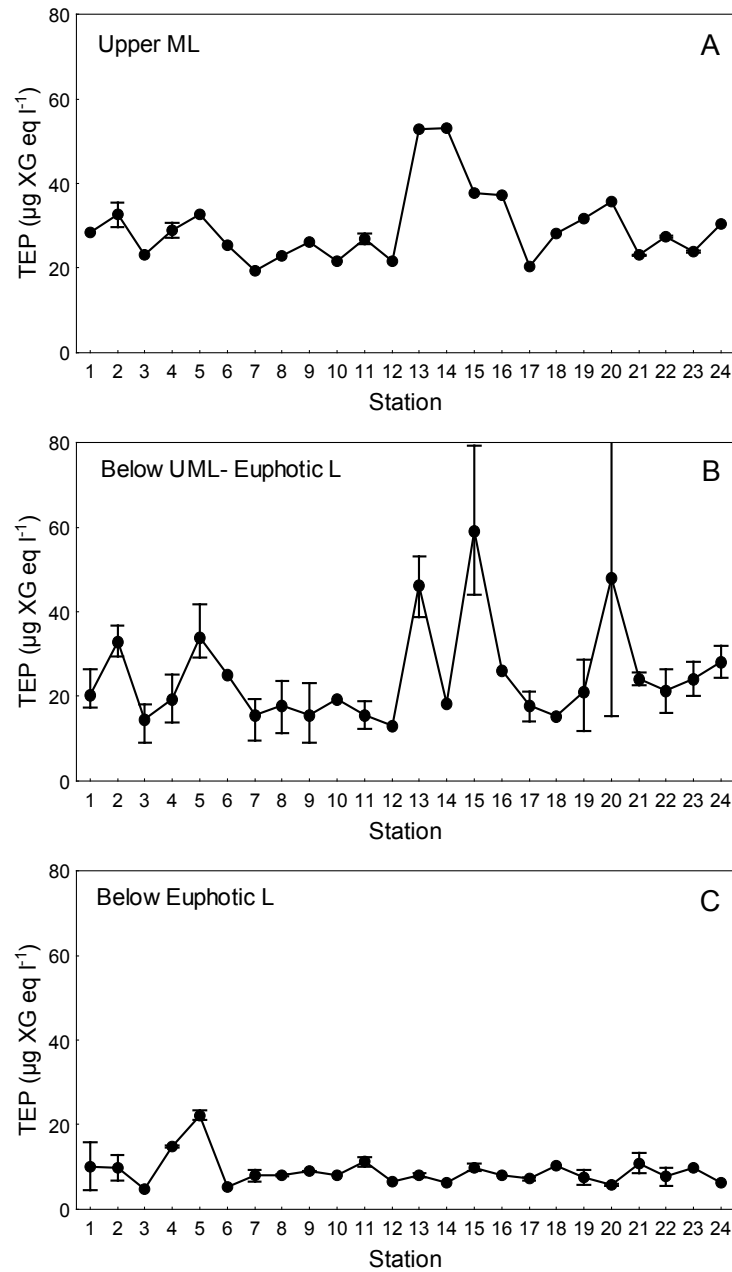


Figure 6.6. Geographical variability of average TEP concentrations within the upper Mixed Layer (A), below UML but within the euphotic Layer (B) and below the euphotic Layer (C) in the different stations. Circles= Average values. Whiskers= Non-outlier ranges.

gean Sea near Greek islands, and #20, in the central Mediterranean, and below the euphotic layer of stations #4 and #5 (Fig. 6.6).

The mean value of the TEP/chl *a* ratio was 505.9 $\mu\text{g XG eq } \mu\text{g chl } a^{-1}$. TEP-C was up to 949% of the Phyto-C and was highest at stations #4 and #5 (Figure 6.4B) and below the euphotic layer (Table 6.1).

The mean value of the TEP/BA ratio was 50.9 XG eq cell⁻¹, and carbon content of TEP (TEP-C) was 191% of that of bacteria and horizontally constant (Fig 6.4C). The highest values were observed within the upper mixed layer (Table 6.1).

TEP concentration was positively related to chl *a* and bacterial abundance and production if all data are considered (Table 6.3). However, the explained variance was low in all cases except for the TEP-BP relationship, where the explained variance was higher than 50% (Table 6.3). The determination of partial coefficients confirmed that BP was the best regressor of TEP concentration (Table 6.4) in the Mediterranean Sea.

Table 6.3. Results of the regression analyses performed between TEP and different biological variables in the Mediterranean Sea (all variables were log₁₀ transformed). SE= Standard Error r²= explained variance p-level = level of significance.

Dependent Var	Independent Var	Intercept	Slope \pm SE	r ²	p level
TEP	Chl <i>a</i> ($\mu\text{g l}^{-1}$)	1.43	0.16 \pm 0.04	0.11	<0.001
($\mu\text{g XG eq l}^{-1}$)	BP ($\mu\text{g C l}^{-1} \text{ h}^{-1}$)	2.07	0.39 \pm 0.03	0.51	<0.001
	BA (cell ml ⁻¹)	-1.46	0.48 \pm 0.10	0.15	<0.001

Table 6.4. Results of partial coefficients obtained in multiple regression between TEP vs. chl *a* and bacterial abundance and production in the Mediterranean S

Dependent var	Independent var	partial coefficient	p level
TEP	Chl <i>a</i>	-0.13	ns
	B Abundance	0.07	ns
	B Production	0.66	<0.001

BACTERIAL TEP GENERATION IN THE MEDITERRANEAN SEA.

The ambient concentrations of chl *a* and TEP and initial concentrations of TEP, DMCHO and DPCHO in the experiments are presented in Table 6.5.

Bacteria increased in both abundance and production in all experiments and treatments (Fig 6.7). The addition of SA did not prevent completely bacterial growth, but inhibited it partially in 3 experiments yielding to significantly lower BA and BP (repeated measures ANOVA, see chapter 3). Daily increases in BA ranged from 0.06 to 2.49×10^8 cell l⁻¹ d⁻¹ (Table 6.6). Cumulative bacterial biomass

Table 6.5. Concentrations (mean \pm standard error) of TEP and chl *a* determined on unfiltered samples from water for at the station and depth selected for the experiments, and TEP, DMCHO and DPCHO at t0 of each regrowth experiment. bdl = below detection limit.

Exp #	St #	Depth	Ambient TEP ($\mu\text{g XG eq l}^{-1}$)	Ambient chl <i>a</i> ($\mu\text{g l}^{-1}$)	TEP t0 ($\mu\text{g XG eq l}^{-1}$)	DMCHO t0 ($\mu\text{g C l}^{-1}$)	DPCHO t0 ($\mu\text{g C l}^{-1}$)
1	2	200m	6.8	bdl	7.6 ± 0.8	13.2 ± 13.2	36.3 ± 12.9
2	2	DCM	29.5	1.15	9.4 ± 1.3	23.4 ± 6.2	53.8 ± 23.1
3	15	200m	9.0	0.06	8.0 ± 0.7	42.6 ± 16.7	23.8 ± 12.9
4	15	DCM	79.2	0.62	20.7 ± 3.8	25.2 ± 9.9	10.0 ± 14.0

Table 6.6. Daily increases in bacterial abundance (BA), bacterial production (BP), TEP and TEP/BA ratios in all experiments and treatments.

Exp	Loca- tion	Depth	Treatment	ΔBA ($\times 10^8$ cell l ⁻¹ d ⁻¹)	ΔBP ($\mu\text{g C l}^{-1} \text{ h}^{-1}$) d ⁻¹	ΔTEP ($\mu\text{g XG}$ eq l ⁻¹ d ⁻¹)	$\Delta\text{TEP/BA}$ (fg XG eq ⁻¹ cell ⁻¹)
1	St #2	200m	+SA	0.30	0.07	10.9	14.3
			Bact	1.56	0.25	17.0	16.1
2		DCM	+SA	0.43	0.08	8.1	12.8
			Bact	2.49	0.31	19.0	19.6
3	St #15	200m	+SA	0.26	0.02	7.3	7.9
			Bact	0.06	0.10	5.4	-3.8
4		DCM	+SA	0.60	0.03	4.8	9.7
			Bact	1.56	0.08	12.3	13.1

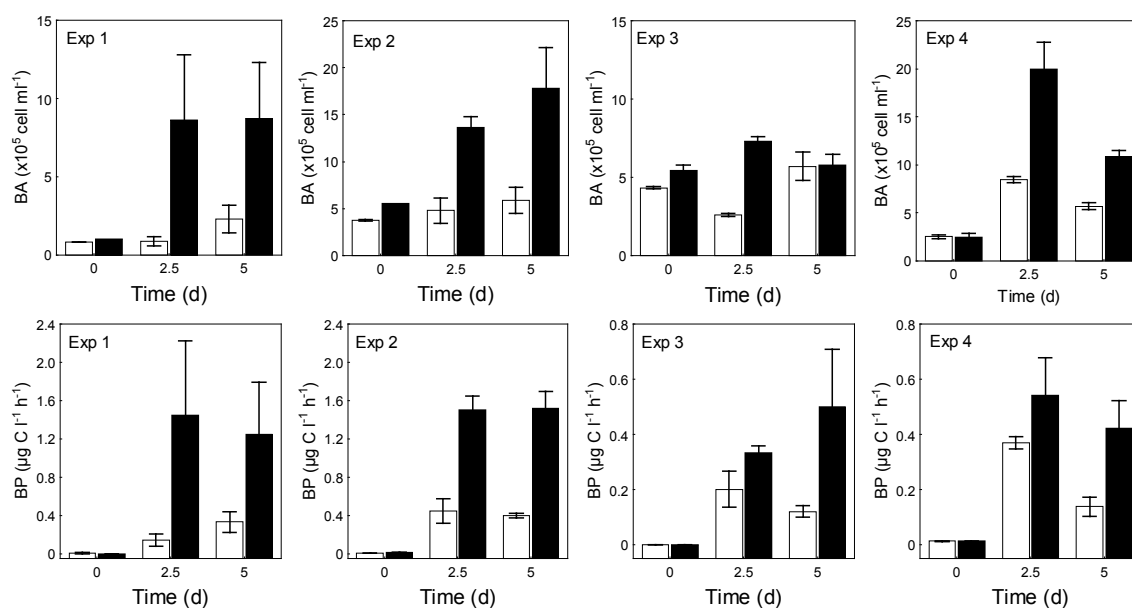


Figure 6.7. Changes in BA (top panels) and BP (bottom panels) over the course of the re-growth cultures performed in the four experiments. White bars: +SA treatments. Black bars: Bact. treatments. Whiskers= Standard Errors. Note the different scales in the y axis.

Table 6.7. Cumulative bacterial biomass (carbon accumulated as bacterial cells), cumulative bacterial production (carbon incorporated as bacteria through the entire incubation time) and cumulative TEP (carbon accumulated as TEP during the whole incubations) in all experiments and treatments.

Exp	Location	Depth	Treatment	Cum. Bacterial Biomass ($\mu\text{g C l}^{-1}$)	Cum. Bacterial Production ($\mu\text{g C l}^{-1}$)	Cum. TEP-C ($\mu\text{g C l}^{-1}$)
1	St #2	200m	+SA	2.9	13.7	40.4
			Bact	15.3	80.1	62.7
2		DCM	+SA	4.2	25.2	29.9
			Bact	24.5	89.4	70.2
3	St #15	200m	+SA	2.7	10.5	29.2
			Bact	0.7	26.4	21.8
4		DCM	+SA	6.4	16.8	19.4
			Bact	16.7	31.2	49.2

at the end of the cultures ranged from 0.7 to 24.5 $\mu\text{g C l}^{-1}$ (mean value 9.2 $\mu\text{g C l}^{-1}$) (Table 6.7).

Daily increases in BP ranged from 0.02 to 0.31 ($\mu\text{g C l}^{-1} \text{ h}^{-1}$) d^{-1} (Table 6.6). Cumulative bacterial production (that is, carbon incorporated to bacteria along the entire incubations) ranged from 10.5 to 89.4 $\mu\text{g C l}^{-1}$ (mean value 36.7 $\mu\text{g C l}^{-1}$) (Table 6.7)

TEP increased in all re-growth cultures (Table 6.6, Fig 6.8), particularly in those without SA additions (Table 6.8). Daily increases in TEP ranged from 4.8 to 19.0 $\mu\text{g XG eq l}^{-1} \text{ d}^{-1}$ (Table 6.6), Cumulative TEP-C during the cultures averaged 40.3 $\mu\text{g C l}^{-1}$, ranging from 19 to 70 $\mu\text{g C l}^{-1}$ (Table 6.7)

The TEP/BA ratios increased in all the re-growth cultures (except in the bact. treatment of experiment 4) from a mean value of 50.3 $\text{fg XG eq cell}^{-1}$ to a mean value of 102.6 $\text{fg XG eq cell}^{-1}$. The TEP/BA ratios were not significantly different (ANOVA, $p > 0.05$) in the treatments with and without SA. Daily increases in TEP/BA ratios ranged from 0.26 to 36.0 $\text{fg XG eq cell}^{-1} \text{ d}^{-1}$ (Table 6.6).

Independently of the initial conditions, daily TEP increases were significant and positively related to daily increases in BA ($r^2 = 0.78$, $p < 0.01$) and BP ($r^2 = 0.78$, $p < 0.01$). The equations that relate daily increases in TEP and daily increases in BA or BP are shown in Figure 6.9. Similar equations were obtained when only treatments without SA additions were considered.

DMCHO concentration increased in 7 of 8 re-growth cultures (Fig 6.10), ranging from a decrease of 3.8 $\mu\text{g C l}^{-1}$ to an increase of 19.6 $\mu\text{g C l}^{-1} \text{ d}^{-1}$ (Table 6.11). By contrast, DPCHO concentration decreased with time in 5 of 8 re-growth cultures (Fig 6.11) and ranged from a decrease of 10.9 $\mu\text{g C l}^{-1} \text{ d}^{-1}$ to an increase of 4.2 $\mu\text{g C l}^{-1} \text{ d}^{-1}$ (Table 6.9). There were no significant differences (ANOVA, $p > 0.05$) between +SA and bact treatments.

Although DPCHO generally decreased with time, these daily decreases were of lower magnitude (average daily change -2.7 $\mu\text{g C l}^{-1} \text{ d}^{-1}$) than daily increases in TEP-C (average daily increase 8.0 $\mu\text{g C l}^{-1} \text{ d}^{-1}$, Table 6.9).

Table 6.8. Results of the ANOVA tests performed to study differences in TEP concentrations in treatments with and without sodium azide additions at the end of all the re-growth cultures. ns= not significant.

Experiment	F	p
1	0.85	ns
2	46.11	< 0.01
3	1.36	ns
4	13.7	< 0.05

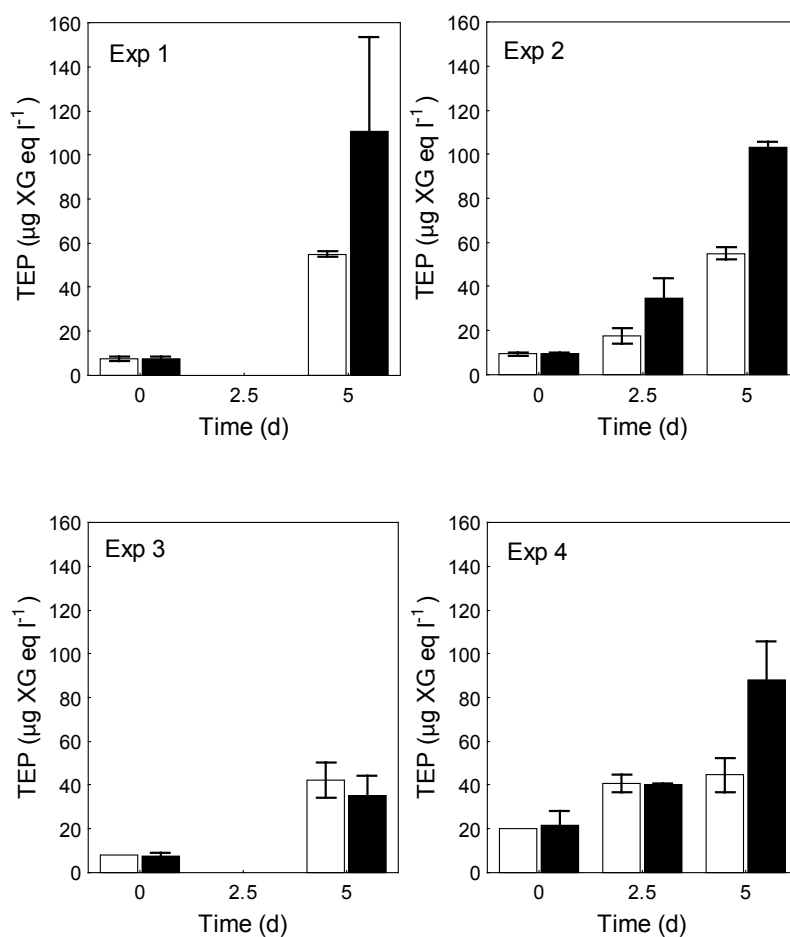


Figure 6.8. Changes in TEP over the course of the re-growth cultures performed in the four experiments. White bars: +SA treatments. Black bars: Bact. treatments. Whiskers= Standard Errors.

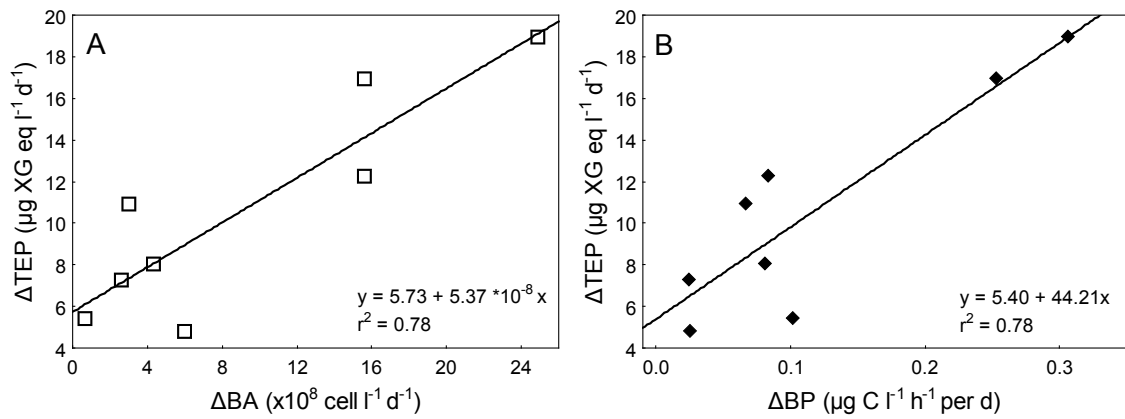


Figure 6.9. Scatterplots between daily increases in TEP (ΔTEP) and daily increases in bacterial abundance (ΔBA , A) and bacterial production (ΔBP , B).

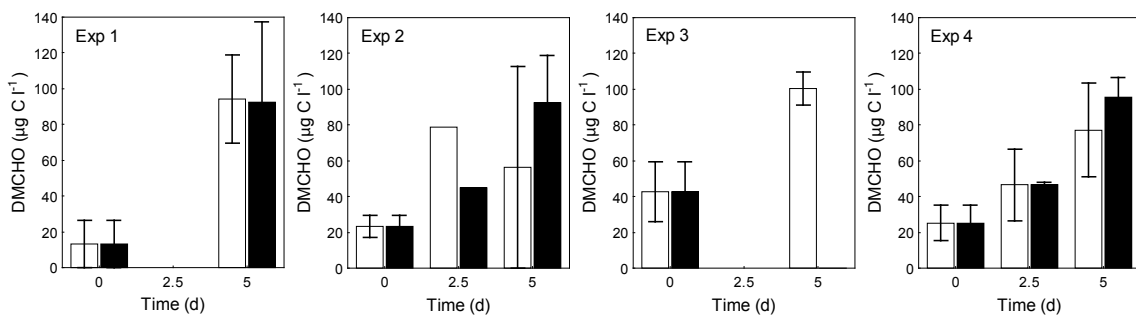


Figure 6.10. Changes in DMCHO over the course of the re-growth cultures performed in the four experiments. White bars: +SA treatments. Black bars: Bact. treatments. Whiskers= Standard Errors.

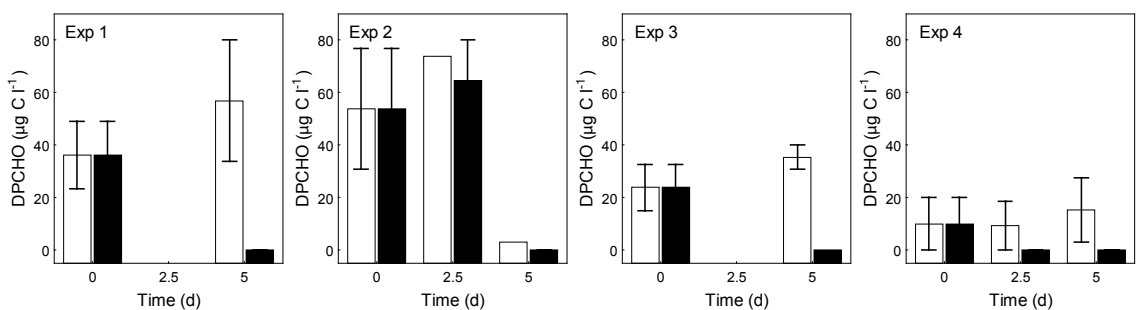


Figure 6.11. Changes in DPCHO over the course of the re-growth cultures performed in the four experiments. White bars: +SA treatments. Black bars: Bact. treatments. Whiskers= Standard Errors.

Table 6.9. Daily increases in TEP-C, DMCHO and DPCHO ($\mu\text{g C l}^{-1} \text{d}^{-1}$), in all experiments and treatments.

Exp	Location	Depth	Treatment	ΔTEP ($\mu\text{g C l}^{-1} \text{d}^{-1}$)	ΔDMCHO ($\mu\text{g C l}^{-1} \text{d}^{-1}$)	ΔDPCHO ($\mu\text{g C l}^{-1} \text{d}^{-1}$)
1	St #2	200m	+SA	8.2	14.3	4.2
			Bact	12.8	16.1	-2.4
2		DCM	+SA	6.1	12.8	-10.3
			Bact	14.3	19.6	-10.9
3	St #15	200m	+SA	5.5	7.9	2.2
			Bact	4.1	-3.8	-2.4
4		DCM	+SA	3.6	9.7	0.0
			Bact	9.2	13.1	-1.9

FIELD EXTRAPOLATION OF BACTERIAL TEP GENERATION.

Daily TEP increases were positively related to time-average BP in the cultures ($r^2 = 0.78$, $p < 0.01$), but were not significantly related to time-average BA ($r^2 = 0.25$, $p > 0.05$). The regression equation obtained (ΔTEP ($\mu\text{g XG eq l}^{-1} \text{d}^{-1}$) = $5.24 + 11.94 \cdot \text{BP}$ ($\mu\text{g C l}^{-1} \text{h}^{-1}$)) was used as the experimental bacterial TEP formation rate by unit of BP. Based on the obtained equation, daily TEP increases normalized per time-average BP ranged from 0.70 to $3.02 \mu\text{g XG eq } \mu\text{gC}^{-1}$ in the cultures.

An extrapolation of these experimental rates (ΔTEP per unit of BP) to field BP average values in the area yielded estimates of a TEP formation rate of $5.4 \mu\text{g XG eq l}^{-1} \text{d}^{-1}$, which would imply a TEP duplication time due to bacterial production of 4 days.

DISCUSSION

Field observations reported in this work suggest a positive influence of bacterioplankton on TEP dynamics. In particular, bacterial activity was the best predictor of TEP distribution in the Mediterranean Sea, and this finding contrasts with previous works that attribute a minor role of bacteria on TEP formation in the field (Passow and Alldredge, 1994; Schuster and Herndl, 1995; Corzo et al., 2005).

In fact, marine aggregates in the Mediterranean are thought to be ultimately of phytoplankton origin (Degobbi, 1989). However, we have observed in our study a weak relationship (low slope and explained variance) between chl *a* and TEP. This weak relationship could be explained by geographical differences in phytoplankton composition or growth status, that would yield specific relationships between chl *a* and TEP, or by nutrient limitation. We observed during this study lowest or undetectable phosphate concentrations in those areas with highest chl *a* (data not shown), corroborating the phosphorus limitation of this ecosystem (Thingstad et al., 2005), and under these conditions TEP can increase due to cell lysis while chl *a* concentrations decrease (Passow, 2002b). This lag time between increases of chl *a* and TEP could explain the observed weak relationship.

By contrast, the significant and positive relationship between BP and TEP suggest that the link between bacteria and TEP in the Mediterranean Sea could be more immediate. The positive of bacterial activity controlling TEP distributions in the area could be explained by different mechanisms: Bacterioplankton can generate or colonize TEP, enhance the abiotic TEP formation, or influence the formation and persistence of algal TEP.

The experimental results allowed us to elucidate the prevalent pathways upon which TEP and bacteria are linked. Because phytoplankton and preexisting TEP were initially removed in the experiments, we can reject an enhancement of algal TEP production or a colonization of these particles as possible mechanisms for this link. In these experiments, increases in TEP followed bacterial growth in abundance and production, suggesting that TEP accumulation was a direct consequence of bacterial activity, consistent with previous studies (Stoderegger and Herndl, 1999; Passow, 2002a; Sugimoto et al., 2007). The bacterial TEP formation rates observed in the experiments yielded to a duplication time of 4 days, which

would imply that 25% of TEP in the field can be daily renewed by bacteria, a similar percentage than that obtained by Sugimoto et al. (2007) when maximum TEP formation rates were monitored.

Bacterial capsules, although are not individual particles as TEP, are also stainable with Alcian Blue and thus cannot be discriminated from TEP with the colorimetric analysis. Although this could yield an overestimation of TEP formed by bacteria, this bias would be also committed in colorimetric determinations of TEP whenever bacteria are present (e.g. natural water samples) if we assume a constant proportion of capsulated bacteria. Indeed, the proportion of capsulated bacteria in cultures is expected to be lower than in the field as grazing stress is absent (Costerton et al., 1978).

In most of the re-growth cultures, an increase in TEP/BA ratios was detected along with time. This is comparable to observed TEP dynamics coupled to phytoplankton growth, where increases in TEP formation have been frequently described at the end of algal blooms (Logan et al., 1995; Corzo et al., 2000; Engel et al., 2002). The higher TEP accumulation at the end of growth stages of microorganisms may be due to the increase in TEP as a result of cell lysis (possibly due to viral infection or grazing) or to a higher TEP release rate due to nutrient depletion. Indeed, bacterioplankton in the Mediterranean Sea, like phytoplankton, are frequently limited by inorganic nutrients (Thingstad and Rassoulzadegan, 1999; Sala et al., 2002).

Trying to elucidate if bacteria generate TEP directly or, alternatively, enhance physically the abiotic TEP formation, we compared increases in TEP-C with decreases in DPCHO in the cultures (that as a bulk measurement of dissolved polysaccharide may include acidic TEP precursors). These increases in TEP were not counterbalanced by a decrease of the same magnitude in DPCHO (Table 6.9), supporting the idea that most TEP accumulated during the experiments were not formed directly by abiotic assembly of dissolved precursor material. The alternative pathway would be an active release of TEP by bacteria rather than their physical influence on abiotic TEP formation. This assertion can be supported by a comparison between the carbon utilized by bacteria and that accumulated as TEP-C. During the course of the experiments there was a mean value of $27.5 \pm 8.4 \mu\text{g C l}^{-1}$ of organic carbon that was incorporated into bacteria but not accumulated as cell biomass at the end of the experiment. This “remaining” amount of

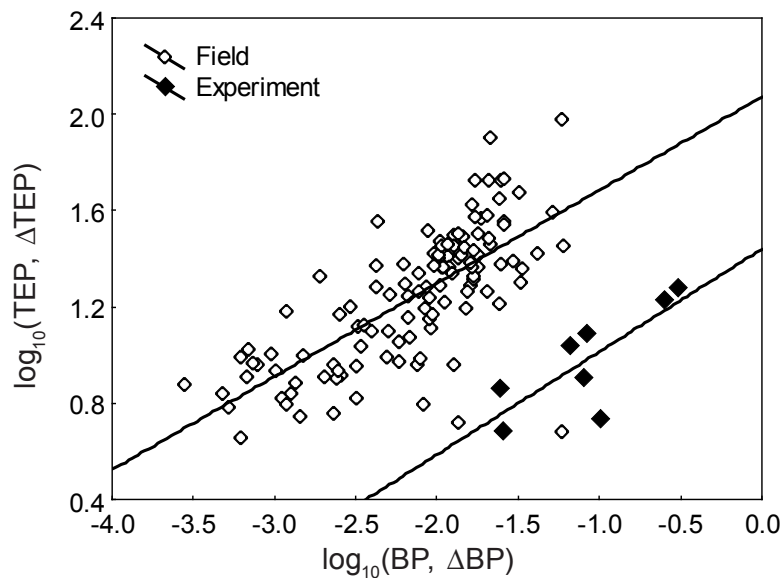


Figure 6.12. Comparative between log-log scatterplots of TEP-BP relationship in the field (white diamonds) and scatterplot of increases in TEP-increases in BP (Δ TEP- Δ BP) in the experiments (black diamonds). Equations are $\log_{10} \text{TEP} = 2.07 + 0.39 * (\log_{10} \text{BP})$ and $\log_{10}(\Delta \text{TEP}) = 1.44 + 0.43 * (\log_{10}(\Delta \text{BP}))$ respectively.

organic carbon was of a similar magnitude that the carbon accumulated as TEP in 5 of 8 cultures (average $40.3 \pm 6.7 \mu\text{g C l}^{-1}$, see Table 6.7), suggesting again that most of TEP produced during the cultures was channeled mostly through bacterioplankton.

In the natural environment, TEP are the result of a balance between sources (not only by bacteria but also by other organisms in general and algae in particular) and sinks (particle sedimentation (Passow et al., 2001; Azetsu-Scott and Passow, 2004), consumption by organisms (Tranvik et al., 1993), Passow 2002b) or polymer cracking by UV radiation (see chapter 7)), which likely govern at different timescales. Interestingly, the relationship between increases in TEP and increases in BP, when expressed as log-log relationship, show a similar slope (0.43) than these for the TEP-BP relationship in the field (0.39) (Fig 6.12). The concordance between experimental and field relationships between TEP and bacteria underline the dominant role that these organisms may play on TEP dynamics in the Mediterranean Sea, suggesting that active TEP production by bacteria would be a significant process occurring in these waters.

The concentrations of DMCHO and DPCHO observed in the study area are in the range of those reported for the Mediterranean Sea (Momzikoff et al., 2004) and other areas of the ocean (Pakulski and Benner, 1994; Mykkestad et al., 1997) using spectrophotometric techniques. Although a positive relationship between DTCHO and TEP was observed, the low explained variance does not warrant a direct relationship between these pools of organic carbon. The proportion of DTCHO from the DOC pool (6.7%) was lower than the reported in the Southern Ocean (23%, see chapter 5) and in other areas (Pakulski and Benner, 1994), but, as for the Southern Ocean, we cannot estimate the proportion of TEP precursors from the bulk measurements of dissolved carbohydrates. Also the high geographical and vertical variability in DMCHO and DPCHO and the weak relationships with any other study variables suggests high dynamicity of these compounds in the field.

The TEP concentration reported in this chapter is lower than those published in different areas of the Mediterranean Sea (Mari et al., 2001; Beauvais et al., 2003). However, this is not surprising if we consider that the few available studies on TEP in the Mediterranean Sea are confined to more eutrophic areas (coastal areas or the Western Mediterranean). Indeed, despite low TEP concentration, the TEP/chl *a* ratios observed in our study were noticeably higher than those reported in other marine systems (see Table 5.5 in chapter 5). The high TEP/chl *a* and also high TEP/BA ratios observed in this system suggests the significant contribution of TEP to particulate organic carbon in these waters. These high ratios could reflect the oligotrophic condition of the Mediterranean Sea, where a limitation by inorganic nutrients (e.g. average NH_4 concentrations of $0.17 \mu\text{M}$ in contrast to average NH_4 concentrations of $1.04 \mu\text{M}$ in the Southern Ocean) can enhance specific TEP production by algae and bacteria. Specifically, high N/P ratios in the Mediterranean Sea have been identified as ultimate causes for the formation of large organic matter aggregates through high extracellular release of polymeric substances by phytoplankton. The formation of TEP from algal-derived dissolved material can be direct by abiotic coagulation or mediated by bacteria through uptake and reprocessing of algal DOM and subsequent release of bacterial exopolymers (Decho and Herndl, 1995), as inferred from our experimental results.

To conclude, the relationship between TEP and bacteria observed in the Mediterranean Sea, that suggests a positive role of these organisms affecting TEP dynamics, is verified experimentally by the direct TEP generation by bacteria in

cultures. According to these results, bacterial release of TEP can act as a dominant process regulating TEP dynamics in the field, yielding to duplication times of few days in the Mediterranean Sea.

REFERENCES

- ALLDREDGE, A.L., U. PASSOW and B.E. LOGAN (1993) The abundance and significance of a class of large, transparent organic particles in the ocean. *Deep-Sea Research Part I-Oceanographic Research Papers*. 40: 1131-1140.
- AZAM, F., T. FENCHEL, J.G. FIELD, J.S. GRAY, L.A. MEYERREIL and F. THINGS-TAD (1983) The ecological role of water-column microbes in the sea. *Marine Ecology-Progress Series*. 10: 257-263.
- AZETSU-SCOTT, K. and U. PASSOW (2004) Ascending marine particles: Significance of transparent exopolymer particles (TEP) in the upper ocean. *Limnology and Oceanography*. 49: 741-748.
- BEAUVAIS, S., M.L. PEDROTTI, E. VILLA and R. LEMÉE (2003) Transparent exopolymer particle (TEP) dynamics in relation to trophic and hydrological conditions in the NW Mediterranean Sea. *Marine Ecology-Progress Series*. 262: 97-109.
- CALVO, S., R. BARONE and L.N. FLORES (1995) Observations on mucus aggregates along Sicilian coasts during 1991-1992. *Science of The Total Environment*. 165: 23-31.
- CORZO, A., J.A. MORILLO and S. RODRÍGUEZ (2000) Production of transparent exopolymer particles (TEP) in cultures of *Chaetoceros calcitrans* under nitrogen limitation. *Aquatic Microbial Ecology*. 23: 63-72.
- CORZO, A., S. RODRÍGUEZ-GÁLVEZ, L. LUBIÁN, P. SANGRÁ, A. MARTÍNEZ and J.A. MORILLO (2005) Spatial distribution of transparent exopolymer particles in the Bransfield Strait, Antarctica. *Journal of Plankton Research*. 27: 635-646.
- COSTERTON, J.W., G.G. GEESEY and K.J. CHENG (1978) How bacteria stick. *Scientific American*. 238: 86-&.
- COTNER, J.B. and B.A. BIDDANDA (2002) Small players, large role: Microbial influence on biogeochemical processes in pelagic aquatic ecosystems. *Ecosystems*. 5: 105-121.
- DECHO, A.W. and G.J. HERNDL (1995) Microbial activities and the transformation of organic matter within mucilaginous material. *Science of The Total Environment*. 165: 33-42.
- DEGOBBIS, D. (1989) Increased eutrophication of the Northern Adriatic Sea - 2nd Act. *Marine Pollution Bulletin*. 20: 452-457.
- ENGEL, A., S. GOLDTHWAIT, U. PASSOW and A. ALLDREDGE (2002) Temporal decoupling of carbon and nitrogen dy-

- namics in a mesocosm diatom bloom. *Limnology and Oceanography*. 47: 753-761.
- ENGEL, A. and U. PASSOW (2001) Carbon and nitrogen content of transparent exopolymer particles (TEP) in relation to their Alcian Blue adsorption. *Marine Ecology-Progress Series*. 219: 1-10.
- ENGEL, A., S. THOMS, U. RIEBESELL, E. RO-CHELLE-NEWALL and I. ZONDERVAN (2004) Polysaccharide aggregation as a potential sink of marine dissolved organic carbon. *Nature*. 428: 929-932.
- GROSSART, H.P., G. CZUB and M. SIMON (2006) Algae-bacteria interactions and their effects on aggregation and organic matter flux in the sea. *Environmental Microbiology*. 8: 1074-1084.
- GUERRINI, F., A. MAZZOTTI, L. BONI and R. PISTOCCHI (1998) Bacterial-algal interactions in polysaccharide production. *Aquatic Microbial Ecology*. 15: 247-253.
- HEISSENBERGER, A., G.G. LEPPARD and G.J. HERNDL (1996a) Relationship between the intracellular integrity and the morphology of the capsular envelope in attached and free-living marine bacteria. *Applied and Environmental Microbiology*. 62: 4521-4528.
- HEISSENBERGER, A., G.G. LEPPARD and G.J. HERNDL (1996b) Ultrastructure of marine snow .2. Microbiological considerations. *Marine Ecology-Progress Series*. 135: 299-308.
- JOHNSON, B.D. and P.E. KEPKAY (1992) Colloid transport and bacterial utilization of oceanic DOC. *Deep-Sea Research Part A-Oceanographic Research Papers*. 39: 855-869.
- KEPKAY, P.E. and B.D. JOHNSON (1988) Microbial response to organic particle generation by surface coagulation in seawater. *Marine Ecology-Progress Series*. 48: 193-198.
- KIRCHMAN, D.L. (1994) The uptake of inorganic nutrients by heterotrophic bacteria. *Microbial Ecology*. 28: 255-271.
- LEE, S. and J.A. FUHRMAN (1987) Relationships between biovolume and biomass of naturally derived marine bacterioplankton. *Applied and Environmental Microbiology*. 53: 1298-1303.
- LOGAN, B.E., U. PASSOW, A.L. ALLDREDGE, H.P. GROSSART and M. SIMON (1995) Rapid formation and sedimentation of large aggregates is predictable from coagulation rates (half-lives) of transparent exopolymer particles (TEP). *Deep-Sea Research Part II-Topical Studies in Oceanography*. 42: 203-214.
- MARI, X., S. BEAUVAIS, R. LEMÉE and M.L. PEDROTTI (2001) Non-Redfield C : N

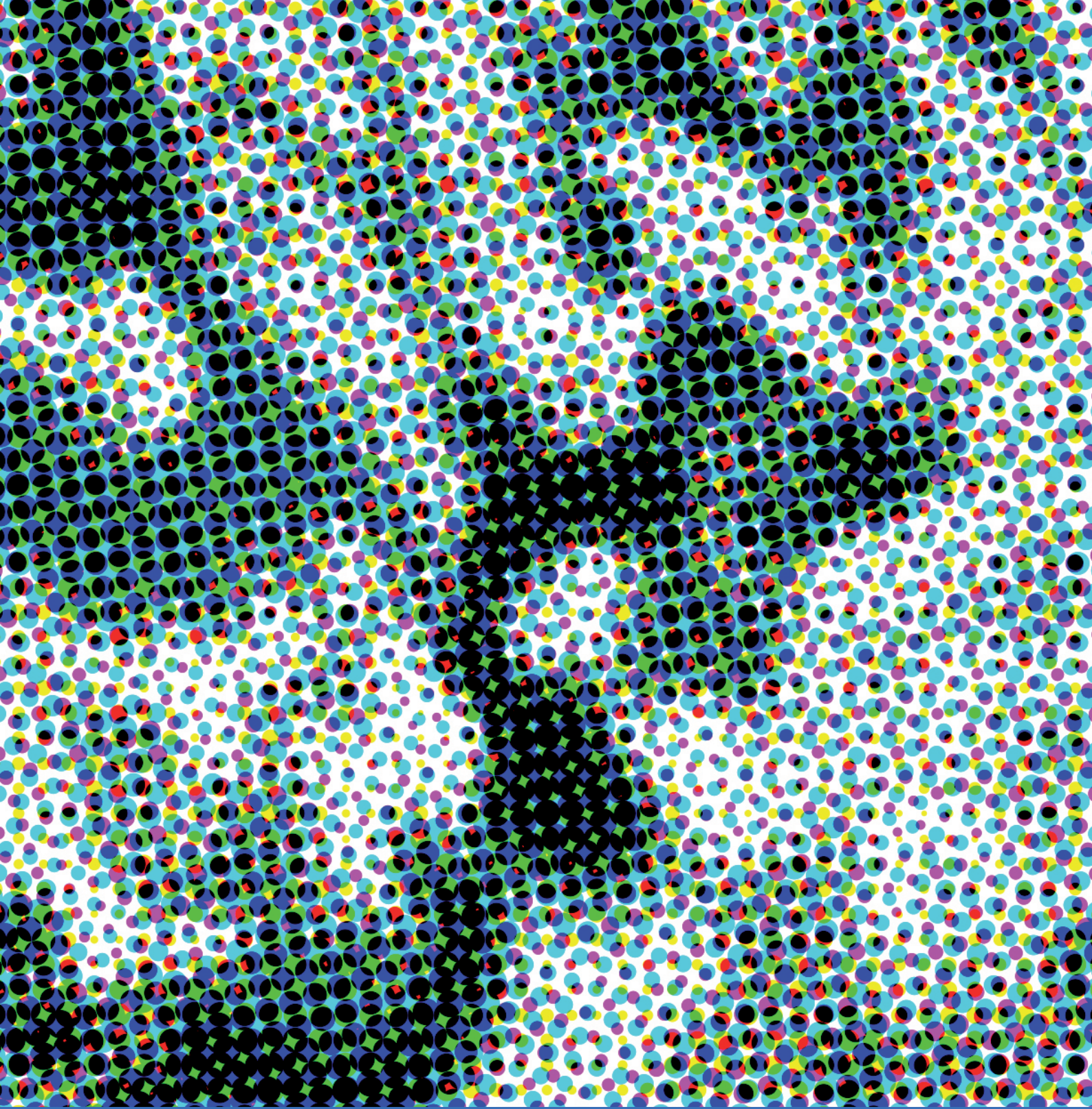
- ratio of transparent exopolymeric particles in the northwestern Mediterranean Sea. *Limnology and Oceanography*. 46: 1831-1836.
- MARI, X. and T. KIORBOE (1996) Abundance, size distribution and bacterial colonization of transparent exopolymeric particles (TEP) during spring in the Kattegat. *Journal of Plankton Research*. 18: 969-986.
- MECOZZI, M., R. ACQUISTUCCI, V. DI NOTO, E. PIETRANTONIO, M. AMICI and D. CARDARILLI (2001) Characterization of mucilage aggregates in Adriatic and Tyrrhenian Sea: structure similarities between mucilage samples and the insoluble fractions of marine humic substance. *Chemosphere*. 44: 709-720.
- MEINERS, K., R. BRINKMEYER, M.A. GRAN-SKOG and A. LINDFORS (2004) Abundance, size distribution and bacterial colonization of exopolymer particles in Antarctic sea ice (Bellingshausen Sea). *Aquatic Microbial Ecology*. 35: 283-296.
- MOMZIKOFF, A., A. BRINIS, S. DALLOT, G. GONDRY, A. SALIOT and P. LEBARON (2004) Field study of the chemical characterization of the upper ocean surface using various samplers. *Limnology and Oceanography-Methods*. 2: 374-386.
- MYKLESTAD, S., E. SKANOY and S. HEST-MANN (1997) A sensitive and rapid method for analysis of dissolved mono- and polysaccharides in seawater. *Marine Chemistry*. 56: 279-286.
- OBERNOSTERER, I. and G.J. HERNDL (1995) Phytoplankton extracellular release and bacterial-Growth - Dependence on the inorganic N-P ratio. *Marine Ecology-Progress Series*. 116: 247-257.
- PAKULSKI, D. and R. BENNER (1994) Abundance and distribution of carbohydrates in the ocean. *Limnology and Oceanography: Methods*. 39: 930-940.
- PASSOW, U. (2002a) Production of transparent exopolymer particles (TEP) by phyto- and bacterioplankton. *Marine Ecology-Progress Series*. 236: 1-12.
- PASSOW, U. (2002b) Transparent exopolymer particles (TEP) in aquatic environments. *Progress in Oceanography*. 55: 287-333.
- PASSOW, U. and A.L. ALLDREDGE (1994) Distribution, size and bacterial-colonization of transparent exopolymer particles (TEP) in the ocean. *Marine Ecology-Progress Series*. 113: 185-198.
- PASSOW, U., R.F. SHIPE, A. MURRAY, D.K. PAK, M.A. BRZEZINSKI and A.L. ALLDREDGE (2001) The origin of transparent exopolymer particles (TEP) and their role in the sedimentation of par-

- ticulate matter. *Continental Shelf Research*. 21: 327-346.
- RADIC, T., I. IVANCIC, D. FUKS and J. RADIC (2006) Marine bacterioplankton production of polysaccharidic and proteinaceous particles under different nutrient regimes. *Fems Microbiology Ecology*. 58: 333-342.
- SALA, M.M., F. PETERS, J.M. GASOL, C. PEDROS-ALIO, C. MARRASÉ and D. VAQUÉ (2002) Seasonal and spatial variations in the nutrient limitation of bacterioplankton growth in the northwestern Mediterranean. *Aquatic Microbial Ecology*. 27: 47-56.
- SCHUSTER, S. and G.J. HERNDL (1995) Formation and significance of transparent exopolymeric particles in the Northern Adriatic Sea. *Marine Ecology-Progress Series*. 124: 227-236.
- SHIBATA, A., K. KOGURE, I. KOIKE and K. OHWADA (1997) Formation of submicron colloidal particles from marine bacteria by viral infection. *Marine Ecology Progress Series*. 155: 303-307.
- STODEREGGER, K. and G.J. HERNDL (1998) Production and release of bacterial capsular material and its subsequent utilization by marine bacterioplankton. *Limnology and Oceanography*. 43: 877-884.
- STODEREGGER, K.E. and G.J. HERNDL (1999) Production of exopolymer particles by marine bacterioplankton under contrasting turbulence conditions. *Marine Ecology-Progress Series*. 189: 9-16.
- SUGIMOTO, K., H. FUKUDA, M.A. BAKI and I. KOIKE (2007) Bacterial contributions to formation of transparent exopolymer particles (TEP) and seasonal trends in coastal waters of Sagami Bay, Japan. *Aquatic Microbial Ecology*. 46: 31-41.
- THINGSTAD, T.F., M.D. KROM, R.F.C. MANTOURA, G.A.F. FLATEN, S. GROOM, B. HERUT, N. KRESS, C.S. LAW, A. PASTERNAK, P. PITTA, S. PSARRA, F. RASSOULZADEGAN, T. TANAKA, A. TSELEPIDES, P. WASSMANN, E.M.S. WOODWARD, C.W. RISER, G. ZODIATIS and T. ZOHARY (2005) Nature of phosphorus limitation in the ultraoligotrophic eastern Mediterranean. *Science*. 309: 1068-1071.
- THINGSTAD, T.F. and F. RASSOULZADEGAN (1999) Conceptual models for the biogeochemical role of the photic zone microbial food web, with particular reference to the Mediterranean Sea. *Progress in Oceanography*. 44: 271-286.
- TRANVIK, L.J., E.B. SHERR and B.F. SHERR (1993) Uptake and utilization of colloidal DOM by heterotrophic flagellates in seawater. *Marine Ecology-Progress Series*. 92: 301-309.
- VANDEVIVERE, P. and D.L. KIRCHMAN (1993) Attachment stimulates exopo-

lysaccharide synthesis by a bacterium.
Applied and Environmental Microbiology. 59: 3280-3286.

VAN LOOSDRECHT, M.C.M., J. LYKLEMA,
W. NORDE and A.J.B. ZEHNDER (1989)
Bacterial adhesion - a physicochemical
approach. Microbial Ecology. 17: 1-15.

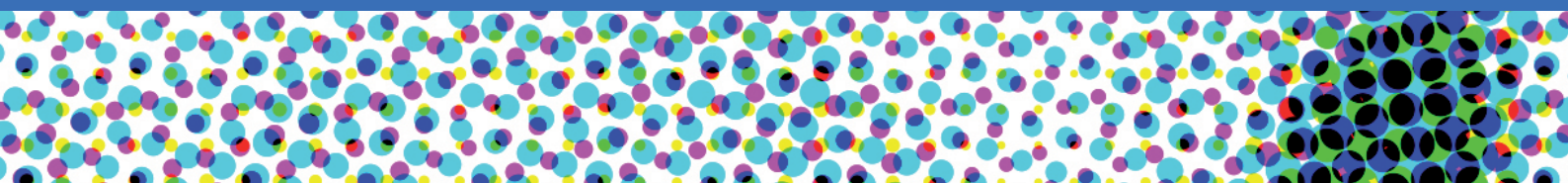
VOLLENWEIDER, R.A. and A. RINALDI
(1995) Special Edition on marine mucil-
lages, with special reference to mucila-
ge events in the Norhtern Adriatic Sea,
the Tyrrhenian Sea and the North Sea.
Science of the Total Environment. 165:
1-235.



Chapter 7: **Impact of UVB on transparent exopolymer particles.**

Ortega-Retuerta, E., Passow, U., Duarte, C.M., and Reche, I.

Abbreviated title: Photoreactivity of TEP



INTRODUCTION

Transparent exopolymer particles are the most ubiquitous and abundant gel particles in the ocean (Passow, 2002). The aggregation of dissolved organic matter precursors to form TEP and their subsequent sedimentation represent a major pathway for dissolved organic carbon (DOC) removal from surface to deep waters (Passow, 2002; Engel et al., 2004). However, owing to their low density, the TEP content of marine aggregates determines their fate in the water column (ascent or settling) (Azetsu-Scott and Passow, 2004; Mari, 2008). In fact, the sea surface microlayer is generally enriched in TEP (Wurl and Holmes, 2008) which affect significantly the air-sea gas exchange (Frew, 1997) with obvious implications for the global carbon cycle. In this context, it is important to understand the mechanisms driving TEP formation and degradation in the ocean.

Abiotic formation of TEP is a function of the size, concentration, and stickiness of precursors and also of the physical environment (e.g. laminar or turbulent shear) (Passow, 2000). In addition, the persistence of TEP is likely dependent on the nature and degree of cross-links generated during the assembly of precursors. Polymers linked by covalent bonds are more stable than particles stabilized by low-energy interactions as Van der Waals forces (Verdugo, 2004; Verdugo et al., 2004). TEP are formed by a surface-active fraction of acidic polysaccharides, that form cationic bridges (e.g. metal ion complexes) and hydrogen bonds (Mopper et al., 1995). Thus, abiotic TEP assembly is likely a reversible process depending on the ionic strength.

To date, the effects of solar radiation on TEP formation and degradation have not been explored. Chromophoric and humic substances are susceptible to be photodegraded to low molecular weight compounds and inorganic forms (dissolved inorganic carbon, carbon monoxide and dioxide) in diverse aquatic ecosystems (Kieber et al., 1990; Mopper et al., 1991; Miller and Zepp, 1995; Reche et al., 1999), as well as humic-like compounds can be generated by the sunlight-mediated condensation of dissolved fatty acids (Kieber et al., 1997) being all these processes widely studied. However, transparent exopolymer particles are formed by acidic polysaccharides. These compounds, where chromophoric groups are lacking, confere high transparency to these particles (Aldredge et al., 1993; Passow, 2002) which also suggest low photoreactivity. UVB radiation can block the abiotic self-assembly of dissolved organic matter into gels, whereas it can completely disperse preexisting gels (Orellana and Verdugo, 2003). The proposed mechanism for this breakage is a loss of anionic charge, which would lead to a decline in polymer network stability. In this case, UVB radiation would result in a decrease in TEP with a subsequent increase in dissolved precursors. Moreover, polysaccharides such as alginic acid, pullullan and laminarin can also be photolysed at high UVB levels (Akhlaq et al., 1990; Kovac et al., 2000). However, to date, there is no available information of the effect of solar radiation, both in the UV and visible ranges, specifically in TEP assembly and/or dispersion. If, according to Orellana and Verdugo (2003), solar radiation blocks gel abiotic formation and also disperses preexisting TEP, then a decrease in TEP linked to an enrichment in dissolved precursors (dissolved mono- and polysaccharides, DMCHO and DPCHO) would be presumable under UVB radiation (Fig 7.1).

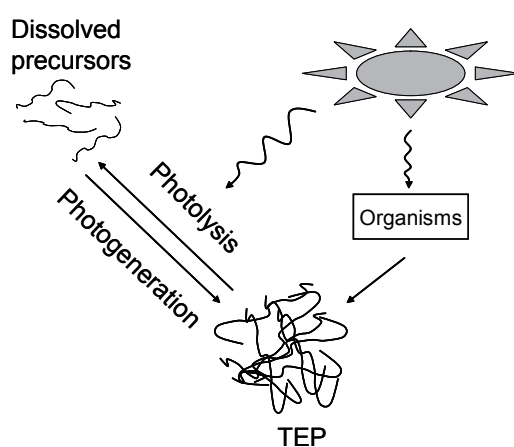


Figure 7.1. Pathways of interaction between TEP and solar radiation.

In this chapter, we experimentally tested three hypotheses: First, UVB radiation can disperse pre-assembled TEP into their dissolved precursors (photolysis). Second, UVB radiation can block the assembly of dissolved precursors to form TEP (photogeneration). Third, TEP generation by microorganisms can be influenced by the light regime.

MATERIAL AND METHODS

Three different types of experiments (Table 7.1) were set up to study the three hypotheses. North Sea water (collected from two locations at the German Bight, see general sampling protocols), was used in four of the experiments, and 3 were conducted with water from a batch culture of *Chaetoceros affinis*. This diatom produces large amounts of TEP and their dissolved precursors (Passow and Alldredge, 1994). These last experiments were conducted with the filtrate (0.2 μm) from the culture that was grown in f/2 media based on North Sea water, with a photoperiod of 12 hours light-12 hours dark at an irradiance of 150 $\mu\text{E m}^{-2} \text{s}^{-1}$ and harvested in the exponential growth phase.

Two experiments were conducted outside on the laboratory roof in a water bath under natural solar radiation and five experiments inside in a temperature constant culture room (15°C) with a light regime of 18:6 hours under artificial

Table 7.1. Summary of the experiments performed, including substrate and the place where the incubations were arranged.

#	Type of experiment	Substrate	Incubation method
1	TEP photolysis	North Sea water (St #2 5m)	Culture room
2	TEP photolysis	<i>C. affinis</i> culture	Culture room
3	TEP photolysis	<i>C. affinis</i> culture	Culture room
4	TEP photogeneration	North Sea water (St #1 5m)	Laboratory roof
5	TEP photogeneration	North Sea water (St #2 5m)	Culture room
6	TEP photogeneration	<i>C. affinis</i> culture	Culture room
7	TEP photoreactivity with microorganisms	North Sea water (St #1 10m)	Laboratory roof

UVB and PAR lamps, receiving a light dose of 0.15 W m^{-2} at UVB, 5.86 W m^{-2} at UVA, and $10 \mu\text{E m}^{-2} \text{ s}^{-1}$ at PAR.

TEP PHOTOLYSIS EXPERIMENTS.

A total of three experiments to determine if TEP photolysis is a significant process were conducted (Fig 7.2). Experiment 1 was performed with natural seawater and experiments 2 and 3 with the filtrate of *C. affinis*. First, North Sea water or water from the batch culture of *C.affinis* were sequentially filtered: first through a $40 \mu\text{m}$ mesh, then through precombusted GF/C and GF/F glass fiber filters ($\approx 1.2 \mu\text{m}$ and $\approx 0.7 \mu\text{m}$, Whatman) and then by $0.2 \mu\text{m}$ polycarbonate filters (Poretics). This procedure removed all particles. The $< 0.2 \mu\text{m}$ filtrate was subsequently incubated in a Couette flocculator for 24 hours at a shear rate of 33.3 s^{-1} . A Couette flocculator consists of a fixed inner and a rotating outer cylinder which provide a quantifiable 2-dimensional laminar shear in the annular space between them (Duuren, 1968). Incubation in a flocculator under these conditions enhances TEP formation from dissolved precursors (Passow, 2000). TEP concentration was

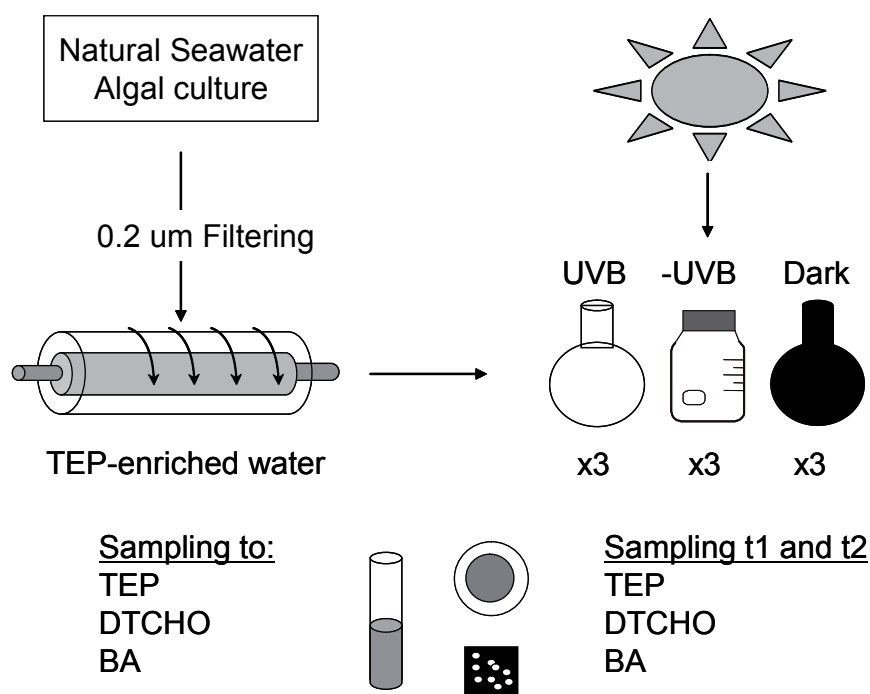


Figure 7.2. Scheme of experimental procedure in TEP direct photolysis experiments.

measured after incubation in the flocculator and compared with controls incubated in a flask. TEP-enriched water from the flocculator was used in these experiments. Each experiment consisted of three treatments in triplicate:

- UVB + UVA + PAR (referred as UVB treatment): water was incubated in 50ml quartz bottles, transparent to UVB light.
- UVA + PAR (- UVB treatment): water was incubated in 50ml borosilicate bottles, opaque to UVB light.
- Dark treatment: water was incubated in aluminium-covered 50ml borosilicate bottles.

The light transmission through borosilicate and quartz bottles was measured in a spectrophotometer. The transmission through the quartz bottles was around 90% in the whole spectra, whereas through the borosilicate bottles it was zero in the UVB range and over 60% in the UVA and PAR ranges (Fig 7.3).

All treatments were incubated inside the culture room. Samples were collected initially and after 1.5 and 3 days to measure TEP and dissolved mono- and

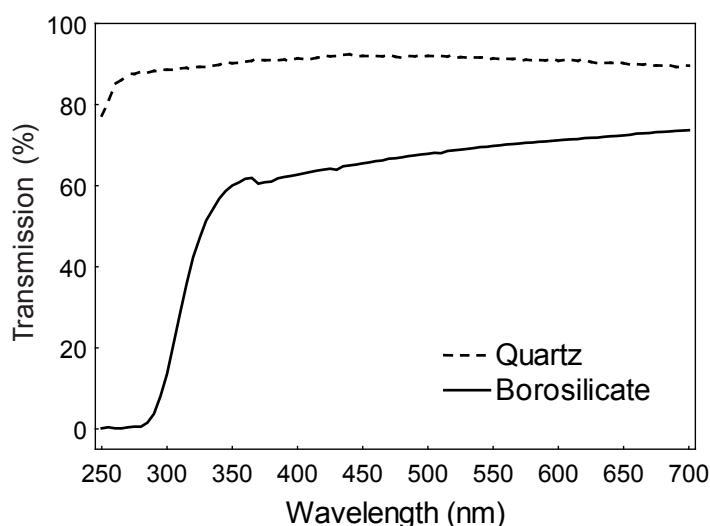


Figure 7.3. Percentage of energy transmission in the experimental bottles for UVB and -UVB treatments (quartz and borosilicate) as a function of wavelength measured on a spectrophotometer.

polysaccharides (DTCHO). Samples for bacterial abundance were also taken as a control.

TEP photolysis rates were calculated after the following expression:

$$-\Delta\text{TEP}(\text{d}^{-1}) = \frac{(\text{TEP}_{t_f} - \text{TEP}_{t_0}) / t}{\text{TEP}_{t_0}} \times 100$$

where t_f and t_0 are final and initial times respectively and t is incubation time in days.

TEP PHOTOGENERATION FROM DISSOLVED PRECURSORS

A total of 3 experiments on the photogeneration of TEP were conducted using natural (experiment 4) or artificial light (experiments 5 and 6) (Fig 7.4). To study

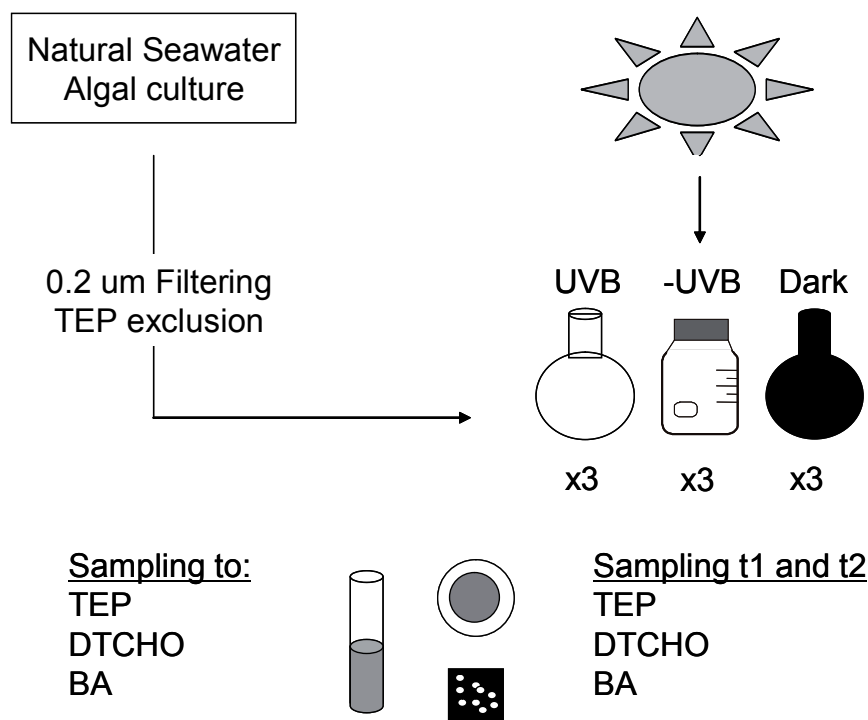


Figure 7.4. Scheme of experimental procedure in TEP photogeneration experiments.

abiotic TEP photogeneration under UVB, -UVB and dark conditions, water from either the North Sea (experiments 4 and 5) or from the *C.affinis* culture (experiment 6) was filtered through 0.2 μm to eliminate all phytoplankton, bacteria and TEP. This $< 0.2 \mu\text{m}$ filtrate was used directly for setting up the experiments. Experiment 5 and 6 consisted of the same three treatments (UVB, -UVB, dark) as described above, whereas experiment 4 was conducted with only two treatments, UVB and dark.

Samples were collected initially, and after 1.5 and 3 days to determine TEP concentration, DTCHO and DOC concentration. Additionally, we took samples for bacterial abundance as a check for bacterial growth. We confirmed the presence of dissolved TEP-precursors in the water used for experiments by incubating an aliquot of the original $< 0.2 \mu\text{m}$ filtered water in a Couette flocculator for 24 hours in the dark.

TEP PHOTOREACTIVITY IN THE PRESENCE OF MICROORGANISMS

Experiment 7 was conducted with unfiltered North Sea water (Station #1, 10m). The experiment consisted of the same three treatments as all prior experiments, with 3 replicates each, and was conducted under natural radiation. Samples were collected initially, and after 4.5 and 9 days for TEP and DTCHO.

STATISTICAL ANALYSES

To test for significant differences between treatments over time in each experiment, repeated measures ANOVA tests were applied. This analysis is useful for experiments where there may be a within-subject effect (incubation time) and a between-subjects effect (UVB, -UVB or total radiation). The analysis tests three types of effects allowing to set out three hypotheses: within-subject effect (does TEP or DTCHO change through incubation time?), between-subjects effect (are TEP or DTCHO different in UVB, -UVB or dark treatments at every incubation time?), and between-subjects by within-subject interaction effect (does the difference between TEP in UVB, -UVB and dark treatments increase through incubation time?).

RESULTS

STUDY AREA CHARACTERIZATION

The average and ranges of DMCHO, DPCHO and TEP determined in the two stations samples in the North Sea are shown in Table 7.2. Dissolved carbohydrates accounted for a 12.7 % of the DOC pool, and TEP-C averaged 671% of bacterial-C. DMCHO, DPCHO and TEP were homogeneously distributed within the two vertical profiles. No significant correlations between DTCHO, TEP and other variables were observed likely due to the low number of samples, although a positive relationship between TEP and BA was observed ($r^2 = 0.44$, slope = 1.13 ± 0.57 , $n = 8$).

Table 7.2. Mean, maximum and minimum values of TEP ($\mu\text{g XG eq l}^{-1}$), carbon content of TEP ($\mu\text{g TEP-C l}^{-1}$), DMCHO ($\mu\text{mol C l}^{-1}$), DPCHO ($\mu\text{mol C l}^{-1}$), percentage of DTCHO relative to DOC and percentage of TEP-C relative to bacterial-C determined in the North Sea stations.

	Mean (ranges)
TEP	200 (112 - 296)
TEP-C	150 (83.7 - 222)
DMCHO	17.8 (13.5 - 20.9)
DPCHO	8.9 (4.9 -11.9)
%DTCHO/DOC	12.7 (9.6 -15.0)
% TEP-C/Bact-C	671 (434 - 1367)

TEP PHOTOLYSIS EXPERIMENTS

TEP concentration decreased markedly in the UVB treatments of all the photolysis experiments. TEP concentrations were undetectable at the end of each experiment (3 days), and very low or undetectable after 1.5 days. In -UVB treatments, TEP decreased, less drastically in experiments 1 and 2, and did not change significantly in experiment 3. In dark treatments, no changes (exp 1) or increases in TEP (exp 2 and 3) were detected (Fig 7.5). The repeated measures ANOVA tests confirmed differences between UVB and dark treatments to be significant (Table 7.3).

Low bacterial growth was detected in UVB and -UVB treatments, ranging from no increases up to 3.15×10^8 cell l⁻¹ in 3 days. However, high bacterial growth was detected in the dark treatments, particularly in those experiments performed with algal culture filtrate (Exps 2 and 3), growing up to 114.3×10^8 cell l⁻¹ (Exp 3 dark treatment).

We used the experimental TEP formation rate due to bacterial growth as calculated in chapter 6 ($\Delta\text{TEP} = 5.73 + 5.37 \times 10^{-8} \Delta\text{BA}$) to estimate the changes in TEP concentration during the experiment that could be attributable to bacterial release. After correction for bacterial production of TEP, the net decrease in TEP was still appreciable in UVB treatments of all experiments and in -UVB treatments of experiments 1 and 2, with no changes in TEP in experiment 3. In the dark treatments, no consistent patterns were detected in TEP concentration after the correction of bacterial contributions (Fig 7.5).

TEP photolysis rates ranged from 27 to 34 % d⁻¹ in the UVB treatments. This rate was constant in all time intervals in experiment 3 (Table 7.4). However, photolysis rates in experiments 1 and 2 were 69 to 71 % in the 1.5 days, leading to almost undetectable TEP concentrations at that time. TEP photolysis rates ranged from 8 to 18% d⁻¹ in the -UVB treatments.

Dissolved mono- and polysaccharides (DTCHO) decreased in the UVB treatments of all experiments. In contrast, there was no consistent pattern in the -UVB and dark treatments, with no changes in experiment 1, decreases in experiment 2 and increases in experiment 3 (Fig 7.6). The effect was significant for UVB radiation in experiment 2 and for total (UVB + PAR) radiation in experiment 3 (Table 7.5).

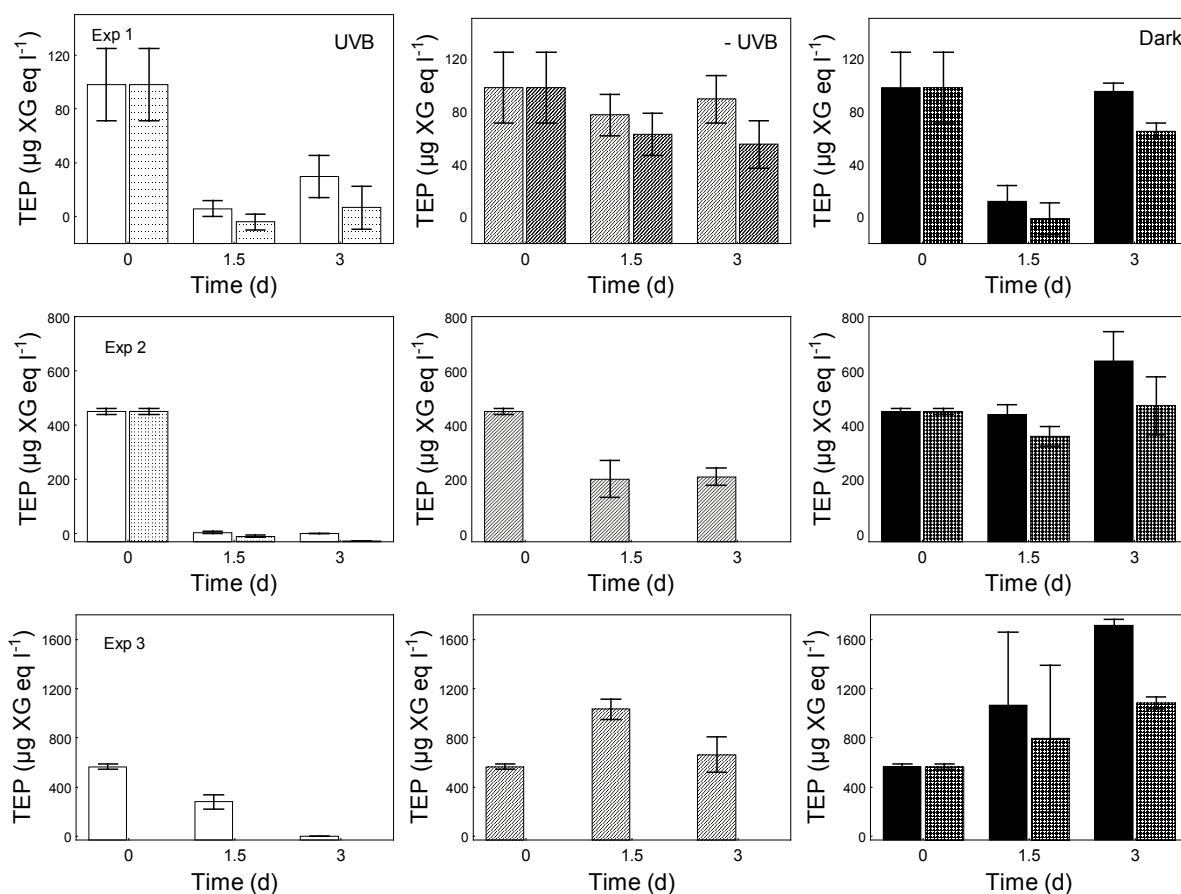


Figure 7.5. Changes in TEP concentrations in UVB, -UVB and dark treatments of TEP photolysis experiments (1 to 3). The pair of bars represent before (left bars) and after (right bars) correcting by bacterial contributions. Experiments where no bacterial growth was detected are only represented with the left bar. Whisker= Standard Error.

Table 7.3. Results of repeated measures ANOVA performed to assess significant differences in TEP concentrations among the different treatments of TEP photolysis experiments (Exp 1 to 3). ns= not significant.

Experiment	Effect	F	p level
1	Full solar spectrum (UVB vs. Dark)	15.1**	< 0.05
	Full sol. sp.*Time		
	UVB (UVB vs. -UVB)	6.0**	ns
	UVB*Time		
	-UVB (-UVB vs. Dark)	0.2	ns
	-UVB*Time		
2	Full solar spectrum (UVB vs. Dark)	23.6	< 0.01
	Full sol. sp.*Time	7.3	< 0.05
	UVB (UVB vs. -UVB)	3.7	ns
	UVB*Time	1.2	ns
	-UVB (-UVB vs. Dark)	7.3	ns
	-UVB*Time	2.9	ns
3	Full solar spectrum (UVB vs. Dark)	509.0	< 0.01
	Full sol. sp.*Time	108.9	< 0.01
	UVB (UVB vs. -UVB)	367.4	< 0.01
	UVB*Time	11.9	< 0.05
	-UVB (-UVB vs. Dark)	47.8	ns
	-UVB*Time	23.2	< 0.05

** simple ANOVA at final time

Table 7.4. TEP photolysis rates (d^{-1}) determined in UVB and -UVB treatments after corrections by bacterial growth.

Experiment	Photolysis rate (% d^{-1})	
	UVB	-UVB
1	-27.3 ± 5.4	-9.8 ± 3.7
2	-34.3	-17.7 ± 2.3
3	-32.2	-8.1 ± 8.2

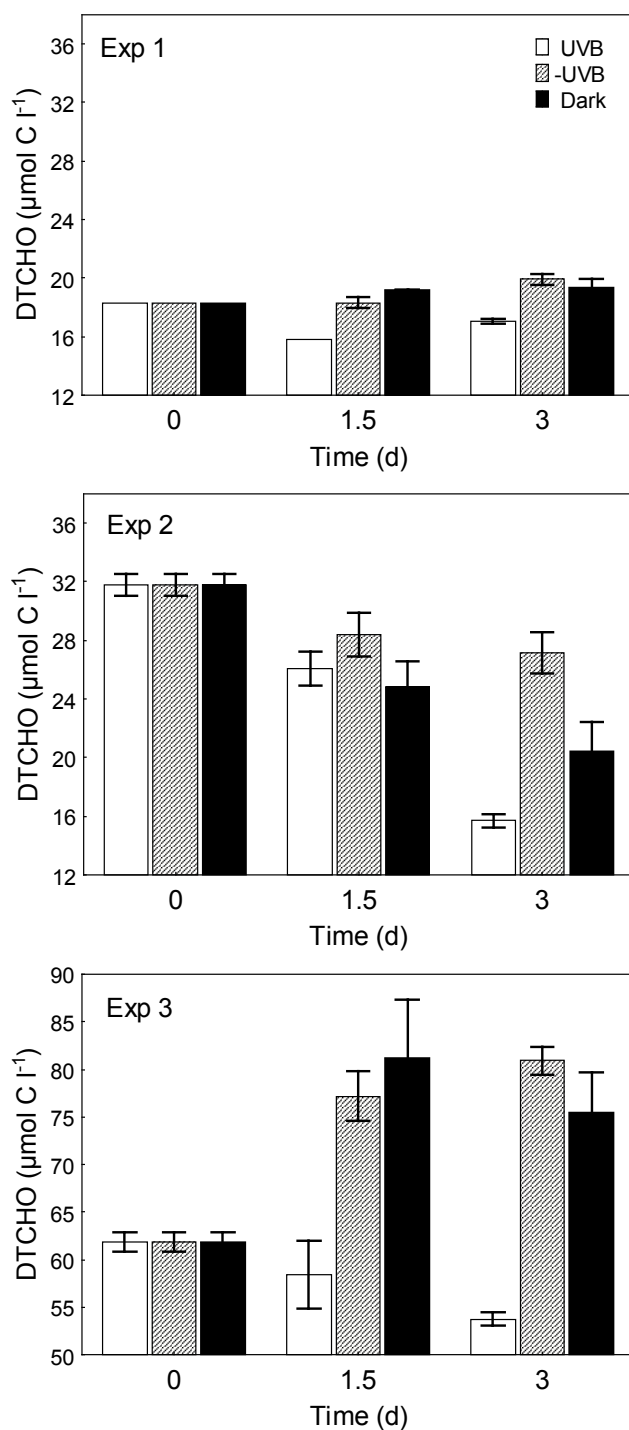


Figure 7.6. Changes in DTCHO concentrations in UVB (white bars), -UVB (striped bars) and dark (black bars) treatments of TEP photolysis experiments (1 to 3). Whisker= Standard Error.

Table 7.5. Results of repeated measures ANOVA performed to study differences in DT-CHO concentrations among the different treatments of TEP photolysis experiments (Exp 1 to 3). ns= not significant.

Experiment	Effect	F	p level
1	Full solar spectrum (UVB vs. Dark)	2.5	ns
	Full sol. sp.*Time	0.4	ns
	UVB (UVB vs. -UVB)	2.4	ns
	UVB*Time	0.3	ns
	-UVB (-UVB vs. Dark)	0	ns
	-UVB*Time	0.1	ns
2	Full solar spectrum (UVB vs. Dark)	0.3	ns
	Full sol. sp.*Time	0.2	ns
	UVB (UVB vs. -UVB)	24.5	< 0.05
	UVB*Time	71.3	< 0.001
	-UVB (-UVB vs. Dark)	2.2	ns
	-UVB*Time	5.2	ns
3	Full solar spectrum (UVB vs. Dark)	93.4	< 0.05
	Full sol. sp.*Time	2.8	ns
	UVB (UVB vs. -UVB)	74.2	< 0.05
	UVB*Time	9.4	ns
	-UVB (-UVB vs. Dark)	0	ns
	-UVB*Time	0.8	ns

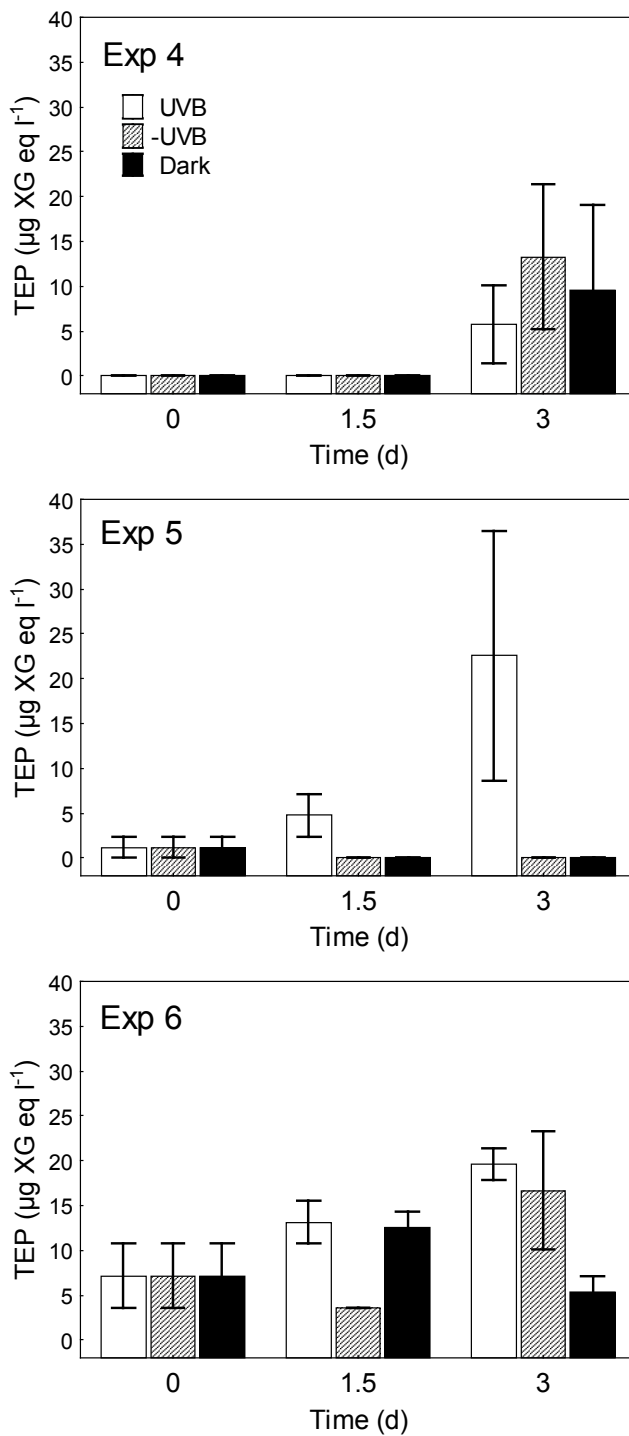


Figure 7.7. Changes in TEP concentrations in UVB (white bars), -UVB (striped bars) and dark (black bars) treatments of TEP photogeneration experiments (4 to 6). Whisker= Standard Error.

TEP PHOTOGENERATION EXPERIMENTS

TEP formation was low or not noticeable in the experiments 4, 5 and 6. The TEP increases observed in all treatments in experiment 4, in UVB treatment of experiment 5, and in UVB and -UVB treatments in experiment 6 (Fig 7.7) were not statistically significant ($p > 0.05$, repeated measures ANOVA).

The flocculator test confirmed the presence of dissolved TEP precursors, as a significant amount of TEP was formed within 24 hours, in experiments 4 and 5 (Fig 7.8). This test was not performed in experiment 6 due to the low volume of water available.

DOC concentration did not change over time in the different photogeneration experiments. DTCHO generally decreased in all photogeneration experiments and treatments, except for the UVB treatment of experiment 4 (Fig 7.9). The differences among treatments, like for TEP generation, were not statistically significant ($p > 0.05$, repeated measures ANOVA). Bacteria did not grow noticeably in experiments 4 and 5. In experiment 6, bacteria reached an abundance of 3.2×10^5 cell ml^{-1} in the dark treatment.

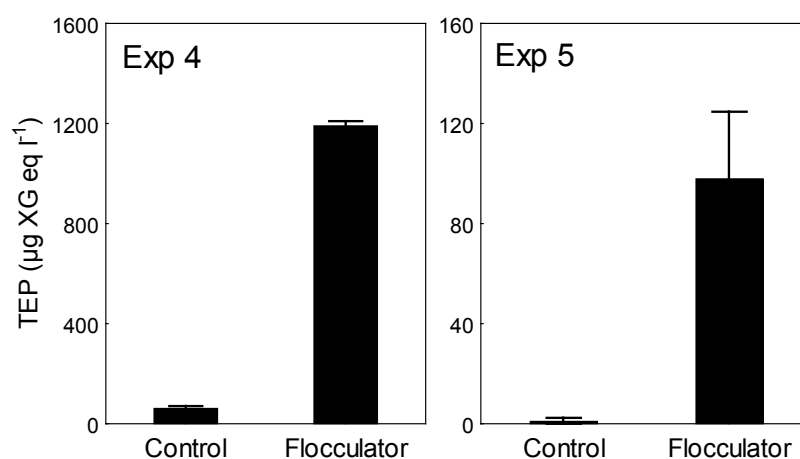


Figure 7.8. Differences in TEP concentration of 0.2-filtered water incubated for 24 hours inside a Couette flocculator vs controls of the same water incubated in parallel in glass flasks at the same light and temperature conditions. Whisker= Standard Error.

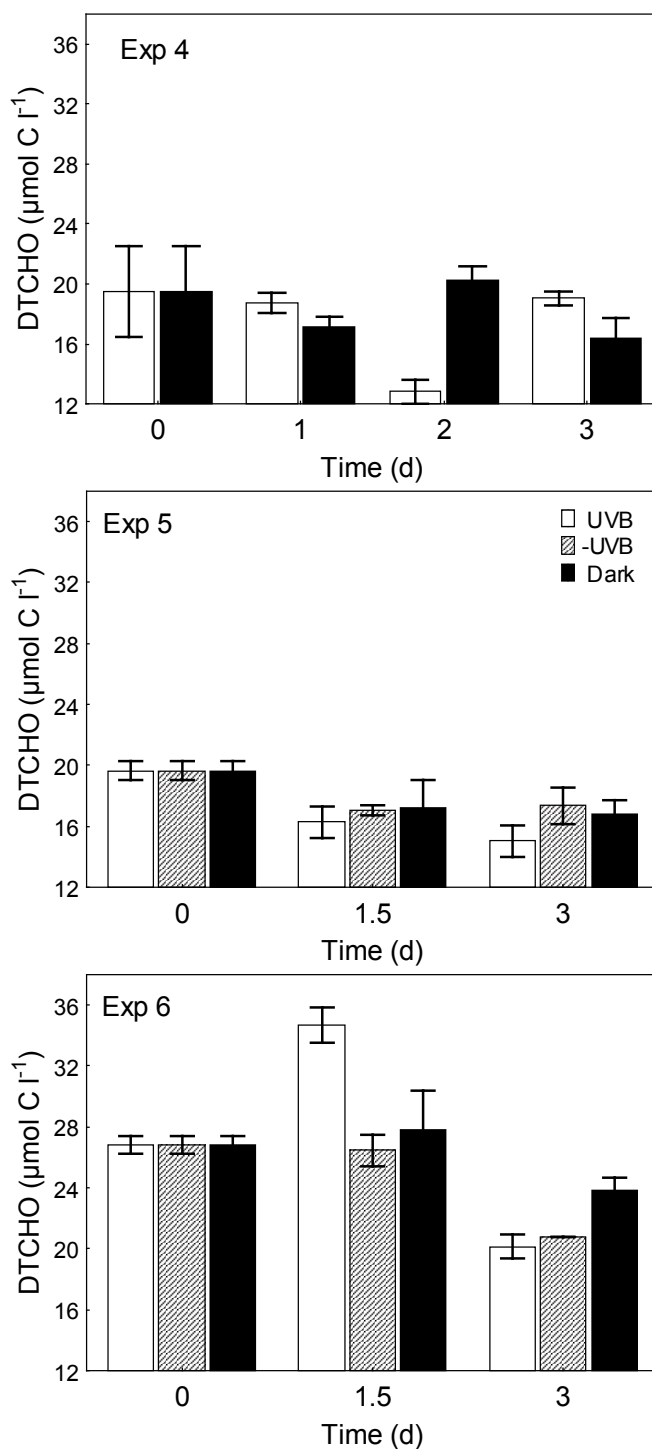


Figure 7.9. Changes in DTCHO concentrations in UVB (white bars), -UVB (striped bars) and dark (black bars) treatments of TEP photogeneration experiments (4 to 6). Whisker= Standard Error.

TEP PHOTOREACTIVITY IN THE PRESENCE OF MICROORGANISMS

In experiment 7, high increases in TEP and DTCHO (Fig 7.10) were observed, particularly in UVB and -UVB treatments. Increases in TEP were significantly higher in the UVB treatment, while increases in DTCHO were higher in the -UVB treatment (Table 7.6).

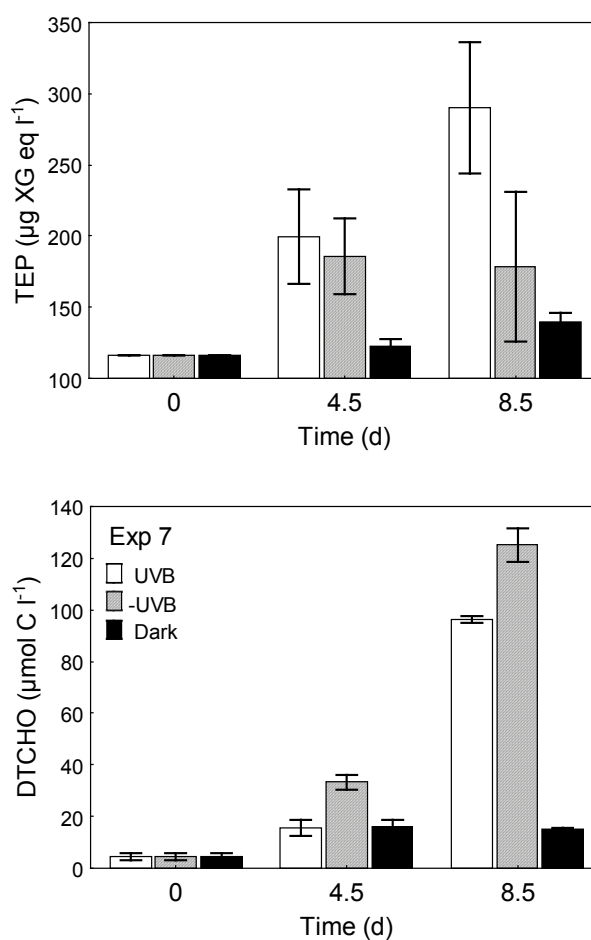


Figure 7.10. Changes in TEP (left panel) and DTCHO (right panel) concentrations in UVB (white bars), -UVB (striped bars) and dark (black bars) treatments of the TEP formation experiment with microorganisms (Exp 7). Whisker= Standard Error.

Table 7.6. Results of the repeated measures ANOVA for differences in TEP and DTCHO among treatments in experiment 7 (TEP photoreactivity with microorganisms). ns= not significant.

Variable	Effect	F	p level
TEP	Full solar spectrum (UVB vs. Dark)	42.9	< 0.01
	Full sol. sp.*Time	16.5	< 0.01
	UVB (UVB vs. -UVB)	6.5	ns
	UVB*Time	0.8	ns
	-UVB (-UVB vs. Dark)	17.3	< 0.05
	-UVB*Time	1.9	ns
DTCHO	Full solar spectrum (UVB vs. Dark)	71910	< 0.001
	Full sol. sp.*Time	160.2	< 0.001
	UVB (UVB vs. -UVB)	82.7	< 0.05
	UVB*Time	7.2	< 0.05
	-UVB (-UVB vs. Dark)	613.0	< 0.01
	-UVB*Time	124.4	< 0.01

DISCUSSION

In this chapter we report the first evidence of direct photolysis or photodispersion of TEP due to UVB light. The particular role of UVB radiation on TEP fragmentation or loss of integrity is consistent with the only published work on gel photodegradation (Orellana and Verdugo, 2003) likely due to a destabilization of polymer networks caused by a loss of net charge. In that study, full dispersion of self-assembled gels was detected in less than 12 hours when submitted to UVB radiation at 0.5 W m^{-2} , that is, 70% higher than those in our study (0.15 W m^{-2}). In our work, we have reported average TEP photolysis rates of $31\% \text{ d}^{-1}$, which would yield complete TEP dispersion or photolysis under UVB light in around 3 days. However, almost undetectable TEP at time 1 of experiments 1 and 2 indicate that TEP photolysis rates are at least 69-71% per day, that is, TEP would disperse completely in around 35 hours or less. Although UVB light appears to be dominant, UVA and PAR radiation likely caused some TEP photolysis, with

rates from 8 to 17% per day (Table 7.4). Thus, TEP photolysis could imply a significant pathway from TEP removal from the water column, compared to other losses such as TEP sedimentation, (Passow et al., 2001) or grazing (Tranvik et al., 1993; Passow and Alldredge, 1999). This process would become crucial as marine aggregates containing TEP, which have a lower density than water, can ascend through the water column (Azetsu-Scott and Passow, 2004) and accumulate in the sea surface microlayer (Wurl and Holmes, 2008), thus being exposed to intense solar radiation.

However, in contrast to expected increases in DTCHO coupled to decreases in TEP, which would be indicative of a photodispersion of TEP into their dissolved precursors, DTCHO generally decreased in the UVB treatments, indicating that they were not the final products of TEP photolysis. TEP photolysis products could be other dissolved organic compounds or, alternatively, dissolved inorganic carbon forms. Photoproduction of inorganic carbon after irradiation of organic matter has been previously reported (Mopper et al., 1991; Miller and Zepp, 1995), and it would imply, therefore, a net loss of organic carbon in the system. Polysaccharides can also be photodegraded into monosaccharides or photomineralized into inorganic forms after the cleavage of glycosidic linkages (Kovac et al., 2000).

Unlike the significant effect of UVB on TEP photolysis or photodispersion, no significant increases in TEP were observed in the photogeneration experiments. This lack of TEP formation, consistent with Thornton (2004), was not caused by the absence of a sufficient amount of precursors in the filtered water, as TEP were formed when submitted to shear inside the flocculator. Previous studies (Mopper et al., 1995; Zhou et al., 1998; Passow, 2000) have demonstrated that freshly released precursors aggregate to form larger colloids, and ultimately TEP, within hours to days, that is, a shorter incubation time than the used in our experiments. Hence, the precursor concentration or the incubation time were not likely the ultimate causes of the low TEP formation, and it is more likely that the physical environment (e.g. turbulence conditions) was not conducive to TEP formation.

In the experiment 7, increases in TEP were high under UVB radiation in the presence of organisms. Most likely production of TEP precursors was higher during growth of phytoplankton in treatments with light availability for photosynthesis. However, the increase in TEP was higher in UVB than in -UVB treatments,

compensating the potential losses of TEP by direct photolysis. The higher TEP production under UVB observed in our study could be a consequence of cell disintegration, as UVB often inhibits photosynthesis and causes cell damage (Cullen et al., 1992; Lesser, 1996; Agustí and Llabrés, 2007).

We conclude that, at similar ambient conditions and in absence of organisms, TEP photolysis by solar radiation, particularly UVB, would be dominant over TEP photogeneration. Hence, photolysis would act as a significant pathway for TEP removal in surface waters, added to other sinks such as sedimentation or biological degradation. TEP are an essential component for the functioning of the biological carbon pump, responsible for the export of carbon from the surface ocean which is in equilibrium with the atmosphere. Changes in TEP concentration due to global change have been hypothesized to result in enhanced carbon flux (negative feedback for the biological pump) (Riebesell and al., 2007) or decreased carbon flux after (positive feed back) (Mari, 2008) to depths. Both scenarios ignore possible consequences of changes in UV radiation for the TEP production. Consequence of global change is also an increase in UV radiation due to ozone depletion (Madronich, 1992). Based in our results, an increase in UVB radiation could lead to a decrease in TEP in the ocean surface, thus decreasing carbon flux into deep waters. However, the higher TEP release by organisms when submitted to UVB light could be compensating direct photolysis.

REFERENCES

- AGUSTÍ, S. and M. LLABRÉS (2007) Solar radiation-induced mortality of marine pico-phytoplankton in the oligotrophic ocean. *Photochemistry and Photobiology*. 83: 793-801.
- AKHLAQ, M.S., H.P. SCHUCHMANN and C. VONSONNTAG (1990) Degradation of the polysaccharide alginic acid - A comparison of the effects of UV-light and ozone. *Environmental Science & Technology*. 24: 379-383.
- ALLDREDGE, A.L., U. PASSOW and B.E. LOGAN (1993) The abundance and significance of a class of large, transparent organic particles in the ocean. *Deep-Sea Research Part I-Oceanographic Research Papers*. 40: 1131-1140.
- AZETSU-SCOTT, K. and U. PASSOW (2004) Ascending marine particles: Significance of transparent exopolymer particles (TEP) in the upper ocean. *Limnology and Oceanography*. 49: 741-748.
- CULLEN, J.J., P.J. NEALE and M.P. LESSER (1992) Biological weighting function for the inhibition of phytoplankton photosynthesis by ultraviolet-radiation. *Science*. 258: 646-650.
- DUUREN, F.A. (1968) Defined velocity gradient model flocculator *Journal of sanitary engineering division*. ASCE. 94: 671-682.
- ENGEL, A., S. THOMS, U. RIEBESELL, E. ROCHELLE-NEWALL and I. ZONDERVAN (2004) Polysaccharide aggregation as a potential sink of marine dissolved organic carbon. *Nature*. 428: 929-932.
- FREW, N.M. (1997) The role of organic films in air-sea gas exchange *In*: P. S. Liss and R. A. Duce (eds.) *The sea surface and global change*. Cambridge University Press, Cambridge. pp. 121-173.
- KIEBER, R.J., L.H. HYDRO and P.J. SEATON (1997) Photooxidation of triglycerides and fatty acids in seawater: Implication toward the formation of marine humic substances. *Limnology and Oceanography*. 42: 1454-1462.
- KIEBER, R.J., X.L. ZHOU and K. MOPPER (1990) Formation of carbonyl-compounds from UV-induced photodegradation of humic substances in natural waters - fate of riverine carbon in the sea. *Limnology and Oceanography*. 35: 1503-1515.
- KOVAC, N., O. BAJT and B. SKET (2000) Photocatalyzed degradation of water soluble polysaccharides. *Fresenius Environmental Bulletin*. 9: 217-224.

- LESSER, M.P. (1996) Elevated temperatures and ultraviolet radiation cause oxidative stress and inhibit photosynthesis in symbiotic dinoflagellates. *Limnology and Oceanography*. 41: 271-283.
- MADRONICH, S. (1992) Implications of recent total atmospheric ozone measurements for biologically-active ultraviolet-radiation reaching the Earth's surface. *Geophysical Research Letters*. 19: 37-40.
- MARI, X. (2008) Does ocean acidification induce an upward flux of marine aggregates? *Biogeosciences Discussions*. *Biogeosciences* 5: 1023-1031.
- MILLER, W.L. and R.G. ZEPP (1995) Photochemical production of dissolved inorganic carbon from terrestrial organic-matter - Significance to the oceanic organic-carbon cycle. *Geophysical Research Letters*. 22: 417-420.
- MOPPER, K., J. ZHOU, K.S. RAMANA, U. PASSOW, H.G. DAM and D.T. DRAPEAU (1995) The role of surface-active carbohydrates in the flocculation of a diatom bloom in a mesocosm. *Deep-Sea Research Part II-Topical studies in Oceanography*. 42: 47-73.
- MOPPER, K., X.L. ZHOU, R.J. KIEBER, D.J. KIEBER, R.J. SIKORSKI and R.D. JONES (1991) Photochemical degradation of dissolved organic-carbon and its impact on the oceanic carbon-cycle. *Nature*. 353: 60-62.
- ORELLANA, M.V. and P. VERDUGO (2003) Ultraviolet radiation blocks the organic carbon exchange between the dissolved phase and the gel phase in the ocean. *Limnology and Oceanography*. 48: 1618-1623.
- PASSOW, U. (2000) Formation of transparent exopolymer particles, TEP, from dissolved precursor material. *Marine Ecology-Progress Series*. 192: 1-11.
- PASSOW, U. (2002) Transparent exopolymer particles (TEP) in aquatic environments. *Progress in Oceanography*. 55: 287-333.
- PASSOW, U. and A.L. ALLDREDGE (1994) Distribution, size and bacterial-colonization of transparent exopolymer particles (TEP) in the ocean. *Marine Ecology-Progress Series*. 113: 185-198.
- PASSOW, U. and A.L. ALLDREDGE (1999) Do transparent exopolymer particles (TEP) inhibit grazing by the euphausiid *Euphausia pacifica*? *Journal of Plankton Research*. 21: 2203-2217.
- PASSOW, U., R.F. SHIPE, A. MURRAY, D.K. PAK, M.A. BRZEZINSKI and A.L. ALLDREDGE (2001) The origin of transparent exopolymer particles (TEP) and their role in the sedimentation of particulate matter. *Continental Shelf Research*. 21: 327-346.

- RECHE, I., M.L. PACE and J.J. COLE (1999) Relationship of trophic and chemical conditions to photobleaching of dissolved organic matter in lake ecosystems. *Biogeochemistry*. 44: 259-280.
- RIEBESSELL, U. et al. (2007) Enhanced biological carbon consumption in a high CO₂ ocean. *Nature*. 450: 545-548.
- THORNTON, D.C.O. (2004) Formation of transparent exopolymeric particles (TEP) from macroalgal detritus. *Marine Ecology-Progress Series*. 282: 1-12.
- TRANVIK, L.J., E.B. SHERR and B.F. SHERR (1993) Uptake and utilization of colloidal DOM by heterotrophic flagellates in seawater. *Marine Ecology-Progress Series*. 92: 301-309.
- VERDUGO, P. (2004) The role of marine gel-phase on carbon cycling in the ocean. *Marine Chemistry*. 92: 65-66.
- VERDUGO, P., A.L. ALLDREDGE, F. AZAM, D.L. KIRCHMAN, U. PASSOW and P.H. SANTSCHI (2004) The oceanic gel phase: a bridge in the DOM-POM continuum. *Marine Chemistry*. 92: 67-85.
- WURL, O. and M. HOLMES (2008) The gelatinous nature of the sea-surface microlayer. *Marine Chemistry*. 110: 89-97.
- ZHOU, J., K. MOPPER and U. PASSOW (1998) The role of surface-active carbohydrates in the formation of transparent exopolymer particles (TEP) by bubble adsorption of seawater. *Limnology and Oceanography*. 43: 1860-1871.

GENERAL SUMMARY

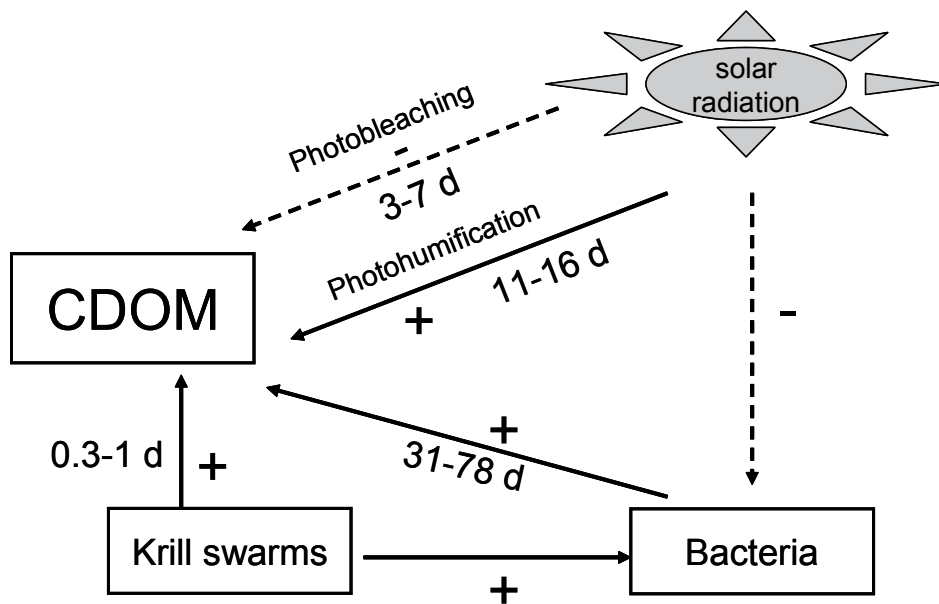
The description of the distribution and dynamics of chromophoric dissolved organic matter in the broadest ocean areas as possible will allow the scientific community to have a better picture of how ocean optics works. Ocean optics has practical applications on the development of analytical models and algorithms for satellite ocean color interpretation (Bricaud et al., 2002) and on the advance in knowledge of how light propagates within the ocean. Light attenuation in the water column has an influence on the rate of carbon fixation by phytoplankton, on the activity of autotrophic and heterotrophic organisms (Herndl et al., 1993; Zepp et al., 1998), and ultimately on carbon export from the upper to deeper ocean (Bricaud et al., 2002). In the first four chapters of this thesis, we described the geographical and vertical distribution of CDOM in contrasting marine ecosystems, and explored field relationships with other biogeochemical variables. In addition, we applied short-term experiments to quantify the effects of significant sources and sinks on CDOM dynamics. The processes measured were CDOM phototransformations (photobleaching and photohumification) and biological CDOM generation by bacteria and krill. Finally, we assessed the validity of the GSM algorithm to successfully retrieve chromophoric dissolved and detrital organic matter (CDM) from satellite observations in the Antarctic Peninsula.

We have pointed out from field observations that, despite the lower dissolved organic carbon (DOC) concentration found in the Southern Ocean, chromophoric dissolved organic matter (CDOM) in this area is around 3-fold higher (mean

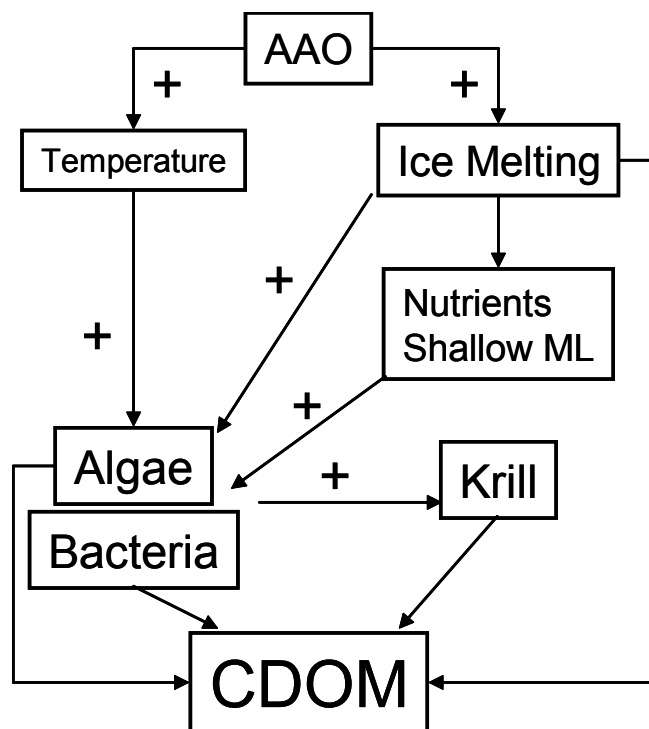
$a_{325} = 0.36 \text{ m}^{-1}$) than in the Mediterranean Sea (mean $a_{325} = 0.11 \text{ m}^{-1}$) which yielded molar absorption coefficients to be much higher (mean $\epsilon_{325} = 6.12$ and $1.69 \text{ m}^2 \text{ mol}^{-1}$ respectively). Moreover, the uncoupling between DOC and CDOM in all study areas suggested that CDOM would be submitted to specific sources and sinks. The experimental results showed in chapter 2 suggested photobleaching as a significant sink of CDOM in the Southern Ocean, with half lives from 3 to 7 days when submitted to natural incident radiation during the austral summer, in contrast to non-significant photobleaching or photohumification in the Mediterranean Sea. If only this sink was considered, lower CDOM in the Southern Ocean than in the Mediterranean Sea would be expectable. In addition, we highlighted the significant but complex role of bacteria affecting CDOM dynamics in the Southern Ocean. The negative short-term impact of CDOM photoproducts on bacterial growth (chapter 2) can be compensated by a relatively higher CDOM generation by these organisms as pointed out in chapter 3. The direct CDOM generation by bacteria was evident and led to field CDOM duplication times within months in both the Southern Ocean and Mediterranean Sea (Scheme 1). The experimental results showed in chapter 3 reveal that bacterial CDOM rates were similar in both ecosystems and dependent on bacterial activity.

Based on these experimental results and remote sensing observations, higher CDOM in the Southern Ocean can be due to higher productivity in the Antarctic Peninsula during austral summer, as chlorophyll *a* and bacterial production were around 2 to 9 fold higher than in the Mediterranean Sea. In addition, CDOM generation by krill, that frequently form large swarms in the Antarctic Peninsula area, could also be compensating photobleaching losses in the Southern Ocean as they can duplicate field CDOM in less than a day (Scheme 1).

From field observations we detected a decoupling between CDOM and chlorophyll *a*. However, when we looked at CDOM dynamics in the Southern Ocean at a longer timescale and over the whole area in contrast to single field stations, we observed that both variables coincide geographically and also covary over time. This results suggest that CDOM is ultimately and likely indirectly produced by algae, and that these variables in the area are subject to the same driving forces, such as the seasonal advance and retreat of ice, and the interannual variability in the Antarctic Oscillation Index (Scheme 2).



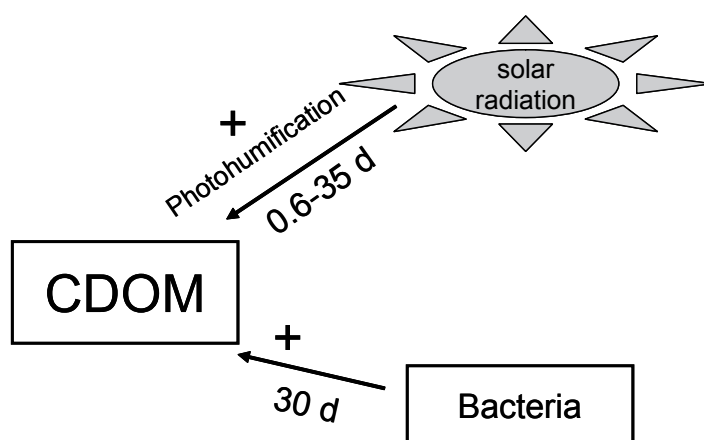
Scheme 1. Sources and sinks of CDOM in the Southern Ocean inferred from experimental results. Continuous arrows= Positive effect. Dashed arrows= Negative effect.



Scheme 2. Principal processes affecting CDOM dynamics around the Antarctic Peninsula.

On the contrary, the oligotrophic status of the Mediterranean Sea results in low CDOM. Although the experiments suggested low CDOM photoreactivity in the Mediterranean Sea (Scheme 3), this ecosystem is submitted to intense solar radiation throughout the whole year, which would be a primary sink of CDOM through photobleaching. This over-year continuous photobleaching would preclude an easy experimental quantification of photobleaching rates. The lower CDOM values in this area than in the Southern Ocean contrast with higher DOC and transparent exopolymer particles (TEP) concentration. This suggests that dissolved organic matter (DOM) in the Southern Ocean is enriched in chromophoric compounds whereas DOM in the Mediterranean Sea is enriched in other compounds, less chromophoric, such as TEP and their precursors.

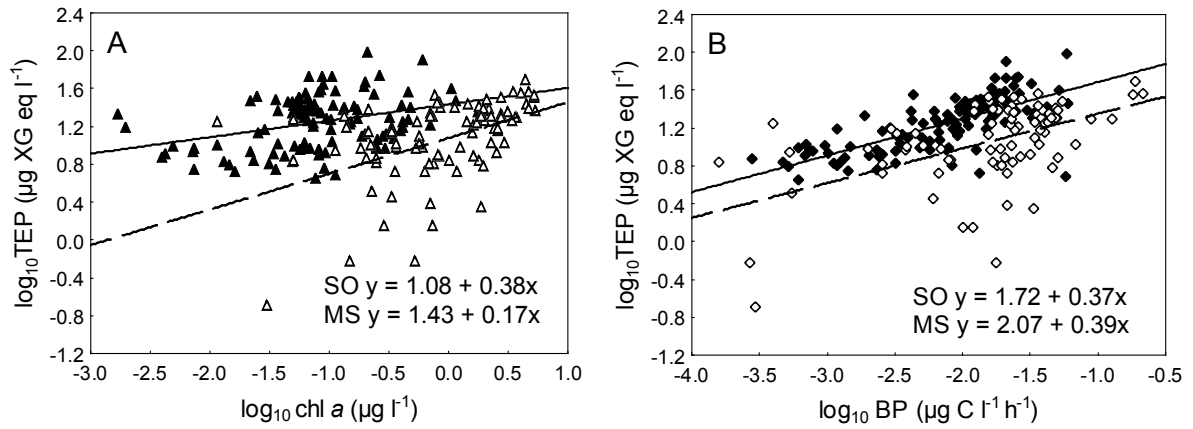
During the second part of this thesis (chapters 5, 6 and 7) we studied the distribution and dynamics of transparent exopolymer particles (TEP) and dissolved carbohydrates (DMCHO and DPCHO) in our study ecosystems, exploring their contribution to dissolved and particulate organic carbon pools, and assessing the role of bacteria and solar radiation (particularly UVB radiation) affecting TEP dynamics. The consideration of organic matter as a continuum from dissolved to particulate phases (Verdugo et al., 2004) is of interest in order to have a more complete view of marine organic matter dynamics. Self-assembling of precursors represents an alternative way to convert dissolved into particulate organic matter in contrast to the microbial loop (Chin et al., 1998; Kerner et al., 2003). In addition, there are important ecological implications as vertical settlement of marine aggregates or ascending and descending movements of gel particles.



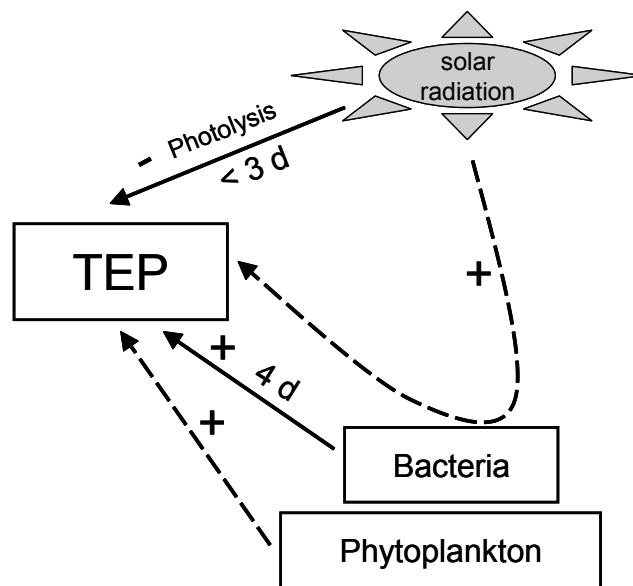
Scheme 3. Sources and sinks of CDOM in the Mediterranean Sea inferred from experimental results.

The low TEP concentrations reported in our study systems in comparison to the previously published studies are in agreement with the general pattern of high TEP concentrations in productive areas. Indeed, TEP have been frequently measured during blooms or in productive coastal sites. In particular, the lower TEP concentration and TEP/chl *a* ratio in the Southern Ocean than in the Mediterranean Sea contrast with its higher productivity. In contrast to TEP concentration, DMCHO and DPCHO concentrations were significantly higher in the Southern Ocean, and a fraction of these dissolved carbohydrates could be attributed to the breakdown of TEP. Indeed, TEP in the Mediterranean Sea tends to accumulate during late spring and summer due to a strong thermal stratification and low water turbulence (Beauvais et al., 2003), while in the Southern Ocean deeper mixed layers, higher turbulence caused by westerly winds, or high UVB radiation during austral summer, could yield to higher TEP degradation. The higher TEP/chl *a* in the Mediterranean Sea than in the Southern Ocean could be explained, added to the more stability of these particles, by higher release of TEP by organisms, likely due to the depletion in inorganic nutrients in this area. This would contrast with the steeper slope of the TEP- chl *a* relationship in the Southern Ocean, that suggests a higher dependence of these particles on phytoplankton (Scheme 4) or a more immediacy of algal TEP production. On the contrary, a lag-time between chl *a* and TEP concentrations in the Mediterranean Sea would impede a tight relationship after simultaneous field observations.

Despite the different link between TEP and chl *a* observed in the study areas, our results suggest consistency in the link between bacteria and TEP. For instance, in waters far from algal influence (below the mixed layer in the Southern Ocean, below the euphotic layer in the Mediterranean Sea), TEP/BA ratios were similar in both areas. In addition, the positive relationships found between TEP and bacterial production in both study areas, showed similar slopes (Scheme 4). This consistency would imply that the relationship between TEP and bacteria is relatively independent on the trophic status of the system. The experimental results showed in chapter 6 support this assertion and propose bacteria as significant sources of TEP in the field. The similar slope in the relationship between the increases in bacterial production and increases in TEP when compared to field measurements of BP and TEP suggests that the active release of TEP by bacteria can be a significant pathway explaining TEP dynamics, accounting for duplication times of 4 days (Scheme 5).



Scheme 4. Scatterplots between (A) chlorophyll a and (B) bacterial production and TEP (log-log scales) in the Southern Ocean (open symbols) and Mediterranean Sea (filled symbols).



Scheme 5. Sources and sinks of TEP in marine ecosystems. Continuous arrows represent processes that have been quantified in the present thesis. Dashed arrows represent processes observed but not quantified.

Alternatively, we have evidenced for the first time the role of UVB radiation as a significant sink for TEPs, with removal times of less than 3 days when exposed to solar radiation. In terms of UV incidence, a UVB daily dose of less than 9000 J m^{-2} would be sufficient for a complete TEP photolysis. These UVB doses are often achieved at the ocean surface during the spring and summer. This process can become of great importance due to the increasing UVB incidence over the Earth's surface (Madronich, 1992) and the role of superficial TEPs on gas exchange between superficial ocean and atmosphere (Riebesell et al., 2007). In this work, we have pointed out the interaction between UVB radiation and microbial activity on TEP generation, which deserves a more detailed addressing and quantification.

FUTURE DIRECTIONS

The study of ocean organic matter has received a great interest among the scientific community, mostly regarding its significance for the global carbon cycle. However, continuous advances in knowledge on the composition, sources, sinks and reactivity of ocean organic matter suggests that there is still much to be learnt.

Needs for future investigation on CDOM comprise, among others, its chemical composition, origin and fate of CDOM in the deep ocean, and biological and optical properties of different classes of CDOM. The novel fluorescence techniques such as excitation-emission matrixes will allow us to more accurately describe CDOM composition and history (Biers et al., 2007; Coble, 2007). In addition, the inclusion of CDOM to develop or improve bio-optical algorithms will lead to high-quality satellite estimations of biogeochemical variables (Bricaud et al., 2002).

Regarding the continuum dissolved-particulate phases, a shift into thinking of organic matter as dynamic compounds whose structure and properties are affected by physical forces (Verdugo et al., 2004) is also of interest. The study of marine organic matter in the context of polymer gel theory is still on its beginning, and its relationship with the biota and fate within the organic matter cycling should be explored.

Although we have studied CDOM and TEP as separate organic matter pools, part of the chromophoric organic matter is also formed by gels. However, a link

between both pools has only been scantily explored (Orellana et al., 2007). The knowledge of optical properties of TEP or structural changes of chromophoric compounds would provide us a broader vision of their dynamics. Finally, we cannot ignore the impact of global change (i.e. UV increase, ocean acidification, temperature increase) on all these processes.

REFERENCES

- BEAUVAIS, S., M.L. PEDROTTI, E. VILLA and R. LEMÉE (2003) Transparent exopolymer particle (TEP) dynamics in relation to trophic and hydrological conditions in the NW Mediterranean Sea. *Mar Ecol Prog Ser.* 262: 97-109.
- BIERS, E.J., R.G. ZEPP and M.A. MORAN (2007) The role of nitrogen in chromophoric and fluorescent dissolved organic matter formation. *Marine Chemistry.* 103: 46-60.
- BRICAUD, A., C.S. ROESLER, J.S. PARSLow and J. ISHIZAKA (2002) Bio-optical studies during the JGOFS-equatorial Pacific program: a contribution to the knowledge of the equatorial system. *Deep Sea Research Part II: Topical Studies in Oceanography.* 49: 2583-2599.
- CHIN, W.C., M.V. ORELLANA and P. VERDUGO (1998) Spontaneous assembly of marine dissolved organic matter into polymer gels. *Nature.* 391: 568-572.
- COBLE, P.G. (2007) Marine optical biogeochemistry: The chemistry of ocean color. *Chemical Reviews.* 107: 402-418.
- HERNDL, G.J., G. MULLERNIKLAS and J. FRICK (1993) Major role of ultraviolet-B in controlling bacterioplankton growth in the surface layer of the ocean. *Nature.* 361: 717-719.
- KERNER, M., H. HOHENBERG, S. ERTL, M. RECKERMANN and A. SPITZY (2003) Self-organization of dissolved organic matter to micelle-like microparticles in river water. *Nature.* 422: 150-154.
- MADRONICH, S. (1992) Implications of recent total atmospheric ozone measurements for biologically active ultraviolet radiation reaching the Earth's surface. *Geophysical Research Letters.* 19: 37-40.
- ORELLANA, M.V., T.W. PETERSEN, A.H. DIERCKS, S. DONOHOE, P. VERDUGO and G. VAN DEN ENGH (2007) Marine microgels: Optical and proteomic fingerprints. *Marine Chemistry.* 105: 229-239.
- RIEBESELL, U., K.G. SCHULZ, R.G.J. BELLERBY, M. BOTROS, P. FRITSCH, M. MEYERHOFER, C. NEILL, G. NONDAL, A. OSCHLIES, J. WOHLERS and E. ZOLLNER (2007) Enhanced biological carbon consumption in a high CO₂ ocean. *Nature.* 450: 545-548.
- VERDUGO, P., A.L. ALLDREDGE, F. AZAM, D.L. KIRCHMAN, U. PASSOW and P.H. SANTSCHI (2004) The oceanic gel phase: a bridge in the DOM-POM continuum. *Marine Chemistry.* 92: 67-85.

■ General Summary

ZEPP, R.G., T.V. CALLAGHAN and D.J. ERICKSON (1998) Effects of enhanced solar ultraviolet radiation on biogeochemical cycles. *Journal of Photochemistry and Photobiology B-Biology*. 46: 69-82.

CONCLUSIONS

1. The Antarctic Peninsula area of the Southern Ocean was generally enriched in CDOM, particularly in areas influenced by ice such as the Weddell Sea. In the Mediterranean Sea, CDOM values were comparatively lower. In the vertical profile, CDOM showed lower values in the upper mixed layer than below it both in the Bellingshausen and Mediterranean Seas.
2. Geographical and vertical patterns of field CDOM in the Southern Ocean and Mediterranean Sea diverged from patterns of chlorophyll a and DOC, underlining the complex and reactive nature of this pool of organic matter at this scale.
3. The net effect of solar radiation on CDOM appears to be dependent on the initial field CDOM. High field CDOM led to CDOM half lives by photobleaching that ranged from 2.3 to 10.2 days, whereas low field CDOM led to duplication times by photohumification that ranged from 1.8 to 35 days. Therefore, CDOM photoreactivity is a process that modifies CDOM in terms of days.
4. Bacterioplankton act as a direct source of CDOM in marine ecosystems, leading to CDOM duplication times from 30 to 78 days. The amount of CDOM generated by bacteria was a function of their activity and its optical quality was related to previous CDOM photoalterations.

5. Antarctic krill, *Euphasia superba*, can directly generate significant amounts of CDOM, leading to CDOM duplication times of less than one day within a krill swarm.
6. The semi-analytic algorithm GSM01 (Garver-Siegel-Maritorena) can retrieve successfully CDM data from satellite measurements of ocean color in the Antarctic Peninsula area.
7. Long-term dynamics and vast distributions of CDM around the Antarctic Peninsula retrieved using remote sensing were closely related to those of chlorophyll *a*. This relationship could be explained by a stimulus of phytoplankton associated to ice melting and, consequently, an indirect fueling of bacterial and krill CDOM generation.
8. The Southern Ocean contained low concentration of TEP and relatively high of dissolved carbohydrates. These variables were not related in the field, pointing out the complexity of TEP formation and degradation processes. TEP was related to chlorophyll *a* in the upper mixed layer and to bacterial production below the mixed layer.
9. Bacterioplankton can directly generate TEP from dissolved organic matter in the Mediterranean Sea. This biogeneration can yield duplication times of four days, and it was the best predictor of TEP dynamics in this marine ecosystem.
10. UVB radiation can cause direct photolysis of TEP resulting in a complete dispersion in less than three days. TEP generation by microorganisms can be enhanced by UVB exposure.

CONCLUSIONES

1. La península antártica mostró en general un enriquecimiento en CDOM, particularmente en áreas influenciadas por el hielo como el oeste del mar de Weddell. Los valores de CDOM fueron comparativamente menores en el mar Mediterráneo. A lo largo de los perfiles verticales, los valores de CDOM fueron menores sobre la capa de mezcla que bajo ésta en los mares de Bellingshausen y Mediterráneo.
2. Los patrones geográficos y verticales de CDOM fueron diferentes de los de clorofila *a* y carbono orgánico disuelto. Este desacople subraya la naturaleza compleja y reactiva de la CDOM a esta escala.
3. El efecto neto de la radiación solar sobre la CDOM depende de los valores de CDOM preexistentes. Unos valores de CDOM inicialmente altos en campo tuvieron una vida media que osciló entre los 2.3 y los 10.2 días debido a la fotodegradación, mientras que valores inicialmente bajos de CDOM sufrieron tiempos de duplicación entre 1.8 y 35 días por fotohumificación. En consecuencia, la fotoreactividad es un proceso que modifica la CDOM en escala de días.
4. El bacterioplancton actúa como una fuente directa de CDOM en ecosistemas marinos, induciendo tiempos de duplicación de la CDOM entre 30 y 78 días. Las bacterias generaron CDOM en función de su actividad,

- y la calidad óptica de la CDOM estuvo relacionada con fotoalteraciones previas.
5. El krill antártico, *Euphasia superba*, puede generar directamente cantidades significativas de CDOM, induciendo tiempos de duplicación de menos de un día dentro de un enjambre de krill.
 6. El algoritmo semianalítico GSM01 (Garver-Siegel-Maritorena) puede obtener datos fiables de CDM a partir de observaciones de satélite del color del océano en el área de la península antártica.
 7. Las dinámicas y distribuciones de CDM a gran escala alrededor de la península antártica obtenidas mediante teledetección estuvieron estrechamente relacionadas con las de clorofila *a*. Esta relación puede explicarse por un estímulo del fitoplancton asociado a la fusión de hielo y, por consiguiente, un inducción indirecta de la generación de CDOM por las bacterias y el krill.
 8. El océano Sur mostró concentraciones bajas de TEP y relativamente altas de carbohidratos disueltos. Estas variables no estuvieron relacionadas en el campo, lo que resalta la complejidad de los procesos de formación y degradación de las TEP. Las TEP estuvieron relacionadas con la clorofila *a* sobre la capa de mezcla y con la producción bacteriana bajo ésta.
 9. Las bacterias pueden generar TEP directamente a partir de material orgánica disuelta en el mar Mediterráneo. Esta biogeneración bacteriana, que puede promover tiempos de duplicación de cuatro días, fue el principal factor controlador de las dinámicas de las TEP en este ecosistema marino.
 10. La radiación UVB puede causar la fotólisis directa de las TEP, provocando una dispersión completa en menos de tres días. La generación de TEP por microorganismos puede verse estimulada por la exposición a la radiación UVB.

LIST OF ABBREVIATIONS

- a_{λ} : Absorption coefficient (m^{-1})
- a_{ph} : Pigment absorption (m^{-1})
- BA: Bacterial abundance
- Bdl: Below detection limit
- BP: Bacterial Production
- CDM: Chromophoric dissolved and detrital matter
- CDOM: Chromophoric dissolved organic matter
- Chl *a*: Chlorophyll *a*
- DCM: Deep chlorophyll maximum
- DMCHO: Dissolved monosaccharides
- DOC: Dissolved organic carbon
- DPCHO: Dissolved polysaccharides
- DTCHO: Dissolved carbohydrates
- ϵ_{λ} : Molar absorption coefficient ($m^2 mol^{-1}$)
- MLD: Mixed Layer Depth
- SA: Sodium Azide
- S_{uv} : Spectral slope of CDOM (290-400nm)
- TEP: Transparent Exopolymer Particles

Exploring the relationship between active bacterioplankton and phytoplankton in the Southern Ocean

E. Ortega-Retuerta^{1,*}, I. Reche^{1,2}, E. Pulido-Villena³, S. Agustí⁴, C. M. Duarte⁴

¹Departamento de Ecología, Facultad de Ciencias, Universidad de Granada, 18071 Granada, Spain

²Instituto del Agua, Universidad de Granada, 18071 Granada, Spain

³Laboratoire d'Océanographie de Villefranche, Villefranche-sur-Mer, France

⁴Institut Mediterrani d'Estudis Avançats (IMEDEA) (CSIC-UIB), Miquel Marqués 21, 07190 Esporles, Illes Balears, Spain

ABSTRACT: Bacterioplankton are a heterogeneous community composed of cells with different physiological states. The consideration of the active fraction of bacterioplankton as a potential factor affecting the strength of the relationship between bacteria and phytoplankton in the Southern Ocean was evaluated in waters around the Antarctic Peninsula. We estimated active bacterioplankton from uptake of ³H-Leucine (bacterial production [BP]) and using vital stains to estimate their proportion within the total bacterioplankton community, based on their relative nucleic acid content (high [HNA] vs. low [LNA]), and by nucleic acid double staining (NADS), based on their membrane permeability. Then we performed a comparative analysis between total and active bacterioplankton and chlorophyll *a* (chl *a*) in this area. Staining with NADS suggested that 61 % of all bacteria were viable, a higher proportion of the total bacterial community than previously reported for the Southern Ocean. HNA bacteria comprised 45 % of all bacteria, indicating that 16 % of bacteria may be viable but with LNA. BP was more strongly related to abundance of LNA cells than NADS-viable or HNA bacteria. The relationship between chl *a* and bacterial abundance (BA) did not increase when considering the abundance of HNA or NADS-viable cells alone, showing that viability/activity of stains did not enhance the linkage between BA and phytoplankton biomass in the Southern Ocean. In contrast, the relationship between chl *a* and BP was stronger than those reported in the literature, suggesting that, in this region, BP is closely dependent on phytoplankton.

KEY WORDS: Active bacteria · NADS · HNA · LNA · Bacterial production · Chlorophyll *a* · Southern Ocean

Resale or republication not permitted without written consent of the publisher

INTRODUCTION

Aquatic bacterioplankton is strongly dependent on organic matter derived from phytoplankton (Cole et al. 1982). This dependence leads to the existence of a general relationship between phytoplankton biomass (as chlorophyll *a*) and bacterial biomass or between primary and bacterial production across broad-spectrum aquatic ecosystems (Cole et al. 1988, Gasol & Duarte 2000).

In Southern Ocean waters, the absence of significant land inputs render bacteria strongly dependent on organic carbon released by algae (Morán et al. 2002). However, instead of an expectedly tight relationship

between bacteria and phytoplankton (i.e. with a steeper slope than previously reported), different field and experimental studies have reported a weaker relationship between bacterioplankton (either abundance or biomass) and chlorophyll *a* (chl *a*) or primary production in this region (Bird & Karl 1999, Duarte et al. 2005). This weaker relationship may be due to several non-exclusive explanations, such as losses due to predation by protists (Vaqué et al. 2002, Duarte et al. 2005), viral lysis infection (Guixa-Boixereu et al. 2002), or low temperatures which preclude an optimal assimilation of organic substrates (Pomeroy & Wiebe 2001). In addition, the use of total bacteria presupposes that they are uniformly active and, thus, large numbers of

*Email: evaor@ugr.es

inactive bacteria could mask the correlation between active bacteria and the substrate that supports them. Indeed, previous studies (Davidson et al. 2004, Pearce et al. 2007) have shown low fractions of active bacteria in the Southern Ocean. Hence, the unique consideration of the active fraction of the bacterial community could lead to a tighter relationship (i.e. higher slope) between bacterial abundance and chl *a*.

The estimates of the active fraction of the bacterial community are strongly dependent on the techniques used (Smith & del Giorgio 2003). Single-cell methods such as microautoradiography or fluorescent *in situ* hybridization are considered very sensitive for enumerating metabolically active bacteria (Hoppe 1976, Karner & Fuhrman 1997). On the other hand, flow cytometry, with nucleic acid stains such as SYTO 13, has been extensively used due to its simplicity and speed, which allows processing of a large number of samples. This technique has revealed the existence of bacterial subpopulations that differ considerably in the degree of staining and, therefore, in the nucleic acid content per cell, allowing classification of cells with relatively high (HNA) and low (LNA) nucleic acid content. The discrimination between HNA and LNA cells has been attributed to different phylogenetic compositions (Zubkov et al. 2001) or used as a proxy for active and non-active components of the bacterial community (Gasol et al. 1999). However, this simple, dichotomous classification has recently come into question (Sherr et al. 2006, Bouvier et al. 2007, Morán et al. 2007). Another easy and helpful technique is nucleic acid double staining (NADS), which is based on simultaneous staining with SYBR Green (staining all cells) and Propidium Iodide (PI, staining only membrane-damaged cells) (Barbesti et al. 2000) that allows discrimination of live (PI-impermeable) vs. dead (PI-positive)

cells in natural assemblages (Grégori et al. 2001, Falconi et al. 2008). Although some authors (Pirker et al. 2005) have found that PI-positive cells can also uptake organic substrates, the proportion of viable (PI-impermeable) cells could be considered an acceptable cut-off in the continuum from inactive to active cells.

In the present study, we determined the magnitude of the active fraction of bacterioplankton in the Southern Ocean using independent techniques in parallel, and we assessed its significance in affecting the relationship between bacteria and chl *a* in waters around the Antarctic Peninsula.

MATERIALS AND METHODS

Study area and sampling. Sampling was carried out during January and February 2004 and 2005 in the 2 ICEPOS oceanographic cruises along the Antarctic Peninsula and Bransfield Strait (Fig. 1). The first cruise (ICEPOS 2004) took place from 14 January to 9 February 2004 aboard RV 'Las Palmas' and 12 stations were selected with 4 to 5 depths each, from surface waters to 150 m. These stations covered 3 transects: from Livingstone Island to (1) Deception Island, (2) Anvers Island, and (3) King George Island (Fig. 1). The second cruise (ICEPOS 2005) took place aboard RV 'Hespérides' from 26 January to 26 February 2005. We selected 18 stations along the eastern Bellingshausen Sea, the Bransfield and Gerlache Straits and the western Weddell Sea (Fig. 1). At each station, 5 to 6 depths were sampled, from surface waters to mid-depth waters, generally 150 to 200 m, below the deep chlorophyll maximum (DCM) located between 15 and 35 m. Water was collected using a Niskin bottle with external spring (Ocean Test, 12 l) during ICEPOS 2004 and a Sea-Bird rosette sampler

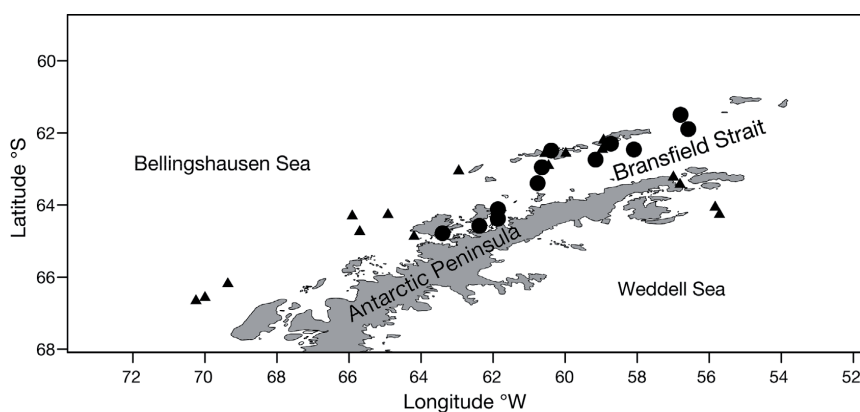


Fig. 1. Stations sampled during ICEPOS 2004 (●) and 2005 (▲) cruises

(24 Niskin bottles, 12 l each) attached to a conductivity/temperature/depth (CTD) system during ICEPOS 2005.

Total, HNA and LNA bacterial abundance. Total bacterial abundance (BA) samples were determined by epifluorescence microscopy (Porter & Feig 1980) during the ICEPOS 2004 cruise. Water subsamples of 4 to 10 ml were filtered through 0.2 μm polycarbonate black filters and stained with DAPI (4,6-diamidino-2 phenylindole) to a final concentration of 1 $\mu\text{g ml}^{-1}$. At least 350 cells in 15 random fields were counted per filter. During ICEPOS 2005, BA was determined by flow cytometry. Subsamples (4 ml) were fixed with 1% paraformaldehyde, allowed 30 min to fix in the dark, deep frozen in liquid nitrogen and then stored frozen at -70°C (Troussellier et al. 1995). Analyses were conducted within a maximum of 2 d from sample collection. The samples were thawed, a 400 μl sample was stained with 4 μl of 5 $\mu\text{mol l}^{-1}$ SYTO13 (Molecular Probes) for 10 min in the dark, and run through a FAC-ScaliburTM flow cytometer (BD Biosciences) fitted with a laser emitting at 488 nm. Samples were run at a low flow rate and data were acquired in log mode until around 10 000 events were acquired. A stock solution (5 μl) of yellow-green 0.92 μm Polysciences latex beads was added as an internal standard per 400 μl of sample. The concentration of the fluorescent beads was calibrated twice during the cruise with TruCounts (Becton Dickinson). Bacteria were detected by their signature in bivariate plots of Side scatter (SSC) vs. FL1 (green fluorescence) and those with HNA or LNA discriminated by their green fluorescence. Data were gated and counted in the SSC vs. FL1 plot using the Paint-a-Gate software (del Giorgio et al. 1996a, Gasol & del Giorgio 2000). HNA and LNA abundances were expressed in cells ml^{-1} . HNA was also expressed as the percentage of the total bacteria counts (% HNA).

Viable bacterial abundance. The Nucleic Acid Double Staining (NADS) flow cytometric protocol was used to quantify cell viability during ICEPOS 2005. This technique is based on the simultaneous use of 2 nucleic acid fluorescent dyes, SYBR Green I and Propidium Iodide (PI). Cell membranes are permeable to SYBR Green I irrespectively of cell viability. However, intact plasmic membranes characteristic of viable cells are impermeable to PI, thus staining with PI indicates compromised, damaged cells (Barbesti et al. 2000). Subsamples were analyzed immediately after collection. Samples (400 μl) were simultaneously stained with 4 μl of SYBR Green I (10-fold dilution of 10 000 \times commercial solution [Molecular Probes] in dimethyl sulfoxide) and 4 μl of Propidium iodide (PI, 1 mg ml^{-1} stock solution [Sigma]), reaching a final concentration of 10 $\mu\text{g ml}^{-1}$, and allowed to stain for 15 min in the dark. This final concentration is similar to the PI concentrations

used and recommended as optimum in previous works (Falcioni et al. 2008). Samples were analyzed by flow cytometry. Bivariate plots of FL1 vs. FL2 (green vs. orange fluorescence, respectively) were obtained by flow cytometry to discriminate PI-impermeable bacteria (green fluorescent, hereafter referred to as viable cells) and PI-permeable bacteria (orange fluorescent) that appeared to have compromised cell membranes. Data were processed with Paint-a-Gate software. We expressed total viable cells in cells ml^{-1} and as a percentage of total BA counts determined with the protocol detailed above.

Bacterial production. Bacterial production (BP) was estimated during ICEPOS 2005 from ^3H -Leucine-protein synthesis following the microcentrifugation technique proposed by Smith & Azam (1992). Briefly, 5 μl of L-[4,5- ^3H] leucine was added to 1.5 ml samples, yielding a final concentration of 52.7 nM, likely to be saturating in this region (Pedrós-Alió et al. 2002), and was incubated for 2 to 5 h. We used a conversion factor from leucine to carbon incorporation of 1.5 kg C mol leu $^{-1}$, which represents a standard, assuming no isotope dilution (Simon & Azam 1989).

Chlorophyll a. Chl *a* concentration was determined fluorometrically by filtering 50 ml subsamples through 25 mm Whatman GF/F filters, extracted into 10 ml of 90% acetone for ca. 24 h in the dark and at 4°C . The fluorescence of the extracts was read in a previously calibrated Turner Design fluorometer (Parsons et al. 1984).

RESULTS

Total BA showed an average value of $5.9 \pm 0.9 \times 10^5$ cells ml^{-1} during ICEPOS 2004 and $7.2 \pm 0.5 \times 10^5$ cells ml^{-1} during ICEPOS 2005. During ICEPOS 2004, total BA ranged from 1.7 to 8.94×10^5 cells ml^{-1} in surface waters and from 1.03 to 3.79×10^5 cells ml^{-1} in waters at 150 m. During ICEPOS 2005, BA ranged from 2.0 to 16.3×10^5 cells ml^{-1} in surface waters and from 0.7 to 15.4×10^5 cells ml^{-1} in waters below the DCM. In ICEPOS 2004, total BA generally decreased with depth (9 of 12 stations) and the highest values were observed inside Port Foster in Deception Island. In 2005, total BA generally decreased with depth (10 stations, Fig. 2a), except in some particular stations where the vertical BA distribution was quite homogeneous (Fig. 2b). The highest total BA values were observed in the stations located in the Weddell Sea (Fig. 2c).

The abundance of HNA cells ranged one order of magnitude. The mean value was $3.0 \pm 0.2 \times 10^5$ cells ml^{-1} , from 0.9 to 9.4×10^5 cells ml^{-1} in surface waters and from 0.52 to 5.71×10^5 cells ml^{-1} in waters below the DCM, showing a similar decreasing pattern with

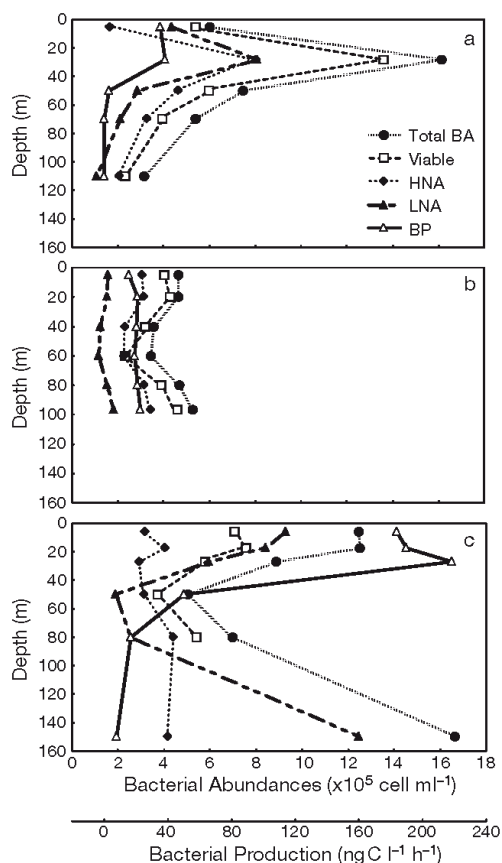


Fig. 2. Vertical profiles of total bacterial abundance (BA), viable cell abundance (Viable), high nucleic acid cell abundance (HNA), low nucleic acid cell abundance (LNA) and bacterial production (BP) in ICEPOS 2005, showing (a) the most common decreasing pattern (Stn 3, Bellingshausen Sea), (b) an exceptionally homogeneous distribution (Stn 8, Antarctic Strait) and (c) particularly high BP values (Stn 9, western Weddell Sea)

Table 1. Correlation matrix among all bacterial variables determined during ICEPOS 2005. See Fig. 2 for abbreviations. *Significant correlations ($p < 0.05$)

n = 63	Total BA (cell ml ⁻¹)	Viable (cell ml ⁻¹)	Percent viable	HNA (cell ml ⁻¹)	LNA (cell ml ⁻¹)	Percent HNA	BP (ng C l ⁻¹ h ⁻¹)
BP (ng C l ⁻¹ h ⁻¹)	0.71*	0.66*	-0.02	0.50*	0.75*	-0.54*	1.00
Percent HNA	-0.46*	-0.26*	0.47*	0.05	-0.69*	1.00	
LNA (cell ml ⁻¹)	0.96*	0.85*	-0.14	0.69*	1.00		
HNA (cell ml ⁻¹)	0.86*	0.92*	0.29*	1.00			
Percent viable	-0.01	0.34*	1.00				
Viable (cell ml ⁻¹)	0.94*	1.00					
Total BA (cell ml ⁻¹)	1.00						

depth as total BA, although this pattern was less accentuated (Fig. 2a). The percentage of HNA cells with respect to total BA generally increased over depth, ranging from $32 \pm 4\%$ in surface waters to $52 \pm 4\%$ in waters below the DCM. This HNA percentage was significant and negatively related to depth ($r = -0.44$, $p < 0.001$, $n = 77$). Total BA was correlated to HNA cells ($r = 0.86$), but the proportion of HNA cells decreased as total BA increased (Table 1). The abundance of LNA cells showed a mean value of $4.1 \pm 0.4 \times 10^5$ cells ml⁻¹ and a wider range than HNA, from 0.6 to 9.5×10^5 cells ml⁻¹ in surface waters and from 0.2 to 7.5×10^5 cells ml⁻¹ in waters below the DCM.

Viable cells after NADS protocol showed a mean value of $4.6 \pm 0.4 \times 10^5$ cells ml⁻¹ and also ranged one order of magnitude, from 2.0 to 10.0×10^5 cells ml⁻¹ in surface water samples and from 0.3 to 9.9×10^5 cells ml⁻¹ in waters below the DCM. Viable cells comprised between 38 and 80% of total BA, generally exceeding the percentage of HNA cells, which indicates that a significant fraction of LNA cells were also viable (Fig. 3). The abundance of viable cells was also correlated to total BA ($r = 0.94$), but the proportion of viable cells was independent of the total BA ($r = -0.01$) (Table 1)

BP showed a similar vertical pattern as total BA, with the lowest values below DCM (13 of 18 stations, Fig. 2a). The BP values ranged 2 orders of magnitude, from 2.0 to 183.8 ng C l⁻¹ h⁻¹ in surface waters and from 0.2 to 46.1 ng C l⁻¹ h⁻¹ in waters below DCM with a mean value of 30.8 ± 3.5 ng C l⁻¹ h⁻¹. Particularly high BP values were observed at the surface waters of the western Weddell Sea (Fig. 2c). BP and total BA were significant and positively correlated (Table 1). BP was also significant and positively correlated to HNA, LNA and viable cells, but this correlation coefficient was higher with LNA cells (Table 1).

Significant and positive relationships between BA and chl *a* concentration were observed in both ICEPOS 2004 and 2005 cruises. Although both regression slopes were lower than 0.4, it was slightly higher for ICEPOS 2005 than for ICEPOS 2004 (Table 2, Fig. 4a).

Table 2. Relationships between chl *a* and all bacterial parameters (BA for each cruise, as well as total HNA, total LNA, total viable and BP for ICEPOS 2005). See Fig. 2 for abbreviations

Cruise	Parameter (vs. chl <i>a</i>)	Slope (\pm SE)	Intercept	r	p	n
ICEPOS 2004	Total BA	0.291 ± 0.053	5.56	0.650	<0.001	50
ICEPOS 2005	Total BA	0.394 ± 0.049	5.79	0.681	<0.001	78
	Viable	0.414 ± 0.057	5.58	0.678	<0.001	64
	HNA	0.280 ± 0.054	5.41	0.512	<0.001	76
	LNA	0.505 ± 0.059	5.52	0.708	<0.001	76
	BP	0.870 ± 0.068	1.26	0.787	<0.001	102

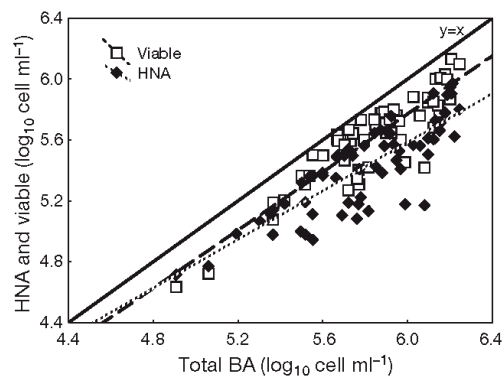


Fig. 3. Scatterplot between total BA and HNA and viable cells. Correlation coefficients are presented in Table 1. See Fig. 2 for abbreviations

All metrics of bacterial abundance (HNA, LNA and viable cells) and BP were significantly correlated with chl *a* in ICEPOS 2005 (Table 2, Fig. 4). A strong relationship was observed between chl *a* and BP, with a log-log regression slope of 0.87 (Table 2). However, lower log-log slopes and correlation coefficients were observed between bacterial abundances and chl *a*. The relationship between viable cells and chl *a* did not show a significantly higher slope than that corresponding to total bacterial abundance (Table 2, Fig. 4). Surprisingly, the relationship between LNA cells and chl *a* showed a significantly higher slope than the slope with HNA cells (Statistica homogeneity-of-slopes model, $p < 0.01$) (Table 2, Fig. 4).

DISCUSSION AND CONCLUSIONS

Our results suggest that viable cells after NADS protocol represent an upper limit with respect to HNA cells (Fig. 3), as the proportion of viable (PI-impermeable) cells (61%) exceeded that of HNA cells (48%), indicating that there are viable bacteria with low acid nucleic content. This high concentration of viable cells

observed in our study, although consistent with other published studies in natural waters (Schumann et al. 2003, Falcioni et al. 2008), contrasts with the only 2 reported studies that use PI stain to measure bacterial viability in the Southern Ocean (Davidson et al. 2004, Pearce et al. 2007), which reported considerably lower proportions (between 2 and 40%). In the work of Pearce et al. (2007), the percentage of viable cells was likely underestimated as higher abundance of total bacteria were observed compared to the sum of viable and non-viable cells. By contrast, in the present study the percentage of viable cells (immediately analyzed with NADS protocol) with respect to total BA cells (previously fixed and stored) would result in an over-estimation of viable cells since a potential loss of cell detection has been observed during storage (Kamiya et al. 2007). However, the potential error in the present study is expected to be minimal due to the short time-lag (up to 2 d) between fixation and analysis.

Total BA, HNA cells and BP obtained in this study were also comparable to those previously reported for the same area (Pedrós-Alió et al. 2002, Vaqué et al. 2002, Corzo et al. 2005) and elsewhere in the Southern Ocean (Ducklow et al. 2000, Granéli et al. 2004). The observed increase in percentage of HNA cells with depth could be explained by selective impact of bacterial grazers. HNA bacteria appear to be preferentially consumed by grazers, whereas LNA escape grazing pressure and will remain abundant (del Giorgio et al. 1996b). Only below the euphotic zone, where the grazing pressure decreases (Vaqué et al. 2002), can HNA bacteria comprise a large proportion of the total bacterial abundance (Jochem 2001, Corzo et al. 2005).

Since ^3H -Leucine incorporation is a bulk measurement of heterotrophic activity, we expected the active fraction of bacterioplankton (either HNA cells or viable cells) to be more closely related to BP than to total BA, which includes bacteria that make little or no contribution to activity. Indeed, some authors (Gasol et al. 1999, Lebaron et al. 2001) have proposed that HNA cells dominate overall bacterial metabolism. However, in the present study LNA cells were more closely related to BP than HNA cells (Table 1, Fig. 4), indicating that

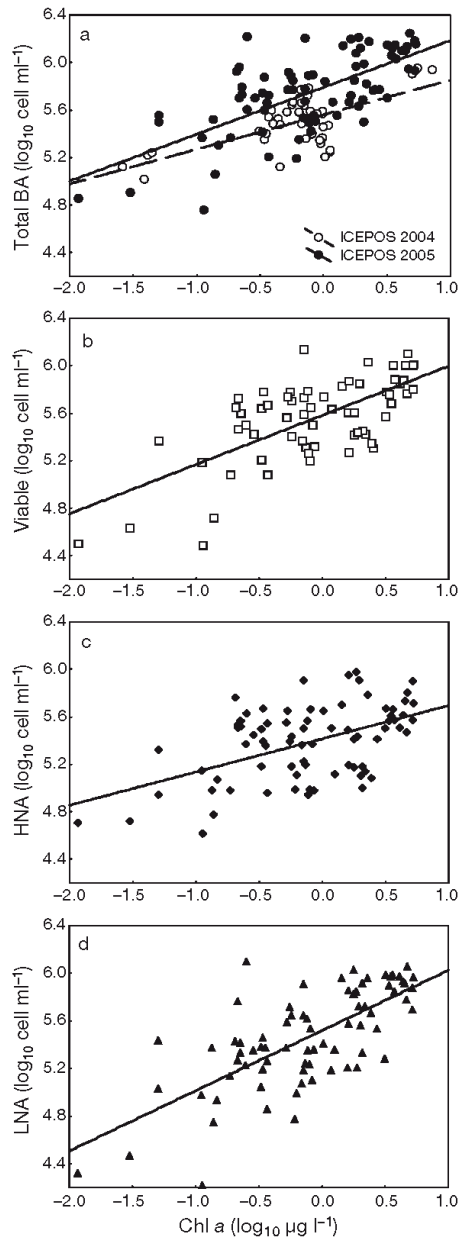


Fig. 4. Scatterplots and regression lines between chl a ($\mu\text{g l}^{-1}$) and (a) total BA (cell ml^{-1}) in both ICEPOS cruises, and (b) viable, (c) HNA and (d) LNA cells (cell ml^{-1}) in ICEPOS 2005. Values for slopes, intercepts, correlation coefficients and levels of significance are presented in Table 2. See Fig. 2 for abbreviations

the discrimination between high and low relative nucleic acid content is not a reliable proxy for the active vs. inactive fractions of the bacterioplankton, supporting recent observations along this line (Sherr et al. 2006). Other studies (Zubkov et al. 2001, Longnecker et al. 2005) also found that LNA cells are responsible for similar or higher fractions of total leucine incorporation than HNA cells in low-chlorophyll waters. Hence, our results corroborate that the simplistic interpretation of HNA and LNA cells as active and inactive subpopulations is also unreliable in Antarctic waters. Rather than differences in activity, HNA and LNA subpopulations appear to represent different fractions with intrinsic properties (e.g. phylogenetically distinct subpopulations), and these fractions may be dynamically linked, with the capacity of LNA cells to shift to HNA and vice versa (Bouvier et al. 2007). In addition, the discrimination of viable cells did not result in a higher correlation with bacterial production (Table 1), as expected from previous reports (Pearce et al. 2007, Falcioni et al. 2008). Like Pirkner et al. (2005), our study showed that the PI stain is not the most reliable method of examining bacterial activity in the field.

There is still a debate about the estimation of active and viable bacterioplankton, which is in part semantic (e.g. actively growing cells, viable but inactive cells with potential activity, inactive and dead cells), but reflects the absence of a widely accepted standard technique. Active bacteria have been determined using a panoply of different techniques yielding divergent estimates (Berman et al. 2001, Schumann et al. 2003, Smith & del Giorgio 2003). Hence, low proportions of activity (<10 to 20%) have been reported, based on the presence of a nucleoid (Berman et al. 2001, Luna et al. 2004) or actively respiring the fluorogenic tetrazolium dye, 5-cyano-2,3 ditolyl tetrazolium chloride (Karner & Fuhrman 1997, Berman et al. 2001), while single-cell approaches, such as fluorescent *in situ* hybridization or microautoradiography, have yielded higher proportions of active cells (Smith & del Giorgio 2003). In comparison, the discrimination of viable bacteria based on their membrane integrity using PI, To-Pro or SYTOX staining, Live/Dead BacLight™ or NADS protocol (Boulos et al. 1999, Davidson et al. 2004, Luna et al. 2004), or active bacteria based on their relative nucleic acid content (HNA vs. LNA; Gasol et al. 1999, Corzo et al. 2005) shows widely variable proportions of active cells. Indeed, this lack of agreement between bacterial activity estimates reflects a continuum of bacterial metabolic states in contrast to the simplistic restriction to discrete categories as active or inactive, and it is unlikely that a single method can capture all the physiological diversity present in bacterioplankton assemblages.

Our aim to assess whether the contribution of specific subpopulations could explain the weak relationship between chl *a* and bacteria found in Antarctic waters gave impetus to discriminating active from inactive bacteria. However, the discrimination of HNA or viable cells within the total abundance in ICEPOS 2005 did not lead to steeper regression slopes or stronger correlation coefficients than the relationship between chl *a* and total BA (Table 2, Fig. 4). This relationship only improved, unexpectedly, when considering LNA cells (Table 2, Fig. 4). Unlike the lower slope observed in the log-log relationship between total BA and chl *a* (slope = 0.3 to 0.4 in comparison to the value of 0.52 reported by Cole et al. [1988]), the slope of the log-log relationship between BP and chl *a* concentration (0.87) was even steeper in the Antarctic communities examined than that in the general relationship (0.62) reported by Cole et al. (1988), and consistent with previous reports of stronger relationships between chl *a* and BP than with BA in the Southern Ocean (Granéli et al. 2004, Duarte et al. 2005). Indeed, previous studies have observed a close coupling between dissolved primary production, a more direct surrogate of algal derived substrates, and bacterial carbon demand in Antarctic waters (Morán et al. 2002), suggesting that in this area bacteria are tightly dependent on algal organic carbon for growth and metabolism, but this dependence is not reflected in terms of total BA, HNA or viable cells. These results suggest that cell abundance was generally more constrained than bacterial protein synthesis, resulting in a significantly steeper slope value for the chl *a*-BP relationship and lower slopes in all the relationships with bacterial abundances. Indeed, the tight trophic linkage between protistan grazers and their prey (Bird & Karl 1999, Vaqué et al. 2002, Duarte et al. 2005), or losses due to viral lysis (Guixa-Boixereu et al. 2002), may preclude significant changes in bacterial abundance, particularly in those cells with high relative nucleic acid (HNA), that appear to be preferentially predated upon. In contrast, protein synthesis usually increases more rapidly than cell duplication to maximize survival, particularly under unfavorable environmental conditions (Ducklow et al. 1992).

In summary, the results of this study revealed a high proportion of viable bacteria in the study area, and the active nature of LNA cells is evidenced by a closer relationship with BP than HNA or viable cells. In addition, although a close relationship between chl *a* and BP was observed, the discrimination between HNA or viable cells from total BA did not result in a stronger relationship between chl *a* and BA in the Southern Ocean, where bacterial abundance may be closely controlled by loss processes rather than resource supply.

Acknowledgements. We thank the crew of the RVs 'Las Palmas' and 'Hespérides' and the Marine Technology Unit for their help and technical assistance, and J.M. Gasol for his help in flow cytometric analyses. We also thank J.M. Gasol and 3 anonymous reviewers for their valuable comments on a previous version of this manuscript. This work was supported by grant REN2002-04165 from the Spanish National Research Program in Antarctica.

LITERATURE CITED

- ▶ Barbesti S, Citterio S, Labra M, Baroni MD, Neri MG, Sgorbati S (2000) Two and three-color fluorescence flow cytometric analysis of immunoidentified viable bacteria. *Cytometry* 40:214–218
- ▶ Berman T, Kaplan B, Chava S, Viner Y, Sherr BF, Sherr EB (2001) Metabolically active bacteria in Lake Kinneret. *Aquat Microb Ecol* 23:213–224
- ▶ Bird DF, Karl DM (1999) Uncoupling of bacteria and phytoplankton during the austral spring bloom in Gerlache Strait, Antarctic Peninsula. *Aquat Microb Ecol* 19:13–27
- ▶ Boulos L, Prévost M, Barbeau B, Coallier J, Desjardins R (1999) LIVE/DEAD (R) BacLight (TM): application of a new rapid staining method for direct enumeration of viable and total bacteria in drinking water. *J Microbiol Methods* 37:77–86
- ▶ Bouvier T, del Giorgio PA, Gasol JM (2007) A comparative study of the cytometric characteristics of high and low nucleic-acid bacterioplankton cells from different aquatic ecosystems. *Environ Microbiol* 9:2050–2066
- ▶ Cole JJ, Likens GE, Strayer DL (1982) Photosynthetically produced dissolved organic-carbon: an important carbon source for planktonic bacteria. *Limnol Oceanogr* 27:1080–1090
- ▶ Cole JJ, Findlay S, Pace ML (1988) Bacterial production in fresh and saltwater ecosystems: a cross-system overview. *Mar Ecol Prog Ser* 43:1–10
- ▶ Corzo A, Rodríguez-Gálvez S, Lubián L, Sobrino C, Sangrá P, Martínez A (2005) Antarctic marine bacterioplankton subpopulations discriminated by their apparent content of nucleic acids differ in their response to ecological factors. *Polar Biol* 29:27–39
- ▶ Davidson AT, Thomson PG, Westwood K, van den Eenden R (2004) Estimation of bacterioplankton activity in Tasmanian coastal waters and between Tasmania and Antarctica using stains. *Aquat Microb Ecol* 37:33–45
- ▶ del Giorgio PA, Bird DF, Prairie YT, Planas D (1996a) Flow cytometric determination of bacterial abundance in lake plankton with the green nucleic acid stain SYTO 13. *Limnol Oceanogr* 41:783–789
- ▶ del Giorgio PA, Gasol JM, Vaqué D, Mura P, Agustí S, Duarte CM (1996b) Bacterioplankton community structure: protists control net production and the proportion of active bacteria in a coastal marine community. *Limnol Oceanogr* 41:1169–1179
- ▶ Duarte CM, Agustí S, Vaqué D, Agawin NSR, Felipe J, Casamayor EO, Gasol JM (2005) Experimental test of bacteria-phytoplankton coupling in the Southern Ocean. *Limnol Oceanogr* 50:1844–1854
- ▶ Ducklow HW, Kirchman DL, Quinby HL (1992) Bacterioplankton cell-growth and macromolecular-synthesis in seawater cultures during the North Atlantic spring phytoplankton bloom, May, 1989. *Microb Ecol* 24:125–144
- ▶ Ducklow HW, Dickson ML, Kirchman DL, Steward G, Orchardo J, Marra J, Azam F (2000) Constraining bacterial production, conversion efficiency and respiration in the

- Ross Sea, Antarctica, January–February, 1997. *Deep-Sea Res II* 47:3227–3247
- Falcioni T, Papa S, Gasol JM (2008) Evaluating the flow-cytometric nucleic acid double-staining protocol in realistic situations of planktonic bacterial death. *Appl Environ Microbiol* 74:1767–1779
- Gasol JM, del Giorgio PA (2000) Using flow cytometry for counting natural planktonic bacteria and understanding the structure of planktonic bacterial communities. *Sci Mar* 64:197–224
- Gasol JM, Duarte CM (2000) Comparative analyses in aquatic microbial ecology: How far do they go? *FEMS Microbiol Ecol* 31:99–106
- Gasol JM, Zweifel UL, Peters F, Fuhrman JA, Hagström Å (1999) Significance of size and nucleic acid content heterogeneity as measured by flow cytometry in natural planktonic bacteria. *Appl Environ Microbiol* 65:4475–4483
- Granéli W, Carlsson P, Bertilsson S (2004) Bacterial abundance, production and organic carbon limitation in the Southern Ocean (39–62°S, 4–14°E) during the austral summer 1997/1998. *Deep-Sea Res II* 51:2569–2582
- Grégori G, Citterio S, Ghiani A, Labra M, Sgorbati S, Brown S, Denis M (2001) Resolution of viable and membrane-compromised bacteria in freshwater and marine waters based on analytical flow cytometry and nucleic acid double staining. *Appl Environ Microbiol* 67:4662–4670
- Guixa-Boixereu N, Vaqué D, Gasol JM, Sanchez-Cámara J, Pedrós-Alió C (2002) Viral distribution and activity in Antarctic waters. *Deep-Sea Res II* 49:827–845
- Hoppe HG (1976) Determination and properties of actively metabolizing heterotrophic bacteria in the sea, investigated by means of micro-autoradiography. *Mar Biol* 36:291–302
- Jochem FJ (2001) Morphology and DNA content of bacterioplankton in the northern Gulf of Mexico: analysis by epifluorescence microscopy and flow cytometry. *Aquat Microb Ecol* 25:179–194
- Kamiya E, Izumiyama S, Nishimura M, Mitchell JG, Kogure K (2007) Effects of fixation and storage on flow cytometric analysis of marine bacteria. *J Oceanogr* 63:101–112
- Karner M, Fuhrman JA (1997) Determination of active marine bacterioplankton: a comparison of universal 16S rRNA probes, autoradiography, and nucleoid staining. *Appl Environ Microbiol* 63:1208–1213
- Lebaron P, Servais P, Agogue H, Courties C, Joux F (2001) Does the high nucleic acid content of individual bacterial cells allow us to discriminate between active cells and inactive cells in aquatic systems? *Appl Environ Microbiol* 67:1775–1782
- Longnecker K, Sherr BF, Sherr EB (2005) Activity and phylogenetic diversity of bacterial cells with high and low nucleic acid content and electron transport system activity in an upwelling ecosystem. *Appl Environ Microbiol* 71:7737–7749
- Luna GM, Dell'Anno A, Giuliano L, Danovaro R (2004) Bacterial diversity in deep Mediterranean sediments: relationship with the active bacterial fraction and substrate availability. *Environ Microbiol* 6:745–753
- Morán XAG, Estrada M, Gasol JM, Pedrós-Alió C (2002) Dissolved primary production and the strength of phytoplankton–bacterioplankton coupling in contrasting marine regions. *Microb Ecol* 44:217–223
- Morán XAG, Bode A, Suárez LA, Nogueira E (2007) Assessing the relevance of nucleic acid content as an indicator of marine bacterial activity. *Aquat Microb Ecol* 46:141–152
- Parsons TR, Maita Y, Lalli CM (1984) A manual of chemical and biological methods for seawater analysis. Pergamon Press, Oxford
- Pearce I, Davidson AT, Bell EM, Wright S (2007) Seasonal changes in the concentration and metabolic activity of bacteria and viruses at an Antarctic coastal site. *Aquat Microb Ecol* 47:11–23
- Pedrós-Alió C, Vaque D, Guixa-Boixereu N, Gasol JM (2002) Prokaryotic plankton biomass and heterotrophic production in western Antarctic waters during the 1995–1996 Austral summer. *Deep-Sea Res II* 49:805–825
- Pirker H, Pausz C, Stoderegger KE, Herndl GJ (2005) Simultaneous measurement of metabolic activity and membrane integrity in marine bacterioplankton determined by confocal laser-scanning microscopy. *Aquat Microb Ecol* 39:225–233
- Pomeroy LR, Wiebe WJ (2001) Temperature and substrates as interactive limiting factors for marine heterotrophic bacteria. *Aquat Microb Ecol* 23:187–204
- Porter KG, Feig YS (1980) The use of DAPI for identifying and counting aquatic microflora. *Limnol Oceanogr* 25:943–948
- Schumann R, Schiewer U, Karsten U, Rieling T (2003) Viability of bacteria from different aquatic habitats. II. Cellular fluorescent markers for membrane integrity and metabolic activity. *Aquat Microb Ecol* 32:137–150
- Sherr EB, Sherr BF, Longnecker K (2006) Distribution of bacterial abundance and cell-specific nucleic acid content in the Northeast Pacific Ocean. *Deep-Sea Res I* 53:713–725
- Simon M, Azam F (1989) Protein content and protein synthesis rates of planktonic marine bacteria. *Mar Ecol Prog Ser* 51:201–213
- Smith DC, Azam F (1992) A simple economical method for measuring bacterial protein synthesis rates in seawater using ³H leucine. *Mar Microb Food Webs* 6:107–114
- Smith EM, del Giorgio PA (2003) Low fractions of active bacteria in natural aquatic communities? *Aquat Microb Ecol* 31:203–208
- Troussellier M, Courties C, Zettelmaier S (1995) Flow cytometric analysis of coastal lagoon bacterioplankton and picophytoplankton: fixation and storage effects. *Estuar Coast Shelf Sci* 40:621–633
- Vaqué D, Guixa-Boixereu M, Gasol JM, Pedrós-Alió C (2002) Distribution of microbial biomass and importance of protists in regulating prokaryotic assemblages in three areas close to the Antarctic Peninsula in spring and summer 1995/96. *Deep-Sea Res II* 49:847–867
- Zubkov MV, Fuchs BM, Burkill PH, Amann R (2001) Comparison of cellular and biomass specific activities of dominant bacterioplankton groups in stratified waters of the Celtic Sea. *Appl Environ Microbiol* 67:5210–5218

Editorial responsibility: Josep Gasol, Barcelona, Spain

*Submitted: September 7, 2007; Accepted: May 29, 2008
Proofs received from author(s): June 2, 2008*

